Titre: Title:	Etude hydrodynamique des lits fluidisés circulants
Auteur: Author:	Larin Godfroy
Date:	1997
Type:	Mémoire ou thèse / Dissertation or Thesis
Référence: Citation:	Godfroy, L. (1997). Etude hydrodynamique des lits fluidisés circulants [Thèse de doctorat, École Polytechnique de Montréal]. PolyPublie. https://publications.polymtl.ca/6809/

UNIVERSITÉ DE MONTRÉAL

ÉTUDE HYDRODYNAMIQUE DES LITS FLUIDISÉS CIRCULANTS

LARIN GODFROY
DÉPARTEMENT DE GÉNIE CHIMIQUE
ÉCOLE POLYTECHNIQUE DE MONTRÉAL

THÈSE PRÉSENTÉE EN VUE DE L'OBTENTION
DU DIPLÔME DE PHILOSOPHIAE DOCTOR (Ph.D.)

(GÉNIE CHIMIQUE)

JUIN 1997

UNIVERSITÉ DE MONTRÉAL

ÉCOLE POLYTECHNIQUE DE MONTRÉAL

Cette thèse intitulée :

ÉTUDE HYDRODYNAMIQUE DES LITS FLUIDISÉS CIRCULANTS

présentée par : GODFROY, Larin

en vue de l'obtention du diplôme de : Philosophiae Doctor

a été dûment accepté par le jury d'examen constitué de :

M. GUY, Christophe, Ph. D., Président

M. CHAOUKI, Jamal, Ph. D, membre et directeur de recherche

M. KENNEDY, Gregory, Ph. D., membre et codirecteur de recherche

M. LEGROS, Robert, Ph. D., membre

M. ZHU, Jing-Xu, Ph. D., membre

À mon père Conrad 1938-1995.

REMERCIEMENTS

En premier lieu, je voudrais remercier tout particulièrement Faiçal Larachi pour ses conseils et son amitié. Sa rigueur exemplaire et sa disponibilité m'ont permis de terminer la rédaction de cette thèse dans des délais acceptables. M. Larachi a été impliqué dès le début du projet en tant que stagiaire post-doctoral au département de génie chimique de l'École Polytechnique. Il est maintenant professeur au département de génie chimique de l'Université Laval.

Je remercie également mon codirecteur de recherche, le professeur Gregory Kennedy du département de génie mécanique. Il a effectué un très bon travail de codirection et s'est impliqué à fond dans le projet. J'ai beaucoup apprécié son implication dans la rédaction des articles et la rapidité avec laquelle il a critiqué et corrigé les travaux.

Un merci très spécial à Gregory Patience pour m'avoir invité à travailler avec lui chez DuPont et pour avoir participé activement à la rédaction de deux articles. Son enthousiasme et son assiduité à la rédaction m'ont permis d'apprécier les mois passés chez DuPont (Delaware) tout en progressant dans mes travaux de recherche. Cette expérience de travail a été marquante et m'a permis d'obtenir un poste au centre de recherche de DuPont Canada à Kingston.

Une attention particulière à toutes les personnes qui n'ont jamais cessé de m'encourager dans la réalisation de mes projets. Je pense entre autre à Émilie, à mes parents et amis sans oublier le personnel de soutien de l'École. Je tiens à remercier particulièrement Messieurs Jean Huard, Robert Delisle, Régent Saint-Pierre, Gérald Lafortune et Carol Painchaud pour leur aide et support technique.

Je désire également exprimer ma gratitute envers les fonds CRSNG et FCAR pour l'aide financière allouée au cours de mes études. Enfin, je ne manquerai pas de remercier le professeur Jamal Chaouki auquel j'ai fait appel à maintes reprises.

RÉSUMÉ

La mise en contact gaz-solide dans les lits fluidisés circulants offre des perspectives intéressantes et ses utilisations industrielles ont connu un grand essor ces dernières années. Cependant, les connaissances relatives à l'hydrodynamique ainsi qu'à la conduite des opérations sont encore bien souvent incomplètes. Ceci constitue un handicap sérieux à la modélisation, à l'optimisation et au design de ces réacteurs. La compréhension de l'hydrodynamique est importante car elle limite le développement de procédés économiquement viables.

L'objectif général de cette étude vise à améliorer la compréhension de l'écoulement dans les lits fluidisés circulants. Dans un premier temps, un modèle hydrodynamique permettant de prédire les caractéristiques macroscopiques moyennes est proposé. Il s'agit d'un modèle complètement empirique qui, à partir des propriétés des particules (ρ_p, d_p) et du diamètre du lit, prédit le profil axial de densité, le profil radial de porosité, le profil radial de vitesse du gaz et des solides et le profil de flux massique.

Les données ayant servi à la validation du modèle proviennent de mesures effectuées dans deux lits fluidisés circulants utilisant deux types de particules (sable et FCC (Fluid Catalytic Cracking)). Le modèle prédit de façon raisonnable les résultats expérimentaux et explique bien les effets radiaux. Il semble mieux adapté dans le cas où ce sont des particules de sable que dans le cas où les particules sont de type FCC.

Le second volet de cette étude analyse de manière plus locale la structure de l'écoulement. Cette étude se veut un raffinement par rapport au modèle hydrodynamique ci-haut mentionné. Il s'agit d'une étude à plus petite échelle où l'intérêt se porte sur les mouvements d'une particule traçante et plus précisément sur ses fluctuations de vitesse. L'utilisation d'un outil innovateur pour investiguer le mouvement des particules dans le lit

fluidisé circulant confère aux nouvelles données expérimentales leur originalité. Cet outil consiste en une technique non-intrusive permettant de mesurer la position instantanée d'une particule traçante. En effet, la technique de poursuite d'une particule radioactive s'est montrée un outil efficace pour décrire le comportement des solides à l'intérieur du lit. La position instantanée est déterminée à partir des comptages obtenus à l'aide de détecteurs radioactifs à scintillation. Les détecteurs sont placés à l'extérieur du lit et l'entourent en partie.

L'application de cette technique à un lit circulant est un défi en soi. La problématique de l'application de cette technique est liée à la résolution spatiale. La technique est entièrement tridimensionnelle et permet de déterminer la position x, y et z de la particule radioactive avec une certaine incertitude. L'incertitude sur les coordonnées (x,y,z) est liée à la nature de la source radioactive (activité et énergie des rayons γ), à la disposition géométrique et au nombre de détecteurs.

Les travaux utilisant la technique de poursuite d'une particule radioactive sont décrits par trois articles:

Le premier article vise à déterminer le meilleur radio-isotope permettant d'améliorer la résolution spatiale. À cette fin, trois radio-isotopes émettant des rayons γ d'énergies différentes ont été étudiés (^{99}Mo (140 keV), ^{198}Au (412 keV), ^{46}Sc (1005 keV)). Les résultats ont permis de démontrer que l'or (^{198}Au) est le meilleur radio-isotope. En effet, l'or permet d'obtenir des comptages plus élevés. Les résultats de cette étape ont été publiés dans le "International Journal of Applied Radiation and Isotopes". Cet article évalue également le potentiel d'un réseau neuronal pour déterminer directement les coordonnées du traceur radioactif à partir des comptages des détecteurs. Ce réseau détermine, en un temps inférieur à la période d'échantillonnage, les coordonnées x, y et z

et permet la visualisation de l'écoulement en temps réel. Cette possibilité peut être recherchée dans de nouvelles applications de la technique.

Un second article montre un essai dynamique de la technique dans un lit fluidisé circulant à l'aide de huit détecteurs radioactifs. À notre connaissance, il s'agit de la première étude décrivant la trajectoire tridimensionnelle d'une particule dans un lit fluidisé circulant. Il s'agit également des premières données obtenues avec ^{198}Au à une fréquence d'échantillonnage de 100 Hz. Ces résultats préliminaires ont été publiés dans le recueil d'articles du 5^{e} congrès sur les lits fluidisés circulants. Les résultats montrent qu'il est possible de déterminer la position instantanée de la particule radioactive. Toutefois, la résolution spatiale dans le plan x,y n'est pas suffisante pour une analyse détaillée des fluctuations de vitesse. Afin d'améliorer la résolution spatiale, il faut donc augmenter le nombre de détecteurs.

Le dernier article décrit le comportement des solides dans le lit fluidisé circulant pour diverses conditions opératoires. Le système de détection utilise seize détecteurs et permet la détermination de la position de la particule cent fois par seconde. La résolution spatiale, définie comme étant l'écart type sur la coordonnée, est en moyenne de 3.5 mm dans la direction x et y et de 4.3 mm dans la direction z. À l'aide de l'ensemble des informations sur la position instantanée d'une particule traçante, le profil de vitesse des particules peut être déterminé. Les essais ont permis de quantifier de façon détaillée l'effet du taux de circulation des solides sur le profil de vitesse des solides. Il appert que la vitesse diminue avec une augmentation du taux de circulation des solides. Ceci est dû à la formation d'agrégats. Les agrégats formés sont évidemment plus volumineux qu'une particule seule et ont des vitesses terminales plus grandes. On observe également que la région près de la paroi, où la vitesse est négative, s'élargit avec l'augmentation du taux de circulation des solides.

Les mêmes données expérimentales permettent, de plus, une analyse des fluctuations de vitesse pour décrire la turbulence. Il s'agit là d'une part de l'originalité de la recherche. Cette analyse permet, entre autres, la détermination des profils de vitesse rms (root mean square), de la fonction d'autocorrélation, du coefficient de dispersion axiale et du coefficient d'anisotropie. Les profils de vitesse rms montrent que les fluctuations de vitesse axiale diminuent légèrement du centre du lit vers la paroi et diminuent avec l'augmentation du taux de circulation des solides. L'analyse des fluctuations de vitesse a également permis de démontrer que l'écoulement n'est pas isotrope et que le coefficient de dispersion axiale des solides diminue avec l'augmentation du taux de circulation des solides.

ABSTRACT

Gas/solids Circulating Fluidized Beds (CFBs) offer good operational perspectives and their use have constantly progressed over the past years. However, the hydrodynamic and operational characteristics of CFBs are not known accurately. This hamper modeling, optimization and design of circulating fluidized bed reactors. The understanding of the hydrodynamic is important and limits the development of new economical processes.

The main objective of this work is to improve the knowledge of mixing behavior in CFB. A fully predictive model for macroscopic hydrodynamic in CFB is proposed: the radial profiles of gas and particle velocities, solids concentration, solids mass flux and axial pressure drop are predicted. The model is validated with experimental data from CFBs operated with both sand and FCC. The model predictions are in good agreement with experimental data over a wide range of operating conditions occurring in catalytic cracking risers and combustion risers.

The second part of this study outlines an investigation of the local flow structure in a CFB. The use of a radioactive particle tracking technique provides original non-intrusive data. The technique is a very powerful tool for investigating the motion of solids. The instantaneous position of a radioactive particle is determined with the help of scintillation detectors surrounding the reactor. The technique allows a mesoscale analysis and is a refinement over the model (macroscopic) discussed above.

Applying the radioactive particle tracking technique to a CFB is challenging. A good spatial resolution is needed. The spatial resolution is a function of the source (activity, γ-ray energy), and the location and number of detectors. These effects need to be

understood and optimized. The work done using the radioactive particle tracking technique is described through three articles:

The first article aims to determine the best radioisotope to improve the spatial resolution. Three radioisotopes have been studied (^{99}Mo (140 keV), ^{198}Au (412 keV), ^{46}Sc (1005 keV)) emitting γ-rays of different energies. The best radioisotope is gold (^{198}Au) which allows higher count rate. The work done leading to this conclusion has been published in the International Journal of Applied Radiation and Isotopes. The potential of neural networks for on-line and real-time visualization of particle movements is also illustrated in the article. This advantage could be appreciated in future application of the technique.

The second article demonstrates the dynamic application of the technique in a circulating fluidized bed using eight detectors. As far as we know, the measurement of the three-dimensional instantaneous position of a single particle has not been investigated before in a CFB. The results were published in the proceedings of the 5th International Conference on Circulating Fluidized Beds. The technique has proven valuable in the measurement of velocity profile. The results were encouraging but the spatial resolution need to be improved. It suggests that further in-depth studies should be done using sixteen detectors.

The third article describes the movements of solids in a circulating fluidized bed under different operating conditions. The tracking system uses a battery of sixteen scintillation detectors and permits accurate determination of the particle position. The spatial resolution, defined as the standard deviation of the coordinate, is 3.5 mm in the radial direction and 4.3 mm in the axial direction. The knowledge of the instantaneous position enables the determination of the instantaneous and mean velocity. Comparison of different axial velocity profiles shows that the velocity across the whole sections decreases with an increase in solids circulation rate. This is explained by the presence of clusters which contributes to an increase in the slip velocities as the solids circulation rate increases. Wall velocities were found to be negative and decreasing with an increase in solids circulation.

The technique also allows an analysis of the particle fluctuating velocities to determine the turbulent mixing characteristics of the flow in a riser. This analysis enables the determination of the root mean square velocities, autocorrelation function, dispersion coefficient and anisotropy coefficient. The analysis of the root mean square velocities shows that the flow is not isotropic and that the axial dispersion coefficient decreases with an increase in solids circulation rate.

TABLES DES MATIÈRES

DÉDICACE IV

REMERCIEMENTS V

RÉSUMÉ VII

ABSTRACT XI

TABLE DES MATIÈRES XIV

LISTE DES TABLEAUX XVII

LISTE DES FIGURES XVIII

LISTE DES SYMBOLES XXI

LISTE DES ANNEXES XXV

AVANT-PROPOS XXVI

INTRODUCTION 1

OBJECTIFS 3

PROBLÉMATIQUE GÉNÉRALE 5

CHAPITRE 1 ARTICLE DE MODÉLISATION DE L'ÉCOULEMENT 7

1.1 Sommaire 7

1.2 Texte de l'article 9

1.2.1 Abstract 9

1.2.2 Introduction 9

1.2.3 Design Considerations 11

1.2.4 Review of Models 12

1.2.5 CFB Workshop 13

1.2.6 Hydrodynamic Model 15
1.2.7 Axial Density Profile 16
1.2.8 Axial Density Profile in the Entrance Region 19
1.2.9 Voidage Profile 20
1.2.10 Gas Velocity Profile 22
1.2.11 Particle Velocity Profile 24
1.2.12 Solids Mass Flux Profile 26
1.2.13 Conclusion 27
1.2.14 List of symbols 30
1.2.15 Greek symbols 31
1.2.16 Subscripts 31

CHAPITRE 2 ARTICLE PUBLIÉ DANS "INTERNATIONAL JOURNAL OF APPLIED RADIATION AND ISOTOPES" 41

2.1 Problématique de l'application de la technique de poursuite d'une particule radioactive 41
2.2 Sommaire de l'article publié dans "International Journal of Applied Radiation and Isotopes 44
2.3 Texte de l'article 46
2.3.1 Summary 46
2.3.2 Background 47
2.3.3 The RPT System 50
2.3.4 Location Algorithms 50
2.3.5 Neural Network and Flow Application 55
2.3.6 Resolution Improvement 57
2.3.7 Conclusion 61
2.3.8 Appendix A 61

CHAPITRE 3 ARTICLE SOUMIS AU 5^{E} CONGRÈS SUR LES LITS FLUIDISÉS CIRCULANTS 73

3.1 Sommaire 73
3.2 Texte de l'article 74
3.2.1 Abstract 74
3.2.2 Introduction 74
3.2.3 Apparatus 76
3.2.4 The Radioactive Particle Tracking System 77
3.2.5 Location Algorithm 78
3.2.6 Results and Discussion 78
3.2.7 Conclusion 81

CHAPITRE 4 ANALYSE DU MOUVEMENT D'UNE PARTICULE TRAÇANTE DANS UN LIT FLUIDISE CIRCULANT 89

4.1 Sommaire 89
4.2 Texte de l'article 91
4.2.1 Abstract 91
4.2.2 Introduction 92
4.2.3 Measurement of Solids Velocities in CFB 93
4.2.4 Circulating Fluidized Bed Riser and RPT Facility 94
4.2.5 Tracer Preparation 95
4.2.6 Spatial Resolution 96
4.2.7 Results and Discussion 96
4.2.8 Conclusion 107

CHAPITRE 5 SYNTHÈSE 127

5.1 Recommandations 132

RÉFÉRENCES 134

LISTE DES TABLEAUX

Table 1.1 Test Matrix for hydrodynamic predictions 32
Table 1.2 Suspension densities under different riser diameters. 32
Table 1.3 Slip factors for FCC powder 33
Table 2.1 Nuclear characteristics of the radionuclides used and measured in this study. .. 62
Table 4.1 Various methods of measuring the velocity of particles (after Oki *et al.* 1978)109
Table 4.2 Calculated values of the slip factor (U_g=4m/s) 110
Table 4.3 Effective dispersion coefficient (after Patience 1990) 111
Tableau AVII.1 Résultats du tamisage 192
Tableau AVII.2 Résultats du tamisage (essai répété) 193

LISTE DES FIGURES

Figure 1.1 Design sequence to determine the geometry and operating conditions. 34
Figure 1.2 Comparison between predicted experimental pressure drop for sand particles. 35
Figure 1.3 Comparison between predicted experimental pressure drop for FCC particles. 36
Figure 1.4 Normalized void fraction as a function of radial position for sand particles. ... 37
Figure 1.5 Normalized void fraction as a function of radial position for FCC particles. ... 38
Figure 1.6 Selected figure showing good agreement (Radial profile of solids mass flux ; sand D=0.4 m, U_g=4.2 m/s, G_s=50kg/m^{2}s). 39
Figure 1.7 Selected figure showing poor agreement (Radial profile of mass flux, FCC D=0.2 m, U_g=11 m/s, G_s=49,196,489,782 kg/m^{2}s). 40
Figure 2.1 Layout of the RPT system. 63
Figure 2.2 Spherical coordinate system used in Monte-Carlo calculation. 64
Figure 2.3 Effect of the number of histories in the Monte Carlo evaluation of the solid angle. 65
Figure 2.4 Neural architecture of the reconstruction model (n=8). 66
Figure 2.5 Tracking a labeled particle in a three-phase fluidized bed using the least-squares search algorithm (I) and the neural network model (II). 67
Figure 2.6 Longitudinal profiles of the mean Eulerian velocities in the radial and longitudinal directions as calculated from the least-squares approach (I) and the neural network model (II) in a three-phase fluidized bed. 68
Figure 2.7 Results of the bias of the located longitudinal component, z, for the three radionuclides (sampling period, 10 ms). 69
Figure 2.8 Longitudinal profiles of the standard deviations σ_y and σ_z of components y and z and the corresponding standard deviations from the detection model (Equation 1), as a function of γ-ray energy (sampling period, 10 ms). 70
Figure 2.9 Predicted resolution σ_z for the ^{198}Au source in a dilute medium. 71

Figure 2.10 Predicted resolution σ_x for the ^{198}Au source in a dilute medium. 72
Figure 3.1 Schematic of the CFB set up. 82
Figure 3.2 Schematic of the RPT system. 83
Figure 3.3a Instantaneous x position (100 Hz) from RPT system after filtering. 84
Figure 3.3b Instantaneous y position (100 Hz) from RPT system after filtering. 85
Figure 3.3c Instantaneous z position (100 Hz) from RPT system after filtering. 86
Figure 3.4 Mean axial velocity profile. 87
Figure 3.5 Number of occurrences of axial velocity measurement. 88
Figure 4.1 Schematic of the circulating fluidized bed apparatus 112
Figure 4.2 Arrangement of the detectors around the CFB riser 113
Figure 4.3 Continuous motion path of the marked particle 114
Figure 4.4 Distribution of downward Lagrangian velocity (U_g=4 m/s) 115
Figure 4.5 Typical occurrences of the location across the section (U_g=4 m/s) 116
Figure 4.6 Solids velocity profiles $v_z(r)$ (U_g=4 m/s) 117
Figure 4.7 Verification for fully developed velocity 118
Figure 4.8 Verification for fully developed velocity 119
Figure 4.9 Axial root mean square velocities ($v'_{z,rms}$) (U_g=4 m/s) 120
Figure 4.10 Radial root mean square velocities ($v'_{r,rms}$) (U_g=4 m/s) 121
Figure 4.11 Anisotropy coefficients as a function of radius $AC(r)$ (U_g=4 m/s) 122
Figure 4.12 Axial autocorrelation functions (f_{zz}) (U_g=4 m/s) 123
Figure 4.13 Effect of Solids Circulation Rate on the Axial Dispersion Coefficients (U_g=4 m/s) 124
Figure 4.14 Residence Time Distributions (U_g=4 m/s) 125
Figure 4.15 Comparison of residence time distributions with model predictions (U_g=4 m/s, G_s=23 kg/m^{2}s) 126
Figure 5.1 Comparaison des profils de vitesse axiale 131
Figure AIII.1 Schéma du montage 181

Figure AIII.2 Schéma de la tuyauterie 182
Figure AIII.3 Schéma du bas du lit 183
Figure AIV.1 Courbe de calibration du rotamètre R3 (P=300 kPa) 185
Figure AIV.2 Courbe de calibration du rotamètre R4 (P=300 kPa) 186
Figure AIV.3 Courbe de calibration du rotamètre R5 (P=300 kPa) 187
Figure AV.1 Courbe de calibration du capteur différentiel de pression pour la mesure de la perte de charge axiale. 189

LISTE DES SYMBOLES

A: source activity (μCi)

$\hat{C}_i$: normalized responses of the detectors (i=1 to n, number of detectors).

C : count recorded by a detector

C_d: drag coefficient

d : thickness of the crystal in the direction given by vector **r** (m)

D: riser diameter (m)

$D_{s,z}$: axial dispersion of the solids (m^2/s)

d_p: particle diameter (m)

e_1 : path length traveled by the γ-ray in the reactor (m)

e_2 : path length traveled by the γ-ray through the reactor wall (mm)

k: kinetic constant

K: parameter (Eq. 4 and 5)

$f_{\alpha\alpha}(\tau)$: autocorrelation function

Fr: Froude number ($U_g/\sqrt{(gD)}$)

Fr_t: terminal Froude number ($V_t/\sqrt{(gD)}$)

g: gravitational constant (m/s^2)

G_s: solids circulation rate (kg/m^2s)

H: riser height (m)

H_j: parameter in equation 4.1 and 4.2

n : external unit vector locally normal to dΣ

n : number of detector

Q: gas flow rate (m^3/s)

$r_{s,0}$: radius at which the axial particle velocity is zero

Re_p: particle Reynolds number ($d_p(V_p-U_g/\varepsilon)\rho_g/\mu$

S: selectivity

t: time (s)

T_L: Lagrangian integral time scale (s)

r : distance between the source and a point on the outer surface of the detector crystal (m)

r: radial component

r_c: radius of the core (m)

R: riser inside radius (m)

T: temperature (°C)

U_g: gas superficial velocity (m/s)

U_{mf}: minimum fluidization velocity (m/s)

V_g: actual gas velocity (m/s)

V_p: particle velocity (m/s)

V_t: terminal velocity (m/s)

Vr': fluctuating radial velocity (m/s)

V_z': fluctuating axial velocity (m/s)

V_z: axial velocity component (m/s)

$Vr_{,rms}$: radial root mean square velocity (m/s)

$V_{z,rms}$: axial root mean square velocity (m/s)

W: catalyst inventory (kg)

w_{jy} : fitting parameters of the neural model

w_{jx} : fitting parameters of the neural model

w_{jy} : fitting parameters of the neural model

w_{jz} : fitting parameters of the neural model

x : coordinate in the plane (m)

$\hat{x}$: normalized coordinates (between 0 and 1) of the tracer

X: conversion

y : coordinate in the plane (m)

$\hat{y}$: normalized coordinates (between 0 and 1) of the tracer

z : axial coordinate

$\hat{z}$: normalized coordinates (between 0 and 1) of the tracer

z : axial coordinate (m)

Z: axial coordinate (m)

Lettre grecque

α :exponent in the gas and particle velocity profile (Eq. 9, 10 and 14)

ΔP :pressure drop (Pa)

ε : void fraction

$\bar{\varepsilon}$: mean void fraction

ε_{cl} : void fraction in the centerline of the riser

ϕ : emission angle in the Monte Carlo calculation

ϕ_s :fraction of the cross-sectional area in which particles ascend

φ : peak-to-total ratio

ψ :slip factor

γ : parameter in Eq. 9 and 12

Ω : solid angle subtended by the detector surface as seen from the source

μ: gas viscosity (Pa s)

μ_D : total linear attenuation coefficients of the detector material

μ_R: total linear attenuation coefficients of the reactor contents

μ_w : total linear attenuation coefficients of the reactor wall

υ: number of γ-rays emitted per disintegration

ρ: suspension density (kg/m^3)

ρ_g: gas density (kg/m^3)

ρ_p: particle density (kg/m^3)

σ : standard deviation in the coordinate

τ : dead-time per recorded pulse

θ :emission polar angle in the Monte Carlo calculation

$\zeta_{s,0}$:non dimensional location at which the particle velocity is zero

ζ : indicates dependence on the non dimensional location

Indice

i : detector i

cl: centerline

mf: minimum fluidization

x : coordinate in the plane

y : coordinate in the plane

r: indicates dependence on radial coordinate

z: indicates dependence on axial coordinate

LISTE DES ANNEXES

Annexe I: Revue de la littérature 146
Annexe II: Article soumis au Groupe Français de Génie des Procédés 171
Annexe III Détails du montage expérimental 179
Annexe IV Courbes de calibration des rotamètres R3, R4 et R5. 184
Annexe V Courbe de calibration du capteur différentiel de pression 188
Annexe VI: Procédure expérimentale 190
Annexe VII Caractérisation de la taille des particules de sable 192
Annexe VIII Réquisition pour l'achat de 8 détecteurs radioactifs 194

AVANT-PROPOS

Depuis 1992, l'École Polytechnique a introduit la possibilité de présenter la thèse par regroupement d'articles. Les articles doivent avoir été soumis pour publication dans des revues avec comité de lecture reconnues dans la discipline. Le jury du travail ne doit pas être lié en aucun cas par les évaluations des articles par les comités de lecture ayant procédés à l'analyse pour publication. Il est souhaitable qu'au moins un des articles utilisés ait été accepté pour s'assurer du sérieux et de la valeur de l'exercice de rédaction.

La présentation d'une thèse par articles constitue une solution de remplacement à la présentation traditionnelle d'une thèse de doctorat. La formule choisie est celle des articles intégrés dans le corps du travail. Chacun des articles utilisés constitue un chapitre du travail et comprend les liens appropriés. Le corps de la thèse comprend quatre articles scientifiques et les annexes en comportent deux autres.

INTRODUCTION

L'étude de l'hydrodynamique, de l'opération, du design et de l'optimisation des lits fluidisés continue depuis maintenant plusieurs dizaines d'années. L'accent mis sur certains régimes d'opération (biphasique à bulles, turbulent, fluidisation rapide, triphasique, etc.) change de décade en décade mais les lits fluidisés demeurent toujours une solution moderne dans les procédés à grande échelle où il y a contact entre un ou des fluides et des particules.

Le développement des réacteurs gaz-solides est particulièrement important pour plusieurs industries. C'est notamment le cas en pétrochimie et en métallurgie (craquage catalytique, synthèse Fisher-Tropsch, calcination de l'alumine, réduction de minerais de fer, etc.), pour la combustion (charbon et déchets) et potentiellement pour plusieurs réactions catalytiques.

Parmi ces réacteurs gaz-solides, le lit fluidisé circulant est avantageux par sa vitesse de gaz élevée et son bon contact particules-gaz. Un lit fluidisé circulant (LFC) est un lit dans lequel la vitesse superficielle de gaz est grande (2-8 m/s), ce qui crée un lit très expansé avec beaucoup d'emportement de solides. Par conséquent, le maintien d'une opération en continu nécessite de recirculer les particules. Les particules entraînées par le courant gazeux à la sortie du lit sont généralement séparées à l'aide de cyclones. Les attraits des lit fluidisés circulants les plus souvent cités sont :

-flexibilité opératoire. Le taux de circulation de solides est indépendant de la vitesse de gaz. Cette caractéristique est importante pour adapter la production à un changement de capacité, de qualité d'alimentation du gaz ou des caractéristiques des solides.

-bon contact gaz-particules et faible temps de résidence (typiquement inférieur à 10 s). Les lits fluidisés circulants sont de bons réacteurs pour les réactions rapides.

-excellentes caractéristiques de transfert de chaleur et du transfert de masse. La température est à toute fin pratique constante dans tout le lit.

-possibilité d'alimentation étagée du gaz et des particules.

-taux de réaction élevé (permet des volumes de réacteurs plus petits).

De plus, la zone de réaction et la zone de recirculation des solides peuvent être à des conditions de température et de pression différentes. Les avantages ci-haut mentionnés font en sorte que les lits fluidisés circulants sont particulièrement intéressants dans le cas où :

a) les réactions requièrent un faible temps de contact par exemple dans le cas où un produit intermédiaire est le produit désiré.

b) le catalyseur se désactive rapidement et où il peut être régénéré dans la zone de recirculation. Il est facile d'ajouter et d'enlever du catalyseur.

c) les réactions requièrent un ajout ou un enlèvement considérable de chaleur et où le solide joue le rôle de transporteur de chaleur.

d) les réactions gaz-solides où un bon contact gaz-particules est essentiel.

e) l'alimentation au réacteur et la demande des produits de la réaction changent, étant donné la flexibilité opératoire.

OBJECTIFS

L'objectif général de cette étude est de caractériser l'hydrodynamique des lits fluidisés circulants. L'atteinte de cet objectif nécessite l'investigation de deux aspects importants de l'hydrodynamique des lits fluidisés circulants : la modélisation macroscopique de l'écoulement et la mesure de la structure locale de l'écoulement. L'étude se trouve ainsi divisée en deux grandes parties.

Dans un premier temps, un modèle hydrodynamique complètement prédictif est présenté pour modéliser de façon macroscopique l'écoulement. Les modèles hydrodynamiques sont utiles pour caractériser l'écoulement du gaz et des particules et pour optimiser, contrôler et mettre à l'échelle les lits fluidisés circulants. L'hydrodynamique affecte la performance du réacteur car elle est intimement liée à la conversion, à la sélectivité et au transfert de chaleur à l'intérieur du réacteur. Les objectifs spécifiques du modèle hydrodynamique sont de prédire les valeurs moyennes du:

- profil axial de densité
- profil radial de porosité
- profil radial de vitesse du gaz
- profil radial de vitesse du gaz
- profil radial de flux massique.

La connaissance de ces variables hydrodynamiques est importante mais ne présente pas toute l'information et n'offre pas le niveau de confiance requis pour faire le design d'un nouveau lit. Par exemple, le modèle prédit qu'un film concentré de particules ayant une vitesse moyenne négative est présent près de la paroi. Le temps que la particule passe dans ce film n'est pas prédit par le modèle, pas plus que les fluctuations de vitesse. Ces caractéristiques affectent le transfert de chaleur entre le lit et la paroi, de même que la

distribution de temps de séjour des particules et par conséquent, les réactions en jeu (conversions et sélectivités).

Pour ces motifs, l'objectif de la seconde partie de cette étude est de caractériser la structure hydrodynamique locale des particules. Les données sont recueillies à l'aide de la technique de poursuite d'une particule radioactive. Le paramètre principalement étudié est l'effet du taux de circulation des solides sur le mouvement d'une particule traçante. Il est cependant nécessaire d'évaluer au préalable si l'outil que représente la technique de poursuite d'une particule radioactive est applicable pour l'étude de la structure locale de l'écoulement des particules dans un lit fluidisé circulant. Ceci constitue donc le dernier objectif, qui est traité dans deux articles présentés respectivement aux chapitres 2 et 3. Enfin, le chapitre 4 présente et discute des résultats obtenus sous différentes conditions opératoires, qui se veut une réponse à l'objectif de privilégier une approche locale.

PROBLÉMATIQUE GÉNÉRALE

La collaboration à la rédaction d'un article de revue de la littérature (annexe I) a permis de dégager la problématique générale à laquelle une nouvelle étude hydrodynamique doit s'attarder. Cette nouvelle étude fait l'objet de la présente thèse et touche deux aspects importants de l'hydrodynamique des lits fluidisés circulants afin de répondre aux objectifs généraux. Le premier aspect concerne la modélisation macroscopique de l'écoulement et le second entre plus dans les détails et s'intéresse à la structure locale de l'écoulement ("mesoscale").

Au niveau de la modélisation macroscopique de l'écoulement, il existe différents modèles hydrodynamiques, qui ont été regroupés en trois grandes catégories selon Harris et Davidson (1994). Les modèles de la première catégorie (type I) prédisent seulement la variation axiale de la concentration moyenne des solides. Les modèles de la seconde catégorie (type II) approximent les distributions radiales de la concentration et de la vitesse moyenne des deux phases en divisant l'écoulement en deux ou plusieurs régions (exemple : modèle de type cœur-anneau). Enfin les modèles de la dernière catégorie (type III) sont basés sur les lois fondamentales de la mécanique des fluides et font intervenir des termes de turbulence permettant entre autres de décrire les fluctuations de vitesse. Les avantages des modèles de type III sont évidents : habileté d'adaptation à des géométries nouvelles, facilité de couplage avec des réactions chimiques, possibilité de traiter l'alimentation étagée, etc. Par contre, la nature même des équations constitutives est controversée et le problème de résolution numérique est de taille. Pour ces raisons, les modèles de type I et II restent toujours les plus fréquemment utilisés. Le modèle hydrodynamique proposé est de type I-II selon la catégorisation de Harris et Davidson (1994). Il se distingue des autres modèles par l'introduction de profils continus de la vitesse du gaz et des particules. L'approche la plus répandue consiste à approximer la distribution radiale par une structure cœur-anneau. Toutefois, cette approximation semble trop simplifiée et ne représente pas bien la structure réelle de l'écoulement.

En ce qui concerne l'aspect étude de la structure locale, il a été exploré à l'aide d'une méthodologie particulière et originale, la technique de poursuite d'une particule radioactive. Cette technique, développée au département de génie chimique de l'École Polytechnique par Larachi et coll. (1994), est toute indiquée pour étudier localement le mouvement des solides. Par contre, la résolution spatiale avec laquelle la position de la particule traçante est déterminée doit être améliorée et constitue le problème majeur à l'utilisation de cette technique. Cette technique constitue un outil efficace pour déterminer le champ moyen et les fluctuations de vitesse et peut être utilisée pour l'investigation de la structure locale de l'écoulement. Elle présente, notamment, l'avantage d'être tridimensionnelle et non-intrusive et ne perturbe ainsi aucunement l'écoulement.

CHAPITRE 1 ARTICLE DE MODÉLISATION DE L'ÉCOULEMENT

1.1 Sommaire

Dans la dernière décennie, plusieurs modèles hydrodynamiques ont vu le jour. Pour plusieurs d'entre eux, les modèles ont été développés dans le but d'exprimer les résultats expérimentaux des auteurs. La plupart du temps, la gamme de conditions opératoires est restreinte et la comparaison est limitée à une géométrie et un type de particules donnés.

Le besoin de déterminer la validité des différents modèles hydrodynamiques a été reconnu au congrès international sur la fluidisation en Australie (1992). Un défi a été lancé à toute la communauté scientifique pour prédire de nouvelles mesures hydrodynamiques à partir de la connaissance des conditions opératoires, de la géométrie des lits fluidisés circulants et des propriétés des particules. Les données expérimentales ont été générées en utilisant deux types de particules et trois lits fluidisés circulants.

Les auteurs intéressés à relever le défi étaient invités à soumettre les courbes prédisants les résultats mesurés. La comparaison entre les données expérimentales et les valeurs prédites par les modèles fut dévoilée au congrès suivant sur la fluidisation (France, 1995). Dix groupes de recherche ont participé à l'exercice et notre groupe, Godfroy, Patience et Chaouki, s'est bien démarqué. Suite à ce succès, nous avons décidé de publier un article sur la modélisation de l'hydrodynamique dans les lits fluidisés circulants. Cet article est présenté à la section suivante. Il a été soumis pour publication dans le journal: "Industrial & Engineering Chemistry Research" au début du mois de décembre 1996.

L'avantage de ce modèle par rapport aux modèles déjà existants est qu'il incorpore un profil radial continu de la vitesse du gaz et des solides. Il s'agit d'un modèle complètement prédictif permettant de décrire: le profil de vitesse axiale du gaz et des particules, la concentration locale des solides, le flux massique local et enfin la perte de charge axiale.

A partir de la taille et de la densité des particules, du diamètre du lit, de la vitesse du gaz, du taux de circulation des solides et d'une corrélation existante sur le facteur de glissement entre le gaz et les particules, le modèle prédit d'abord la concentration moyenne des solides dans la zone où l'écoulement est développé. Le modèle utilise alors une approche semi-empirique basée sur un bilan de force sur une particule pour prédire le profil axial de concentration des solides dans la zone d'accélération au bas du lit. Afin de déterminer le profil radial de concentration des solides, le modèle suppose une forme adimensionnelle qui est uniquement fonction du rayon. Les expressions des profils de vitesse du gaz et des particules sont déterminées à l'aide de bilans de masse. Les profils de vitesse du gaz et des solides suivent un profil exponentiel ayant la même forme. La vitesse du gaz est nulle à la paroi alors qu'elle est négative pour les particules.

1.2 Texte de l'article

Radial Hydrodynamics in Risers

soumis au Industrial & Engineering Chemistry Research Journal

en décembre 1996

Larin Godfroy[1], Gregory S. Patience[2] and Jamal Chaouki[1]

[1] Department of Chemical Engineering, École Polytechnique de Montréal, C.P. 6079, Succ. Centre-Ville, Montréal, Québec, Canada H3C 3A7

[2] E.I. du Pont de Nemours & Co., Wilmington, DE, U.S.A. 19880-0262

1.2.1 Abstract

A fully predictive model for the hydrodynamics of circulating fluidized beds is proposed: the radial profiles of gas and particle velocity, solids concentration, solids mass flux and axial pressure drop are predicted. Starting from the knowledge of powder size, particle density, riser diameter, gas velocity and solids circulation rates, the model combines an existing slip factor correlation to determine the cross-sectionally average void fraction and pressure drop in the fully developed flow region. It uses a semi empirical approach based on a momentum balance to define the density profile in the acceleration region. The variation of voidage with the radius is assumed to be a unique function of radial distance when normalized. Both gas and velocity profile follow a power law type expression with zero gas velocity and negative particle velocity at the wall. The model predictions are in reasonably good agreement with experimental data over a wide range of operating conditions occurring in catalytic cracking risers and combustion risers.

1.2.2 Introduction

Circulating Fluid Bed (CFB) hydrodynamic models are useful for understanding gas-solid mixing, scale-up, plant optimization and control. Hydrodynamics impact reactor performance, conversion, selectivity and heat transfer. Furthermore, CFB riser operating conditions affect the efficiency of downstream equipment such as cyclones, filters,

standpipes, etc. Hydrodynamic modeling is useful for understanding and optimizing plant conditions but they do not offer the level of confidence required to design, a priori, a new commercial plant. Rather, new commercial facilities are designed based on extensive piloting and conservative extrapolations of pilot plant basic data. Pilot plants, at a sufficiently large scale, minimize risk of projecting performance to commercial scale and provide the means with which to test alternative designs rapidly and economically. Three examples of this approach include the NUCLA power generation facility (Reh 1995), Mobil's short contact time catalytic cracker (Avidan *et al.* 1990), and DuPont's butane to maleic anhydride process (Contractor *et al.* 1994).

In the last decade, significant advances have been made in experimental measurements of riser hydrodynamics and a number of models have emerged to characterize these data. However, most models are developed based on a limited data set and their extrapolation to conditions outside the range is not well documented. For this reason J. Chen proposed that a "Benchmark Modeling Exercise" be prepared to compare model predictions against unpublished experimental data that cover a wide range of operating conditions. T. Knowlton prepared the exercise and invited modelers to predict axial pressure drop, radial void fraction and mass flux in two different risers. He disclosed the CFB geometry, particle characteristic and operating conditions. Eleven teams accepted this challenge and T. Knowlton, D. Geldart and J. Matsen presented the results of the exercise at the 1995 International Conference on Fluidization in France.

In this paper, we discuss the Benchmark Modeling data base and describe in detail the model proposed by Chaouki, Godfroy and Patience. We also summarize the approaches different modelers have adopted to predict riser hydrodynamics. Throughout this discussion, we highlight some difficulties in measuring experimental data and the strengths and weaknesses of the model.

1.2.3 Design Considerations

Operational flexibility is of particular importance in many CFB applications. In both combustion and fluid catalytic cracking, operators often require the ability to treat a variety of feedstocks. Flexibility is an advantage of CFB technology but, at the design stage, this flexibility often translates into uncertainty. The largest uncertainty relates to predicting the solids volumetric fraction - solids hold-up or inventory - as a function of geometry and operating conditions. Hold-up increases with solids circulation rate and decreases with gas velocity. The solids hold-up does not only affect riser pressure drop but it may also affect reactor performance: for example, in FCC units, higher solids hold-up resulting from increasing the circulation rate may alter the temperature profile and, thus, the hydrocarbon product distribution.

Designing fixed bed tubular reactors and fluid beds is less complicated than CFB design because solids inventory is independent of operating conditions. The relation between geometry, design parameters and operating variables are different with a CFB. The geometry of a fixed bed is set to minimize pressure drop and maximize heat transfer. In a CFB, superficial gas velocity, solids circulation rate and reactor geometry affect solids hold-up, which determine specific reaction rates. Figure 1.1 shows a design flow diagram to determine the geometry and operating conditions of a CFB. Generally, we require a certain production rate (Q) and set conversion (X) and selectivity (S) to meet economic objectives. These parameters, coupled with reaction kinetics, determine solids inventory (W). As with a fixed bed, kinetic considerations may form the basis for the gas flow rate (Q) and catalyst inventory (W) in a CFB. With these two parameters, we first pick a diameter (D) and calculate a gas velocity (U_g), which should be sufficiently low to avoid excessive solids attrition (typically <30 m/s). Gas velocity (U_g) together with solids mass flux (G_s) determine the suspension density, from which the height (H) is determined to satisfy solids inventory requirements. The riser height must be sufficiently large such that its pressure drop (ΔP_{riser}) is less than that across the recycle loop ($\Delta P_{recirculation}$) otherwise solids will circulate at rates lower than design. In the case of low circulation rates, solids

inventory in the recycle loop becomes prohibitively high and this can negatively impact overall economics: so, the ratio of riser solids to solids in the recycle loop should be maximized.

Independent parameters that impact riser hydrodynamics include geometry - entrance and exit configuration as well as bed diameter - gas velocity, circulation rate and particle characteristics. These parameters form the basis of hydrodynamic models and are used to predict the overall riser pressure drop, and radial density and velocity profile.

1.2.4 Review of Models

Several modeling efforts employing very different mathematical formulations have appeared in the recent literature to predict the relationship between solids hold-up, operating conditions and riser geometry. Harris and Davidson (1994) classified the models into three broad categories: (I) those that predict the axial solids suspension density profile, but not the radial profile, (II) those that predict the radial profile by assuming two or more regions, such as core-annulus or clustering annular flow models, (III) those that employ the fundamental equations of fluid dynamics to predict two phase gas-solid flow. Type III models, because of their generality, are suitable for predicting the effects of complex geometry (Harris and Davidson (1994)). However, the constituent equations for two-phase gas-solid flow is not well developed and the numerical complexity often discourages their use. Proponents of the type I and II models cite ease of understanding and usage along with generally very good agreement with experimental data as the main advantages. However, detractors argue that the assumptions of the flow structure associated with such model oversimplify the complex flow pattern. One important consideration in selecting a modeling approach is its intended application: type I and II models may best be employed as a design tools to investigate the effects of operating conditions and riser dimensions on the riser flow structure as well as control models. In addition, they may be easily coupled with reaction kinetic models to simulate the performance of CFB reactors (Pugsley *et al.* (1992), Patience and Mills (1994), Bolkan-

Kenny *et al.* (1994)). Type III models, on the other hand, are well suited to investigate the riser local flow structure and the impact of geometry, such as corner effects in CFB combustors, or a unique inlet configuration such as those studied by Pita and Sundaresan (1993). They could also be useful for control development and testing. However, they might be overly complex to use directly in control algorithms. The three classes of models described may further be characterized by the mathematical approach taken. This characterization is obvious for type III models in which a system of equations contains the continuity, momentum, and pseudo-thermal energy balances, and constitutive relations are solved. However, types I and II may involve the use of correlations based on experimental data, referred to as the "lumped approach" or a combination of correlations and fundamental relationships. The equations found in the three categories are found in an extended review of CFB hydrodynamics (Berruti *et al.* (1995)) (Annexe I).

1.2.5 CFB Workshop

Over the past several years significant advances have been made in both the experimental measurements of riser hydrodynamics and characterization. To highlight recent advances and define future directions a Benchmark Modeling was proposed in the 1992 International Conference on Fluidization in Australia. The geometry of the units along with the operating conditions and particle characteristics of the solids would be made available to the research community with an invitation to predict the hydrodynamics. Comparison between model predictions and experimental data were disclosed at the 1995 International Conference on Fluidization in France. Authors only sent their prediction graphically without explanation.

One riser was 14.2 m tall and 0.2 m in diameter and the other was 9 m tall and 0.4 m in diameter. Both risers were equipped with round smooth elbows at the top and solids were fed at the bottom through L-valves. Sand and FCC were the test solids and air was the fluidizing medium. Data were collected over a wide range of conditions - $2.4 < U_g < 11$ m/s ; $15 < G_s < 800$ kg/m^{2}s as summarized in Table 1. This information was given to the

modelers in January 1995 with the challenge to predict axial pressure profiles, radials solids mass flux profiles, and radial solids density profiles. Ten research groups; Bernard; Sundaresan; Arastoopour and Kim; Gidaspow and Sun; Johnsson; Chaouki, Godfroy and Patience; Pugsley and Berruti; Rhodes and Wang; O'Brien and Syamlal; and Chen participated in the exercise. Comparison between predictions and the experimental data were presented by Knowlton, Matsen and Geldart. At Fluidization VIII in France, the results were announced at a special CFB hydrodynamics workshop: two plots were shown for each participating group - one which represent good agreement between experimental data and model predictions and the other in which the agreement was considered poor.

Most of the groups did not attempt to model all the test conditions, nonetheless the exercise provided a good perspective of the state-of-the-art in CFB modeling. Only type II and type III modelers participated. Conclusions drawn from the exercise are as follows: (a) no single model adequately predicted all the conditions and trends in data; (b) type III models did not show as good agreement with data as did type II models; (c) some models are good over a limited range of conditions; (d) most models failed to properly represent radial density and solids mass flux profile of FCC catalyst at the highest mass flux; (e) no model adequately predicted the increase in suspension density at the top of the riser; (f) Bernard's model predicted FCC data quite well; (g) the models of Chaouki, Godfroy and Patience; and; Pugsley and Berruti provided the best overall agreement with the experimental data; and; (h) the best type III model was presented by Gidaspow and Sun that matched some significant trends in the radial mass flux profiles.

During subsequent discussion, the necessity of including additional criteria in the assessment of the different models was pointed out. One of the most crucial requirements is user-friendliness and speed in generating results. The benchmark modeling test provided a fair representation of the accuracy and applicability of present hydrodynamic models and it indicated some direction for future developments.

1.2.6 Hydrodynamic Model

The model assumes that solids are entrained at high velocities in the central region of the riser and descend near the wall. Most experimental data show strong radial velocity and solids volume fraction gradients at the wall. To characterize this phenomena, we approximate the radial profiles of particle velocity and suspensions density with continuous functions. The input parameters are: the superficial gas velocity (U_g), the solids circulation rate (G_s), the riser diameter (D) and the particles density and diameter.

The model predicts:

1- axial density profile
2- radial void fraction
3- radial gas velocity profile
4- radial particle velocity profile
5- radial solids mass flux profile

Predicting the hydrodynamic properties of a CFB riser is difficult. Controversial data arise in the open literature and trends of different effects (U_g, G_s, D, ρ_p, d_p) are not always clear. As an example, the effect of diameter on the mean void fraction for constant gas velocity and solids mass flux is not clear. Avidan's (1980) experiments in a 7.6 and 15.2 cm FCC CFB showed that the mean void fraction is higher in the 15.2 cm diameter column compared in the 7.6. He reported density in the fully developed region of 39 and 20 kg/m^3 respectively in the 7.6 and 15.2 cm diameter riser at superficial velocity of 4 m/s and solids circulation rate of 60 kg/m^2s.

As shown in table 1.2, Avidan reported lower density in the larger column at the same operating conditions: 39 kg/m^3 in a 7.6 cm column versus 20 kg/m^3 in a 15.2 cm diameter column. These treads are also reported by Rhodes *et al.* (1992a). They showed that the

density increases by factor of two with the riser twice the diameter. The decrease of void fraction in the smaller unit was attributed to solids friction and wall phenomena (condensation of solids at the wall), the later being dominant. At the wall, velocities are much lower and solids may tend to agglomerate. Proportionately more solids will tend to condense in small riser compared to large diameter risers (surface-to-volume ratio effect). However, although the trends in the two studies agree, the absolute values differs by a factor of almost 3: the density reported by Rhodes *et al.* (1992a) is 56 kg/m^3 in a 15.2 cm column compared to only 20 kg/m^3 in Avidan's test. That difference is greater than the diameter effect. Discrepancies, such as these are not uncommon in the literature and contribute to lack of convergence of a unique interpretation of hydrodynamics trends.

The wall phenomena effect is also not clear. Solids condensation at the wall cannot account for experimental findings of Contractor *et al.* (1992). They reported lower densities after introducing surface area in the form of a vertical heat transfer tube. The increased surface area due to the tube should condense solids and increase the solids fraction. The reasons of this maybe attributed to the lack of accuracy in the measurements of the superficial gas velocity and solids circulation rate. Many authors considered that they operate their CFB at atmospheric pressure. For tall reactors (5 m and more) it is not uncommon that the pressure in the bottom of the bed is 0.1 to 0.2 atm. Thus the true superficial velocity will be 10 to 20 % lower than what is reported is some regions.

1.2.7 Axial Density Profile

In industrial sized FCC risers, Matsen (1976) reported that the ratio of the gas velocity to solids velocity - slip factor - was about 2 (ψ =2).

Patience *et al.* (1992) correlated data from a number of experimental risers using this concept and developed a non-dimensional expression to account for the effects of particle characteristics, riser diameter and gas velocity.

$$\psi = 1 + 5.6/Fr + 0.47\, Fr_t^{0.41} = (U_g / \bar{\varepsilon}) / V_t \qquad (1)$$

where Fr is the Froude number $(U_g/(g\ D)^{0.5})$and Fr_t is the terminal Froude number $(V_t/(g\ D)^{0.5})$. Solving for the mean void fraction, $\bar{\varepsilon}$ we obtain:

$$\bar{\varepsilon} = \frac{1}{1 + G_s \psi / (U_g \rho_g)} \qquad (2)$$

Void fraction increases with increasing gas velocity, decreasing solids circulation rate and decreasing slip factor. Slip factor decreases with increasing gas velocity; The three main variables that affect (ψ) are the gas velocity, particle characteristics and riser diameter. The correlation predicts that the void fraction increases with increasing diameter. This trend is opposite to results of Rhodes *et al.* (1992a) and Avidan (1980).

Figure 1.2 compares the calculated pressure gradient with experimental data for the two risers using sand as the test solids. In the fully developed region, agreement between the model and data is good for experiments run using sand in the 20 cm and 40 cm diameter riser (Figure 1.2). In the 20 cm riser, two experiments were reported at constant mass flux of 29 kg/m^{2}s and gas velocities of 4 and 5.8 m/s. We predict the correct trend in as much as the pressure gradient - solids hold-up - decreases with increasing gas velocity. In the 40 cm diameter riser, gas velocity was 4.2 m/s and mass flux was 50 kg/m^{2}s; same gas velocity as in the experiment in the 20 cm unit with almost twice the mass flux. Again we show good agreement in the fully developed region, which suggests that the slip factor correlation adequately predicts the influence of the diameter for this data set.

FCC data are compared with model predictions in Figure 1.3. In the fully developed region, we consistently over predict the pressure gradient by about 30%. However, the model predicts well the relative change in suspension density with a change in gas superficial velocity. For example, at a height of 8.2 m, the experimental pressure drop

decreases from 870 Pa/m at 7.6 m/s to 490 Pa/m at 5.2 m/s. A difference of 380 Pa/m. For the same conditions, the model predicts a drop of 415 Pa/m.

As shown in Table 1.3, slip factors reported by Knowlton for FCC are very low. Typical FCC risers operate near 11 m/s and slip factors in 1 m diameter units are around 2 (Patience *et al.* 1992).

The correlation for the slip factor is based on a number of studies with sand and FCC powders. The data base for FCC at high gas velocities and mass flux was taken from van Swaaij *et al.* (1970). The slip factors in Van Swaaij *et al.'s* data report is in the range of 1.6 to 2.2, which is much higher than what reported by Knowlton. More recently, Contractor *et al.* (1994) published data for FCC in the same operating range in a 15 cm riser and their results agree well with those of Van Swaaij *et al.*

Correlation data in the FCC regime is largely based on data published by Van Swaaij. As shown in table 1.3, slip factors in the 6-11 m/s gas velocity range are between 1.6 to 2.3 for FCC. The data published by Contractor *et al.* (1994) in a 15 cm riser for FCC in the same range of conditions also show slip factors around 2 for similar conditions reported by Knowlton.

Difficulties in measuring on-line solids circulation and gas velocities might have an effect. The variation of the riser gas velocity with height is substantial for tall risers. Furthermore, at very high solids circulation rate, the interstitial gas contained around the particle in the standpipe can contribute to a significant amount of the gas in the riser. For example, at a superficial gas velocity of 5.2 m/s and a solids circulation rate of 489 kg/m^2s, the interstitial gas in the solids could increase the superficial gas velocity by 10%. Underestimation of the gas velocity in the riser could be one of the cause of the reported low slip factors.

Viitanen (1993) measured both solids and gas velocity using radioactive tracers. In his 1.3 riser m riser, he reported solids and gas velocity from 12 to 14 m/s and solids velocities between 6 and 8 m/s, which gives a slip factor near 2. The experimental data of Rhodes et al. (1992a) and Avidan (1980) suggest that the slip factor increases with decreasing diameter. If this observation is scaleable from a 1 m diameter to 0.2 and 0.4 diameter, we would expect factors much greater than two in the smaller equipment. The data set in the workshop is not consistent with the industrial measurements.

1.2.8 Axial Density Profile in the Entrance Region

In labscale risers, the entrance region occupies a significant fraction of the total height. Generally, when solids enter horizontally from an L-valve, the density appears to decay exponentially to an asymptote. We refer to the region where solids density is essentially constant as the fully developed region. The length of the acceleration region depends most on operating conditions: it increases with suspension density, higher at lower gas velocities and higher solids mass flux. To describe this phenomena, Pugsley et al. (1994) adopted the force balance equation for one-dimensional motion of single particles through fluids,

$$\frac{\pi}{6}\left(d_p\right)^3 \rho_p \frac{dV_p}{dt} = C_d \frac{(U_g / \bar{\varepsilon}_s - V_p)^2}{2} \rho_g \frac{\pi}{4} d_p^2 + \frac{\pi}{6} d_p^3 (\rho_g - \rho_p) g \qquad (3)$$

where V_p is the local particle velocity integrated over the entire cross-section and the drag coefficient is

$$C_d = K / \mathrm{Re}_p^{0.6} \qquad (4)$$

Under dilute conditions where particle interactions are negligible K equals 18.5 (Stokes' Law regime: $2 < \mathrm{Re}_p < 500$). To account for particle interactions, i.e. dense phase conditions, we substitute Eq. 4 into the momentum balance (Eq. 3) and solve for K.

$$K = \frac{4}{3}\frac{(\rho_p/\rho_g - 1)}{(\Psi - 1)^2}\frac{\mathrm{Re}_p^{0.6}}{Fr_p^2} \tag{5}$$

The parameter K lumps together the effect of particle-particle interactions and radial non-uniformity. To calculate the void fraction as a function of height, Equation Eq. 3 is solved simultaneously with the solids flux balance and an equation relating axial coordinate and the mean particle velocity - Equations 6 and 7,

$$(1 - \bar{\varepsilon}_s)\rho_p V_p = G_s \tag{6}$$

and

$$\frac{dZ}{dt} = V_p \tag{7}$$

To solve this set of equations, two boundary conditions are required; one for the initial void fraction and one the initial height. We assume that $\bar{\varepsilon}$ is equal to ε_{mf} at $t = 0$ and that $Z = 0$ at $t = 0$. The two major contributions to the pressure drop are due to solids hold-up and solids acceleration. We ignore gas density and frictional effects. Figures 1.2 and 1.3 illustrate the change in pressure drop with respect to height. Model predictions agree very well with data generated with sand, but with FCC powder at high mass flux, we overestimate the pressure drop. However, the shape of the curves agree reasonably well with the experimental data. The difference is due to the poor fit in the fully developed region where we overpredict the solids hold-up, which in turn affects the parameter K.

1.2.9 Voidage Profile

Zhang *et al.* (1991) reported radial void fraction profiles for four different powders in three different risers up to 0.3 m in diameter. They found that the normalized radial void fraction was a unique function of radial distance. Data reported by Herb *et al.* (1989), Mineo (1989) and Tung *et al.* (1989) also support this observation. Zhang et al. correlated their data and found that the centerline void fraction was best approximated by

$\varepsilon_{cl} = (\bar{\varepsilon})^{0.191}$. However, this expression appears to underestimate the actual void fraction in as much as it poorly accounts for the observed trends in solids mass flux. Solids mass flux is the product of local density and particle velocity. The velocity at the centerline is maximum as is often the case for mass flux. However, when we use Zhang's correlation with solids velocity data, we calculate a local minimum for centerline mass flux. For this reason, Patience and Chaouki (1995) recorrelated Zhang's data with mass flux data and developed the following relationship

$$\frac{\bar{\varepsilon}^{0.4} - \varepsilon_{\xi}}{\bar{\varepsilon}^{0.4} - \bar{\varepsilon}} = 4\xi^{6} \tag{8}$$

The only input parameter is $\bar{\varepsilon}$ - the average void fraction. The denominator, $(\bar{\varepsilon}^{0.4} - \bar{\varepsilon})$ is the difference between the centerline and the average void fraction while $(\bar{\varepsilon}^{0.4} - \varepsilon_{\xi})$ is the difference between the centerline void fraction and the void fraction at the non-dimensional distance, ξ.

One important difference between Eq. 8 and the correlation of Zhang is the calculated void fraction at the centerline. The exponent proposed by Zhang takes a value of 0.191, while we propose that it should be higher and have found that 0.4 agrees well with Zhang's void fraction data and mass flux data. In the turbulent and bubbling fluidization regimes, the centerline void fraction is higher; data published by Abed (1983) suggest that the range is from $\bar{\varepsilon}^{0.5}$ to $\bar{\varepsilon}^{1.0}$; the exponent increases with decreasing gas velocity.

As shown in Figure 1.4, overall agreement between the experimental void fraction data with sand and that predicted by Eq. 8 is good. At the center, the void fraction is a minimum and it increases towards the wall. At constant mass flux, void fraction increases with increasing gas velocity; it decreases with increasing mass flux at constant gas velocity.

Scatter near the wall is large and may be attributable to the difficulty with the experimental method; the disturbance introduced by the measuring probe is greatest closest to the wall.

The curves show the same characteristic shape, which is consistent with Zhang et al.'s postulate that the reduced radial profile is a unique function of radial distance. In Figure 1.5, we show all the experimental FCC data compared with Eq. 8 in its reduced form.

With FCC, under dilute operating conditions, the reduced radial void fraction profile appears to depend on radial distance only; agreement between model predictions and experimental data is generally good at high gas velocities. However, at low gas velocities and high mass fluxes - high suspension densities - the shape of the curve changes. For example, at 7.6 m/s and 489 kg/m^{2}s, the reduced void fraction is about two for $\xi > 0.75$. The solids density at the wall appears to reach a limiting value; with further increases in suspension density (either by increasing solids circulation rate at constant gas velocity, or decreasing gas velocity at constant circulation rate) solids at the wall do not compact further, rather they migrate toward the center, thus increasing the average local density until it reaches the limiting value. Presumably, the limiting void fraction at the wall is largely a function of gas velocity.

1.2.10 Gas Velocity Profile

van Zoonen (1962) reported that the local solids hold-up was greater near the wall compared to the centerline and that the radial particle velocity was nearly parabolic. Based on these observations, Rowe (1962) suggested that the gas might have a similar radial velocity distribution. He reasoned that the presence of solids would dampen turbulence and cause the gas to be in streamline flow. Data reported from the NUCLA power plant experimental program support this hypothesis. They sampled the gas stream over the radius at two heights 7 m apart and found similar radial concentration profiles. If radial gas mixing was significant, then we would expect that the concentration profile might become flat. However, steady state injection of helium gas in experimental risers showed

that gas backmixing declines with increasing gas velocity (Cankurt and Yerushalmi, 1978) but that radial dispersion can be an important effect (Yang et al., 1983).

Other important issues remaining concerning gas phase hydrodynamics relate to the wall boundary condition and entrance effects. Some data suggest that gas is carried down by the solids along the wall, while other data indicate that the no slip boundary condition is an appropriate approximation. Under certain conditions of high mass flux and suspension density, solids have been reported to ascend at the wall, and this effect has not yet been well documented.

In our model, we assume that the radial gas velocity profile is continuous and can be approximated by a power law type expression, similar to that proposed by Martin al. (1992). We assume the no slip boundary condition at the wall and that the velocity is maximum at the center

$$V_{g,\zeta} = U_g / \gamma \left(1 - \xi^{\alpha}\right) \tag{9}$$

The value of alpha varies between 1 and 7, where 1 approximates a triangular profile, 2 is parabolic and 7 approximates a turbulent profile. Patience et al. (1996) correlated experimental data - both gas velocity and solids velocity data - to identify parameters that affect the velocity profile. The data set included both sand and FCC powders and covered a large range of operating conditions and riser diameters up to 0.3 m. They found that the profile depends most strongly on gas velocity and to a lesser extent on mass flux and riser diameter,

$$\alpha = 1 + 0.036\, Fr\left(U_g \rho_p / G_s\right)^{0.5} \tag{10}$$

With increasing gas velocity, solids suspension density decreases and the velocity profile approaches turbulent. Decreasing mass flux has the same effect on suspension density; the velocity profile approaches turbulent at lower mass flux. The correlation predicts an interesting affect with respect to riser diameter: at a constant gas velocity and mass flux, the velocity profile tends toward a turbulent profile with decreasing diameter. This trend is consistent with the slip factor model, which predicts that the solids hold-up increases with increasing diameter. However, as already mentioned, the effect of diameter on suspension density is not well documented and it is less well understood for gas hydrodynamics.

The value of γ in Eq. 9 is calculated from a mass balance on the gas,

$$\int_{\xi=0}^{1} U_{g,\xi}\, 2\xi\, d\xi = \int_{\xi=0}^{1} \varepsilon_{\xi} V_{g,\xi}\, 2\xi\, d\xi = U_g \tag{11}$$

where $U_{g,\xi}$ is the local superficial velocity. Solving for γ gives

$$\gamma = \bar{\varepsilon} - \frac{2\bar{\varepsilon}^{0.4}}{\alpha + 2} + \frac{8\left(\bar{\varepsilon}^{0.4} - \bar{\varepsilon}\right)}{\alpha + 8} \tag{12}$$

1.2.11 Particle Velocity Profile

Based on van Zoonen's (1962) experimental data, Rowe (1962) suggested that both gas and solids might have a similar parabolic velocity profile. He further postulated that the slip velocity between the two phases would also be similar at all radii. We assume that the slip velocity at the center equals the particle terminal velocity

$$V_{p,cl} = V_{g,cl} - V_t \tag{13}$$

At the center, solids hold-up is low and the particles are well dispersed. For the radial solids velocity profile, we use a power law expression with the same exponent (α) used in the radial gas velocity profile, Eq. 10 :

$$V_{p,\xi} = V_{p,cl}\left(1 - (\xi / \phi_s^{1/2})^{\alpha}\right) \tag{14}$$

where, ϕ_s is the fraction of the cross-sectional area in which particles ascend. Gas and solids radial velocity profiles are similar but the slip velocities across the radius are not equal, as Rowe (1962) postulated. At the wall, particle velocities may be negative and considerably greater than the particle terminal velocity while the gas velocity is zero. The expression for the radial velocity profile has the same form as for the gas velocity profile except that the velocity is negative for $r > r_{s,0}$ (or $\xi > \xi_{s,0}$). ϕ_s is calculated based on an overall mass flux balance :

$$\int_{\xi=0}^{1} \rho_p (1 - \varepsilon_\xi)\, V_{p,\xi}\, 2\xi\, d\xi = G_s \tag{15}$$

The solids mass flux is the integral of the product of the local solids hold-up (Eq. 8) and the local solids velocity (Eq. 14). Integrating this product and solving for ϕ_s gives :

$$\phi_s = \left(\frac{\frac{2\left(1 - \bar{\varepsilon}^{0.4}\right)}{\alpha + 2} + \frac{8\left(\bar{\varepsilon}^{0.4} - \bar{\varepsilon}\right)}{\alpha + 8}}{(1 - \bar{\varepsilon}) - G_s / \left(\rho_p V_{p,cl}\right)} \right)^{2/\alpha} \tag{16}$$

With increasing gas velocity at fixed mass flux, the value of ϕ_s will also increase. The value of ϕ_s is not strongly affected by a change in solids circulation rate. With larger riser diameter, Eq. 16 predicts that the cross-sectional area in which solids descend along the wall is greater. This trend is consistent with the slip factor model and Eq. 1 relating the gas velocity profile with operating conditions: in larger diameter risers, suspension densities are higher, the velocity gradient is steeper and more solids descend along the wall.

1.2.12 Solids Mass Flux Profile

Solids mass flux is a product of the local velocity and local suspension density

$$G_{s,\xi} = V_{p,\xi}\,\rho_p(1-\varepsilon_\xi) \tag{17}$$

where the local solids velocity is calculated based on Eq. 14 and the local void fraction is from Eq. 8. During the Fluidization Workshop, J. Matsen was charged with the task of presenting a graph from each participating research group in which agreement between experimental data and model predictions was the closest. D. Geldart had the misfortune to compare a graph that showed the least agreement between experimental data and model predictions. Matsen selected Figure 1.6 as the example where our model agreed well with the data. In the 0.4 m diameter riser, mass flux at the centerline is almost three times the average. The wall mass flux is negative and about four times the average mass flux. The transition from upflow to downflow occurs at $\phi_s^{1/2} = 0.9$. All of these characteristics were captured by the model remarkably well.

Geldart chose Figure 1.7 as the example where the model predictions fit the experimental data poorly. He pointed out that we overpredict the centerline mass flux and show negative values at the wall (although the experiments do not include data near the wall). He did add that the model captured some unique characteristics of the data and in fact "was not that bad". For example, the centerline velocity is at a local minimum and the absolute maximum is nearer to the wall. The model fits the experiments conducted at mass flux below 200 kg/m^{2}s very well.

The agreement is poor at the highest mass flux because of an error in the reported value. Integrating the experimental local flux gives 640 kg/m^{2}s compared to their reported value of 782 kg/m^{2}s. At an average mass flux of 640 kg/m^{2}s, our model predicts 875 kg/m^{2}s at the center, whereas we calculated 1100 kg/m^{2}s with 782 kg/m^{2}s. Regardless of the error

in the reported mass flux, we still overpredict G_s at the center. A contributing factor to the difference may be due to the slip factor model that overpredicts the average density: higher densities in the center will result in higher local mass flux.

1.2.13 Conclusion

A brief review of the models used for predicting the riser hydrodynamic in circulating fluidized bed riser has been presented. A fully predictive two-dimensional model was developed and applied successfully to describe the hydrodynamic behavior in a circulating fluidized bed riser. An algorithm describing all the equations involved in the model predictions was detailed and the performance of the model predictions was compared with data available in the literature. The CFB riser model was tested against data from Knowlton presented at the Fluidization VIII CFB workshop (Tours, France, May 1996) (12-14 m height, 0.2-0.4 m ID, FCC and sand) operated in the ranges 4.2-11 m/s and 15-780 kg/m^{2}s of superficial gas velocity and solids mass flux respectively. It is clear that the specific design of CFB risers can greatly influence particle and gas motion , and hence other dependent properties like solids concentration and velocity. The entry and exit geometry, cross-sectional shape, wall contour and roughness, and baffles all can cause significant variations in local flow. An effort has been made to solve the model without the use of any experimental information.

The model is able to predict:

- the axial density profile
- the radial void profile
- the radial gas velocity profile
- the radial particle velocity profile
- the radial solids mass flux profile

The essential features of the hydrodynamic model are:

- the slip factor is approximately equal to 2 in the fully developed region;
- a semi-theoretical model that relate the cross sectionaly average particle velocity and voidage and a momentum balance has been proposed to predict the axial pressure drop in the acceleration region;
- the normalized void fraction profile is a unique function of radial distance;
- the centerline void fraction is equal to the average raised to the power 0.4;
- the gas velocity at the wall is zero;
- the gas velocity profile follows a power law and the exponent is a function of Fr, Ug, G_s and particle density;
- at the center, the slip velocity equals the single particle terminal velocity;
- the particle velocity profile follows a power law with the same exponent as the gas profile;
- the solids wall velocities are calculated based on a solids flux balance; finally,
- the mass flux is the product of the local density and particle velocity.

The model predicts axial pressure gradient for experiments conducted with sand quite well but not as accurately for FCC. Discrepancies in FCC data are largely attributable to the difference between the experimental and predicted solids hold-up in the fully developed region. The model overpredicts the density in the fully developed region when FCC were

fluidized. In spite of these malpredictions, the model seems to behave in a physically feasible way and give reasonable predictions of the riser hydrodynamic in circulating fluidized beds. The reason for the poorer fit with FCC data may be due to the historical data base upon which the slip factor correlation was developed. Another possibility is that FCC particles were fluidized in tall risers. For these such tall risers, it is not allowed to neglect the change in superficial velocity with change in pressure along the riser and the interstitial amount of air that enter in the riser with the high solids circulation rate that affect the effective gas superficial velocity.

The model predictions in the acceleration region show a good trend; the axial pressure drop decay exponentially with height. However, the length of acceleration is underpredicted as could be seen in Figure 1.2 and 1.3. In the acceleration region, the gravity, buoyancy and drag forces are not the only factors contributing to particle motion and hence pressure drop. Particle-particle interactions play a key role in this dense region and are lumped together in Eq. (5) and apparently does not capture all factors affecting the pressure drop in the acceleration region.

It was shown that the normalized void fraction is a unique function of radial distance and that the centerline void fraction is equal to the sectionaly average void fraction raised to the power 0.4. The model assume that the radial gas velocity profile can be approximated by a power law type expression with no slip boundary condition at the wall and maximum velocity in the center. The value of the exponent is based on correlated experimental data. The expression for the radial particle velocity profile has the same form as the gas velocity profile except that the velocity near the wall is negative. The value of the radius at which the particle velocity is zero is calculated from a particle flux balance. Finally, the location where the transition from upflow to downflow occurs is calculated based on a mass flux balance.

The exit region was not considered in the present model. It was stated at the Fluidization VIII Conference that deeper knowledge of the hydrodynamics is still needed for further modeling. Especially the investigation of entrance and exit effects is of importance. These research needs are commonly accepted for catalytic and combustion systems. A detailed answer of these open questions is needed to solve-up problems, for which solutions are still missing. In future work, the microscopic interaction between gas-phase eddies and dispersed particles need to be considered. The model predicts the average flow structure in the CFB riser. The dynamic change in flow structure exhibits significant fluctuation which are important in mass and heat transfer between particles and fluid.

1.2.14 List of symbols

C_d: drag coefficient

D: riser diameter (m)

d_p: particle diameter (m)

k: kinetic constant

K: parameter (Eq. 4 and 5)

Fr: Froude number ($U_g/\sqrt{(gD)}$)

Fr_t: terminal Froude number ($V_t/\sqrt{(gD)}$)

g: gravitational constant (m/s^2)

G_s: solids circulation rate (kg/m^2s)

H: riser height (m)

Q: gas flow rate (m^3/s)

$r_{s,0}$: radius at which the axial particle velocity is zero

Re_p: particle Reynolds number ($d_p(V_p-U_g/\varepsilon)\rho_g/\mu$

S: selectivity

t: time (s)

T: temperature (°C)

U_g: gas superficial velocity (m/s)

V_g: actual gas velocity (m/s)

V_p: particle velocity (m/s)

V_t: terminal velocity (m/s)

W: catalyst inventory (kg)

X: conversion

Z: axial coordinate (m)

1.2.15 Greek symbols

α :exponent in the gas and particle velocity profile (Eq. 9, 10 and 14)

ΔP :pressure drop (Pa)

ε : void fraction

$\bar{\varepsilon}$: mean void fraction

ε_{cl} : void fraction in the centerline of the riser

ϕ_s :fraction of the cross-sectional area in which particles ascend

ψ :slip factor

γ : parameter in Eq. 9 and 12

μ: gas viscosity (Pa s)

ρ: suspension density (kg/m^3)

ρ_g: gas density (kg/m^3)

ρ_p: particle density (kg/m^3)

$\zeta_{z,0}$:non dimensional location at which the particle velocity is zero

1.2.16 Subscripts

cl: centerline

mf: minimum fluidization

z: indicates dependence on axial coordinate

ζ: indicates dependence on the non dimensional location

Table 1.1 Test Matrix for hydrodynamic predictions

FCC, d_p=76μm, ρ_p=1712 kg/m^3, D=0.2 m				
U_g, G_s	49 kg/m^{2}s	196 kg/m^{2}s	489 kg/m^{2}s	782 kg/m^{2}s
5.2 m/s			X	
7.6 m/s			X	
11 m/s	X	X	X	X
Sand, d_p=175μm, ρ_p=2145 kg/m^3, D=0.2 m				
U_g, G_s	15 kg/m^{2}s	29 kg/m^{2}s	51 kg/m^{2}s	
2.4 m/s		X		
4 m/s	X	X	X	
5.8 m/s		X		
Sand, d_p=120μm, ρ_p=2600 kg/m^3, D=0.4 m				
U_g, G_s	50 kg/m^{2}s			
4.2 m/s	X			

Table 1.2 Suspension densities under different riser diameters.

Study	D cm	U_g m/s	G_s kg/m^{2}s	ρ kg/m^3
Avidan (1980)	7.6	4	60	39
Avidan, (1980)	15.2	4	60	20
Rhodes *et al.* (1992a)	15.2	4	60	56
Rhodes *et al.* (1992a)	30.5	4	60	29

Table 1.3 Slip factors for FCC powder

U_g	G_s	D	$\psi^{(1)}$	$\psi^{(2)}$	$\psi^{(3)}$	$\psi^{(4)}$
m/s	kg/m^{2}s	m				
11	500	0.2	1.16			1.9
7.6	500	0.2	1.45			2.3
5.2	500	0.2	1.74			2.7
11	500	0.18	1.9			1.6
7.6	300	0.18		2.3		2.2
5.7	300	0.18		2.3		2.5
8.9	500	0.18		2.0		2.1
10.1	500	0.18		2.3		2.0
5.6	550	0.15			2.5	2.5
7	550	0.15			2.2	2.2
9	550	0.15			1.9	2.0

(1) Knowlton, (2) Van Swaaij *et al.*(1970), (3) Contractor *et al.* (1994),
(4) Equation 1

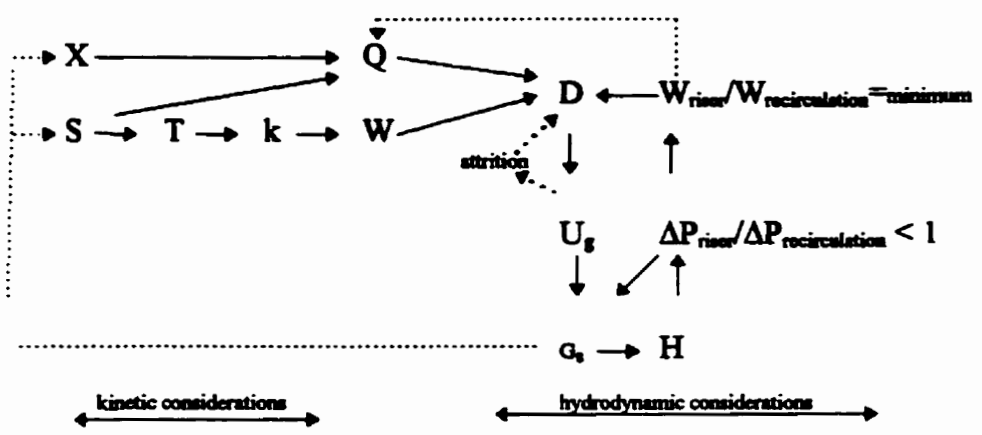

Figure 1.1 Design sequence to determine the geometry and operating conditions.

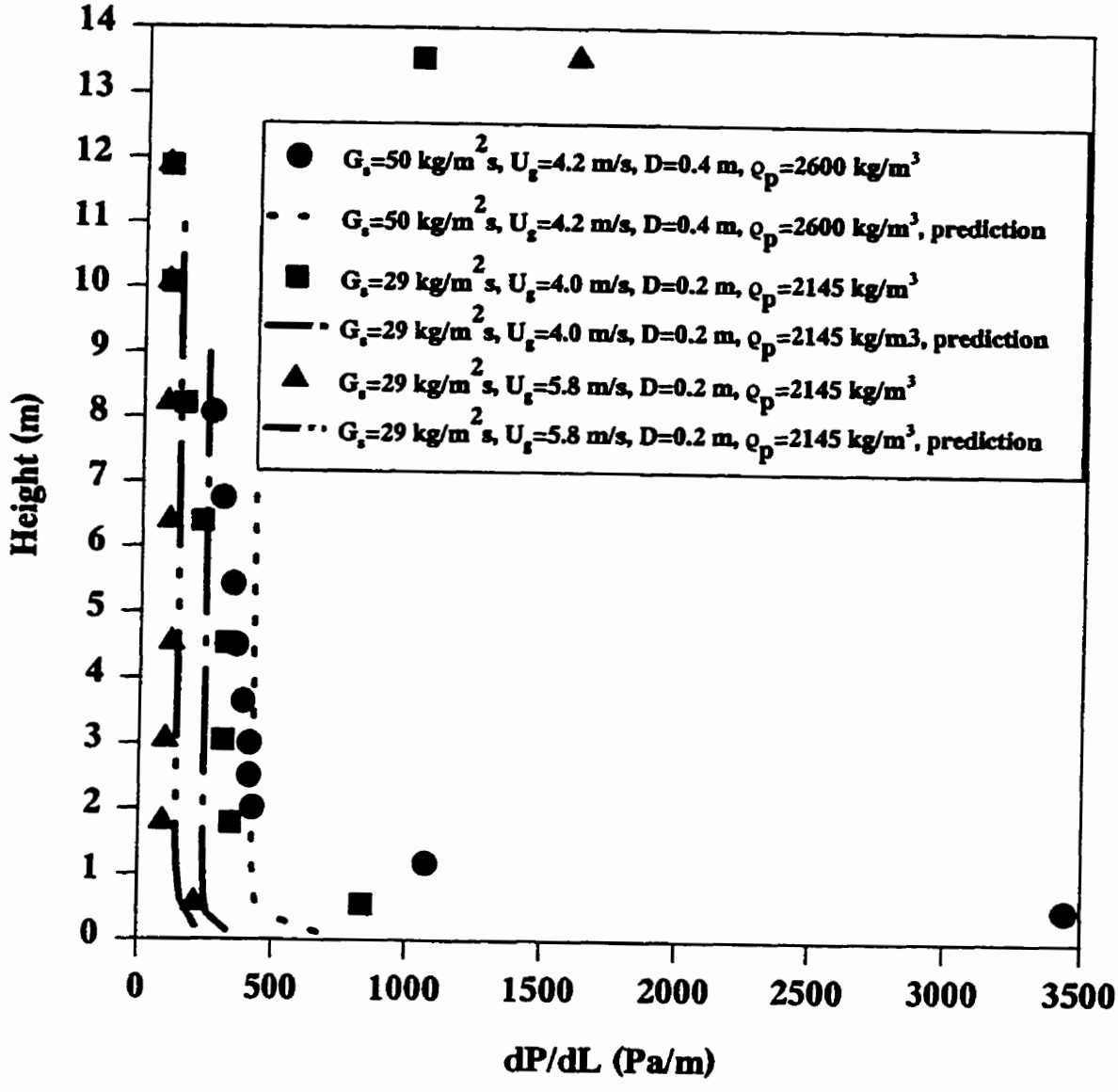

Figure 1.2 Comparison between predicted experimental pressure drop for sand particles.

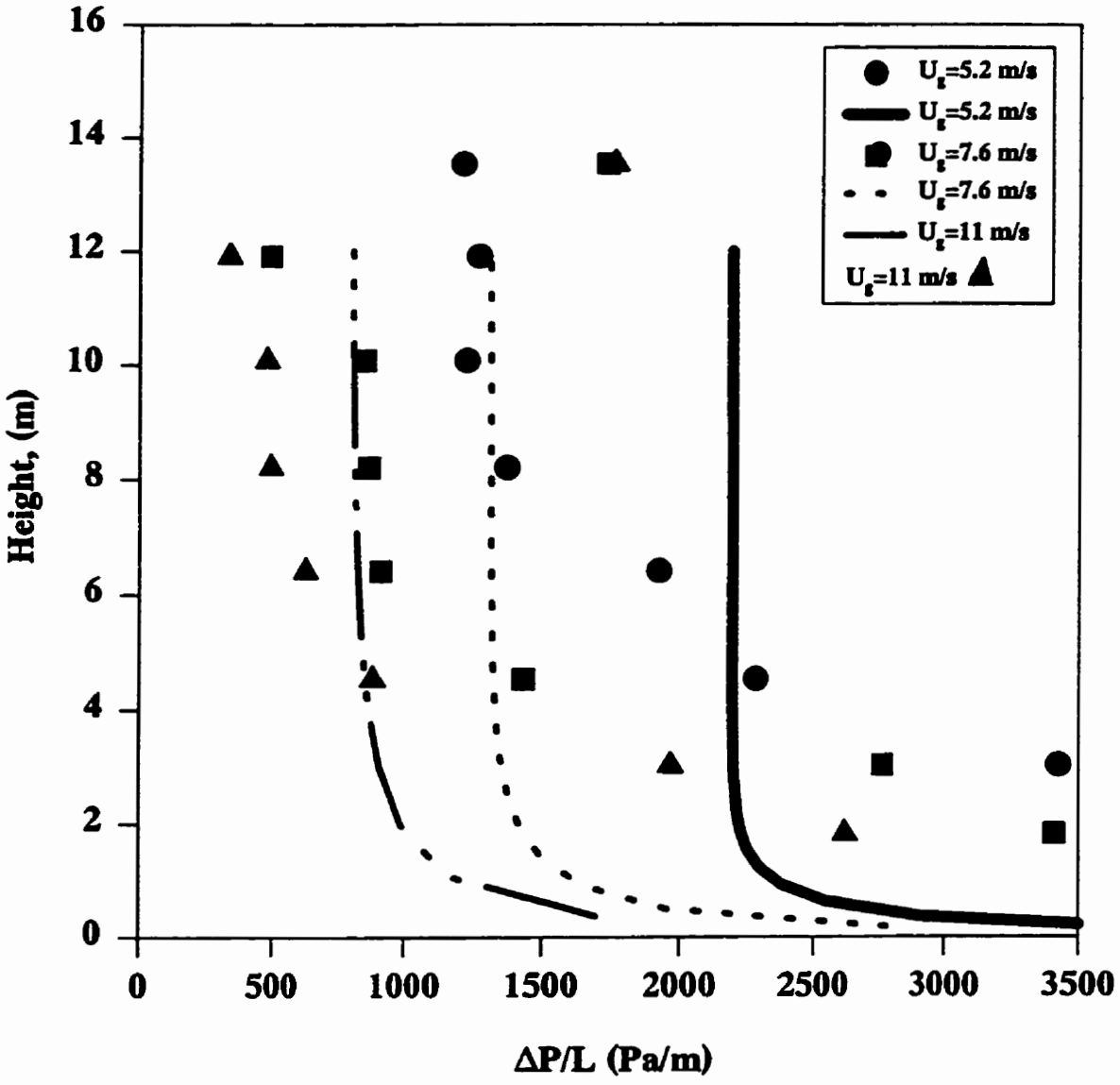

Figure 1.3 Comparison between predicted experimental pressure drop for FCC particles.

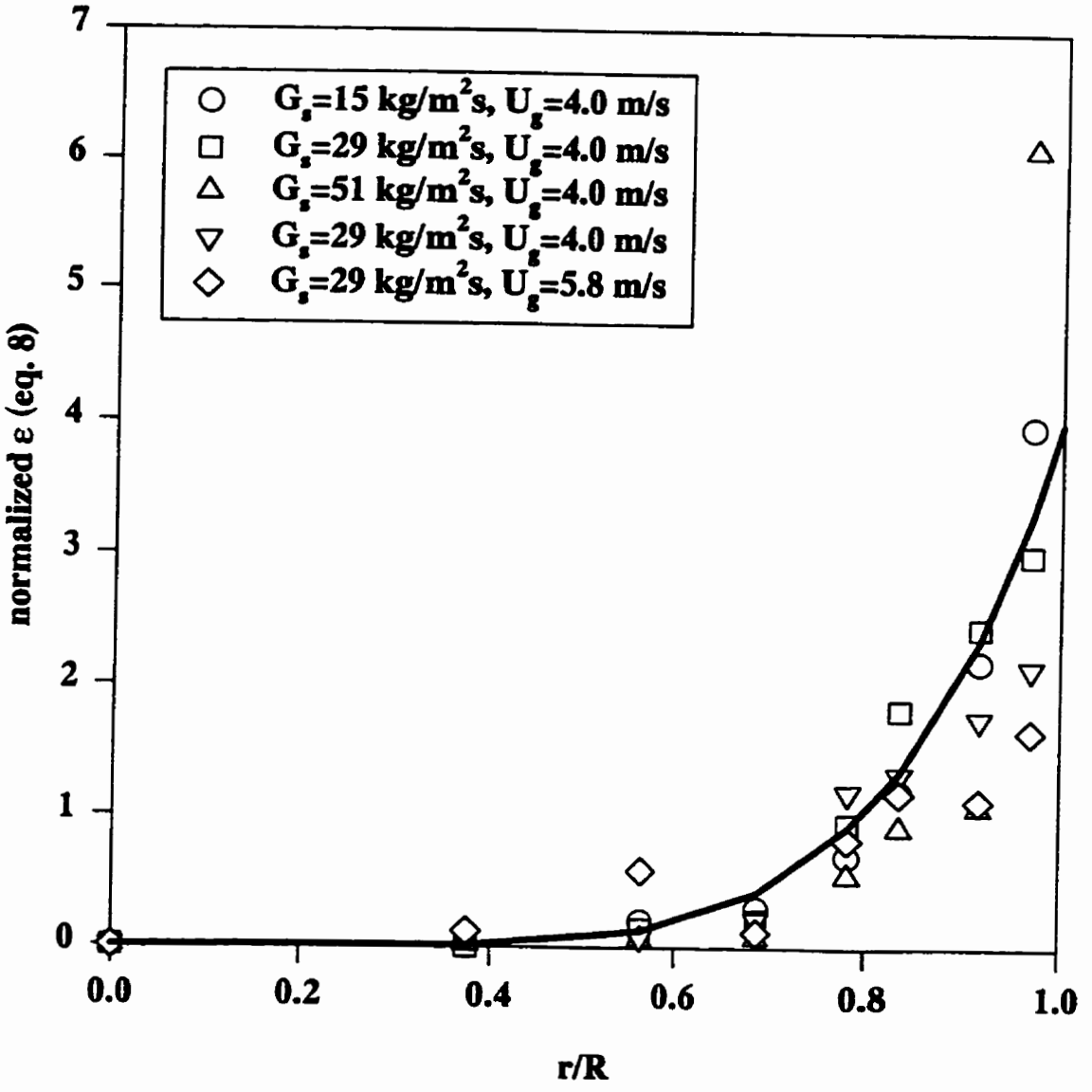

Figure 1.4 Normalized void fraction as a function of radial position for sand particles.

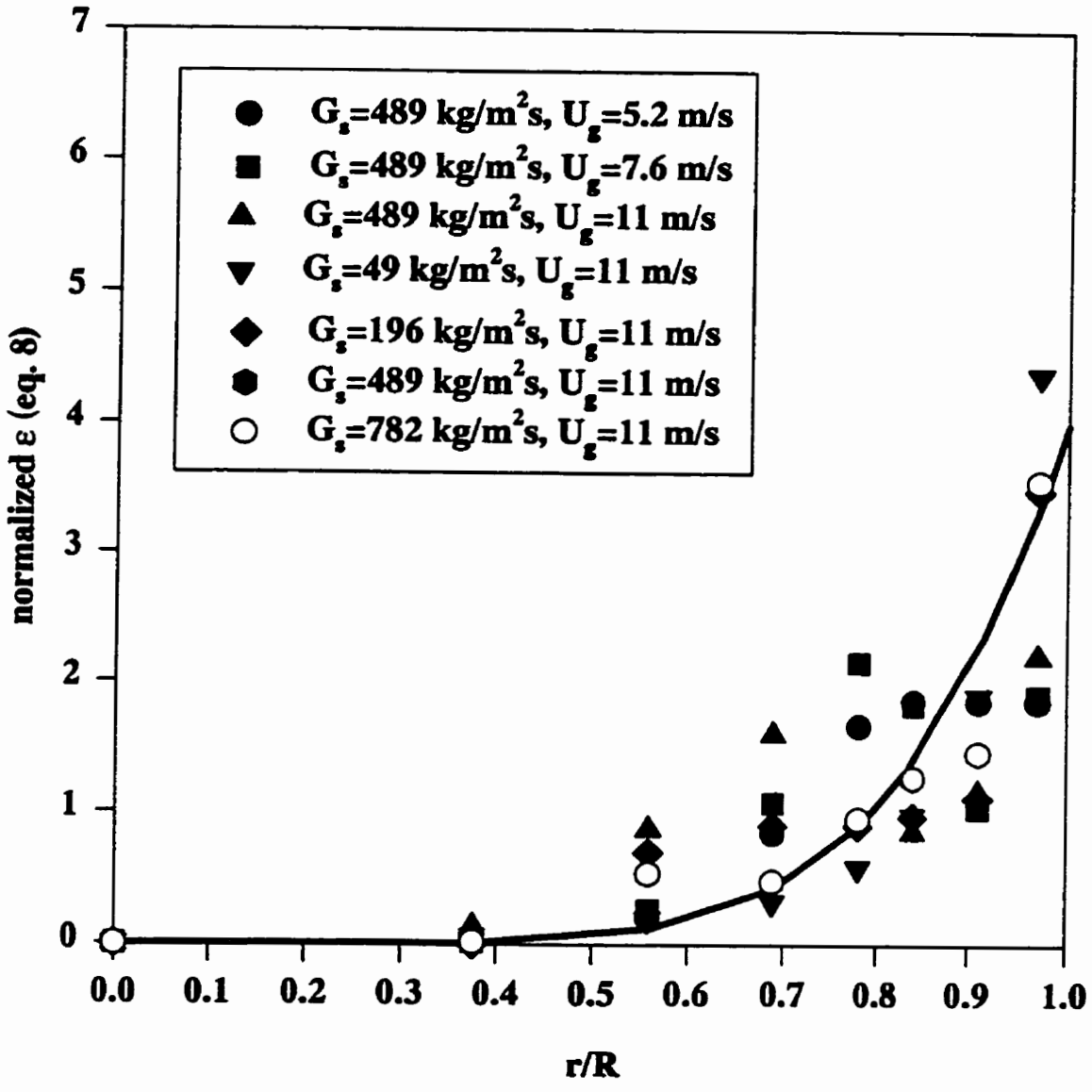

Figure 1.5 Normalized void fraction as a function of radial position for FCC particles.

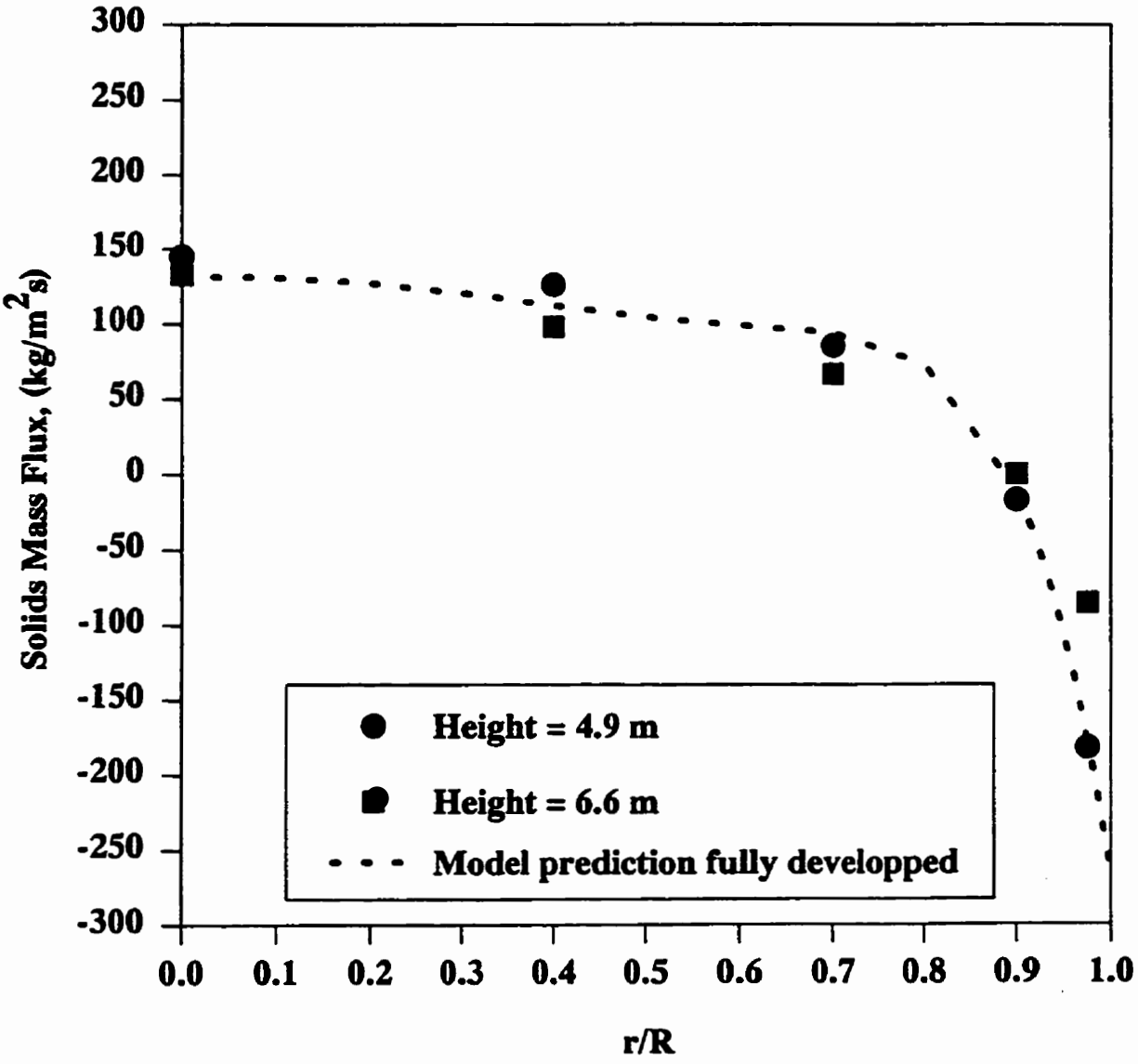

Figure 1.6 Selected figure showing good agreement (Radial profile of solids mass flux ; sand D=0.4 m, U_g=4.2 m/s, G_s=50kg/m^{2}s).

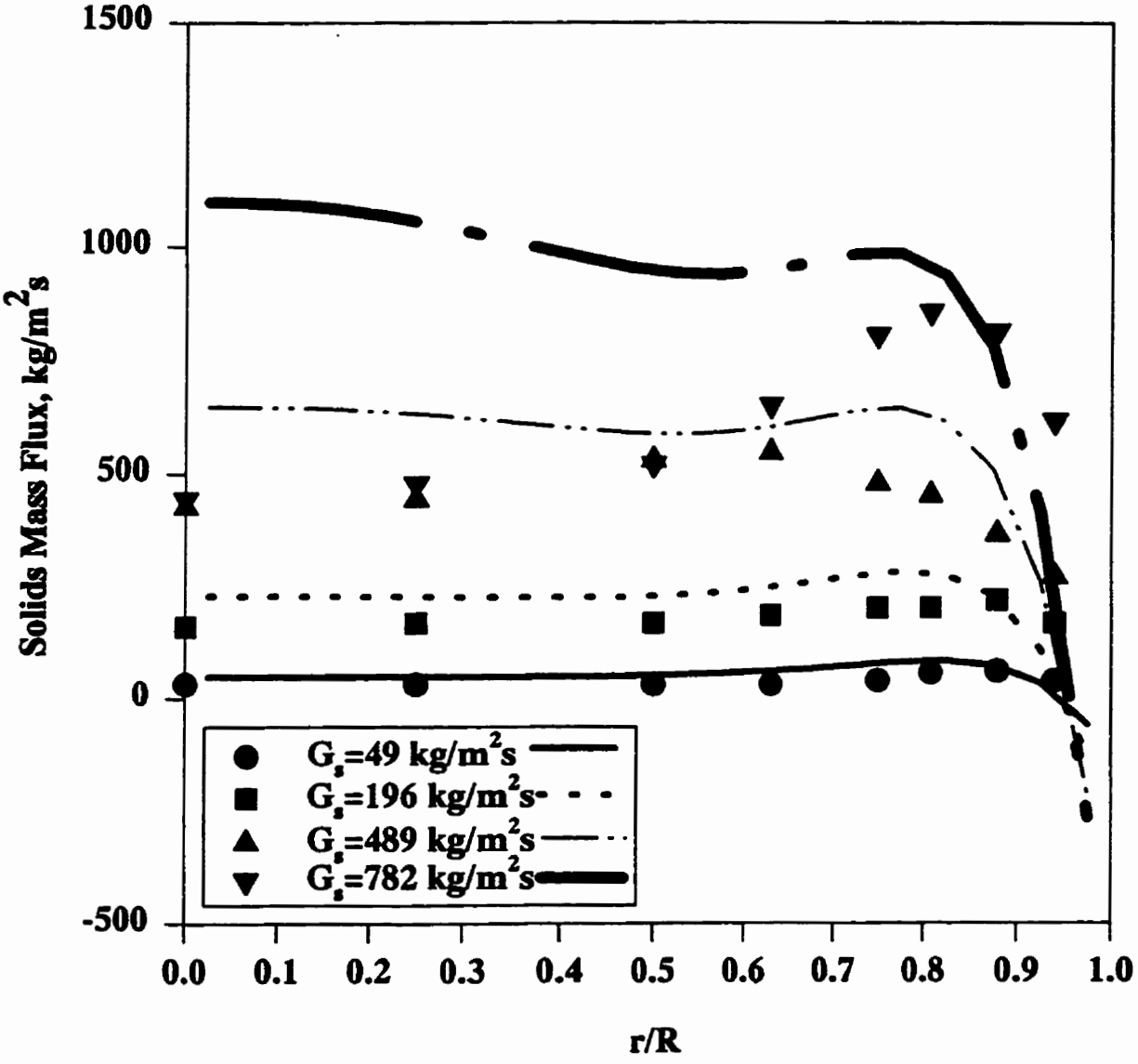

Figure 1.7 Selected figure showing poor agreement (Radial profile of mass flux, FCC D=0.2 m, U_g=11 m/s, G_s=49,196,489,782 kg/m^{2}s).

CHAPITRE 2 ARTICLE PUBLIÉ DANS "INTERNATIONAL JOURNAL OF APPLIED RADIATION AND ISOTOPES"

Ce chapitre introduit la seconde partie de la thèse, qui vise à caractériser la structure hydrodynamique locale des particules. Rappelons que la méthode expérimentale utilisée est la poursuite d'une particule radioactive. La technique de poursuite d'une particule radioactive telle que développée par Larachi et coll. (1994) doit être améliorée afin de pouvoir être appliquée à une étude dans un lit fluidisé circulant. Le but visé par ce chapitre est de trouver un radio-isotope qui peut améliorer la résolution spatiale de la technique.

2.1 Problématique de l'application de la technique de poursuite d'une particule radioactive

La technique de poursuite d'une particule radioactive développée par Larachi et coll. 1994 s'est montrée un outil performant pour étudier le mouvement des particules dans un lit fluidisé liquide-solides, dans un lit fluidisé triphasique (D=10 cm, H=40 cm, d_p=3000 mm) (Larachi et coll. 1995a,b) et dans un lit à jet (D=10 cm, H=40 cm, d_p=3000 mm) (Roy et coll. 1994). La problématique de l'application de cette technique au lit fluidisé circulant est la suivante:

-À cause des vitesses en jeu dans les LFC, il faut diminuer la période d'échantillonnage par rapport aux études antérieures (10 ms au lieu de 30 ms). Dans les applications précédentes, les mouvements des particules sont lents (vitesses inférieures à 1-2 m/s). La méthode doit être améliorée pour permettre de mesurer des vitesses limites d'environ 5 m/s. L'augmentation de la fréquence d'échantillonnage par un facteur trois réduit d'autant le comptage des détecteurs pendant la période d'échantillonnage. La résolution spatiale de la technique s'en trouve réduite.

- Dans les applications précédentes, la région d'intérêt où la position de la particule est déterminée est petite. Les hauteurs du lit fluidisé liquide-solides, du lit fluidisé

triphasique et du lit à jet ne sont que de 40 cm. Or, la hauteur du lit fluidisé circulant est de 7 mètres et il n'est évidemment pas possible d'utiliser la technique de poursuite sur tout le lit. L'étude se concentre donc sur une partie du lit où l'écoulement est établi. Le système de détection doit couvrir une portion importante du lit. En effet, le nombre de positions instantanées mesuré est proportionnel au volume couvert par le système. L'augmentation du volume couvert par le système diminue la "densité d'information" et réduit par le fait même la résolution spatiale de la technique.

- La technique a été appliquée à des lits denses à paroi d'acrylique. L'atténuation de la paroi du lit a été prise en considération en supposant que l'atténuation des photons dans celle-ci est identique à l'atténuation dans le lit. Cette approximation est justifiée dans le lit fluidisé liquide-solides, dans le lit fluidisé triphasique et dans le lit à jet mais pas dans le lit fluidisé circulant. La paroi du lit circulant est faite d'acier inoxydable d'une épaisseur de 2.6 mm. Le lit fluidisé circulant est dilué (densité lit<100 kg/m^3) et l'atténuation y est très différente que dans l'acier. Il faut donc modifier les programmes pour tenir compte de l'atténuation dans la paroi d'acier.

Avant d'appliquer la technique au lit fluidisé circulant, il faut nécessairement l'améliorer. Il est clair que le coeur du problème est la résolution spatiale. Larachi et coll. (1995) estime localiser la particule à 5 mm près dans le plan x-y (écart type sur la position x et y) et à 7 mm près axialement (écart type sur la coordonnée z). Il faut obtenir des résolutions semblables dans le lit circulant. Le problème est que la "densité d'information" est de beaucoup réduite par rapport aux applications précédentes. La densité d'information est réduite par un facteur six (un facteur trois lié à l'augmentation de la fréquence d'échantillonnage et un facteur deux lié à l'augmentation du volume de contrôle du système de détection).

Pour obtenir une bonne résolution dans le lit fluidisé circulant, les paramètres suivants doivent être optimisés:

-les propriétés de la source (activité et énergie des rayons γ émis)

-la configuration des détecteurs.

Ces paramètres sont discutés dans un article publié en février 1997 dans la revue "Journal of Applied Radiation and Isotopes". Une copie de cet article est présentée dans les pages qui suivent.

2.2 Sommaire de l'article publié dans "International Journal of Applied Radiation and Isotopes

Le choix de la source s'est fait en comparant les résolutions expérimentales obtenues à l'aide de trois radio-isotopes différents, ^{99}Mo, ^{198}Au et ^{46}Sc. L'article discute également d'un moyen innovateur de calculer les coordonnées instantanées de la particule à partir des comptages mesurés par les détecteurs. Le grand intérêt de ce moyen, un réseau neuronal, réside dans le fait qu'il permet de calculer rapidement les positions x,y et z, directement à l'aide des comptages obtenus par les huit détecteurs.

La conclusion la plus importante pour la poursuite de ce projet de recherche est la suivante:

-l'or (^{198}Au) est le meilleur radio-isotope pour l'application dans le lit circulant. Deux qualités le rendent plus intéressant que le radio-isotope utilisé par Larachi et coll. (1994, 1995a,b) et Roy et coll. (1994), le ^{46}Sc. L'effet le plus marqué est le photopic (0.55 pour ^{198}Au comparé à 0.4 pour ^{46}Sc) qui permet d'évaluer le nombre de photons utiles. Cela se traduit par le fait que jusqu'à 55000 photons utiles par seconde peuvent être comptés par chacun des détecteurs avec ^{198}Au alors qu'il n'est que de 40000 avec ^{46}Sc. Le nombre de photons utiles (photons détectés dans le photopic) est ainsi augmenté de 38%. L'utilisation de ^{198}Au améliore donc la résolution spatiale de la technique puisque les comptages mesurés sont supérieurs. Le second effet vient du fait que l'or émet des rayons γ de plus faibles énergies qui sont plus atténués. La plus grande atténuation des rayons γ rend le comptage des détecteurs plus sensible à la position de la particule radioactive et améliore ainsi la résolution spatiale.

De plus, la faible demi-vie (2.7 j) est intéressante parce qu'il est pratiquement impossible de récupérer les particules radioactives à la fin d'une expérience dans le lit fluidisé circulant et il est donc nécessaire que la demi-vie ne soit pas trop grande.

L'article démontre également que la résolution spatiale du système peut être prédite pour une configuration de détecteurs et une source données. Ce résultat est fondamental pour optimiser

la position des détecteurs. Ainsi, il est possible de déterminer de façon quantitative si une configuration donnée est meilleure qu'une autre. Il est aussi possible d'imaginer une optimisation de l'activité de la source et de la configuration des détecteurs mais ceci demanderait beaucoup de temps de calcul.

2.3 Texte de l'article

On-Line Flow Visualization in Multiphase Reactors using Neural Networks

(Appl. Radiat. Isot. Vol. 48, No. 2, pp. 225-235, 1997)

L. Godfroy[a], F. Larachi[b], G. Kennedy[c], B. Grandjean[b] and J. Chaouki[a]

[a] Department of Chemical Engineering, École Polytechnique, C.P. 6079,
Station "Centre-Ville", Montréal, Québec, Canada H3C 3A7, Fax: 514-340-4159

[b] Department of Chemical Engineering, Laval University,
Sainte-Foy, Québec, Canada G1K 7P4

[c] Nuclear Engineering Institute, École Polytechnique, C.P. 6079,
Station "Centre-Ville", Montréal, Québec, Canada H3C 3A7

2.3.1 Summary

The success of the radioactive particle tracking system (RPT) developed at École Polytechnique (Montréal) and applied to the study of particle motion in a variety of chemical reactors (three-phase fluidized bed, gas spouted bed and liquid fluidized bed) has motivated us to continue improving this technique (in terms of accuracy and resolution) and to apply it to new reactor types. Our goals are: i) enhance the original search location algorithm in order to permit on-line flow visualization and ii) extend RPT to very fast solids flows such as those encountered in circulating fluidized beds (particle velocities higher than a few meters/s).

The potential of neural networks for on-line and real-time visualization of particle movements in multiphase reactors will be illustrated. The original least-squares search location algorithm (Larachi *et al.* 1994) has been replaced with an enhanced algorithm which uses a three-layer feedforward neural network. The results obtained from the two algorithms for particle tracking in a three-phase fluidized bed reactor are compared.

The RPT system employs eight NaI(Tl) scintillation detectors to study the movement of solid particles in chemical reactors. The performance of the system was investigated using particles containing the radioisotopes ^{46}Sc (γ–ray energy 1005 keV), ^{99}Mo (γ–ray energy 140 keV) and ^{198}Au (γ–ray energy 412 keV). The 3-D spatial resolution was measured in empty and water-filled tubes simulating highly diluted and dense media. The best results were obtained using ^{198}Au with which the particle can be located to within 7 mm in water and 9 mm in air 100 times per second.

Keywords: Particle tracking, neural network, multiphase reactors, visualization, chemical engineering

2.3.2 Background

It is well recognized that the measurement of particle trajectories and related dynamic phenomena in fluid-particulate flow systems is particularly difficult because the particles usually exhibit complex motion patterns and the flow field very often is spatially non-uniform. Conventional measurement devices such as fiber optics or electrical capacitance probes give large errors because they disturb the flow; they also do not provide full flow field measurements. Given accurate knowledge of the particle movement, one can infer a wealth of transient and steady-state information on the particulate phase, such as the circulation time distribution and the time-averaged velocity field. Notable examples of two and three-phase flow conditions where accurate trajectory measurements of solid particles are critical are found in fluid-solids transport processes such as drying, combustion, and hydrorefining. In each of these areas, the accurate and non-invasive measurement of particle movement would advance the physical understanding and the modeling of the related technologies.

In the last decade, important progress has been made in the development of advanced non-invasive nuclear particle tracking techniques specifically suited for the characterization of three-dimensional flow fields of discrete or continuous batch phases in dilute/dense and opaque multiphase systems (Chaouki *et al.* 1997). Two photon emission-based tracking techniques are

currently in application on laboratory scale reactors: "positron emission particle tracking (PEPT)"(Broadbent *et al.* 1993); and "γ–ray emission radioactive particle tracking (RPT)" (Lin *et al.* 1985, Moslemian *et al.* 1992 and Larachi *et al.* 1994). Both use the detection and counting of highly penetrating γ–rays emitted by radiolabeled flow followers which are dynamically similar to the tracked phase. They use the detected γ-rays to provide the instantaneous coordinates (x(t),y(t),z(t)) of the moving tagged particle.

The success of the radioactive particle tracking system developed at École Polytechnique (Larachi *et al.* 1994) and applied to the study of particle motion in three-phase fluidized beds, gas spouted beds and liquid fluidized beds has motivated us to continue improving the technique (in terms of accuracy and resolution) and to apply it to new reactor types. Our first RPT system used an array of 8 scintillation detectors surrounding the reactor under study, Figure 2.1, and detected the 1005 keV γ–rays emitted from a particle labeled with ^{46}Sc. One of our goals is to extend RPT to very fast solids flows such as those encountered in circulating fluidized beds (particle velocities higher than a few meters/s). This requires increasing the sampling frequency of the system without increasing the error associated with locating the tracer particle. However, as will be shown below, an increase in the sampling frequency necessarily worsens the resolution by a factor equal to the square-root of the increase in frequency. This effect must therefore be compensated by an equivalent improvement in resolution achieved by optimization of the γ–ray detection system.

The aim of the present study is to address the following two issues:

i) The first issue deals with the improvement of computational speed of the reconstruction method to permit on-line visualization of the tracer coordinates from the measures γ–ray counts. Indeed, the RPT system used did not meet the requirements of on-line and real-time visualization due to computation times far exceeding the sampling time interval. The original time-consuming least-squares search (Larachi *et al.* 1994) is now replaced by an enhanced neural network which calculates the tracer positions directly from the signals from the eight

detectors. The potential of the neural network location algorithm, in terms of accuracy and reduction in cpu time will be investigated for a particle tracking experiment in a three-phase fluidized bed.

ii) The second issue is to address the improvement in spatial resolution using various static tracers emitting γ–rays of different energies, and embedded either in dilute or dense media. Improvement in spatial resolution (or position standard-deviation, see Eq. 3 below) will permit sampling faster movements and thus will extend RPT to explore applications where rapid granular flows occur. In addition to this, minimizing the position standard-deviations leads to measuring tracer trajectories with low noise-to-signal ratio allowing thus access to flow parameters calculated from velocity fluctuations such as turbulence coefficients, normal and shear stresses, etc. For instance to calculate the genuine turbulent (or root-mean-square) velocity due to flow, one has to subtract in quadrature the spurious velocity (due to noise) from the noise-embedded measured velocities.

It was shown that to achieve good spatial resolution both high γ–ray counts and a high detector sensitivity are needed (Larachi et al. 1996). This occurs only when the tracer-to-detector distance is not too large. To obtain a detector response with maximum sensitivity, radioactive sources emitting low energy γ–rays have to be chosen in order that small displacements of the source will produce appreciable changes in the counts due to attenuation in the medium. Better sensitivity is also achieved with low energy γ–rays because a higher fraction of counts is recorded in the photopeak. Both these effects should contribute to providing the highest spatial resolutions with low energy γ–rays. Unfortunately, a decrease in the γ-ray energy will decrease the full-width-at-half-maximum of the detector thus narrowing the region of space where the detector is most sensitive. For a tracer located at an appreciable distance from the detector, the low number of γ-rays and the low sensitivity both contribute in worsening the spatial resolution. At these distances high energy γ-rays are more appropriate as they are less attenuated in the medium and lead to more counts. In actual practice the trade-off between high and low energy

γ-rays remains one of the basic problems in RPT detection. It is one of the objectives of this work to suggest radioisotopes emitting γ-rays of optimum energy yielding the best spatial resolution.

2.3.3 The RPT System

The reactor contains a radioactive particle (the tracer), whose flow properties match those of the solids whose flow is being studied, and is surrounded by eight uncollimated NaI(Tl) scintillation detectors as shown in Figure 2.1. γ-rays emitted from the particle may be absorbed by the materials in the reactor and the reactor wall. A computer simultaneously registers the number of γ-rays detected by each detector in each sampling time interval. The number of counts in each of the 8 detectors is used to calculate the coordinates of the particle. Data are acquired for several hours (typically a million particle locations are determined) in order to characterize the movement and the velocity field with sufficient accuracy in all regions of the reactor. RPT has already been applied by us to gas spouted beds (Roy *et al.* 1994), three-phase and liquid fluidized beds (Larachi *et al.* 1995a,b), and by other investigators to bubble columns (Devanathan *et al.* 1990) and gas fluidized beds (Lin *et al.* 1985 and Moslemian *et al.* 1992).

2.3.4 Location Algorithms

Three methods have been used to determine the location of the particle using the number of counts recorded by the detectors. In the first, the detector is considered as a "virtual point" and the distance to the particle is a polynomial function of the number of counts recorded. The polynomial is fitted to calibration data obtained by positioning the tracer at known locations in the reactor (Lin *et al.* 1985 and Moslemian *et al.* 1992). This approach suffers from low accuracy and resolution in dense flows, especially when the detectors are not flush-mounted with the reactor wall. The second uses a rigorous phenomenological model which describes the interactions of radiation with matter for the geometry of the system (Larachi *et al.* 1994). A map of detector counts versus location is generated by Monte Carlo calculation and is adjusted to calibration measurements. Subsequently, each location of the tracer is determined by a least-squares search for the grid point on the map which best matches the counts registered in the detectors (Larachi *et al.* 1994). This location is refined by a least-squares search in the

neighborhood of this grid point using a simplified model. The third method, which is developed in this study, is an enhanced algorithm where the searches of the second method are replaced by a direct and faster neural network model.

This section briefly summarizes the theory of radiation detection used by RPT and the steps required for locating the particle.

2.3.4.1 Detection Model

The number of photopeak counts, C, recorded by a detector during a sampling time interval T from a source of radioactivity A placed at a location (x,y,z) inside the reactor can be expressed by the following relationship (Tsoulfanidis 1983):

$$C = \frac{T \upsilon A \varphi \iint_{\Omega} \frac{\mathbf{r}\cdot\mathbf{n}}{r^3} \exp\left(-\mu_R e_1 - \mu_w e_2\right)\left(1-\exp\left(-\mu_D d\right)\right) d\Sigma}{1+\tau \upsilon A \varphi \iint_{\Omega} \frac{\mathbf{r}\cdot\mathbf{n}}{r^3} \exp\left(-\mu_R e_1 - \mu_w e_2\right)\left(1-\exp\left(-\mu_D d\right)\right) d\Sigma} \qquad (1)$$

where υ is the number of γ-rays emitted per disintegration, r is the distance between the source and a point on the outer surface of the detector crystal, e_1 the path length traveled by the γ-ray in the reactor, e_2 the path length traveled by the γ-ray through the reactor wall and d the thickness of the crystal in the direction given by vector r (see Figure2.1). Ω is the solid angle subtended by the detector surface as seen from the source and n is an external unit vector locally normal to $d\Sigma$. μ_R, μ_w and μ_D are the total linear attenuation coefficients of the reactor contents, the reactor wall and the detector material, respectively. τ is the dead-time per recorded pulse and φ is the peak-to-total ratio. μ_R, μ_w, μ_D and φ depend on the γ-ray energy.

2.3.4.2 Accuracy Analysis in Monte Carlo Calculation

The Monte Carlo treatment consists of following and categorizing a large number of photon histories from emission at the source to absorption in the detector. For each photon, the emission angles θ and ϕ are determined as follows: the polar angle θ (see Figure 2.2) is scanned and the angle ϕ is determined by a random number. These angles are used to determine the photon path and collision site in the detector, modified from Beam *et al.* 1978.

The number of photon histories followed in the Monte Carlo calculation was studied here in order to determine the number necessary for sufficient accuracy and reasonable computation time. Figure 2.3 shows the effect of the number of histories in the Monte Carlo evaluation of the solid angle Ω representing the position of the particle in the center of the column. The solid angle is calculated at 21 positions representing locations where the particle is just in front of the detector to 20 cm away axially. The ordinate in Figure 2.3 is calculated using:

$$f = \sqrt{\frac{1}{21}\sum_{p=1}^{21}\left(\frac{\Omega(n)-\Omega(10^7)}{\Omega(10^7)}\right)^2} \qquad (2)$$

where $\Omega(n)$ is the solid angle calculated using n photon histories in the Monte Carlo calculation and $\Omega(10^7)$ using 10^7 histories. "f" is a measure of the accuracy of the Monte Carlo calculation. 1000 histories have been used in all calculations and as Figure 2.3 illustrates, the accuracy is approximately .04 %. The accuracy in the solid angle calculation is good enough to ensure that the main factor contributing to the spatial resolution is the statistical fluctuation (Poisson statistics) in the number of γ-rays registered by each detector.

2.3.4.3 Theoretical Resolution

The spatial resolution of the particle tracking system is defined as the variation of the determined particle location, or more precisely, the standard deviations σ_x, σ_y and σ_z of the statistical distributions of the determined coordinates x, y and z. The resolution can be determined experimentally by fixing the particle at a given location and observing the fluctuation in the location calculated from the repeatedly measured counts in the detectors. Factors contributing to fluctuation are: i) statistical fluctuations (Poisson statistics) in the number of γ-rays registered by each detector, ii) density fluctuations of the material in the reactor, and iii) propagation of error through algorithmic computations in the location algorithm.

Assuming that the first factor dominates (which will likely be the case when the sampling time is very short and the number of counts is low), it is possible to estimate the resolution theoretically. Thus, the variance of the calculated x coordinate is given by:

$$\frac{1}{\sigma_x^2} = \sum_{i=1}^{n} \left(\frac{\partial C_i}{\partial x} \right)^2 \tag{3}$$

where n is the number of detectors.

Similar relations hold for σ_y and σ_z. The C_i and the derivatives of the C_i with respect to x, y, and z are obtained from the detection model (Equation 1). The details of the derivation of Equation 3 are given in Appendix A.

2.3.4.5 Least-squares Search Location Algorithm

Equation 1 cannot be calculated analytically, rather it is evaluated numerically using a Monte Carlo technique (Larachi *et al.* 1994). For each detector, a map is computer-generated using a Monte Carlo calculation for 19,200 grid points throughout the reactor (60 vertical coordinates, 8 radii and 40 azimuthal angles). The map is the detector response as a function of tracer position. In order to accomplish the ultimate objective of obtaining the particle positions, the set of counts recorded by the detectors for each time interval must be converted into a spatial location. With the previously published method (Larachi *et al.* 1994), the 1,000 grid points closest to the best grid point for the previous time interval were searched for the best match. This was accomplished by least-squares minimization between the set of γ-ray counts of each of the grid points and the measured set of counts. The search was further refined in the neighborhood of the best grid point using the "virtual point" detector assumption within the volume delimited by the adjacent grid points (Larachi *et al.* 1994). Because the time required for one position to be calculated far exceeded the sampling time period, this algorithm, although very accurate, did not lend itself to real-time point-by-point trajectory reconstruction. This has led to consider other approaches capable of drastically reducing the cpu time per calculated position without sacrificing accuracy.

2.3.4.5 Neural network model

A neural network is proposed to calculate the tracer position directly from the counts recorded by the detectors. Backpropagation (or feedforward) neural network models are known to be very effective for capturing the non-linear relationships which may exist between variables in complex systems (Wasserman 1989, Lippmann 1987). In essence, a backpropagation neural network model can be viewed simply as a large regression model between input and output variables. Various applications of these models are reported in chemical engineering mainly in process modeling and control, and fault diagnosis. For additional references in this field, the reader is referred to recent papers by Morris *et al.* 1994 and Watanabe *et al.* 1994.

A three-layer feedforward neural model is built to express the normalized coordinates (between 0 and 1) of the tracer, $(\hat{x},\hat{y},\hat{z})$, as a function of the normalized responses of the detectors, $\hat{C}_i$ (i=1 to n, number of detectors). Figure 2.4 shows the schematic representation of the three-layer feedforward neural network which has been used in this investigation. Explicitly, the mathematical form for the tracer coordinates consists of the following set of equations:

$$H_j = \frac{1}{1 + \exp\left(-\sum_{i=1}^{n+1} W_{ij}\,\hat{C}_i\right)} \qquad (4.1)$$

$$1 \le j \le J-1 \quad \textit{with} \quad \hat{C}_{n+1} = 1$$

$$\hat{x} = \frac{1}{1 + \exp\left(-\sum_{j=1}^{J} W_{jx}\,H_j\right)}$$

$$\hat{y} = \frac{1}{1 + \exp\left(-\sum_{j=1}^{J} W_{jy}\,H_j\right)} \qquad (4.2)$$

$$\hat{z} = \frac{1}{1 + \exp\left(-\sum_{j=1}^{J} W_{jz}\,H_j\right)}$$

$\hat{C}_9$ and H_J, which are set equal to 1, are referred to as the bias. The vectors $\hat{C}$, H and $(\hat{x},\hat{y},\hat{z})$ define the input, hidden and output layers of the neural model, respectively. The value of J

(number of hidden neurons) has to be chosen empirically and increases with the complexity of the problem. Basically, the coefficients w_{j0}, w_{jx}, w_{jy} and w_{jz} in the summations, which are referred to as the weights, are the fitting parameters of the neural model. Parameter determination, known as the learning or training of the neural model, consists of least-squares regression analysis performed on a set of predetermined (experimental or simulated) input and output data. The powerful feature of neural models, as proved by Cybenko 1989 and Hornik *et al.* 1989, is that Equations 4.1 and 4.2 allow the approximation of any function providing a sufficiently high value of J. In this investigation, a value of J=14 has been used, resulting in a neural model which contains 159 fitting parameters.

One of the most important aspects of a neural network is the learning process whereby representative examples of knowledge to be acquired are presented to the network so that it can integrate this knowledge within its structure. In our case, the training set, for which the inputs and outputs are known, is given by the computer-generated maps obtained from the Monte Carlo simulation. Thus, the learning process randomly selects 12,250 grid points among the 19,200 points of a map and regression analysis using Marquardt's method (Press *et al.* 1988) is performed to determine the 159 weights w_{j0}, w_{jx}, w_{jy} and w_{jz} that produce the best fit over the training set. The optimum number of selected grid points was found by trials and errors to ensure a good fit. The remaining 6,950 grid points are used for a preliminary testing of the generalizing capability of the neural model. A more complete evaluation of the generalization will be performed using an actual tracking experiment which contains over than 720,000 data.

2.3.5 Neural Network and Flow Application

2.3.5.1 Experimental

The potential of the neural network technique for on-line visualization of particle movement in a three-phase fluidized bed was investigated. The experiment aimed at determining whether neural network method could accurately reproduce the particle trajectory in a real system and whether it could locate the particle in a calculation time significantly less than the sampling

interval. A 3 mm glass bead was irradiated to produce approximately 50 μCi of ^{46}Sc and was followed in a three-phase fluidized bed of internal diameter 100 mm. The superficial velocities of air and water were 25 mm/s and 60 mm/s, respectively, and the solids inventory was made of 3 mm glass beads. The particle locations were determined by the neural network model and by the least-squares search algorithm for comparison.

2.3.5.2 Results

The neural model was trained using 12,250 of the 19,200 grid points of the reactor map. It was tested on the remaining 6,950 points and the average error in the locations calculated was well below 1 mm. This excellent accuracy should not be confused with that attainable on experimental data with statistical fluctuations. A set of tracer coordinates is calculated in 0.16 cpu ms on an IBM RISC 6000-375 with the neural model, which is 500 times faster than with the least-squares search algorithm. The neural model was found to be still sufficiently fast for on-line visualization on a 66 MHz 80486 PC: a position is calculated in 0.5 ms.

The results of the three-phase fluidized bed experiment carried out to test the neural network model are shown in Figure 2.5. The curves show a 60 s portion of a typical set of y and z components as calculated with the least-squares search (continuous line, I) and the neural model (dashed line, II). The sampling period was 30 ms. Overall, the results from the two location algorithms show very good agreement; the differences (standard deviations) calculated over 720,000 positions were 1.5, 1.4 and 14.8 mm for x, y and z, respectively. The discrepancies noted for the longitudinal component z were most visible in the entrance region and in the inversion region of the bed (top of the bed), and were possibly due to an overfitting by the neural model (Normandin *et al.* 1993). Neglecting both the entrance and inversion regions, the standard deviation for z is comparable with those of x and y. It is important to stress that even though a good fit to a large number of data (12,250) is obtained with the model, there is no guarantee of deriving a model robust for data not contained in the training data set. An iterative learning procedure needs to be carried out in order to minimize the risk of getting an overfitted neural model. It is thought that by adding more data to the training set

from the bed regions where an abnormal behaviour is expected, the model will respond better for the z component. This aspect is currently under study.

After converting the instantaneous coordinates (x,y,z) into cylindrical coordinates, components of the velocities (u_r,u_Θ,u_z) are determined by subtracting the coordinates of successive positions (r,Θ,z) and dividing by the counting time interval. Using a cylindrical grid covering the fluidizing medium, the column is divided into 3,840 sampling compartments (30 longitudinal, 8 radii and 16 azimuthal) in order to determine compartment-averaged velocities. Each resulting velocity vector (u_r,u_Θ,u_z) is assigned to the center of the sampling compartment that contains the midpoint between two successive locations. For each compartment, the instantaneous velocity components are ensemble-averaged by summing each velocity component and dividing by the total number of assignments made to the compartment under consideration. By assuming solids flow axisymmetry, one dimension is taken out by averaging azimuthally the ensemble averaged velocities. Figure 2.6 shows longitudinal profiles of the radial and longitudinal mean Eulerian velocities at radial position r/R=0.19 (close to the centerline) using the trajectories calculated from the least-squares approach and the neural model. As expected, the average velocities resulting from the two calculation methods compare very well, except for the ends where, for the reason mentioned above, slight differences are observed.

Lets now review what strategy should be followed for true on-line experiment. First we have to calibrate the phenomenological model by using a limited number of experimental points (30 to 100). Three parameters, A, τ and μ_R (see equation 1) are thus determined. Then we have to generate counts by Monte Carlo calculation for each detector in many position (≈12,000). These "pseudo-experimental" data will enable us to optimize the 159 parameters of the neural network. After the optimum parameters are found, we are ready for a true on-line experiment.

2.3.6 Resolution Improvement

The radioisotope study addresses improvement in spatial resolution for static measurements. The implication is that higher spatial resolution due to more favorable radiation transport

characteristics for localization will permit higher velocities/shorter counting times by trading improvements in spatial resolution for increased variance in detection statistics.

2.3.6.1 Experimental

Tracking fast moving particles requires high sampling frequencies (short counting intervals). The detectors thus record few counts in each interval which implies important statistical fluctuations and poorer spatial resolution. To increase the number of counts the source activity is adjusted so that the detectors receive a near-saturation count-rate when the particle is at its closest position. Radionuclides emitting low-energy γ-rays may give better resolution because of increased attenuation in the reactor and because low-energy γ-rays have a higher probability of depositing all of their energy in the detector leading to more recorded counts relative to rejected events which only contribute to saturating the detector.

Measurements were carried out to determine the resolution attainable with three radionuclides: ^{46}Sc (2 γ-rays/disintegration, 1120 keV and 889 keV), ^{198}Au (0.96 effective γ-rays/disintegration, 412 keV) and ^{99}Mo (0.97 effective γ-rays/disintegration, 140 keV). The labeled particles were approximately 2 mm diameter spheres containing a few milligrams of $^{45}Sc_2O_3$, ^{197}Au and ^{98}Mo, which were irradiated using the SLOWPOKE nuclear reactor of École Polytechnique. As different numbers of γ-rays are emitted per disintegration from each radionuclide, the radioactivity level generated in each particle was adjusted so as to have approximately the same γ-ray flux ($3.7\ 10^6$ γ/s) for the three sources, which gives the same maximum total count-rate in the detectors. Other characteristics of the radionuclides are summarized in Table 1.1. For each radionuclide, two sets of experiments were carried out in a 500 mm high, 88.9 mm OD and 2.6 mm thick Schedule 10 stainless steel pipe. The particles were placed at 30 positions inside the pipe. Measurements were carried out with the pipe empty and filled with water to simulate highly diluted and dense flows respectively.

To measure the resolution, data were recorded for 1,000 ten millisecond counting intervals at each point and the variation in the located positions was calculated for the three radionuclides in air and in water.

2.3.6.2 Results

In the experiments carried out with the three radionuclides, the distances from the particle to any of the detectors varied from 100 to 450 mm, which corresponded to recorded counts of roughly 20,000 to 1,000 events per second. For each point, the particle position was calculated 1,000 times, and the mean location was compared to the true position; the standard deviation of the locations about this mean was then calculated for each of the three coordinates. During those experiments, the particle is not moving. The least-squares search location algorithm gave accurate results, with the mean calculated locations agreeing very well with the true locations. This is illustrated in Figure 2.7, where the mean calculated longitudinal coordinates, z, are compared with the true geometrical longitudinal coordinates for the six sets of experiments.

Figure 2.8 shows the standard deviations of the calculated y and z coordinates as a function of z (the longitudinal coordinate) obtained with the three tracers in the water-filled pipe. The standard deviations of the x coordinate are similar to those for y. The lines are the standard deviations predicted by Equation 3. Several features are apparent. First, ^{198}Au and ^{99}Mo give better x and y resolution than ^{46}Sc and ^{198}Au gives the best z resolution. For this size reactor (88 mm diameter, 420 mm height) low energy γ-rays give better resolution partly because attenuation in water gives a faster variation in recorded counts as a function of position. Also, φ, the fraction of the γ-rays which give all of their energy to the detector and are therefore recorded, is greater for ^{198}Au and ^{99}Mo (Table 1.1). From detection considerations alone, the φ for 140 keV γ-rays should be greater than that for 412 keV γ-rays. However, the φ for ^{99}Mo is reduced because of X-rays and other γ-rays which are also emitted. In fact, no radioisotope exists which emits uniquely γ-rays with energy near 100 keV. Thus, the attainable resolution is limited by the existence of suitable radioisotopes. For larger reactors, higher energy γ-ray emitters like ^{46}Sc may be preferable.

The resolutions measured in the empty pipe were always worse than those measured in the water-filled pipe which confirms that γ-ray attenuation in the water contributes to improving the resolution. For a sampling period of 10 ms, the average three-dimensional resolutions were found to be 7 mm in water and 9 mm in air for ^{198}Au, 9 mm and 11 mm respectively for ^{46}Sc and 7.5 mm and 12 mm respectively for ^{99}Mo. For a sampling period of 30 ms and a water-filled pipe, the average three-dimensional resolution was found to be 6 mm for ^{46}Sc, which is very close to that of ^{198}Au for a sampling period three times shorter. The aim of compensating the loss of resolution due to the shorter sampling period has thus been achieved by optimization of the γ-ray energy.

Figure 2.8 also shows that the resolutions predicted by Equation 3 agree quite well with the measurements. This confirms the validity of Equation 3 and the fact that the resolution depends essentially on the statistical fluctuations in the numbers of γ-rays recorded. This signifies that, as far as the statistical fluctuations in the number of γ-rays dominate, the RPT resolution might be further improved by numerical simulations using Equations 1 and 3. Indeed, for different reactors geometries and sizes, the optimal γ-ray energy and the optimal arrangement of the detectors can be found and the attainable resolution can be predicted by the simulations before any experiments are carried out.

Figure 2.9 shows the predicted resolution of σ_z on an axial plane in the column (.082 m in diameter) for a 100 μCi ^{198}Au source in a dilute medium. In this simulation, 4 detectors are located at an elevation of 80 mm and 4 others are located at 300 mm. The wall is 2.6 mm thick and the sampling period is 10 ms. The resolution in axial position is a strong function of the axial position but not of the radial position. Figure 2.9 also clearly indicates the effect of the detectors placed on two different levels. The spatial resolution (σ_z) is worsened near the two axial positions where the detectors are held. This confirms that the arrangement of the detectors is not optimal and could be improved to obtain a more uniform distribution. The

resolution is worst just in front of the center of the detectors (7-8 mm at 80 mm and 300 mm) because the detectors are insensitive to an axial displacement in their surrounding. The resolution σ_z is at its best in the middle of the column (4.5-5.5 mm at 150 mm < z < 250 mm) where all the detectors contribute significantly to the reduction of σ_z. It is believed that a spiral disposition of the detectors will improve the uniformity in the spatial resolution. New experiments will be conducted in a circulating fluidized bed to confirm this point.

Figure 2.10 shows the predicted resolution of σ_x on the same plane. The resolution is better near the wall because the attenuation in the stainless steel wall plays a role in increasing the change in count rate with position. The effect of the wall would be less significant with a lighter wall material (Plexiglass for example). The resolution is better just in front of the detectors (3.5-5.5 mm at 80 mm and 300 mm) because the detection solid angle is sensitive to a change in position of the particle. Both σ_x and σ_z worsen at elevations below 30 mm and above 350 mm, away from all the detectors.

2.3.7 Conclusion

An enhanced location algorithm based on a three layer feedforward neural network has made possible extremely fast position calculations using the γ-ray counts measured by an array of detectors. The potential of such a reconstruction technique for on-line visualization purposes was illustrated for a particle tracking experiment in a three-phase fluidized bed reactor.

This research has investigated the use of new radioisotopes for improving the spatial resolution in tracking radioactive tracer particles using RPT. The improved resolution achieved with ^{198}Au has been shown to be promising for potential application to fast particulate flow systems. This radioisotope should be use in new experiment using the original least-squares search algorithm or the neural network.

2.3.8 Appendix A

Given the average number of counts, C_i, recorded in detector #i during a time interval, the standard deviation in this information is $\sigma_i=\sqrt{C_i}$. Consider the effect of this uncertainty on the

determination of the x coordinate of the particle. Each C_i contributes to the determination of the value of x, and the variance in x arising from the uncertainty in C_i can be written as

$$\left(\frac{\partial x}{\partial C_i}\sigma_i\right)^2$$

Considering x as the weighted average of the contributions from each of the detectors, the resulting variance in x is the combination of the contributions of the C_i. The procedure for calculating the variance of a weighted average (Bevington 1969) yields the following expression for σ_x:

$$\frac{1}{\sigma_x^2}=\sum_{i=1}^{n}\left(\frac{1}{\left(\frac{\partial x}{\partial C_i}\sigma_i\right)^2}\right)=\sum_{i=1}^{n}C_i\left(\frac{\partial \ln C_i}{\partial x}\right)^2 \qquad \text{(A1)}$$

where $\frac{\partial \ln C_i}{\partial x}$ is calculated by the detection model (Equation 1). A similar relation holds for σ_y and σ_z.

Finally, the three-dimensional spatial resolution σ_{3D} is given by the following relation:

$$\sigma_{3D}=\sqrt{\sigma_x^2+\sigma_y^2+\sigma_z^2} \qquad \text{(A2)}$$

Table 2.1 Nuclear characteristics of the radionuclides used and measured in this study.

Radio-nuclide	Half-life (d)	E-γ (keV)	n	φ	A (μCi)	μ_{w} Stainless Steel (mm^{-1})	μ_{H2O} (mm^{-1})
^{46}Sc	83.3	1005	2.00	0.40	50	.046	.007
^{198}Au	2.7	412	0.96	0.55	100	.070	.010
^{99}Mo	2.8	140	0.97	0.52	104	.166	.015

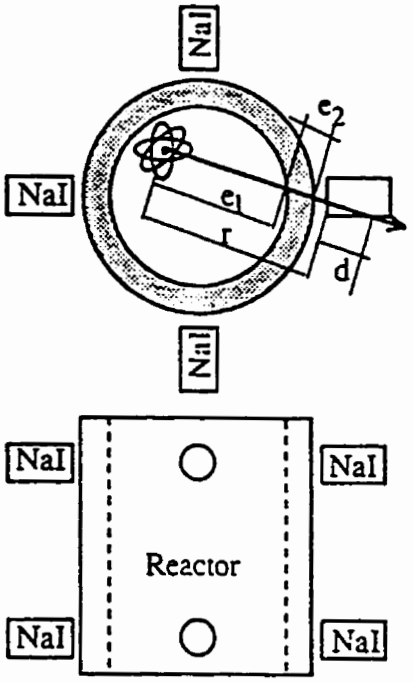

Figure 2.1 Layout of the RPT system.

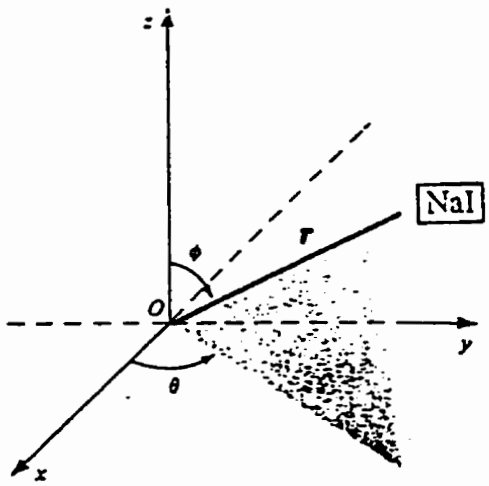

Figure 2.2 Spherical coordinate system used in Monte-Carlo calculation.

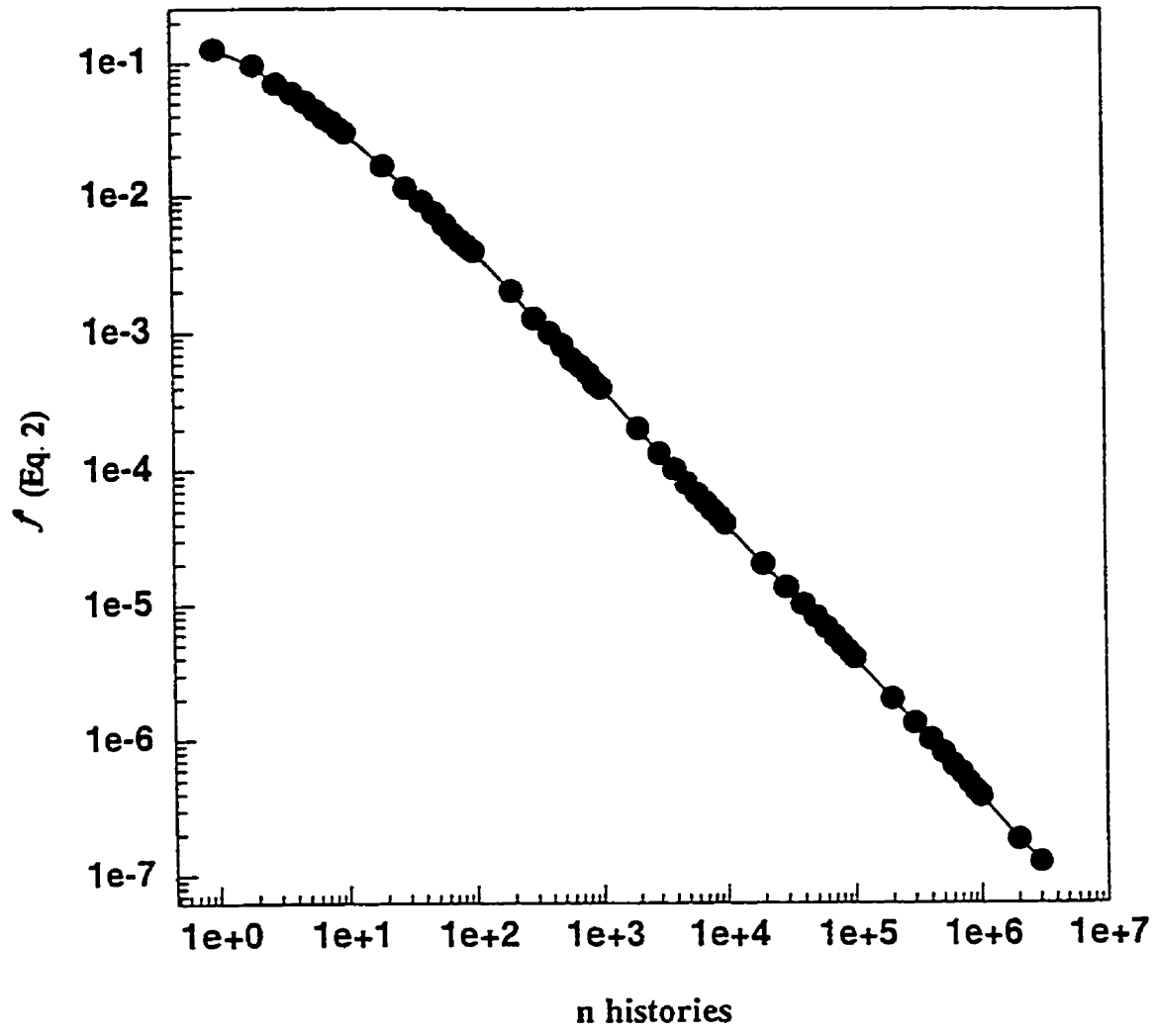

Figure 2.3 Effect of the number of histories in the Monte Carlo evaluation of the solid angle.

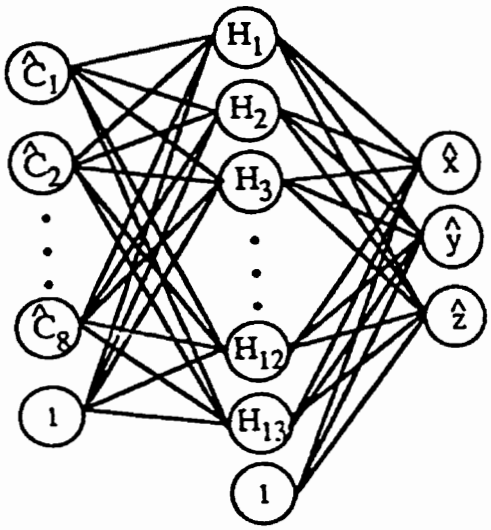

Figure 2.4 Neural architecture of the reconstruction model (n=8).

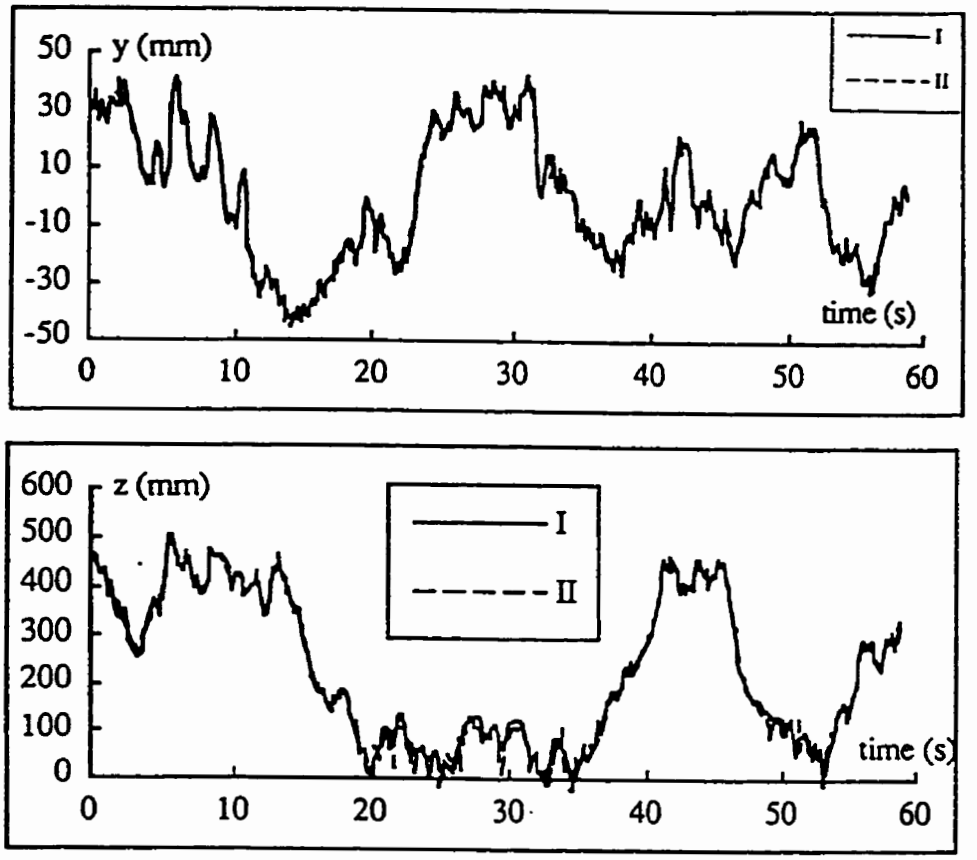

Figure 2.5 Tracking a labeled particle in a three-phase fluidized bed using the least-squares search algorithm (I) and the neural network model (II).

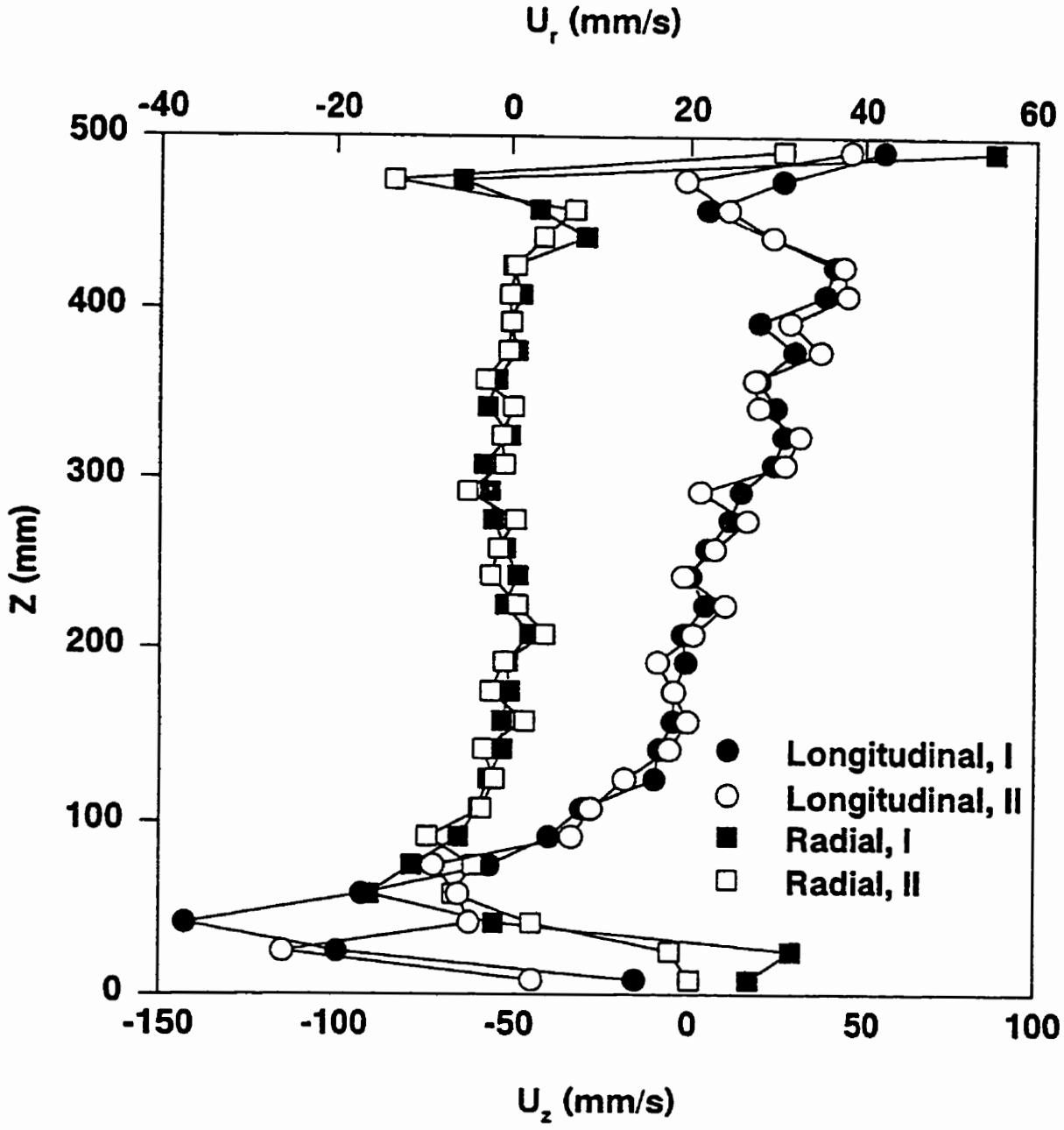

Figure 2.6 Longitudinal profiles of the mean Eulerian velocities in the radial and longitudinal directions as calculated from the least-squares approach (I) and the neural network model (II) in a three-phase fluidized bed.

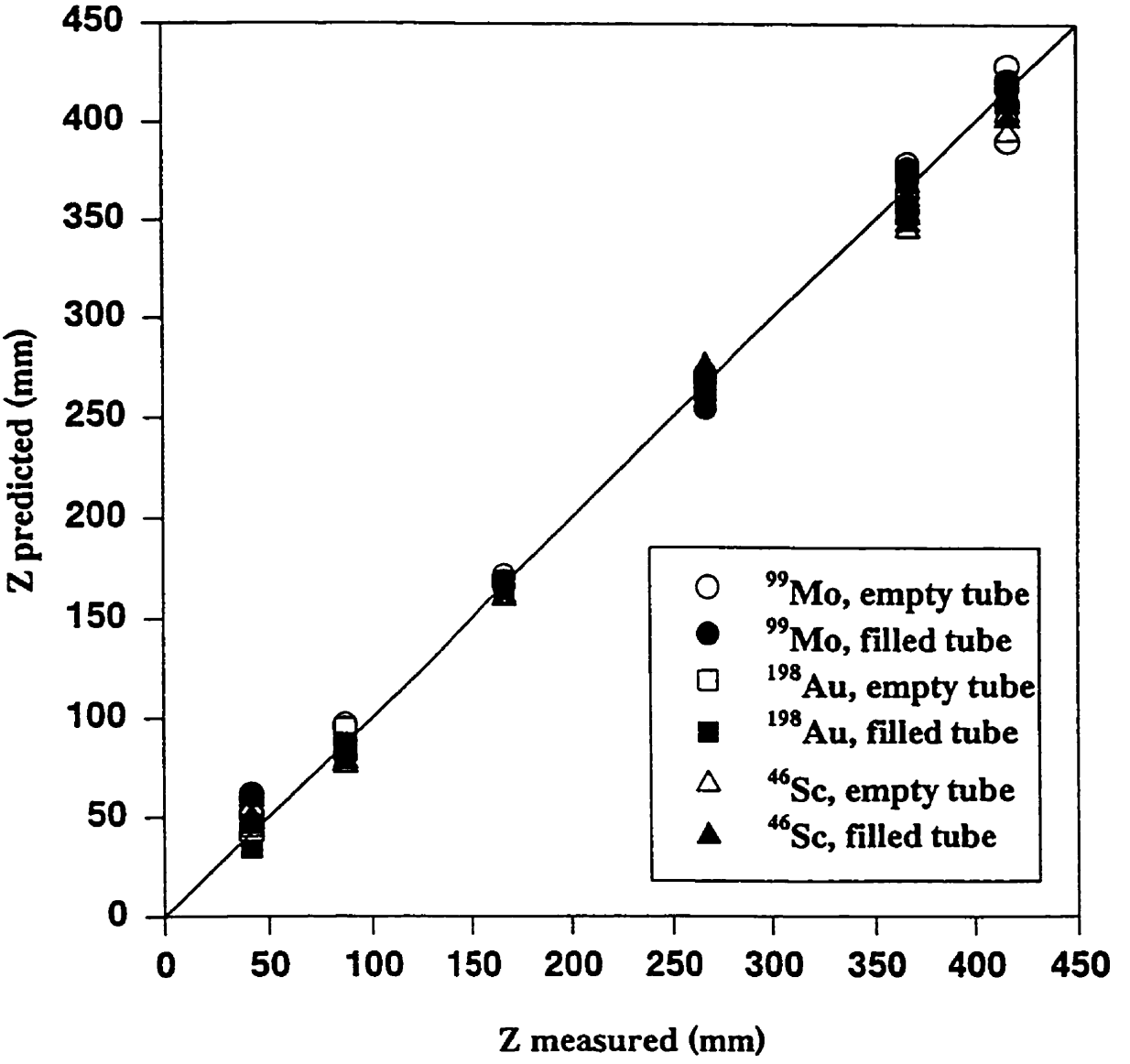

Figure 2.7 Results of the bias of the located longitudinal component, z, for the three radionuclides (sampling period, 10 ms).

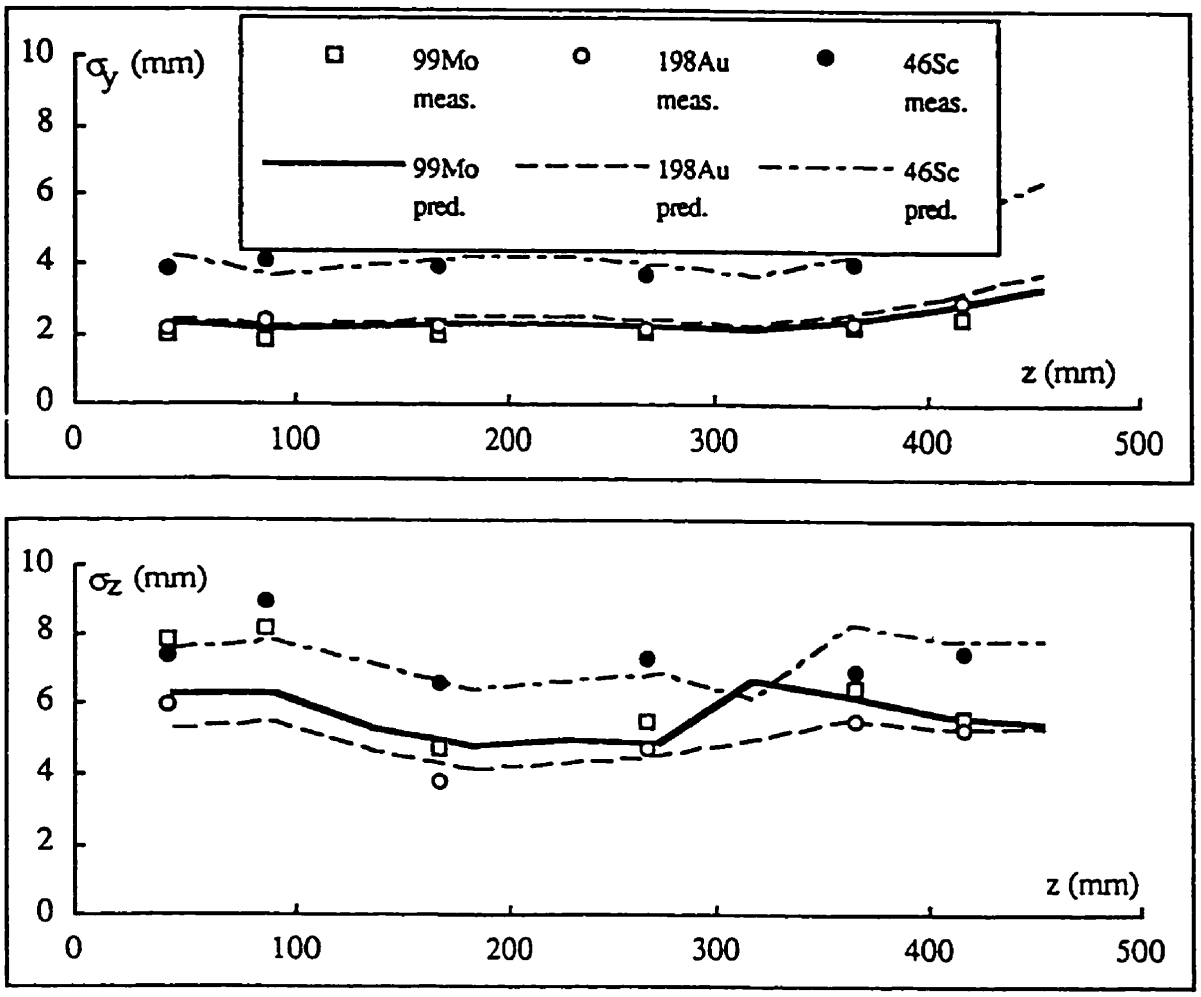

Figure 2.8 Longitudinal profiles of the standard deviations σ_y and σ_z of components y and z and the corresponding standard deviations from the detection model (Equation 1), as a function of γ-ray energy (sampling period, 10 ms).

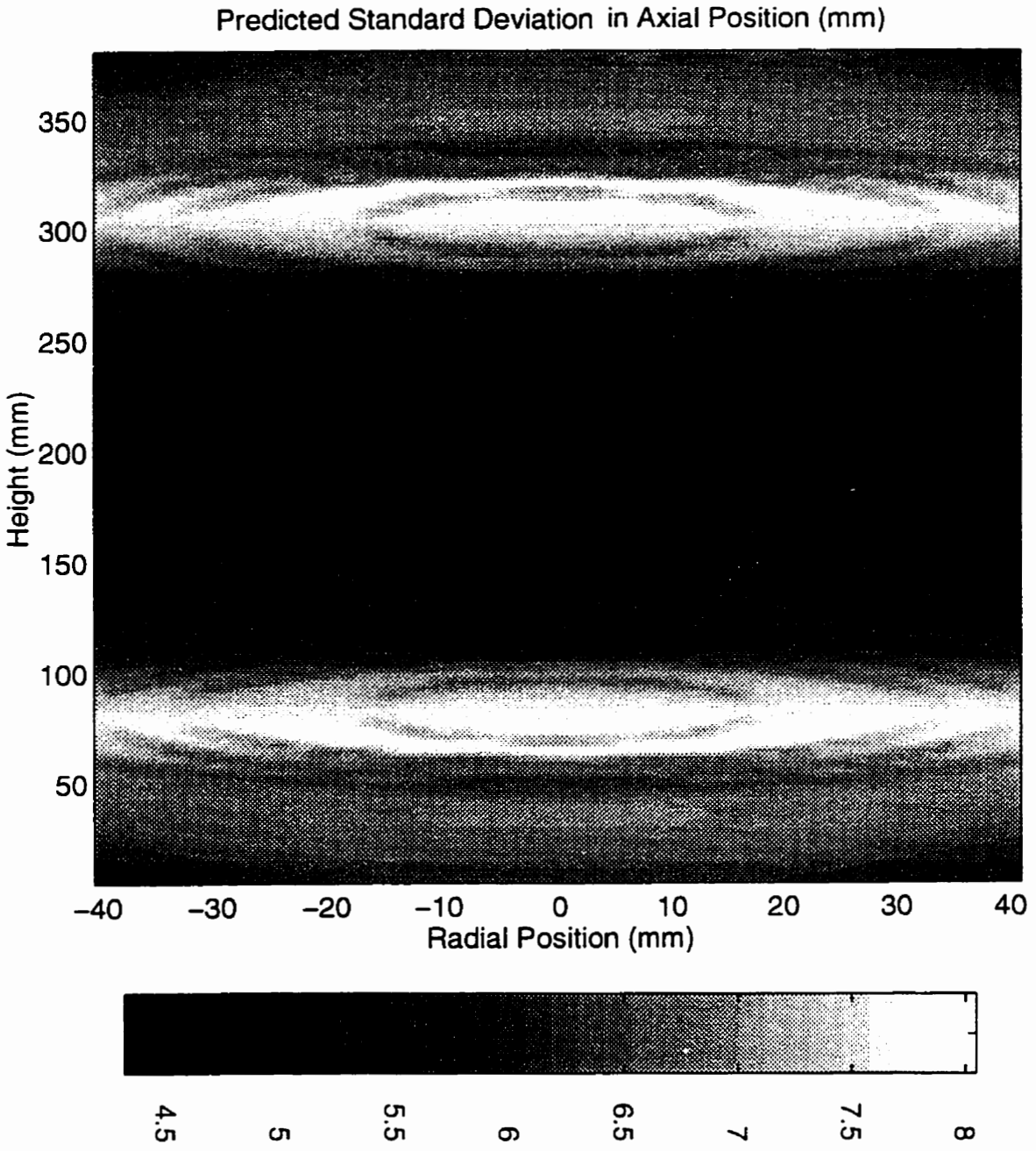

Figure 2.9 Predicted resolution σ_z for the ^{198}Au source in a dilute medium.

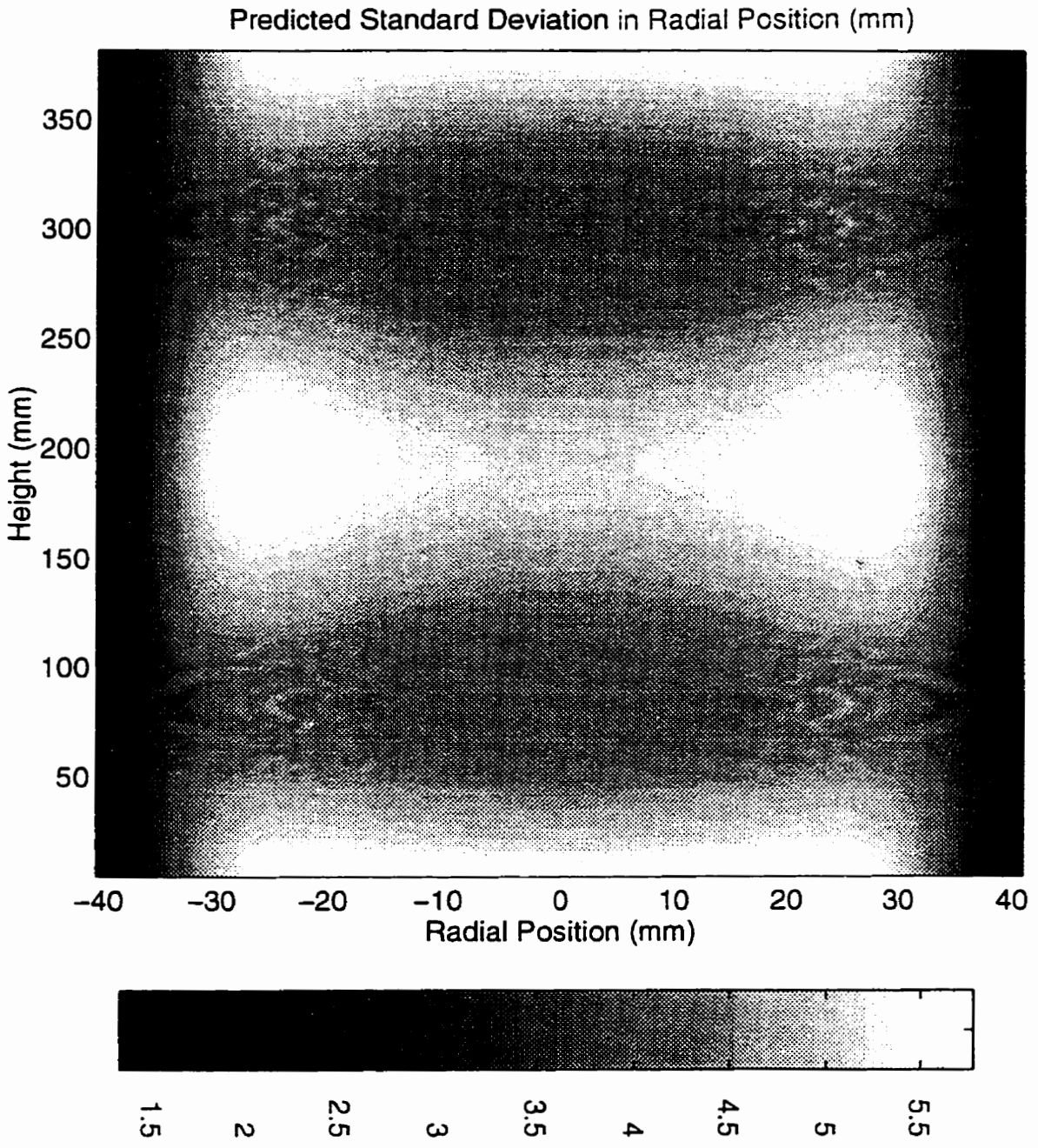

Figure 2.10 Predicted resolution σ_x for the ^{198}Au source in a dilute medium.

CHAPITRE 3 ARTICLE SOUMIS AU 5E CONGRÈS SUR LES LITS FLUIDISÉS CIRCULANTS

Le chapitre précédent a permis de conclure que l'or était le meilleur radio-isotope parce qu'il améliore la résolution spatiale en permettant la mesure de comptages plus élevés. Rappelons que la comparaison des différents radio-isotopes est basée sur des tests statiquea (où le particule ne bouge pas). Le but de ce chapitre est de démontrer si l'outil que représente la technique de poursuite d'une particule radioactive est applicable pour l'étude du mouvement d'une particule traçante dans un lit fluidisé circulant. Les détails sur l'unité de lit fluidisé circulant sont décrits à l'annexe III.

3.1 Sommaire

Un article soumis (2 février 1996) pour publication dans le compte rendu de conférence du 5e Congrès International sur les Lits Fluidisés Circulants (Beijing, Chine 28 Mai- 1er juin 1996, page MI2-1 à MI2-6) rapporte des résultats préliminaires. L'article a été sélectionné et accepté par un comité de lecture pour être publié après la conférence dans un recueil d'articles formant le livre "Circulating Fluidized Bed Technology V". Une copie de cet article est présentée dans les pages qui suivent.

La conclusion la plus importante pour la poursuite des travaux est la suivante:

> -Malgré les hautes vitesses de solide inhérentes aux lits fluidisés circulants, il est possible de localiser instantanément la particule dans le plan x-y à l'aide de huit détecteurs; toutefois, les prochaines expériences seront réalisées à l'aide seize détecteurs afin d'augmenter la résolution spatiale.

3.2 Texte de l'article

Simultaneous Measurement of the 3-D Position and Velocity of a Single Radioactive Particle in a CFB Riser at High Velocity

L. Godfroy*, F. Larachi**, G. Kennedy* and J. Chaouki*

*École Polytechnique de Montréal, Montréal, (Québec), Canada

** Université Laval, Québec, (Québec), Canada

3.2.1 Abstract

Investigating hydrodynamic behaviour in a multiphase reactor is a complex task. A dynamic non-invasive technique was recently developed to determine the position and velocity of a radioactive particle. This technique is based on the use of a phenomenological model to predict the count of a scintillation detector as a function of the particle position. While it has already been proven successful in three phase fluidized bed and in spouted bed, this technique is applied for the first time to .082 m diameter, 7 m height riser of a circulating fluidized bed.

The technique is a very powerful tool of investigation and permits the study of local hydrodynamics of CFBs. Its main advantages lie in its non-intrusive characteristics and in the fact that it gives the instantaneous position of the particle. The position and velocity of a radiolabeled particle are determined every 10 ms with eight NaI(Tl) scintillation detectors surrounding the riser section of the CFB.

3.2.2 Introduction

Investigating the hydrodynamic behaviour in Circulating Fluidized Bed (CFB) is a complex task. Recent advances in the study of local two-phase flow structure have revealed non-uniform solids velocities and concentrations in the cross section of the flow. Although numerous studies have been conducted on this subject, the hydrodynamic behaviour of

CFBs remains very difficult to understand, and predictive models are still unable to offer an accurate description of the two-phase flow. Many hydrodynamic models have attempted to predict the mean particle velocity profile; yet, very little is known about local particle velocities.

Towards this end, many measurement techniques have been applied. Conventional measurement devices such as sampling probes, fiber optic or electrical capacitance probes have been associated with significant errors, due to the fact that they disturb the flow. Although non-invasive techniques are superior in this area, they do have a number of weaknesses. For instance, the phase Doppler Particle Analyzer permits the measurement of only one velocity component; The laser sheet technique or any video camera system can be used only for dilute flow and transparent wall. Hence, the need to develop a non-invasive technique that is free from these limitations is important.

In the last decade, important progress has been made in the development of advanced non-invasive nuclear particle tracking techniques that are particularly suitable for the characterization of three-dimensional flow fields of discrete or continuous batch phase in dilute/dense and opaque multiphase systems. Two photon emission-based tracking techniques are currently in application on laboratory scale reactors, "positron emission particle tracking (PEPT)" (Broadbent *et al.*, 1993); and "γ-ray emission radioactive particle tracking (RPT)" (Lin *et al.*, 1985, Moslemian *et al.*, 1992 and Larachi *et al.*, 1994). Both use the detection and counting of highly penetrating γ-rays emitted by radiolabeled flow followers which are dynamically similar to the tracked phase. They use the detected γ-rays to provide the instantaneous coordinates (x(t), y(t),z(t)) of the moving tagged particle. These techniques also allow the determination of the 3-D instantaneous components of velocity -- an improvement over other techniques measuring only one velocity (axial) component (although another component (radial) could be measured by a 90° rotation of the equipment).

The use of Positron Emission Particle Tracking (PEPT) has been limited to studies at low velocities (up to 1.5 U_{tf}) and for coarse particles . PEPT has not as yet been used in CFB (Seville *et al.*, 1995). The success of the radioactive particle tracking system developed at École Polytechnique (Larachi *et al.*, 1994) and applied to the study of particle motion in gas spouted bed (Roy *et al.*, 1994), three-phase and liquid fluidized beds (Larachi *et al.*, 1995a,b), and by other investigators to bubble columns (Devanathan *et al.*, 1990) and gas fluidized beds (Lin *et al.*, 1985 and Moslemian *et al.*, 1992) has motivated us to continue improving the technique (in terms of accuracy and resolution) , and to apply it to a CFB.

The aim of this study is to demonstrate the applicability of the 3-D particle tracking to high velocity flow in a CFB , and to present results at a superficial gas velocity of 4 m/s and solids circulation rate of 25 $kg/m^2.s$.

In this work, extended time series of positions of a solid tracer freely moving in the CFB riser are analyzed. The tracer has nearly the same properties as the particles constituting CFB inventory. The tracer mimics the solid phase, and its position is obtained each 10 ms (100 Hz) by a non-invasive radioactive particle tracking technique. The particle tracking technique illustrates the actual path of one of the solid particles in the CFB. This path would represent the motion of any equivalent particle at different instants if the tracking were long enough (Cassanello *et al.*, 1995). Therefore, this technique allows us to capture the average dynamics of solids motion across the riser by providing instantaneous information sampled over all the riser cross section.

3.2.3 Apparatus

The CFB set up is shown in Figure 3.1. The riser is .082 m inside diameter, 3.048 mm thick stainless steel wall and 7 meters high. Solids are introduced into the riser by 4 orifices in the riser just above an orifice plate distributor. They are entrained in the upward flowing gas, before exiting through a smooth exit, and finally separating from the gas

phase by two cyclones in series. The particles are returned to the riser bottom and the gas is vented into atmosphere. The air flow rate is measured by pressure drop across an orifice. The solids circulation rate is measured by collecting the solids at the exit of the first cyclone for a timed period and by weighting. The simultaneous measurements of the 3-D position and velocity are taken by a radioactive particle tracking system. Measurements are done between heights of 4 and 5 meters above the distributor, in the fully developed region, and away from end effects.

150 mm sand particles with density of 2600 kg/m^3 are used. The radioactive particle (the tracer) is made of a mixture of epoxy resin and very fine gold particles (<10 μm). The particle contains approximately 50 μg of gold. Its diameter is 500 μm and the particle is approximately spherical. The density is about 2000 kg/m^3. To ensure that the tracer is attrition resistant, it is covered by a thin layer of super glue. It should be noted that the tracer particle is not exactly representative of the bulk material; work continues on reducing the size of the tracer. Finer particles could be made but the relatively low content of Au would take a long time for nuclear activation. The particle is activated in a thermal neutron flux in a Slowpoke reactor for 32 hours. The resulting activity is approximately 100 μCi of ^{198}Au emitting γ-rays of energy 412 keV (half-life=2.8 d).

3.2.4 The Radioactive Particle Tracking System

The reactor contains a radioactive particle (the tracer), whose properties match as close as possible those of the solids in the bed. The reactor is surrounded by eight uncollimated 3" X 3" NaI(Tl) scintillation detectors as shown in Figure 3.2. Detectors are located 110 mm apart axially and the distance between the detectors and the reactor wall is approximately 65 mm. The detectors are arranged in spiral with 90° spacing between two consecutive detectors. γ-rays emitted from the particle may be absorbed by the materials in the reactor and the reactor wall. A computer simultaneously registers the number of γ-rays detected by each of the 8 detectors. The counts of the 8 detectors are used to calculate the coordinates of the particle. Data were acquired for several hours in order to get a number

of passes sufficient to characterize the movement and the velocity field with reasonable accuracy in the entire cross section of the riser. The particle coordinates x,y,z could only be calculated when the radioactive particle is in the riser in front of the RPT system. Unfortunately, the particle spent most of the time outside the riser section covered by the RPT system. In fact, we have about 1 to 1.5 seconds of useful information every time the particle passes through the entire circulation loop (12 minutes).

3.2.5 Location Algorithm

The location algorithm uses a rigorous phenomenological model (Beam *et al.*, 1978) which describes the interactions of radiation with matter for the system geometry. A map of detector counts versus location is generated by Monte Carlo and is adjusted to calibration measurements. The calibration procedures permit the evaluation of three parameters for each detection system, the activity of the source, the attenuation coefficient, and the dead time. Once the parameters are determined, a dictionary of 19200 positions (60 axial, 8 radii and 40 azimuthal positions) containing the count predicted for each detector is computer generated. Subsequently, each location of the tracer is determined by least-squares search for the grid point in the dictionary which best matches the counts registered in the detectors (Larachi *et al.*, 1994). This location is refined by least-squares search in the neighborhood of this grid point using a simplified model. Calculation is done off line using a fast computer. A set of tracer coordinates is calculated in 80 cpu ms on an IBM RISC 6000-375. An enhanced location algorithm using a three layer feed-forward neural network model can also be used for extremely fast position calculation for on-line visualization purposes (Godfroy *et al.*, 1997a).

3.2.6 Results and Discussion

Figures 3.3a,b,c present typical positions x,y,z calculated by the RPT technique (Note that z is relative to the RPT system, not to the riser distributor). In the first part of the graphs, the particle is going down while it is going up in the second part. It is noted that the signal is noise imprinted. In order to get a velocity, we must differentiate a coordinate (x,y or z). Direct differentiation led to erroneous velocities. Consequently, the time series signal

corresponding to positions was filtered. The Figures also show the resulting filtered positions represented by smooth lines. Data were filtered using a 4th order low-pass digital Butterworth filter design. With the help of Fast Fourrier Transform, we were able to identify the cut-off frequency. The cut-off frequency is 0.3 times the sampling rate. A zero-phase forward and reverse digital filtering was used. The instantaneous values of the slope (V_z) in Figure 3.3c are comparable when the particle is going down and when it is going up. However, it is clear that the particle spent more time to go through the same distance (approx. 900 mm) while going down. In general, the particle moves faster when ascending than descending. This will later be shown by the mean velocity profile.

The position of the detectors affects the spatial resolution of the RPT technique. The original development (Larachi *et al.*, 1994) used 8 detectors placed on two levels. The four detectors on each level surrounded the reactor with 90° spacing. That configuration gives a good x and y resolution but a poor z resolution. In our case, the detectors were well distributed axially over the region of interest, and the z resolution was good to the detriment of x and y. The effect of the filtering does not change significantly the mean axial component of the velocity. The filtering allows us to find the most probable location in the x,y plane where that velocity is measured. The axial velocity is accurately measured but its location in the x,y plane is less well defined.

To improve the resolution, new experiments will be done using a set of 16 scintillation detectors covering approximately the same section of the riser (approx. 1 m). The improvement in resolution obtained by doubling the number of signals is especially important in the x,y plane and will allow a more accurate calculation of the mean axial velocity profile. The 16 detector assembly is currently under construction.

Averaging all instantaneous axial velocities at each radius allows us to compute the mean velocity profile. The mean axial velocity profile is presented in Figure 3.4. Its shape is parabolic with a positive maximum in the center and negative values in the wall region.

The shape of the velocity profile is similar to those found by other techniques (pitot tube, Bader *et al.*, 1988; isokinetic probe, Harris *et al.*, 1994; laser Doppler velocimetry, Yang *et al.*, 1991, 1992b, Wang *et al.*, 1993; optical fiber probes, Hartge *et al.*, 1988, Horio *et al.*, 1988 Ishii *et al.*, 1989, Katoh *et al.*, 1993, Qian and Li 1994). The velocity profile is not well defined in the center (r/R<.5) where the data are scattered. The profile is better defined near the wall and generally is smoother. Figure 3.5 shows the number of occurrences over which velocity (Figure 3.4) is calculated. It shows that the occurrence is very high at the wall, enabling a good representation of the mean velocity in that region.

If we define a core-annulus structure and define the limit between the core and the annulus as the location where the particle velocity is zero, then we find that r_c/R is equal to .89. This value is similar to those predicted by Harris and Davidson (1994) and Rhodes (1990) using a core-annulus model. The annular region is 4.5 mm thick and occupies 21% of the cross sectional area. Based on the occurrence, the particle spent 39 % of the time in the annular region. There are two reasons why the particle spent that much time in the wall region. First, the wall region is denser than the central region. Secondly, the particle velocity is lower in the wall region and the solids residence time is thus longer than in the fast moving central region.

Knowing the mean velocity profile, the occurrence and the average void fraction, the voidage fraction profile can in principle be estimated. However, that calculation could not be made due to insufficient data points (the occurrence is not high enough). A sufficient number of data points is obtained for the velocity profile measurement but the number of data points required for estimation of the void fraction is not attained. It is expected that convergence to the void fraction is very slow. The total occurrence of velocity measurements is 5404, maybe 100 times lower than what is necessary for the evaluation of the local void fraction.

3.2.7 Conclusion

Flow analysis of the hydrodynamics obtained with this non-invasive radioactive particle tracking technique can lead to a better understanding of the phenomena involved in the motion of discrete particles in CFB than can be obtained using any of the previously available techniques. Further experiments will be conducted using several radioactive particles (3 or 4) with exactly the same activity. The number of passes will increase proportionally which will increase the accuracy of the velocity field.

The technique has proven valuable in the measurement of the velocity profile in a CFB at a superficial gas velocity of 4 m/s and a solids circulation rate of 25 $kg/m^2.s$. The velocity profile has a parabolic shape with maximum values in the center and negative values at the wall. The wall region (annulus) occupies 21% of the cross section, where the particle spends almost 40% of the time.

Further in-depth hydrodynamic studies will be done using the improved 16 detector RPT system.

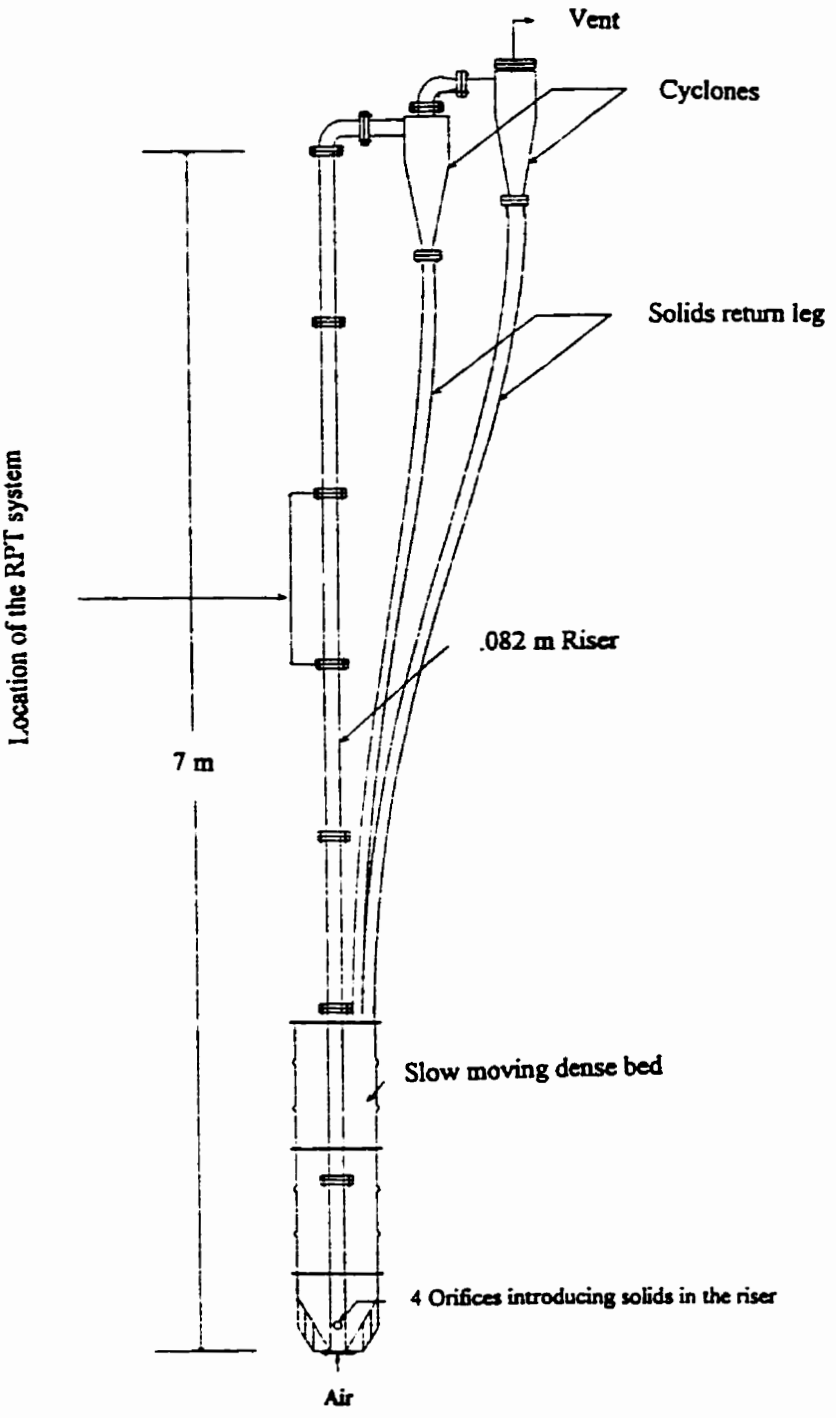

Figure 3.1 Schematic of the CFB set up.

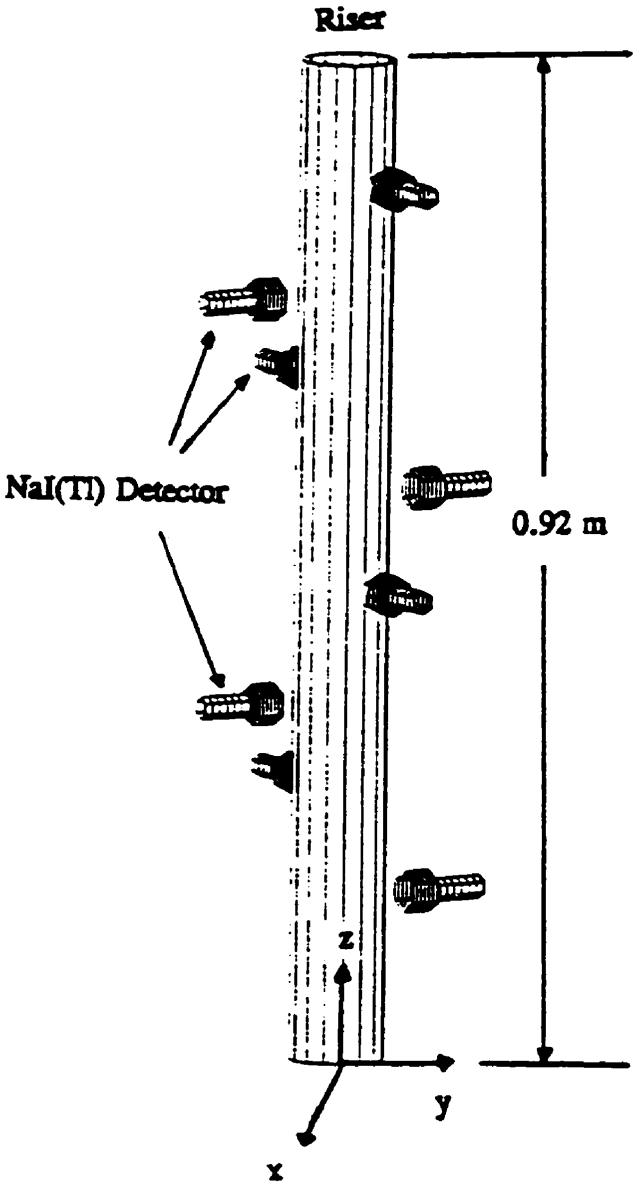

Figure 3.2 Schematic of the RPT system.

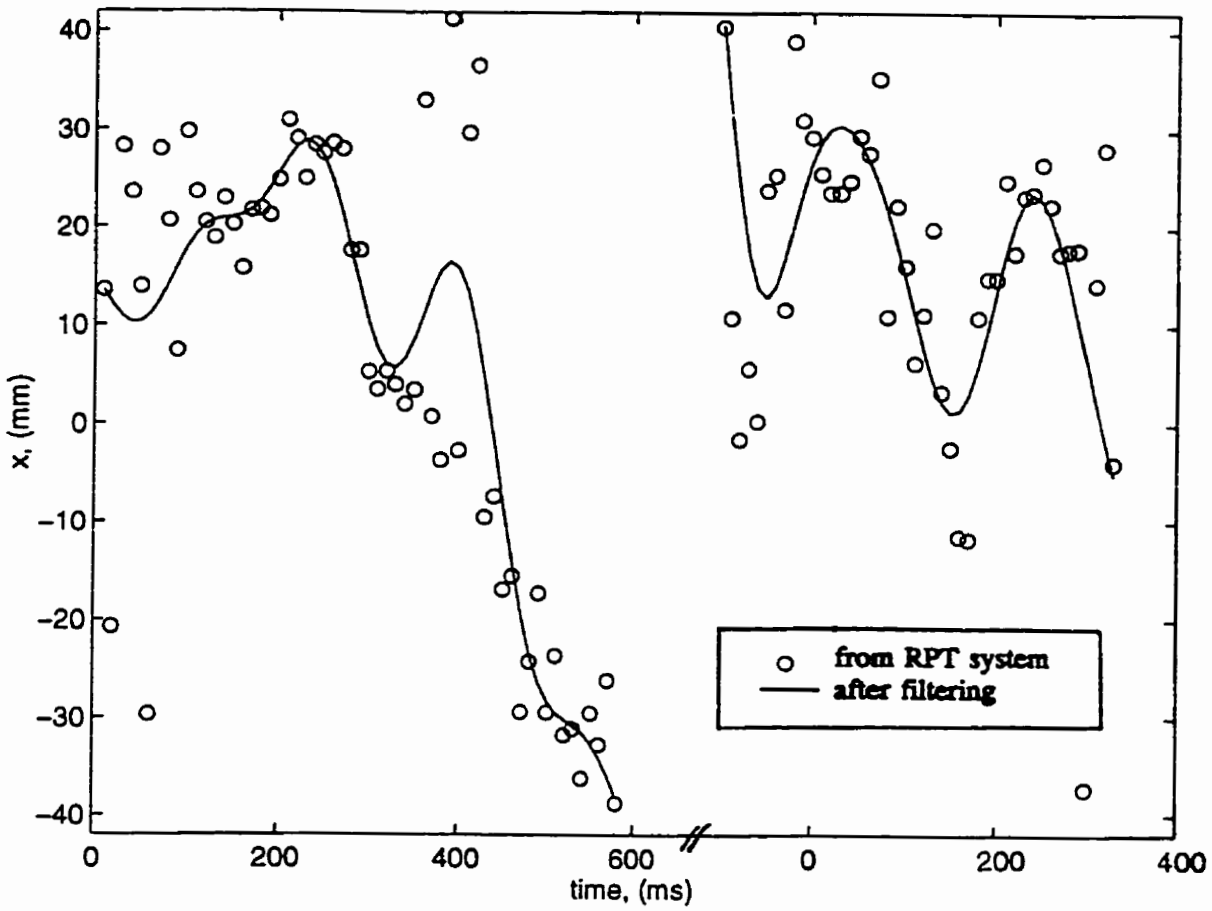

Figure 3.3a Instantaneous x position (100 Hz) from RPT system after filtering.

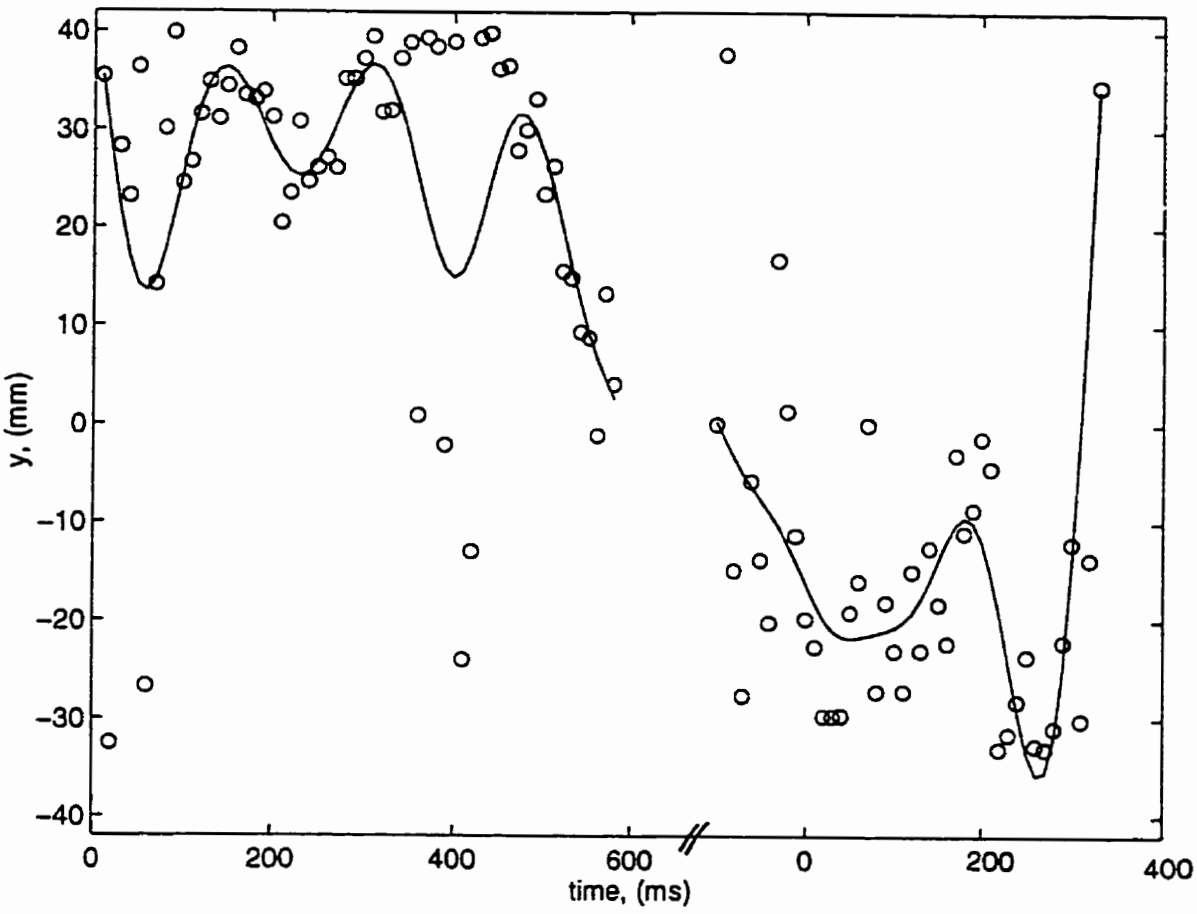

Figure 3.3b Instantaneous y position (100 Hz) from RPT system after filtering.

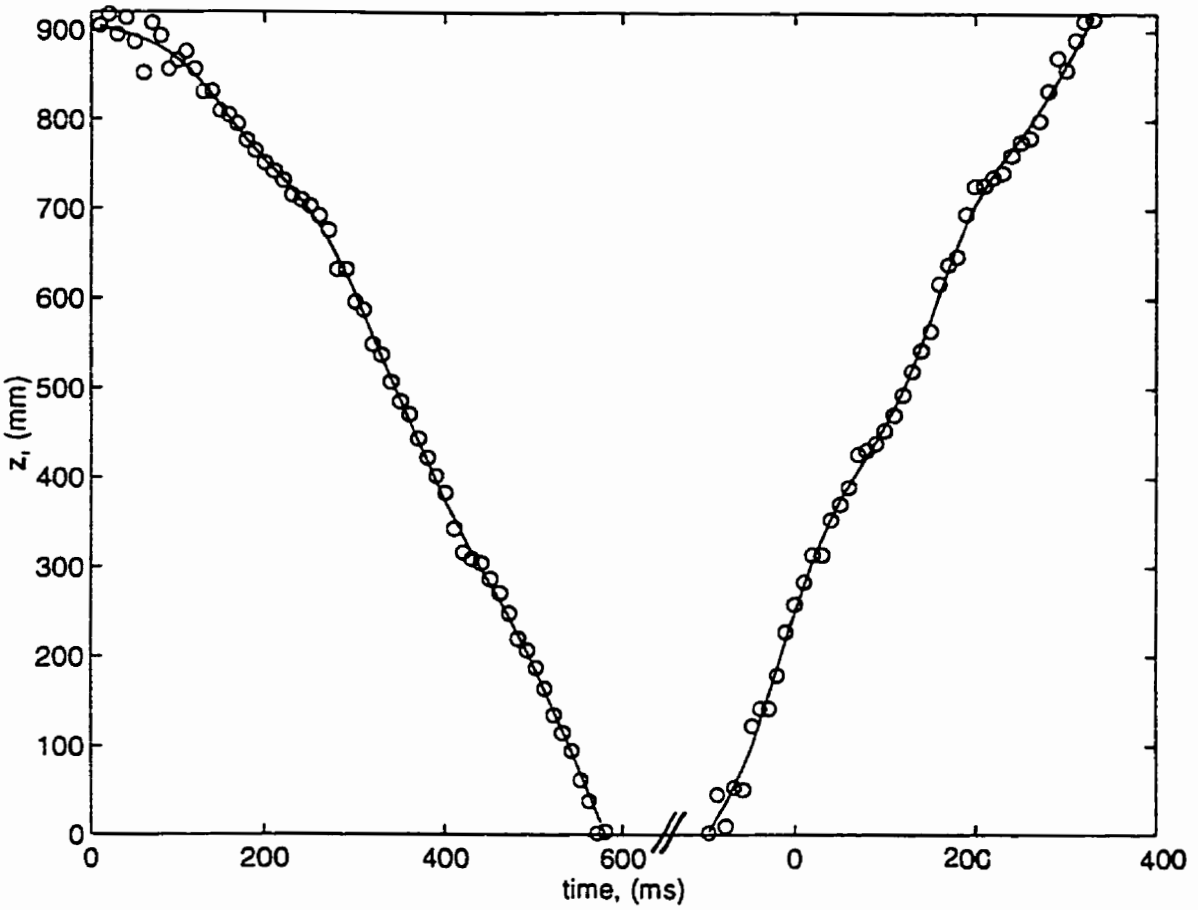

Figure 3.3c Instantaneous z position (100 Hz) from RPT system after filtering.

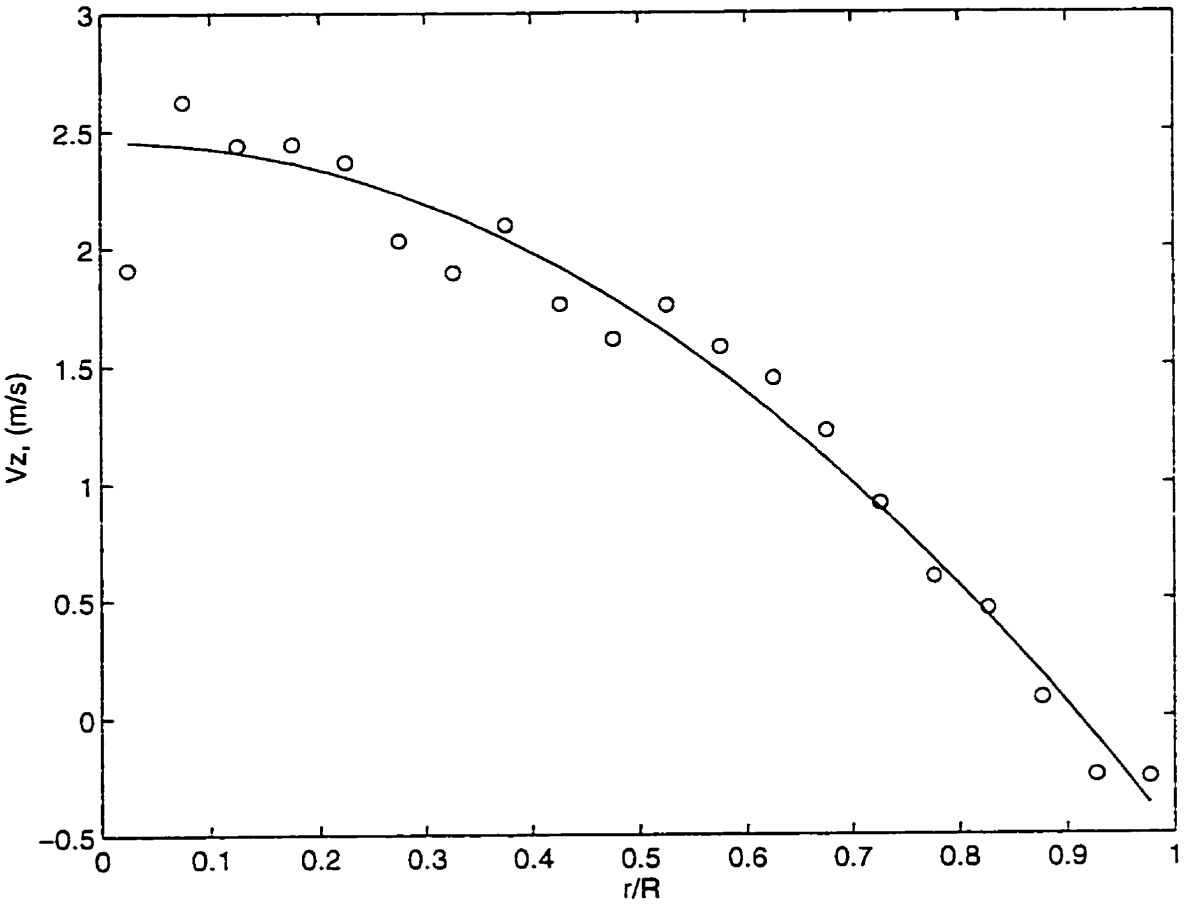

Figure 3.4 Mean axial velocity profile.

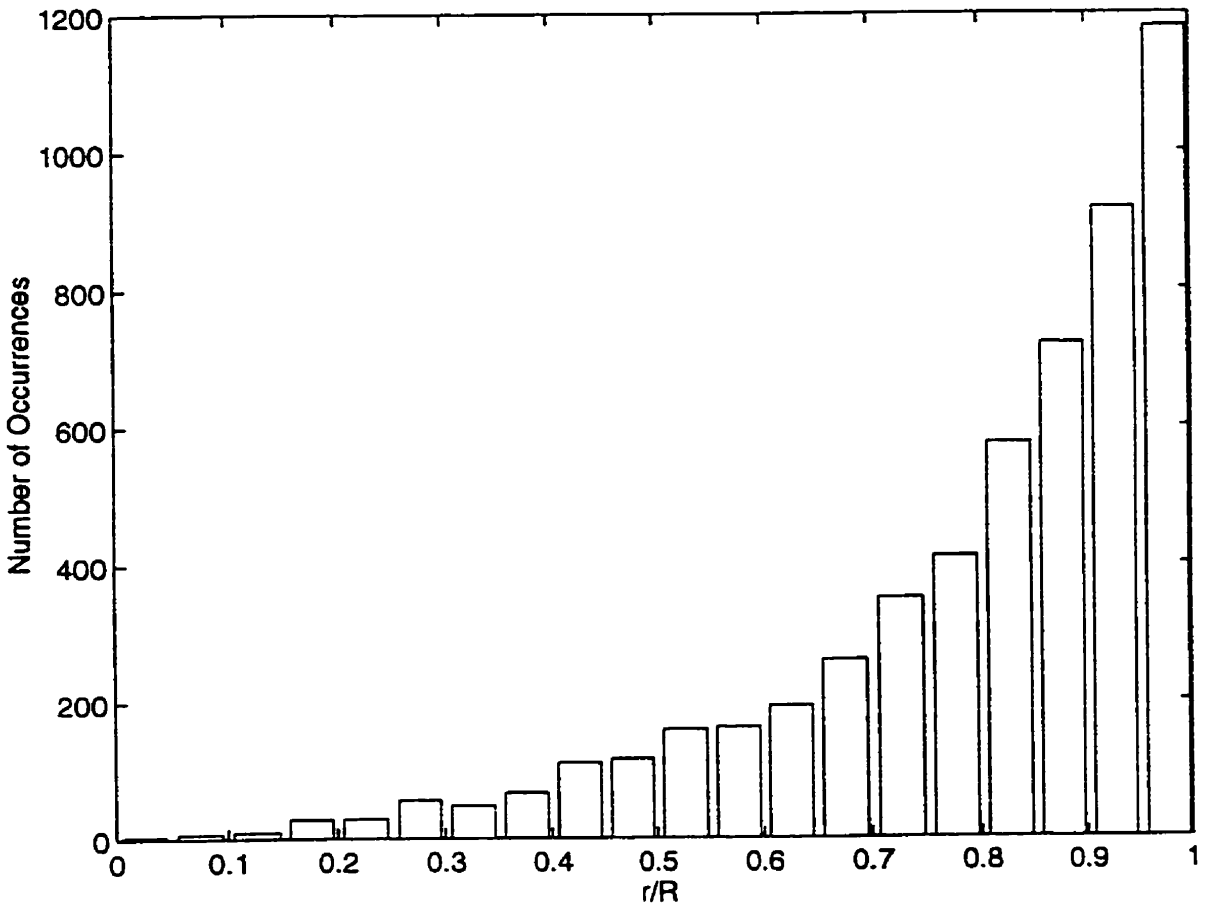

Figure 3.5 Number of occurrences of axial velocity measurement.

CHAPITRE 4 ANALYSE DU MOUVEMENT D'UNE PARTICULE TRAÇANTE DANS UN LIT FLUIDISE CIRCULANT

4.1 Sommaire

Le but de ce chapitre est de présenter et d'analyser les résultats du mouvement d'une particule traçante dans un lit fluidisé circulant. Le chapitre 2 a permis de choisir le meilleur radio-isotope et le chapitre 3 a permis de démontrer l'applicabilité de la technique de poursuite d'une particule radioactive au lit fluidisé circulant. Ce chapitre se concentre sur l'analyse des résultats du mouvement de la particule traçante dans un lit fluidisé circulant.

Ce chapitre est le plus original de la thèse puisqu'il apporte une contribution unique aux mesures hydrodynamiques des solides dans un lit fluidisé circulant. Il répond à l'un des objectifs généraux du projet de recherche, celui de privilégier une approche locale. L'article discute des profils et des fluctuations de vitesse. L'analyse des fluctuations de vitesse est particulièrement intéressante pour les chercheurs développant des modèles hydrodynamiques complexes basés sur la résolution des équations du mouvement.

Plusieurs conclusions ont été tirées de cette étude :

- Du point de vue hydrodynamique, on observe une diminution de la vitesse axiale des solides avec une augmentation du taux de circulation à vitesse de gaz constante. La diminution de la vitesse axiale sur toute la section est attribuée à la formation d'agrégats. Les agrégats sont formés d'un ensemble de particules ayant une vitesse terminale plus importante que celle d'une particule simple et leur vitesse est plus faible.

- L'analyse des fluctuations de vitesse a permis de démontrer que celles-ci diminuent légèrement avec un rayon croissant. Cette analyse a également permis de démontrer que l'écoulement n'est pas isotrope, surtout près de la paroi.

- Enfin, l'analyse des fluctuations de vitesse a également permis d'évaluer le coefficient de dispersion de turbulence axiale (turbulent dispersion coefficient). Ce dernier diminue avec une augmentation du taux de circulation des solides. Cette diminution est liée à la diminution des fluctuations des vitesses axiales.

4.2 Texte de l'article

Position and Velocity of a Large Particle in a Gas/Solid Riser Using the Radioactive Particle Tracking Technique.

L. Godfroy*, F, Larachi▼, J. Chaouki* and G. Kennedy†

*Dept. Chem. Eng., †Dept. Mech. Eng., École Polytechnique de Montréal,

C.P. 6079 succ. Centre-Ville, Montréal, Québec, Canada, H3C 3A7

▼Dept. Chem. Eng. Université Laval, Sainte-Foy, Québec, Canada, G1K 7P4

4.2.1 Abstract

The flow behavior of the solids phase in the fully developed region of a laboratory-scale circulating fluidized bed riser was studied using an assembly of sixteen NaI detectors to determine the position of a 500 μm radioactive particle, 100 times per second. The particle location was inferred from the number of γ-rays recorded by the assembly. The knowledge of the instantaneous positions enables the determination of the instantaneous and mean velocity fields. Tests were conducted in a 0.082 m diameter, 7 m tall riser using 150 μm silica sand particles. Data were obtained at a gas superficial velocity of 4 m/s and solids mass fluxes in the range of 23 to 75 kg/m^{2}s. Radial profiles of axial particle velocity show that the solids velocity decreased with an increase in solids circulation. Correspondingly, turbulent particle velocities and solids dispersion coefficient in the longitudinal direction were found to decrease as the solids circulation rate increased. The cross-sectional area where, in average, solids downflow takes place increased with an increase in solids circulation rate.

Keywords: particle motion, circulating fluidized bed, turbulence, Radioactive Particle Tracking

4.2.2 Introduction

Gas/solid contactors are extensively employed in various industrial applications related to the chemical, petrochemical and metallurgical industries, in the manufacture of fine powders and ceramics, in combustion and in environmental remediation. One specific type of gas/solid reactors, the circulating fluidized bed (CFB), is finding broad applications in many industrial processes because of its intrinsic properties such as efficiency, operational flexibility and overall profitability. CFBs are widely used for the combustion of coal in power stations as well as for heavy oil cracking in the petroleum industry. A number of new applications of CFBs are expected in the near future according to the recent reviews by Berruti *et al.* (1995) (Annexe I) and Grace *et al.* (1997).

Quantification of the flow patterns and backmixing is essential for proper design and scale-up of CFB risers. Existing models often suffer from a lack of pertinent experimental data for model validation. The gas/solid flow in the CFB riser is characterized by a strong heterogeneity. Yet, experimental investigations have demonstrated that the solids distribution is nonhomogeneous in both axial and radial directions in the CFB riser. For example, the nonhomogeneous character of the solids distribution in the axial direction was attributed to the acceleration of particles entering with low velocities at the bottom of the riser. Harris *et al.* (1994) and Grace (1996) have also shown that the riser exit geometry may have an impact on the gross hydrodynamic behavior of the riser. The nonhomogeneous solids distribution in the radial direction, a less well understood subject, may cause significant downflow of particles near the wall (Nieuwland *et al.*, 1996a). As outlined by Sinclair and Jackson (1989) and Pita and Sundaresan (1993), the solids lateral segregation may be the cause of the nonhomogeneity. According to Sinclair and Jackson (1989), the central problem in constructing a satisfactory model for riser systems is to understand the mechanism that gives rise to lateral particle segregation.

Gas-solid flows satisfy the principle of mass, momentum and energy balances. While the Navier-Stokes equations govern the motion of the gas phase, there is yet no universal

agreement on how to describe the particulate phase. One approach, called the two-fluid model, treats this phase as a continuum and uses some form of averaging of the balance equations together with closure and constitutive relationships. The essential features of gas-particle flows can indeed be captured by solving the continuity and the momentum balance equations for the two phases and the pseudo-thermal energy balance equation for the solids. The terms involved in the balance equations and terms appearing in the closure equations are described in detail by Lun *et al.* (1984), Johnson and Jackson (1987), and Ding and Gidaspow (1990). The hold-up, pressure and velocity of both phases are the basic variables. For such an approach to be successful, it is essential to measure these basic variables for model validation. Although sustaining research efforts have lead to precise determination of the gas-phase variables, those for the solids were less easy to obtain due to the difficulty of probing the particulate phase.

This work describes the very first application of the radioactive particle tracking (RPT) to study the non-invasively 3-D movements of a single radioactive tracer in the riser section of a CFB. This tracer consists of a 500 μm particle evolving among a solids inventory made of 150 μm sand particles. Analysis of the 3-D trajectories in the Eulerian and Lagrangian framework gave access to mean advective and turbulent velocity profiles, axial dispersion coefficients, residence time distributions, Lagrangian autocorrelations and macroscale times, etc.

4.2.3 Measurement of Solids Velocities in CFB

Oki *et al.* (1978) described and compared various methods for measuring local particle velocities as presented in table 4.1. Even though a large number of papers have been published recently on the improvement of various methods, measuring principles have been known for a long time. The RPT technique used in this work is not an exception. Kondukov *et al.* (1964) recorded continuously the particle positions in a fluidized bed using six scintillation detectors fixed in pairs along three mutually perpendicular axes. Using calibration curves, the signals received by each pair of detectors were used to

calculate the tracer particle coordinates. Lin *et al.* (1985) improved the signal processing scheme utilizing the redundancy of signals to increase accuracy by reducing the influence of intrinsic noise due to the quantized nature of gamma emission. The Radioactive Particle Tracking (RPT) technique developed by Larachi *et al.* (1994) was in principle similar to that of Lin *et al.*(1985) but it yielded improved spatial resolution owing to a phenomenological model that was incorporated to describe the interactions of the γ-rays with the vessel geometry. Thorough descriptions of the RPT are provided elsewhere (Larachi *et al.*, 1994) and will not be given here. In the present study, we determine the particle motion in a circulating fluidized bed using sixteen scintillation detectors at a sampling interval of 10 ms. Time differentiation of the displacements yields the local instantaneous velocities. Correspondingly, ensemble-averaged velocity distribution and turbulence quantities can be computed after acquiring data for a sufficient length of time. As far as we know, the continuous recording of the particle position in a circulating fluidized bed riser in a full three-dimensional field has not been reported previously. Other successful approach towards the understanding of complex multiphase flows using non-invasive monitoring technique have been recently presented by Chaouki *et al.* (1997)

4.2.4 Circulating Fluidized Bed Riser and RPT Facility

The CFB hydrodynamic is studied in a cold flow CFB unit which is shown in Figure 4.1. Sand particles (d_p=150 μm, ρ_p=2600 kg/m^3) are air-fluidized in a tall (7 m) riser. The riser column is comprised of seven sections of schedule-10 stainless-steel pipe 1 m long and 0.082 m in diameter joined with flanges. The solids are fed symmetrically via an annular moving dense bed into the riser column through 4 orifices (D_{or}=4.8 cm) located in the riser wall, 15 cm above the air distributor (annexe III). The bottom of the riser is surrounded by a 2 m high dense moving bed in which particles are slowly moving downwards. The solids flux is controlled by the amount of air fed into the dense moving bed. At the exit of the riser column, two cyclones separate the particles from the fluidizing air. The particles are recirculated back to the dense moving bed at the bottom of the riser through a flexible galvanized steel pipe (D_{return}=70 mm). The solids circulation rate is determined from the

weight of solids collected over a short period of time after closing a butterfly valve located on top of the dense bed.

Figure 4.2 shows the arrangement of the detectors around the CFB riser. The detectors of the RPT system are arranged in helix, with 90° spacing between two consecutive detectors. The RPT system is located in the fully developed region, 4 to 5 m above the distributor. The detector arrangement offers the advantage that where ever the tracer is, there are several detectors nearby providing a good sensitivity and a good spatial resolution. Data recording by the sixteen detectors begins when a particle moving upwards is detected in the lower part of the riser. A 17th detector located 2.5 m above the distributor is connected to a stand-alone personal computer timing system, and triggers simultaneously the sixteen detectors for data acquisition each time a count-rate threshold is exceeded. After each passage of the tracer particle, the RPT system is in a waiting mode until triggered by another passage of the tracer.

For the open configuration used here, an experiment in the riser of the CFB results in the determination of 15,000 instantaneous positions. The useful time, which could be defined as the time the particle spends passing through the RPT system, is very small compared to the duration of an experiment, typically 0.25% of the total experimental time.

4.2.5 Tracer Preparation

The radioactive particle is made of a mixture of epoxy resin and fine pure gold powder (<2 μm). Gold powder and epoxy are mixed together in proportions which give a mixture density equal to that of sand (ρ_p=2600 kg/m^3). After hardening, a piece of the mixture is cut and hand-rounded to make a 500 μm (±20 μm) particle. The particle contains approximately 50 μg of gold (^{197}Au). The particle is coated with a very thin layer of hard super-glue to make it attrition-resistant. It is activated in the École Polytechnique SLOWPOKE nuclear reactor for 32 h at a neutron flux of $5*10^{11}$/cm^2. It should be noted that the tracer particle is not exactly representative of the bulk material (150 μm sand) and

work continues on reducing the size of the tracer until it reaches that of fluidized particles. Finer particles could be made but the relatively low amount of Au would necessitate a longer activation time or a higher neutron flux which is not achievable at the present time. The tracer particle has an activity of 100 μCi (±0.7 μCi) of ^{198}Au which emits 412 keV γ-rays.

4.2.6 Spatial Resolution

The spatial resolution of the particle tracking system is described in terms of the standard deviation σ_x, σ_y and σ_z of the statistical distributions of the determined coordinates x, y and z as was shown by Godfroy *et al.* (1997a). It is possible to predict the resolution theoretically from the model developed by Larachi *et al.* (1994). The spatial resolution is computed from algebraic manipulation of the directional partial derivatives of the counts with respect to position. For a sampling period of 10 ms with a 100 μCi ^{198}Au source and a sixteen detector assembly, the average x,y resolution (σ_x, σ_y) is 3.5 mm and the average axial resolution (σ_z) is 4.3 mm.

4.2.7 Results and Discussion

4.2.7.1 Motion of the particle

The discussion which follows is concerned with the movement of a large 500 μm tracer among 150 μm sand particles. Figure 4.3 presents an example of the continuous motion within the various zones of the riser of the marked particle. The flow directions in these zones are such that particles are transported upwards with the gas in the core zone (Figure 4.3.a), whereas in the wall region the particles move downwards (Figure 4.3.b). An average Lagrangian downward velocity can be calculated from each segment of trajectory where the particle is moving downwards, irrespective of the position in the x,y plane. The distribution of downward Lagrangian velocity is presented in Figure 4.4. The maximum frequencies are close to -1 m/s and the average is -1.4 m/s. This average velocity is fairly constant and is equal to -1.4 m/s at a mass flux in the range of 23-75 kg/m^{2}s for a constant gas velocity (U_g=4 m/s).

Contrary to the downward motion, the average Lagrangian velocity of a particle traveling upwards decreases slightly as the solids circulation rate increases. The average upward velocity is 2.08 m/s at $G_s = 23$ kg/m^{2}s and 1.86 m/s at $G_s = 75$ kg/m^{2}s.

Also during its motion, the particle exhibits fluctuating radial movements. These radial fluctuations are less marked during upward motion than during downward motion. Apparently, a weak radial mixing predominates in the core. As Figure 4.3.b shows, the particle may travel long and uninterrupted distances downwards contributing to a significant backmixing of the solids in the wall region. In general, the trajectory of the particle in the wall region is characterized by rapid changes from positive to negative velocities. At some location, the particle may re-enter the dilute core phase where upflow predominates and move upwards. As shown by Zethraeus (1996), the gas shear stress at the core-annulus boundary may be the cause. Sometimes, the particle is transported from the core zone towards the wall due likely to intermittency in the wall boundary layer as defined by Brereton and Grace (1993). The tendency to concentrate in the wall region is shown clearly by the radial distribution of the normalized occurrences per unit horizontal area in Figure 4.5. These occurrences may be thought of as a residence time mapping or stagnancy mapping of the tracer passages per pixel. It is also indicative of the radial profile of normalized solids hold up in the CFB riser section. The local void fraction could not be estimated only from the RPT technique. The RPT technique shows only how solids are radially distributed and requires the cross-sectionnally average solids hold-up for estimation of the local solids hold-up. The average solids hold-up could be calculated from pressure drop measurements assuming that the time average pressure drop is attributable only to the hydrostatic head of solids. As should be expected, the occurrence profile presented in Figure 4.5. is flat in the core and increases toward the wall. Interestingly, the normalized radial stagnancy profiles do not seem to depend on the solids circulation rate, and are very akin to the universal solids hold-up profiles already reported by Zhang *et al.* (1991) and Rhodes *et al.* (1992b).

4.2.7.2 Axial Velocity Profile

The motion path data, illustrated in Figure 4.3, are converted into instantaneous and average particle velocities in the three directions of space. For the purpose of calculating velocity profiles, the column is divided into 20 compartments in the radial direction. Details of the Eulerian velocity calculations are described by Dudukovic *et al.* (1991).

For each radial compartment, and consistent with flow axisymmetry in the riser, the measured average radial and azimuthal velocities are near zero and none were indeed found to differ significantly from zero. Typical profiles for the radial variation of axial particle velocity are shown in Figure 4.6 for test conditions of constant gas superficial velocity (U_g=4 m/s) and solids mass flux in the range 23 kg/m^{2}s $\leq G_s \leq$ 75 kg/m^{2}s. Note that it was found that 250 instantaneous velocity measurements were sufficient to ensure that the average cumulative velocity is within 5% of its asymptotic value. Thus the accuracy is always better than 5% for reduced radius (r/R) greater than about 0.4. The shapes of the profiles are consistent with those reported by other workers (Bader *et al.* (1988); Harris *et al.* (1994), Yang *et al.* (1993)). The axial velocities ($v_z(r)$) vary considerably with radial position and models predicting those variations are emerging (Godfroy *et al.* 1997b). The shapes are approximately parabolic near the wall. In the center, the velocity profiles flatten and diverge from the parabolic trend. There, the particle velocity was found to be of the order of the gas superficial velocity. This seems to be different from the finding of Bader *et al.* (1988) who measured particle velocities using a sampling probe. Bader *et al.* (1988) reported particle velocities in the center of the riser to be 2 to 3 times the superficial gas velocity under similar conditions (U_g=3.7 m/s, G_s=98 kg/m^{2}s) in a 30.5 cm diameter riser with 76 μm FCC catalyst. Harris *et al.*(1994) measured the radial variation of the 60 μm FCC grain volume fraction and velocity using iso-kinetic and Pitot tubes, and reported that, in the center, the particle velocity was approximately twice the gas superficial velocity (U_g=4.4 m/s) for various solids circulation rates (26 kg/m^{2}s$\leq$Gs$\leq$52 kg/m^{2}s) in a 0.14 m diameter riser. Similarly, Tanner *et al.*

(1994) measured solids velocity and concentration profiles using optical probes, and reported a particle velocity in the center of about 7 m/s (U_g=4.5 m/s, G_s=78 kg/m^{2}s, D_{riser}=.41 m, d_p=110 μm, ρ_p=2500 kg/m^3). The behavior of a large tracer particle embedded in a clump of smaller particles is expected to differ from that occurring with a monodispersed lot of particles. It is intuitive that particle inertia is a major cause for the discrepancies in particle velocities observed between the present study and those of the other authors. Therefore the differences between the measured axial particle velocity in this study and those observed by other authors are significant, especially in the core region.

Fully developed flow of the velocity profile presented in Figure 4.6 could be verified by plotting the axial velocity as a function of height as shown in Figure 4.7 and 4.8. Those plots also show that instantaneous velocities are evenly distributed among the mean and do not vary with height. Also shown in Figure 4.7 and 4.8 are the line corresponding to the average velocity plus and minus the root mean square velocity as will later be defined by Equation 4.

In addition, the results in Figure 4.6 show that the velocity in the fully developed zone of the riser decreases with an increase in solids circulation rate. This interesting result is explained by the presence of clusters. For a given gas velocity and low solids circulation rate, the particles tend to move independently from one another, and the local slip velocity between the gas and the particles is close to the particle terminal velocity. As the solids circulation rate increases, the flow becomes denser and particle-particle interactions are no longer negligible and the tendency to form clusters increases. This tendency occurs even at low solids circulation rate as found by Horio *et al.* (1993) using a laser sheet technique. These clusters move with a higher slip velocity than the particle terminal velocity. The slip velocity may be many times larger than the single particle slip velocity. Bai *et al.* (1995) reported slip velocities of up to four times the terminal velocity at conditions similar to ours. The tendency to form clusters increases with increasing solids circulation rate.

Figure 4.6 shows that the wall region gets thicker with an increase in solids circulation rate, and that the absolute values of the velocities are higher (≈0 at G_s=23 kg/m^{2}s and 0.25 m/s at Gs=75 kg/m^{2}s). These higher absolute wall velocities should not be confused with the constant Lagrangian downward velocity (-1.4 m/s). The former velocities are ensemble-average (Eulerian) velocities and the later velocity is calculated from an average on each segment of trajectory where the particle is moving downwards. Figure 4.6 also indicates that a significant part of the particles near the wall may move upwards, especially at low solids circulation rates.

Note that for one experiment the particle velocity at the wall is slightly positive. At first sight, this observation might be surprising. Because the gas velocity is zero at the wall, one might expect the particles to fall. In fact, there is a region near the wall where the particles can acquire a velocity higher than that of the gas. This effect is due to the shear stress in the particle phase. Particles further from the wall are lifted by the gas and, through collisions, transfer momentum to particles closer to the wall (Louge *et al.* 1991). As stated by Pita and Sundaresan (1993), it is essential that a dense region of particles develops in the vicinity of the wall to yield downflow of particles there.

The experimental velocity profiles (Figure 4.6) suggest that the concept of a sharply defined core/annulus boundary with one-dimensional flow on either side of this boundary is an oversimplification. The velocity profiles are smooth rather than having a sharp transition at a core/annulus boundary. Similar conclusions are also suggested from reactant concentration profiles (Grace and Lim, 1997).

It is difficult to model the velocity profile obtained in this study because no model exist to predict the behavior of a large tracer particle embedded in a clump of smaller particles. Recently, Godfroy *et al.* (1997b, Chapitre 1) have submitted a fully predictive semi-empirical model for radial hydrodynamic in risers. The model predicts the radial profiles of

gas and particles velocity, solids concentrations, solids mass flux and the axial pressure drop profile.

The key parameter in the model is estimated from the slip factor correlation proposed by Patience *et al.* (1992). The slip factor is the ratio of the actual gas velocity to average particle velocity.

$$\psi = (U_g / \bar{\varepsilon}) / V_p \qquad (1)$$

where ψ is the slip factor, $\bar{\varepsilon}$ is the average void fraction and V_p is the average axial particle velocity. This ratio is about 2 at different operating conditions (Matsen 1976).

Calculated values of the slip factor are presented in Table 4.2. The experimental slip factor is calculated with the average axial particle velocity from Figure 4.6 and with void fraction assuming that the time averaged pressure drop is attributable only to the hydrostatic head of the solids. The hydrodynamic model assumes that the slip factor is not a function of solids circulation rate whereas the experimental results show the opposite. The slip factor is close to 2 for experiments at mass fluxes of 23 and 33 kg/m^{2}s. Thus for those conditions, model predictions are adequate. The slip factor correlation presented by Patience *et al.*(1992) should be revised to account for a change in the slip factor with solids circulation rate. Further details on the model are not presented here for brevity.

4.2.7.3 Analysis of Particle Velocity Fluctuations

Root Mean Square (RMS) velocities, calculated from RPT, are made up of two parts : RMS due to the hydrodynamics and RMS due to the noise associated with measurement error. Statistical fluctuations in γ-ray count rates cause uncertainty in the particle coordinates and thus in the derived velocities (Moslemian 1987).

$$V^2_{\alpha,\text{rms with noise}} = V^2_{\alpha,\text{rms hydro}} + V^2_{\alpha,\text{rms noise}} \qquad (2)$$

The noise component is given by the following equation :

$$V_{\alpha,rms\ noise} = \frac{\sqrt{2}\,\sigma_\alpha}{P} \tag{3}$$

where σ_α is the standard deviation in the instantaneous measurement of the α coordinate of the particle position, P is the sampling period. Details of the calculation of σ_α can be found elsewhere (Godfroy *et al.*, 1997a). Finally, the genuine hydrodynamic component of the root mean square velocity is computed as:

$$V_{\alpha,rms} = \sqrt{V^2_{\alpha,rms\ with\ noise} - \left(\frac{\sqrt{2}\,\sigma_\alpha}{P}\right)^2} \tag{4}$$

Some sample curves of the distribution of particle velocity fluctuations in streamwise and in cross-stream directions are shown in Figures 4.9 and 4.10. The particle RMS velocities in the cross-stream direction are smaller than that in the streamwise direction. This behavior occurs due to the quasi-unidirectional trajectories of particles. This conclusion is important for modelers. For example, Jenkins and Savage (1983) in their original kinetic theory model of cohesionless granular material assumed the magnitude of the velocity fluctuations to be constant and equally likely in all directions (isotropy). We see here that the constancy of the axial velocity fluctuations is a good assumption (homogeneous turbulence), but the fluctuations are not equally likely in all directions; the turbulent motion is not isotropic. An anisotropy coefficient (AC) may be computed to quantify the degree of anisotropy between axial and radial direction :

$$AC = \frac{v^2_{r,rms}}{v^2_{z,rms}} \tag{5}$$

Radial profiles of AC are presented in Figure 4.11. There is a tendency for AC to increase at the center of the riser (tendency toward less anisotropy). AC is approximately 0.35 in the core of the riser and decreases rapidly in the wall region due to the low value of the radial RMS velocity. Kinetic theory would greatly benefit from clarifying the questions of

what assumptions must be abandoned or what ingredients must be added in order to improve the theory and to extend it to a realistic description of the CFB flow phenomena.

4.2.7.4 Autocorrelation and Axial Dispersion Coefficient

It seems that very little is known about the particle velocity autocorrelation in a CFB riser. To quantify the statistical behavior of the particle motion, the autocorrelation of the fluctuating velocities has been evaluated. The correlation between the values of the fluctuating velocity at two different times is referred to as the autocorrelation. The Lagrangian autocorrelation function is defined as :

$$f_{\alpha\alpha}=\frac{\langle v'_\alpha(t)\quad v'_\alpha(t+\tau)\rangle}{\langle v'_\alpha\rangle^2} \tag{6}$$

where $\langle\rangle$ denotes the ensemble average and v'_α is the α-component of the instantaneous fluctuating velocity. The fluctuating velocities were obtained by subtracting the mean (or ensemble average) $\overline{v_\alpha(r)}$ from their respective instantaneous velocities $v_\alpha(r,t)$.

$$v'_\alpha(t)=v_\alpha(r,t)-\overline{v_\alpha(r)} \tag{7}$$

The autocorrelation function decreases as the time lag, τ, increases if the velocities $v'_\alpha(t)$ and $v'_\alpha(t+\tau)$ become less correlated with increasing lag time. As defined in Eq. 7, and Eq. 6, $v'_\alpha(t)$ is not a function of the radius but is only a function of the time. The autocorrelation function thus computed represents an average over the whole field of view.

As shown in Figure 4.12, the axial autocorrelation function decays slowly suggesting a strongly correlated flow. Within the limits of experimental scatter, the autocorrelation function always decay monotony. The correlation is stronger at the low solids circulation rates compared to the higher circulation rate. This is due to higher particle-particle interactions at a high solids circulation rate. The particle travels a shorter distance before colliding with another particle or a cluster resulting in a lost of autocorrelation.

The Lagrangian integral time scale is defined as:

$$T_{L,\alpha} = \int_0^{\infty} f_{\alpha\alpha}(\tau)\, d\tau \tag{8}$$

The Lagrangian integral time scale is defined as the zeroth order moment of the autocorrelation function $f_{\alpha\alpha}(\tau)$. At the lower solids circulation rates, the integral was evaluated from $\tau=0$ to $\tau_{5\%}$ where the autocorrelation function reaches the plateau within 5% of error. The axial Lagrangian integral time scales $\left(T_{L,z}\right)$ were not found to vary significantly with solids circulation rate. The average value is 0.25 s the for conditions shown in Figure 4.12.

The Lagrangian integral time scale is used for the determination of the axial dispersion coefficient, $D_{s,z}$. The axial solids dispersion coefficient is given by:

$$D_{s,z} = T_{L,z} \left\langle v_{z,rms}^2 \right\rangle \tag{9}$$

where $\left\langle v_{z,rms}^2 \right\rangle$ is the cross-sectionally averaged root mean square axial velocity illustrated in Figure 4.9. Figure 4.13 shows the variation of the axial solids dispersion coefficient with solids circulation rate. The average value of the axial solids dispersion is 0.85 m^2/s. The dispersion coefficient decreases with an increase in solids circulation rate due to a decrease in turbulent axial velocities. The order of magnitude of the axial dispersion coefficients agrees with Patience (1990) data. Using different sizes of tracer particles, Patience (1990) found an average effective dispersion coefficient of 0.9 m^2/s (ranging from 0.22 to 1.67 m^2/s) under different operating conditions ($4.0 \le U_g \le 6.2$ m/s, $40 \le G_s \le 170$ kg/m^2s) as summarized in Table 4.3.

4.2.7.5 Residence Time Distribution

Each particle path across the RPT system has an attribute which can give information about the internal solids flow characteristics. This attribute is called age and is the time that the particle has spent in the system. The particle trajectories measured by the RPT

technique can be used to compute the Residence Time Distribution (RTD). The particle generally will not remain in the RPT system for exactly the same time for successive passages as particle will follow a different path. Particles have zero age when they first enter at the bottom of the RPT system and acquire age at a rate equal to the time spent within the system boundaries. The injection corresponds to a perfect delta function of tracer particles at the bottom at time t=0. This precision is important because the output curves depends in subtle ways on the exact method used for injecting and detecting the tracer particles (Nauman, 1981). The initial and boundary conditions are important and correspond to a closed system. The residence time distributions are presented in Figure 4.14. Each distribution is calculated based on approximately 250 trajectories across the RPT system. The rapid rising peaks are due to particles rapidly moving up in the core. The highly skewed RTD shows pronounced "tailing" due to pulsating radial movement in some particle paths and the existence of a relatively more stagnant wall region. These observations are consistent with the observations of Patience (1990) who measured the particle residence time distribution by injecting a sample of radioactive particles. When solids circulation rate increases, the peak time increases, the peak height decreases and it gets wider. The fluctuations in the tail of the distribution are due to the relatively small number of observations provided by the RPT technique. It should be noted that the apparent fluctuations in the tail are not due to noise. Those longer residence times have a physical meaning and correspond actually to particle spending a longer time. Curl and McMillan (1966) illustrated the extreme importance of tails in estimates derived from RTD measurements. This is notably the case in the measurement of residence time distributions using a radioactive sample. Another problem arising in general with radioactive sample is from the assumption that the count rate of a detector is proportional to the sectionally averaged concentration of tracer in front of the detector. This assumption is questionable. The count rate of a radioactive detector is especially a function of distance (solid angle) and source activity of the tracer in front of the detector. For example, the count rate over time measured from a weak source moving slowly close to the detector could be the same as a more radioactive source moving with a higher velocity further away from the detector.

This illustrates that different hydrodynamic phenomena could be lumped together when using traditional radioactive method for determining residence time distributions.

4.2.7.6 Modeling of Residence Time Distribution

Interestingly, the RTD could be estimated effectively based on the velocity profile as shown in Figure 4.15. The agreement between the predicted RTD and the experimental RTD is good. Thus, the RTD can effectively be predicted only with the knowledge of the velocity profile. This conclusion is important since many authors have concentrated their effort on measuring RTD and assuming two or more radial zone such as a core-annulus model with mass transfer between the two zones. The results presented here suggest that accurate measurement of velocity profile could be used to estimate RTDs.

The agreement between the predicted RTD and the experimental RTD could be further increased by allowing axial dispersion. Turbulent dispersion is simply added to the velocity profile as a random component of the instantaneous velocity with null average and a standard deviation equal to the axial root mean square velocity determined in Figure 4.9. The predicted RTD is calculated in similar conditions as the experimental RTD. The predicted RTD is calculated by following a large number of particles. All particles are injected at time t=0 at an axial location corresponding to the beginning of region covered by the RPT system (z=0, relative to RTP system). The axial position of each particles is then calculated by following relation :

$$z_{t+\Delta t} = z_t + v_{z\,inst}\,\Delta t \tag{10}$$

where $v_{z\,inst}$ is the instantaneous axial velocity given by :

$$v_{z\,inst} = \overline{v_z(r)} + \text{randn} * v_{z,rms} \tag{11}$$

where $\overline{v_z(r)}$ is the average axial velocity profile calculated from Figure 4.6, $v_{z,rms}$ is the constant axial root mean square velocity determined from Figure 4.9 and randn is a normally distributed random number with mean 0 and variance 1. The exit time of a

particle (or residence time) is determined by the time at which the particle first leave the system at an axial location (z max ≅ 1 m) corresponding to the limit of the RPT system.

The model predictions with axial mixing is presented in Figure 4.15. As expected, the introduction of axial mixing spread the distribution and does not affect the peak time of the distribution .

Radial mixing could be introduced with the same idea behind the development of Equations (10) and (11), allowing particles to change radial component and thus axial average velocity. Figure 4.15 also shows the predicted RTD with radial mixing with the exception that $v_{r,rms}$ is not constant but a function of the radius as estimated from Figure 4.10.

The introduction of radial mixing shift significantly the distribution toward higher residence time. The radial fluctuating velocity (Figure 4.10) is such that particles in the center are allowed to move significant distance radially due its high value. Thus particle in the center could easily reach the wall region. However, when a particle is trapped in the wall region, the fluctuating radial velocity is much lower and do not allow many particles to get back to the center region of the riser. The radial root mean square velocity in the center is probably overestimated in Figure 4.10 ; such a high root mean square velocity would induce a much higher concentration of particle near the wall than experimentally determined in Figure 4.5. Of course axial mixing could also be introduced with radial mixing. Again the effect of axial mixing is to spread the distribution and lower the peak height.

4.2.8 Conclusion

The axial particle velocity was found to decrease with increasing solids circulation rate which was attributed to the presence of clusters. The wall region where particle velocities

are negative grows in size with increasing solids circulation rate. However, since the tracer used in this work is larger than bulk particle, its physical properties influence the observed flow pattern.

The analysis of the root mean square velocities shows that the solids flow is not isotropic and that the axial solids dispersion coefficient decreases with increasing solids circulation rate. The average axial solids dispersion coefficient was found to be 0.85 m^2/s.

The residence time distribution of solids could be estimated based only on the average axial velocity profile. Thus, models predicting radial variation of axial solids velocity are helpful for predicting residence time distributions. However, improved estimation of the residence time distribution could be obtained by adding axial mixing. The axial mixing is added as a superimposed velocity fluctuating component to the axial velocity profile. This fluctuating component was found to be constant over the cross-section of the riser and vary with operating conditions.

Table 4.1 Various methods of measuring the velocity of particles (after Oki *et al.* 1978)

	Method		Principle	Detector or device	Measured velocity
I	Drag force method	a	Conversion of mass flow rate variation into the variation of the strain of a small object	Piezoelectric crystal transducer	Linear velocity Mass velocity
		b	Conversion of mass flow rate variation into the rotation rate of a small impeller	Rotation rate to frequency conversion device Digital counter	Mass velocity Linear velocity
II	Heat transfer method		Conversion of mass flow rate variation into the variation of heat transfer rate	Thermister Integrator	Mass velocity
III	Tracer method	a	Measurement of a track of radioactive isotope tracer	Scintillation counter	Linear velocity
		b	Measurement of a track of radiopill tracer	Radiopill Aerial coil Radio receiver	Linear velocity
IV	Correlation method		Statistical determination of the transit time of particles between two fixed points	Optical fiber Light detector	Linear velocity

Table 4.2 Calculated values of the slip factor (U_g=4m/s)

G_s (kg/m^{2}s)	V_p (m/s)	$\bar{\varepsilon}$	$\psi = (U_g / \bar{\varepsilon}) / V_p$
23	1.82	.9935	2.2
33	1.58	.9922	2.6
42	1.23	.9898	3.3
75	.83	.9814	4.9

Table 4.3 Effective dispersion coefficient (after Patience 1990)

U_g (m/s)	G_s (kg/m^{2}s)	d_p (mm)	D (m^2/s)
4.1	42	108	0.57
4.1	50	275	0.43
4.3	45	275	0.39
4.3	40	513	0.22
6.0	70	275	0.90
6.1	70	275	0.92
5.8	99	275	1.12
5.9	99	275	1.65
6.2	151	275	1.67
6.1	166	275	1.23

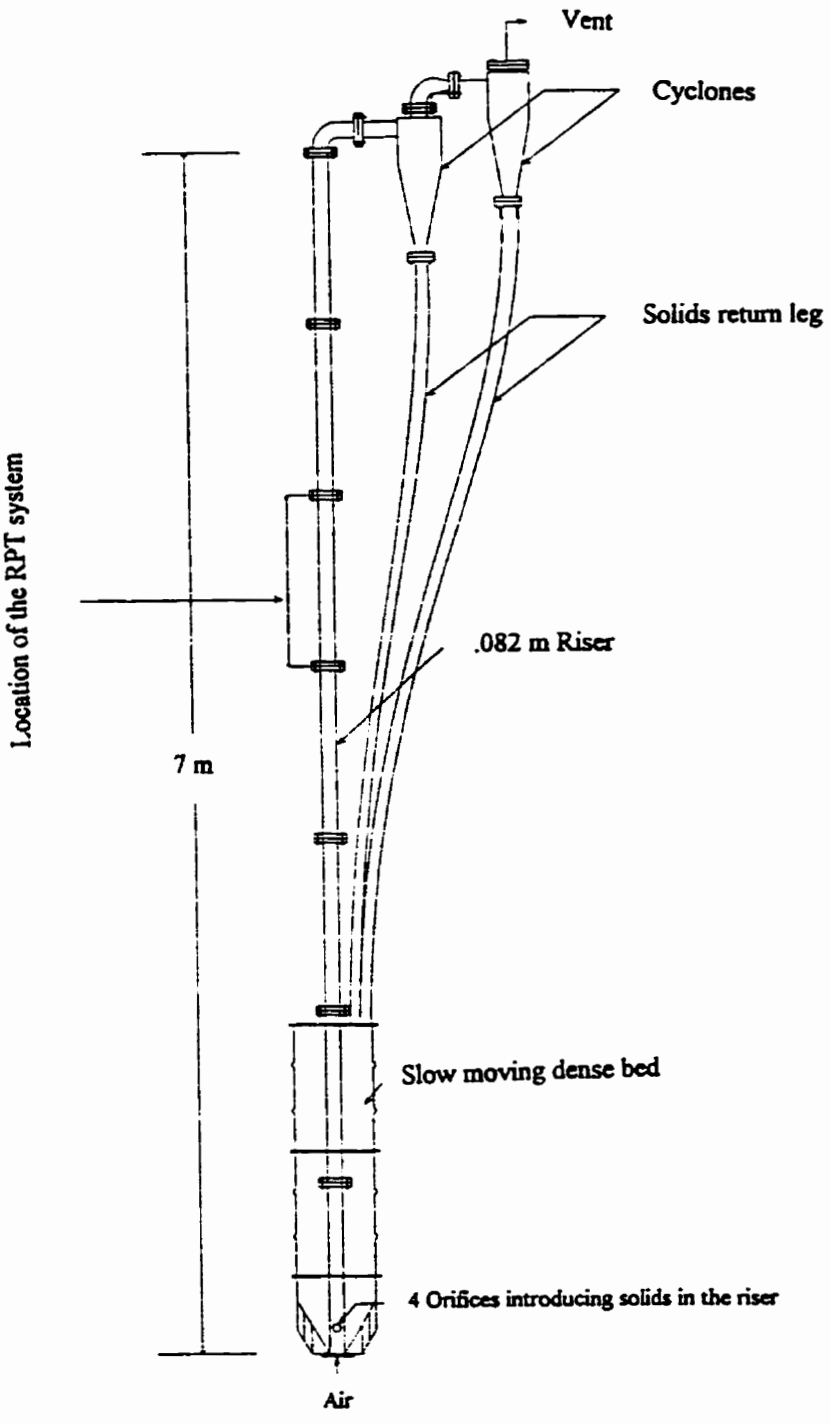

Figure 4.1 Schematic of the circulating fluidized bed apparatus

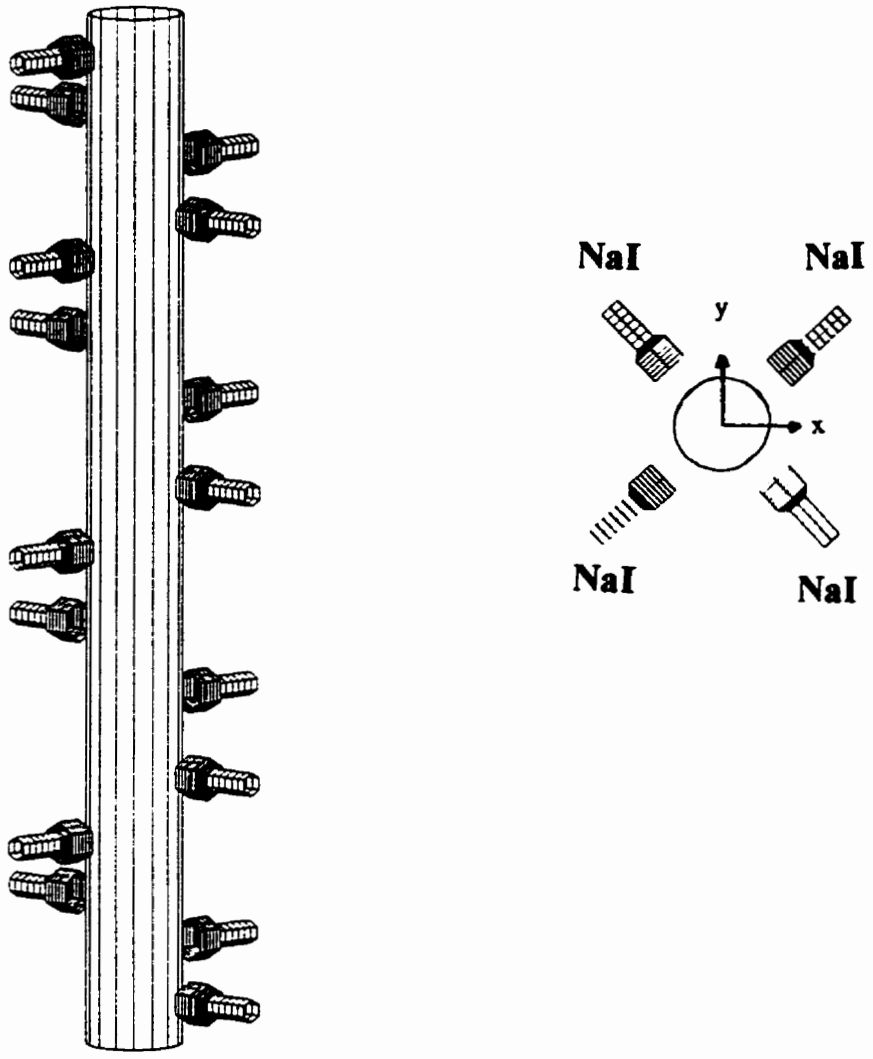

Figure 4.2 Arrangement of the detectors around the CFB riser

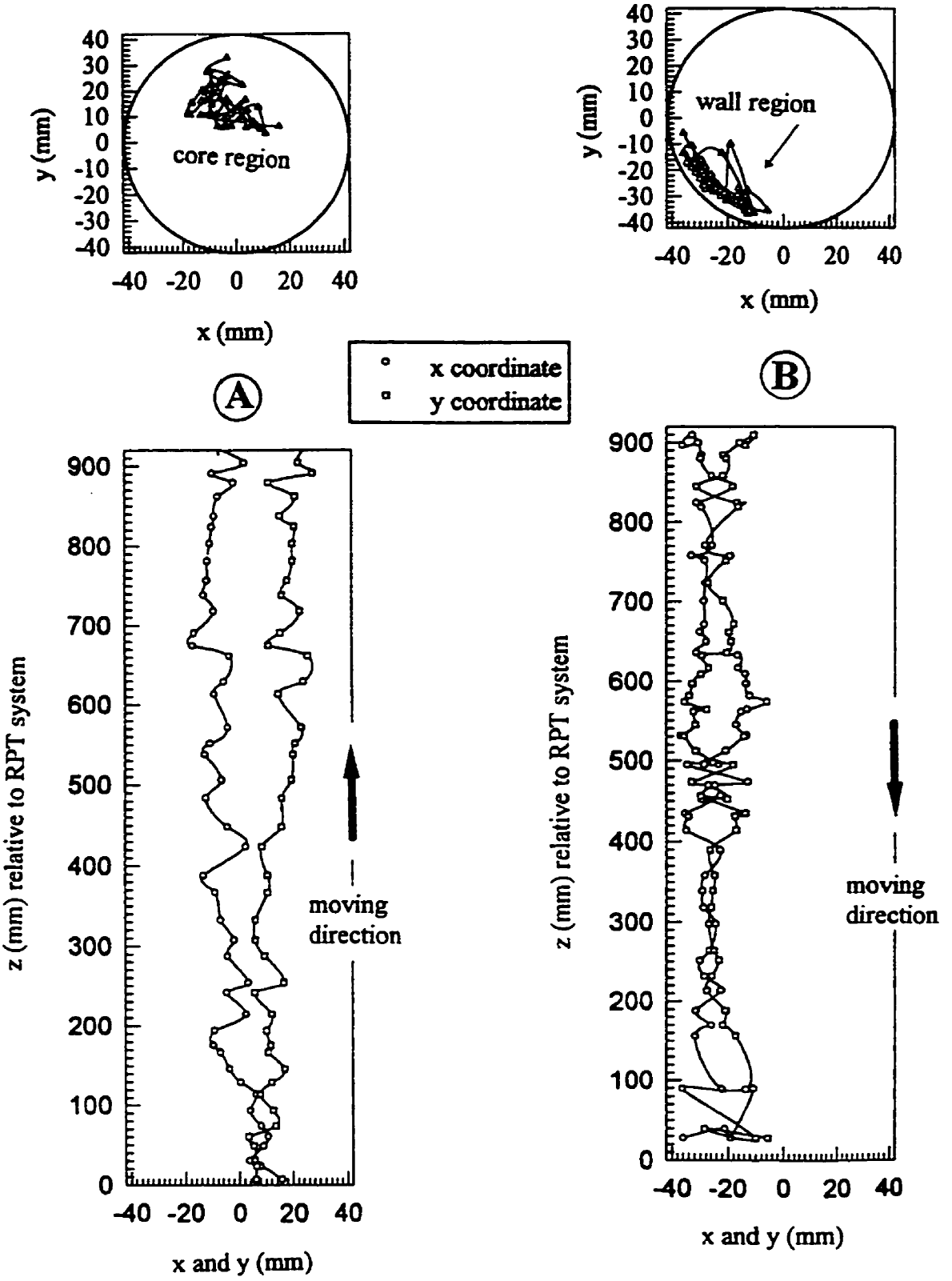

Figure 4.3 Continuous motion path of the marked particle

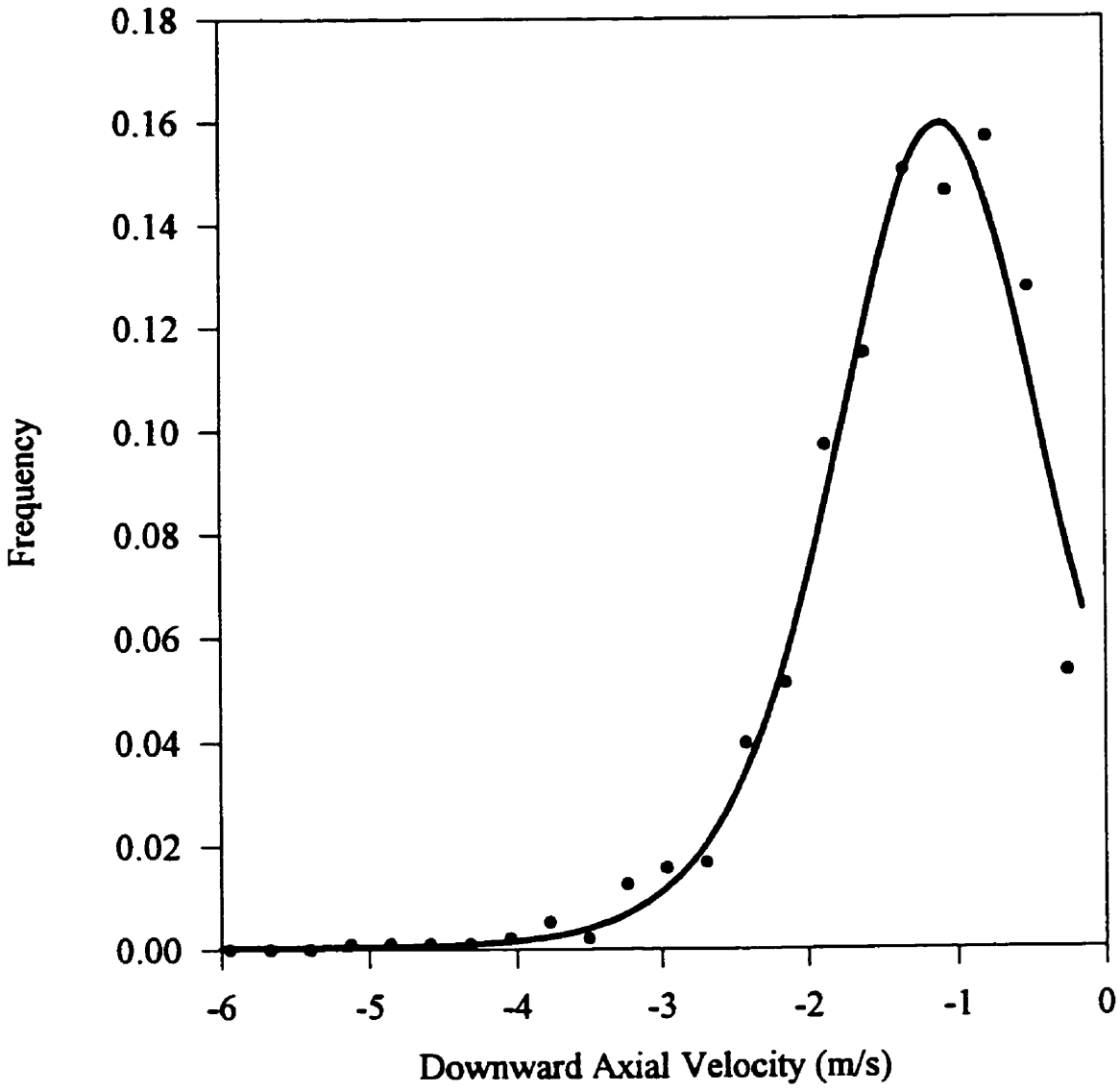

Figure 4.4 Distribution of downward Lagrangian velocity (U_g=4 m/s)

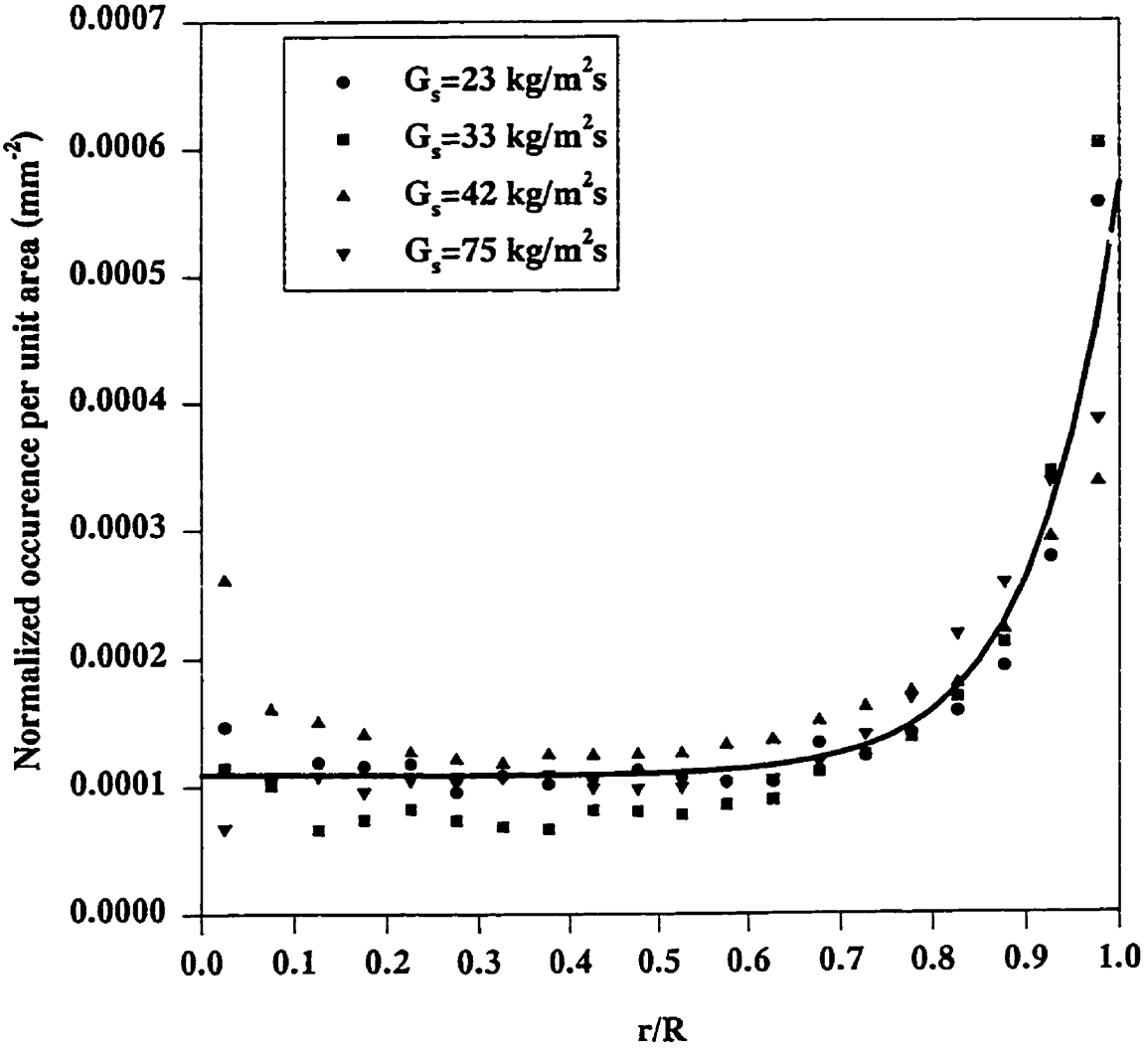

Figure 4.5 Typical occurrences of the location across the section (U_g=4 m/s)

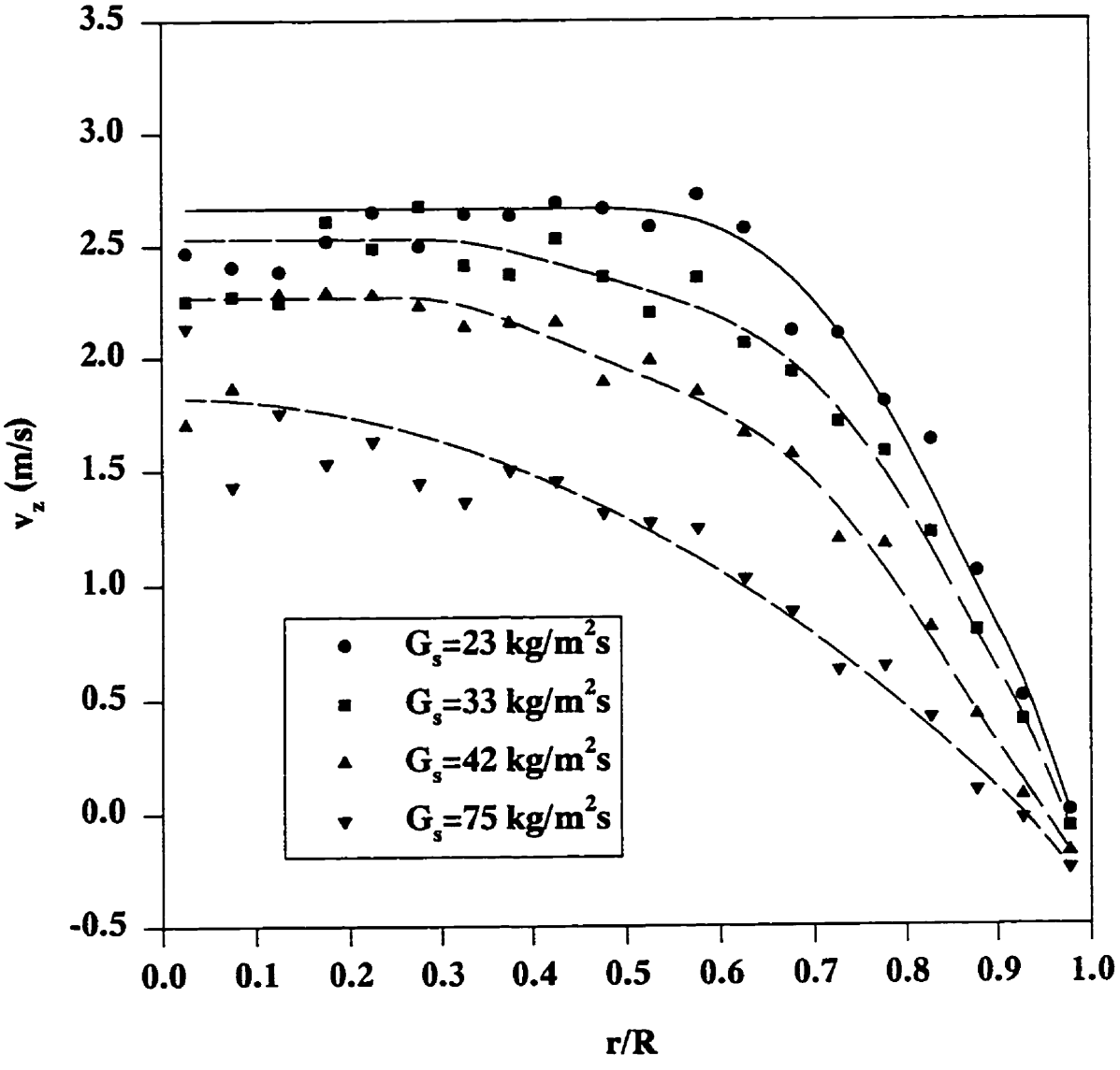

Figure 4.6 Solids velocity profiles $v_z(r)$ (U_g=4 m/s)

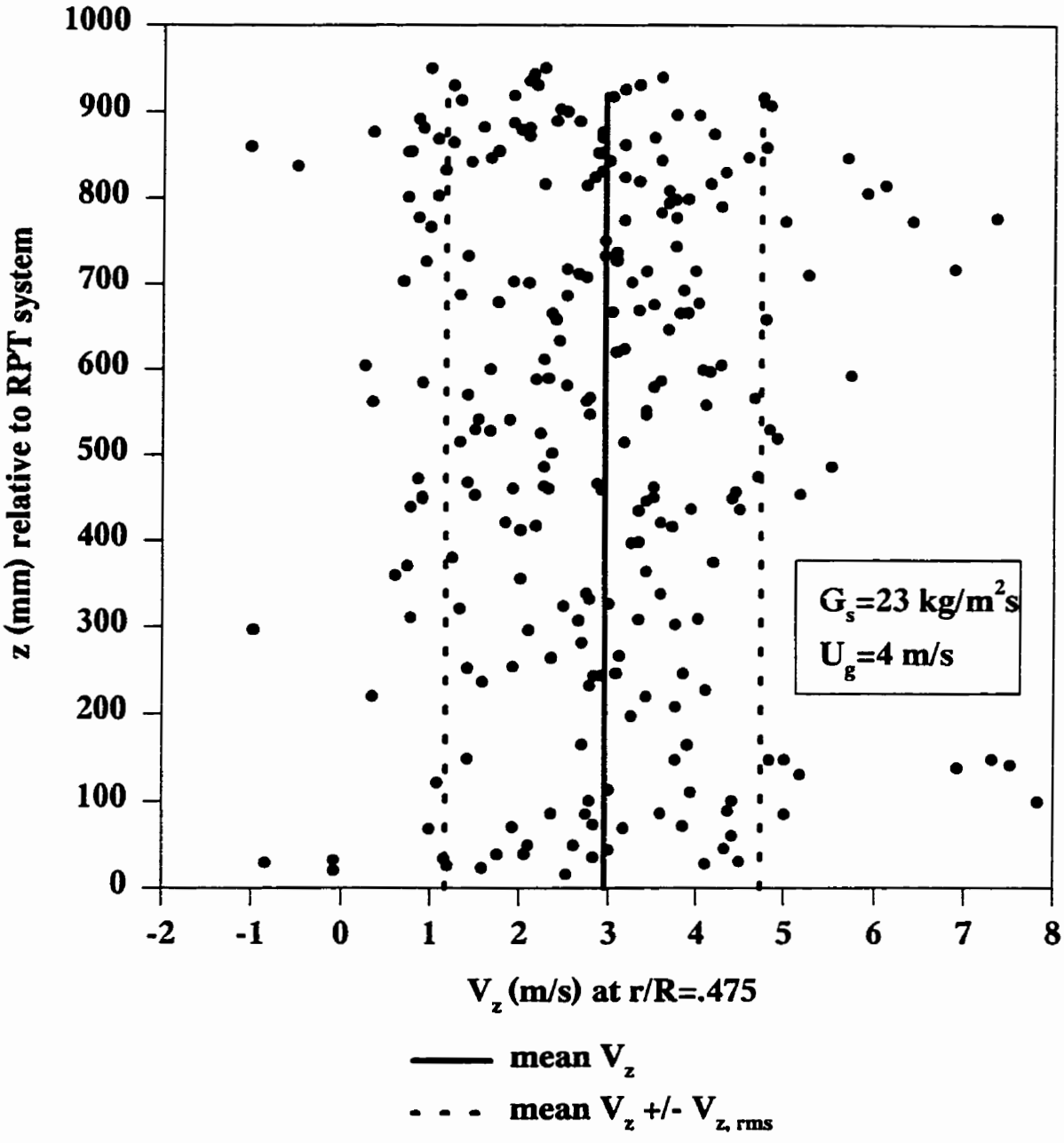

Figure 4.7 Verification for fully developed velocity

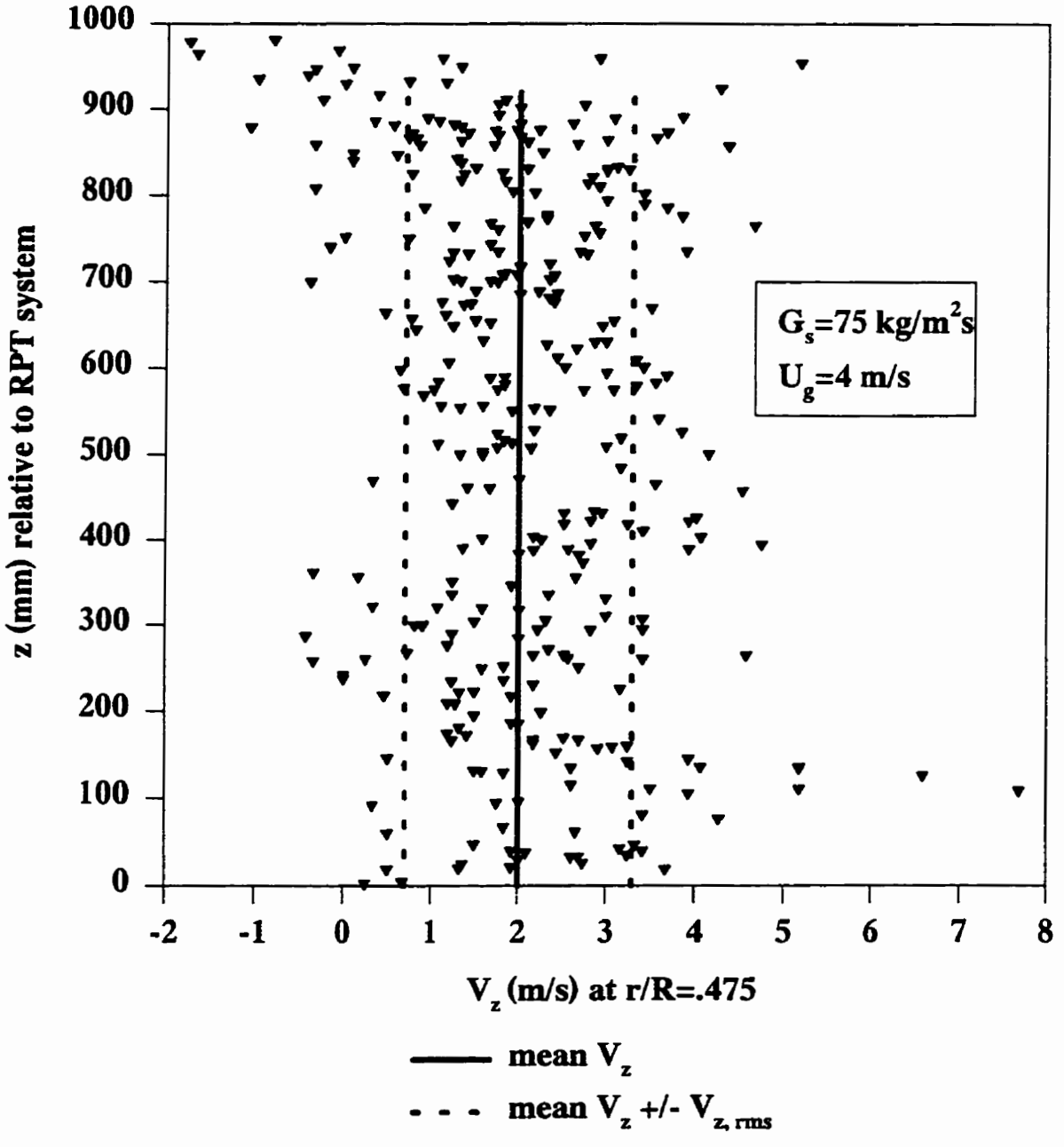

Figure 4.8 Verification for fully developed velocity

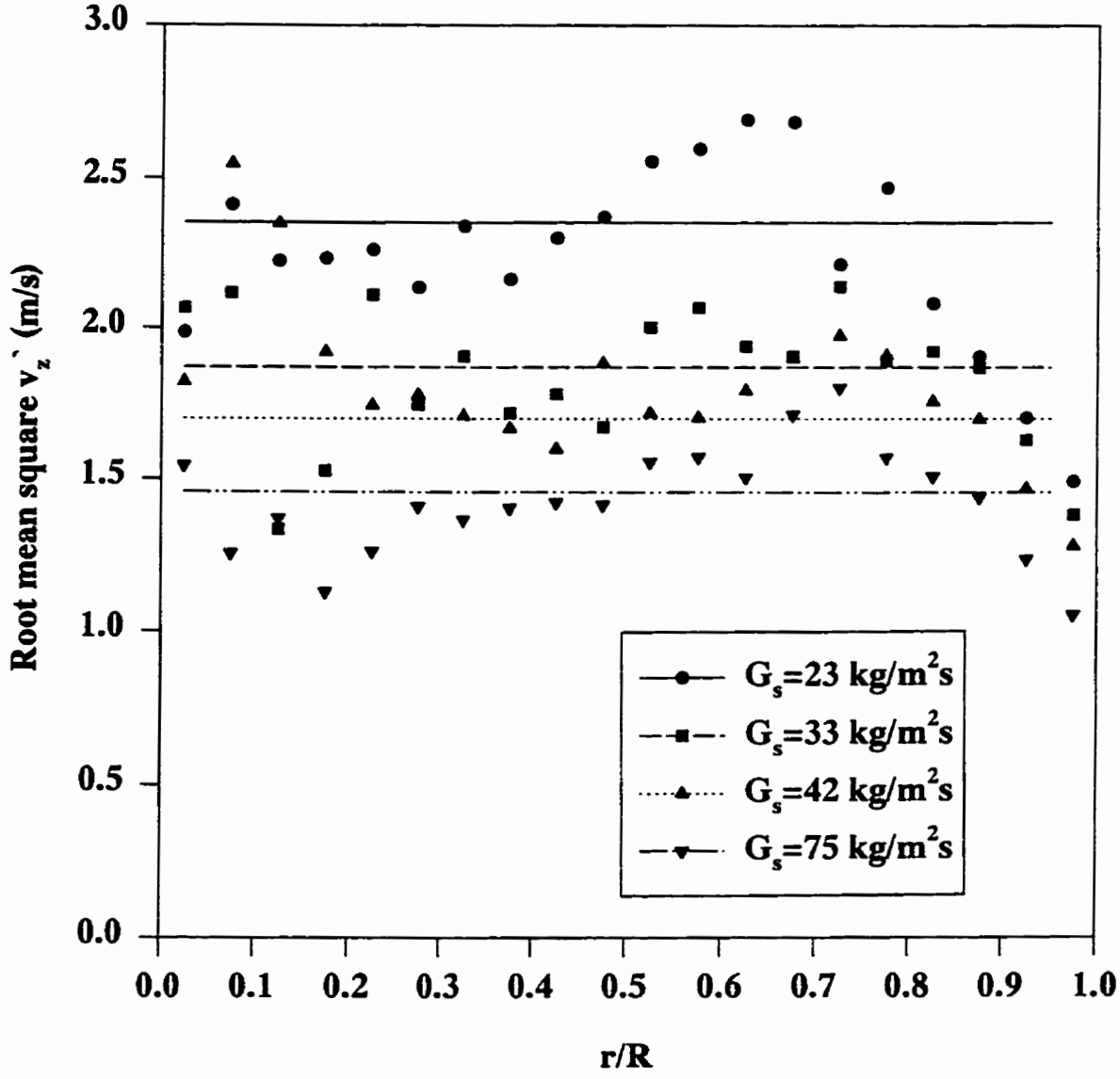

Figure 4.9 Axial root mean square velocities ($v'_{z,rms}$) (U_g=4 m/s)

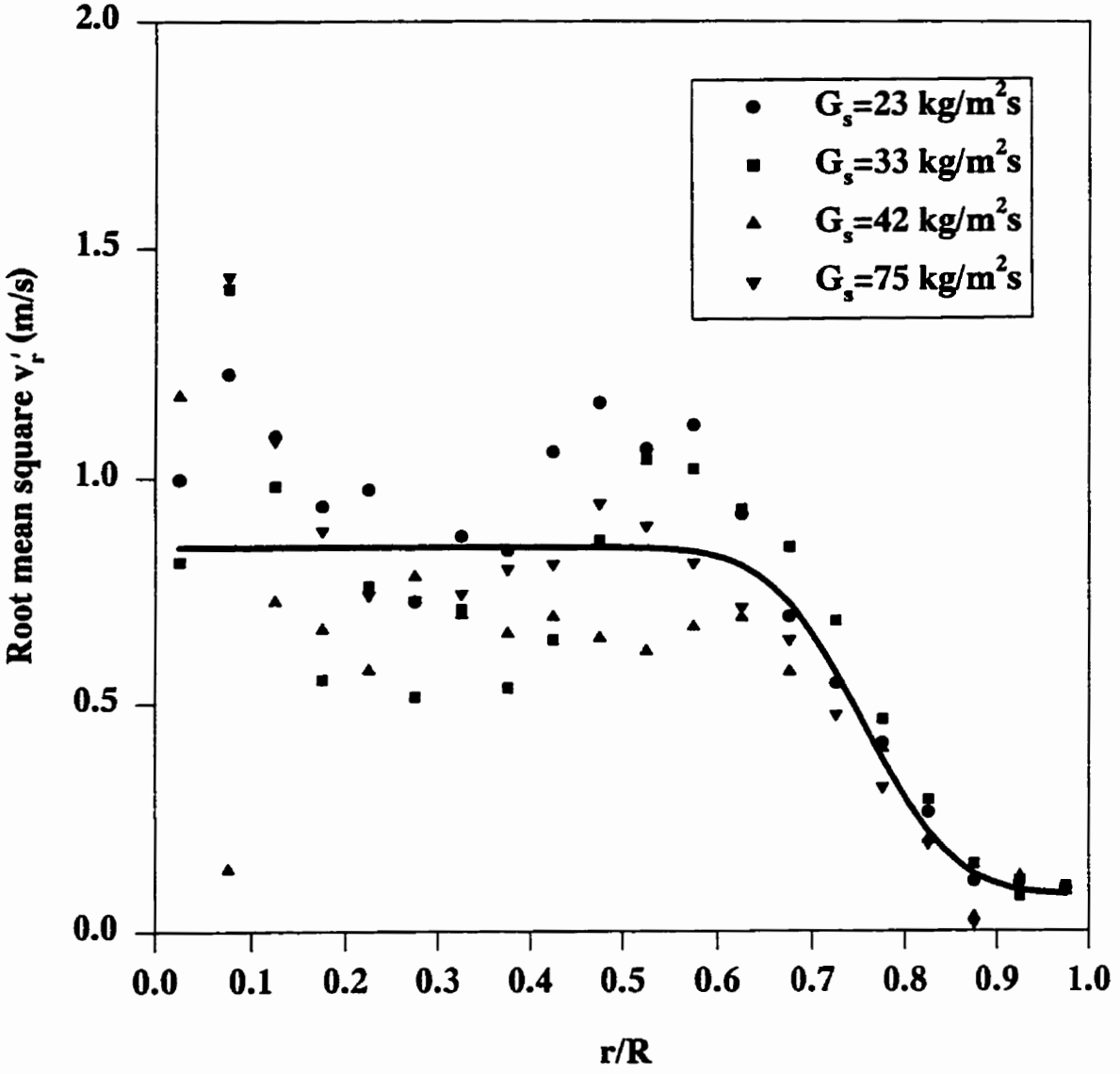

Figure 4.10 Radial root mean square velocities ($v_{r,rms}$) (U_g=4 m/s)

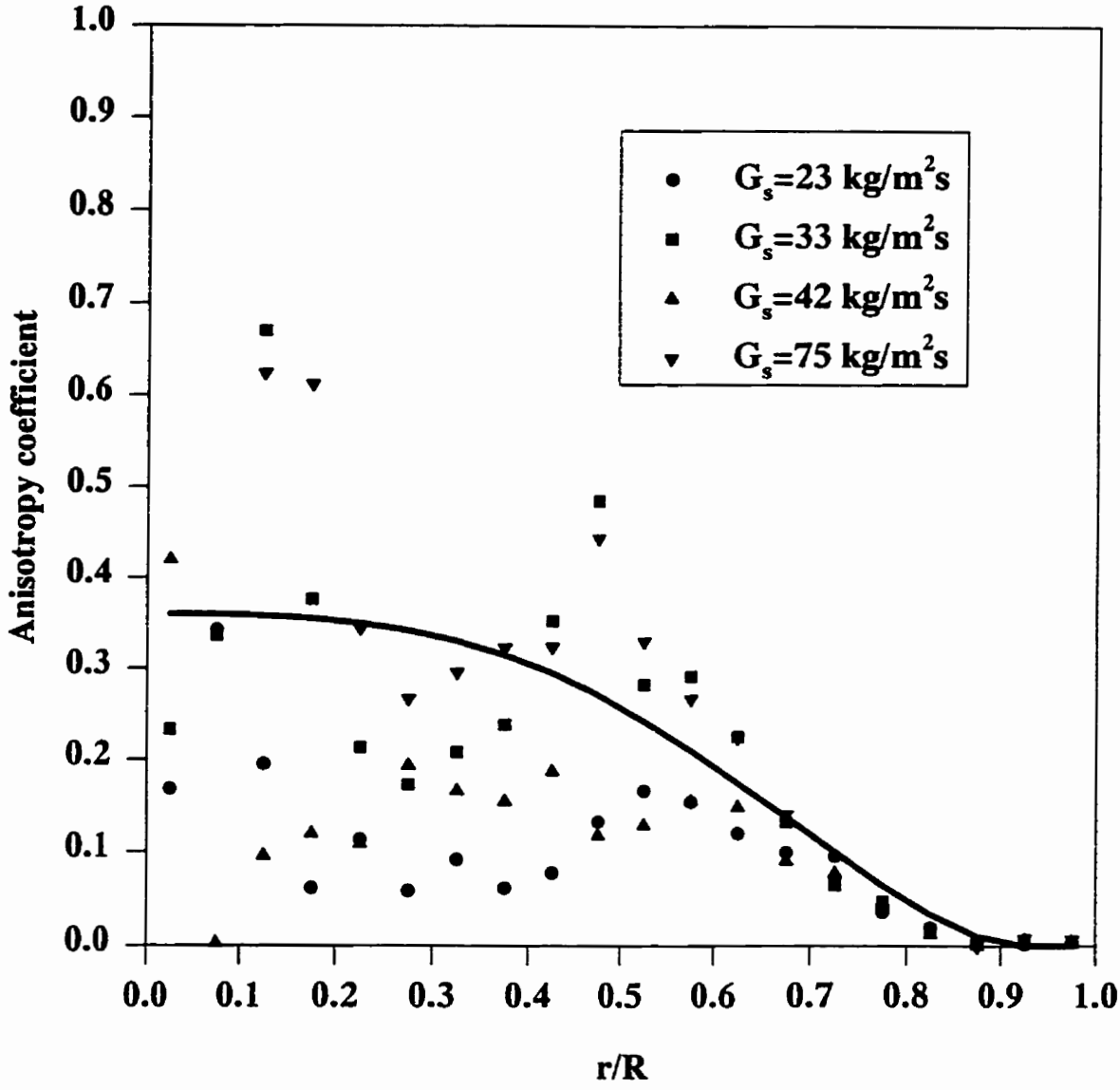

Figure 4.11 Anisotropy coefficients as a function of radius $AC(r)$ (U_g=4 m/s)

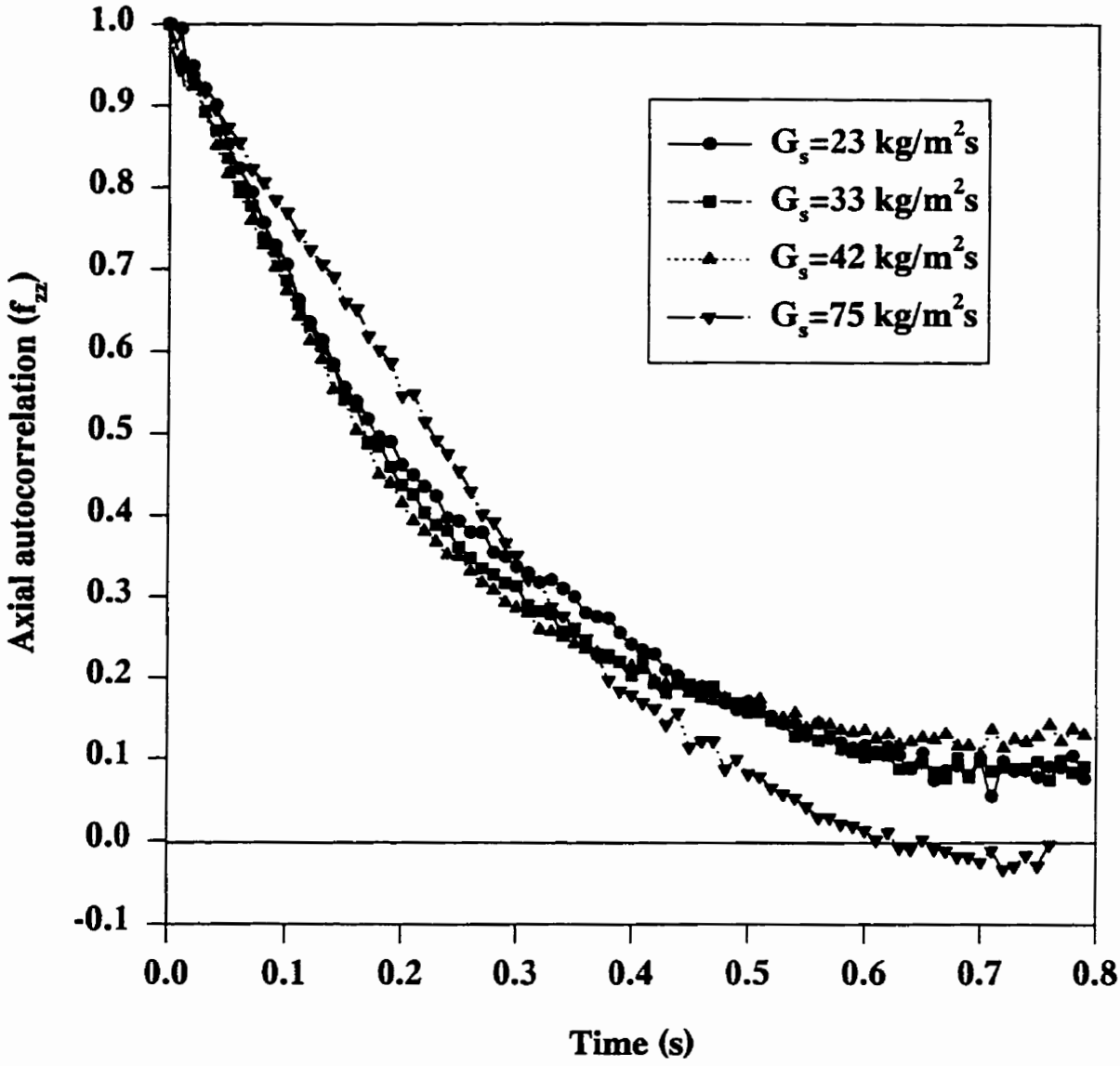

Figure 4.12 Axial autocorrelation functions (f_{zz}) (U_g=4 m/s)

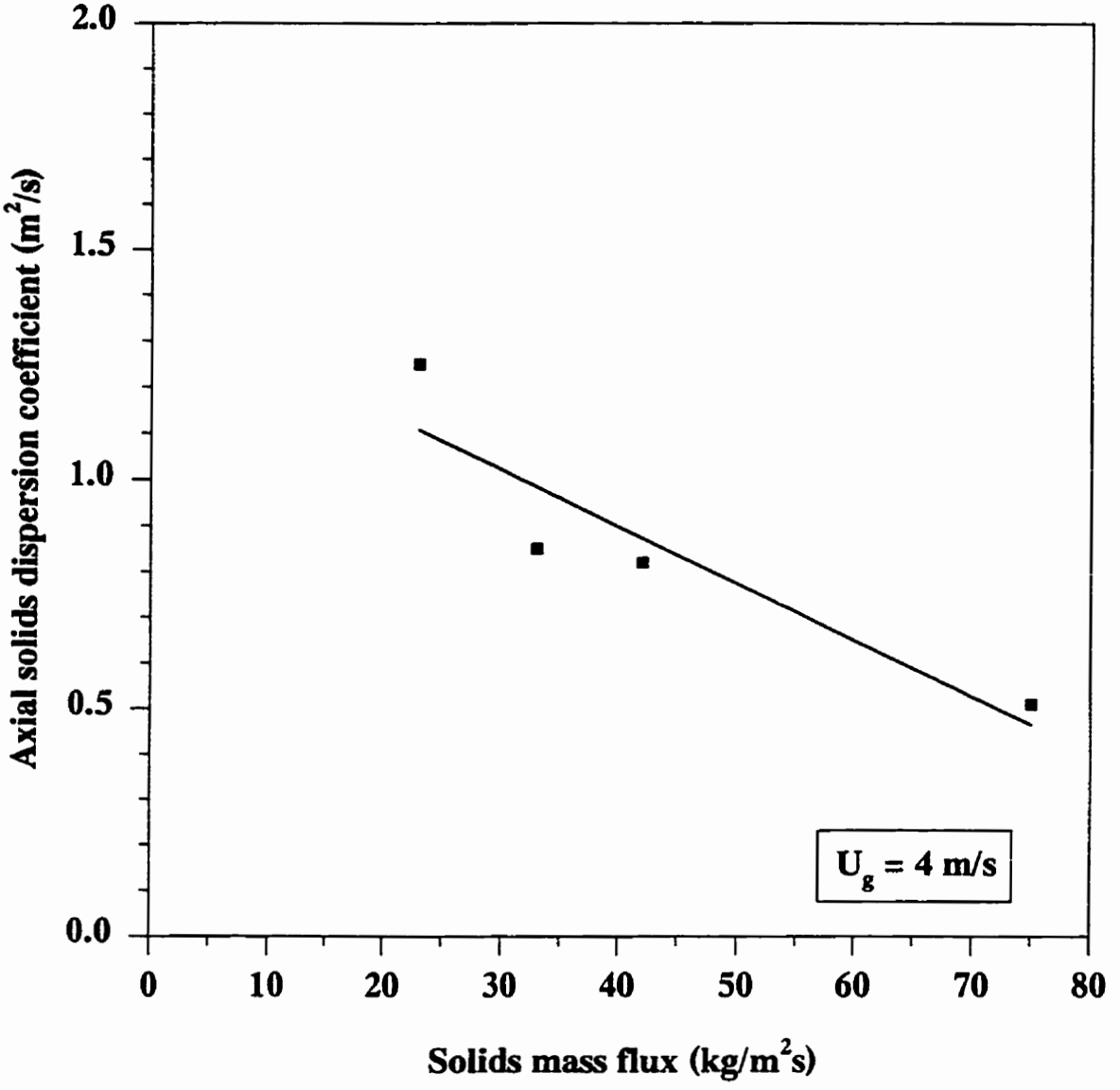

Figure 4.13 Effect of Solids Circulation Rate on the Axial Dispersion Coefficients (U_g=4 m/s)

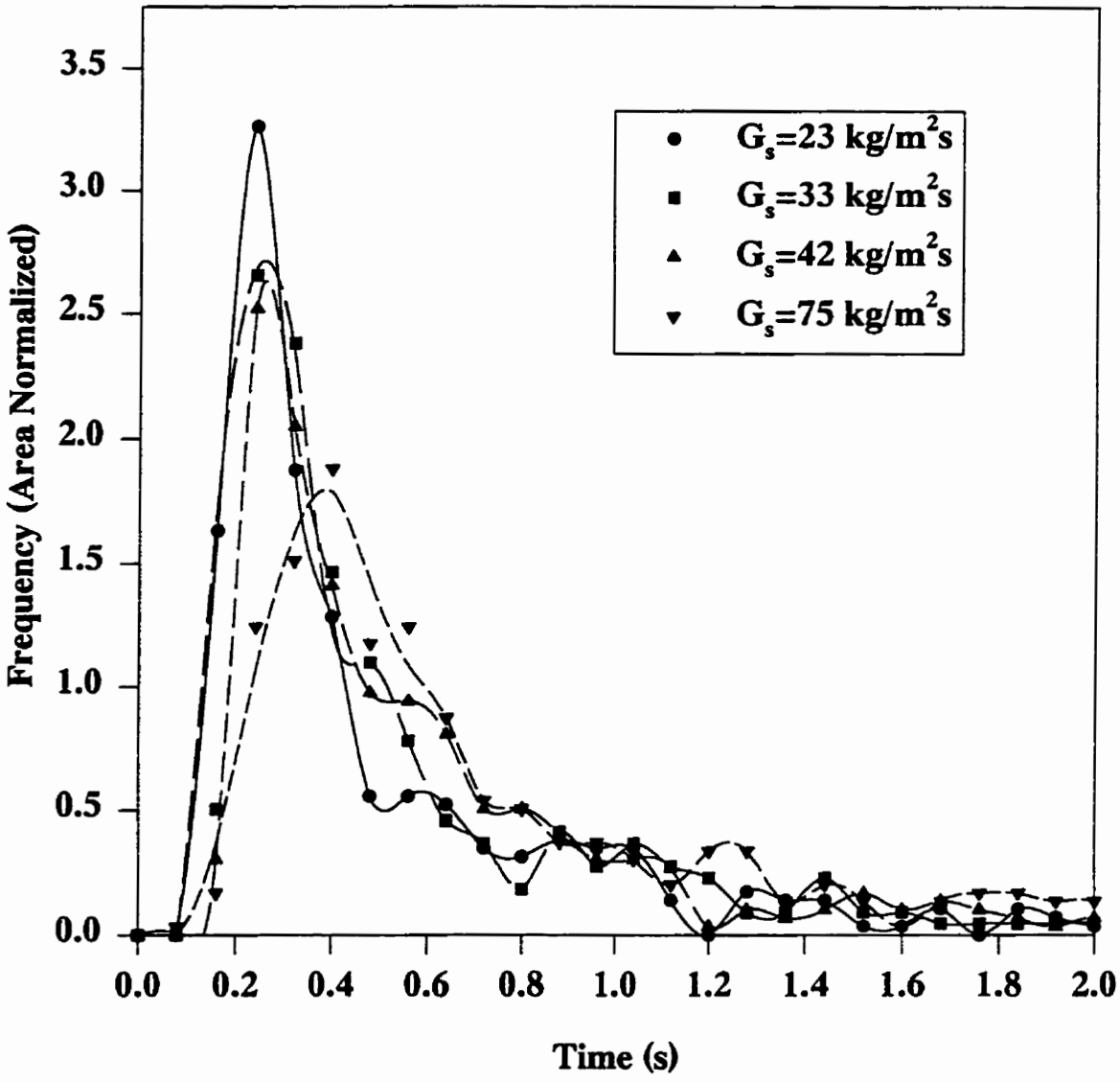

Figure 4.14 Residence Time Distributions (U_g=4 m/s)

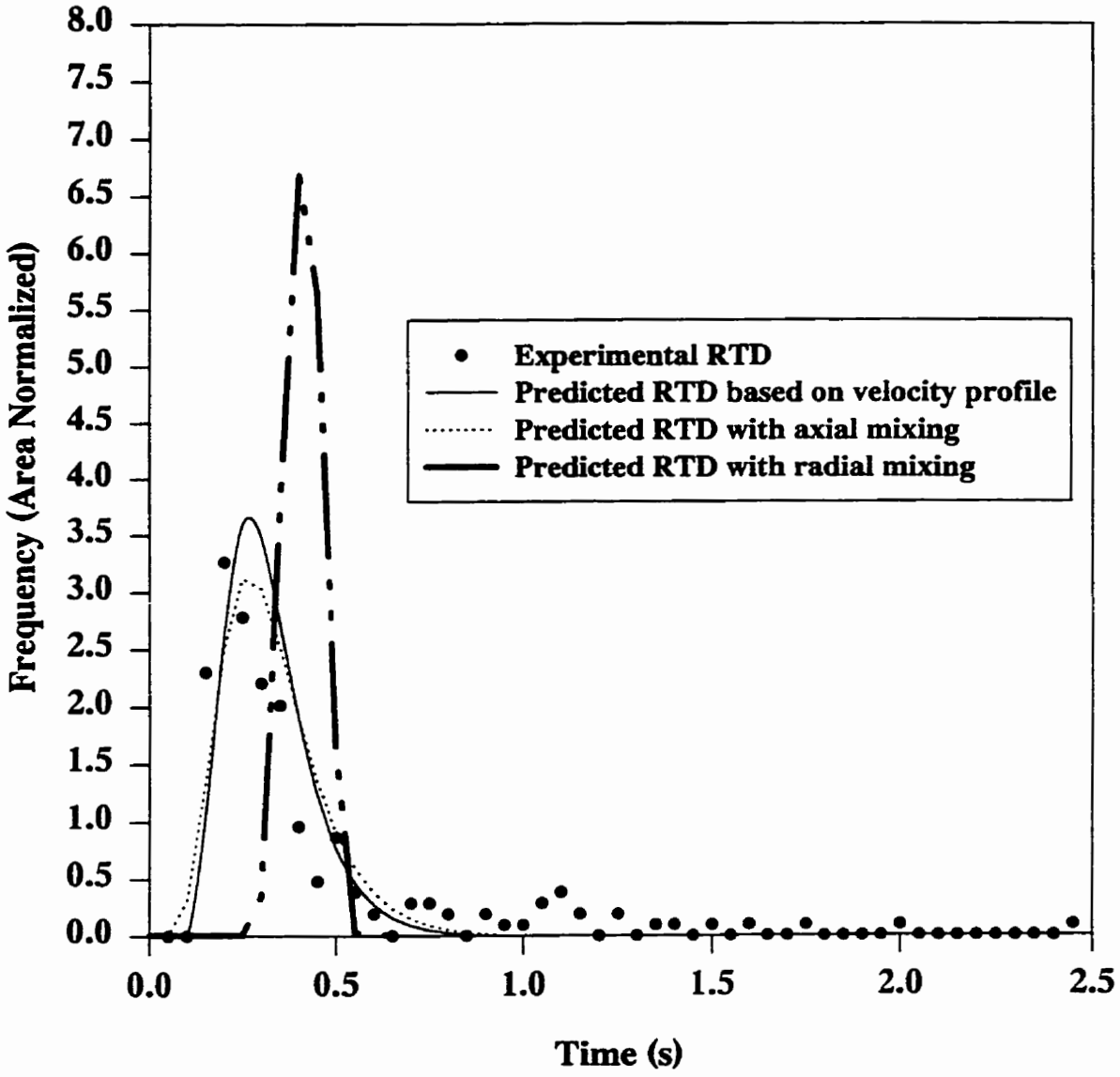

Figure 4.15 Comparison of residence time distribution with model prediction (U_g=4 m/s, G_s=23 kg/m^{2}s)

CHAPITRE 5 SYNTHÈSE

Ce chapitre fait la synthèse des contributions apportées à l'étude hydrodynamique dans les lits fluidisés circulants. La première contribution a été de participer à un article de revue de littérature qui est présenté à l'annexe I. La seconde contribution est un modèle hydrodynamique complètement prédictif. Les conditions de développement de ce modèle sont quelques peu inhabituelles. Le modèle s'est montré efficace pour prédire les variables hydrodynamiques mesurées dans des conditions nouvelles. Il n'a été soumis pour publication que par la suite. Il faut insister sur le fait qu'aucun lissage de paramètres n'a été fait pour assurer l'ajustement des variables expérimentales prédites.

Le modèle prédit le profil de vitesse axiale du gaz et des particules, la concentration locale des solides, le flux massique local et enfin la perte de charge axiale. Le modèle présenté dans cette étude se distingue des autres modèles par l'introduction de profils continus de la vitesse du gaz et des particules. Le modèle prédit les valeurs moyennes de ces variables hydrodynamiques. Cependant, la connaissance de ces variables hydrodynamiques ne présente pas toute l'information et n'offre pas le niveau de confiance requis pour faire le design d'un nouveau lit. Par exemple, le modèle prédit qu'un film concentré de particules ayant une vitesse moyenne négative est présent près de la paroi. Le temps que la particule séjourne dans ce film n'est pas prédit par le modèle pas plus que les fluctuations de vitesse. Ces caractéristiques affectent la distribution de temps de séjour des particules et par conséquent les réactions en jeu (conversions et sélectivités). Pour ces motifs, l'objectif de la seconde partie de cette étude est de caractériser la structure hydrodynamique locale des particules.

La seconde partie de cette thèse regroupe plusieurs articles et constitue une partie importante des travaux de recherche. La méthode utilisée pour cette étude est la technique de poursuite d'une particule développée par Faiçal Larachi au département de génie

chimique. Cette technique s'était déjà montrée un outil fort intéressant et prometteur. Il fallait bien sûr adapter la technique pour son application à un lit circulant. Le chapitre 2 a discuté de la problématique de l'application de la technique au lit circulant. Le problème principal est lié à la résolution spatiale. On doit augmenter la fréquence d'échantillonnage et augmenter le volume à l'intérieur duquel il est possible de déterminer la position de la particule.

L'article "On-line Flow Visualization in Multiphase Reactors using Neural Networks" présente la recherche d'un meilleur radio-isotope et montre que la résolution spatiale peut être prédite pour une configuration des détecteurs et une source données. Ce résultat est fondamental pour optimiser la position des détecteurs. La conclusion la plus importante pour la poursuite des travaux est que l'or est le meilleur radio-isotope et peut améliorer la résolution spatiale du système de détection. Le choix du meilleur radio-isotope s'est effectué en mode statique *i.e.* que la particule radioactive n'est pas en mouvement. La validation dynamique est présentée au chapitre suivant, le chapitre 3. L'article publié s'intéresse également à la démonstration de calculs permettant très rapidement la détermination des coordonnées de la particule traçante à partir des comptages des détecteurs. Il s'agit là d'une méthode originale qui rend possible la visualisation de l'écoulement en temps réel en utilisant un réseau neuronal.

Le chapitre 3 présente les résultats préliminaires obtenus dans le lit fluidisé circulant. La conclusion principale de cet article est qu'il est possible de localiser instantanément la particule traçante dans des conditions rencontrées dans le lit fluidisé circulant. Toutefois, la résolution spatiale doit être améliorée en utilisant un plus grand nombre de détecteurs.

Le chapitre 4 présente une analyse détaillée du mouvement d'une particule traçante dans un lit fluidisé circulant. Une diminution de la vitesse axiale des solides est observée avec une augmentation du taux de circulation des solides à vitesse de gaz constante. Cette diminution de la vitesse axiale est attribuée à la formation d'agrégats. L'analyse des

fluctuations de vitesse a permis de démontrer que les fluctuations de la vitesse axiale diminuent également avec une augmentation du taux de circulation des solides. Cette diminution de fluctuations de la vitesse axiale entraîne une diminution du coefficient de dispersion turbulente. L'ordre de grandeur du coefficient de dispersion axiale turbulente est de 1 m^2/s. L'analyse des fluctuations de vitesse a également permis de démontrer que l'écoulement des solides n'est pas isotrope puisque les fluctuations des vitesses axiales sont plus importantes que celles radiales.

La modélisation de la distribution de temps de séjour a clairement permis de démontrer que cette dernière peut être prédite simplement à l'aide du profil radial de vitesse axiale. Cette conclusion montre à quel point la connaissance du profil de vitesse est importante. Ainsi, il est important de modéliser le profil de vitesse des particules par une approche comme celle présentée au chapitre 1. La figure 5.1 compare les profils de vitesse axiale mesurées expérimentalement et ceux prédits par le modèle hydrodynamique discuté au chapitre 1. Les valeurs prédites par le modèle sont assez près ($\pm$0.5 m/s) des valeurs expérimentales, surtout au centre du réacteur ($r/R \leq 0.8$). Près de la paroi, les différences entre les deux profils sont plus importantes et peuvent atteindre 1 m/s. Les tendances de la variation de la vitesse axiale prédites par le modèle sont toutefois opposées à celles mesurées expérimentalement. Le modèle prédit que la vitesse augmente avec une augmentation du taux de circulation des solides alors qu'une diminution de la vitesse est observée. Dans le modèle, le bilan de masse sur le gaz cause une augmentation de la vitesse des particules. Expérimentalement, la diminution de la vitesse axiale avec une augmentation du taux de circulation des solides est attribuée à la formation d'agrégats. Cette tendance est probablement liée à la taille de l'ensemble des particules et en particulier à la taille de la particule traçante. Il serait très intéressant de poursuivre les expériences avec toute une gamme de tailles de particules radioactives. Il serait alors possible d'évaluer l'effet de la taille d'une particule sur son comportement hydrodynamique.

D'autres expériences sont requises pour déterminer l'importance de cette formation d'agrégats.

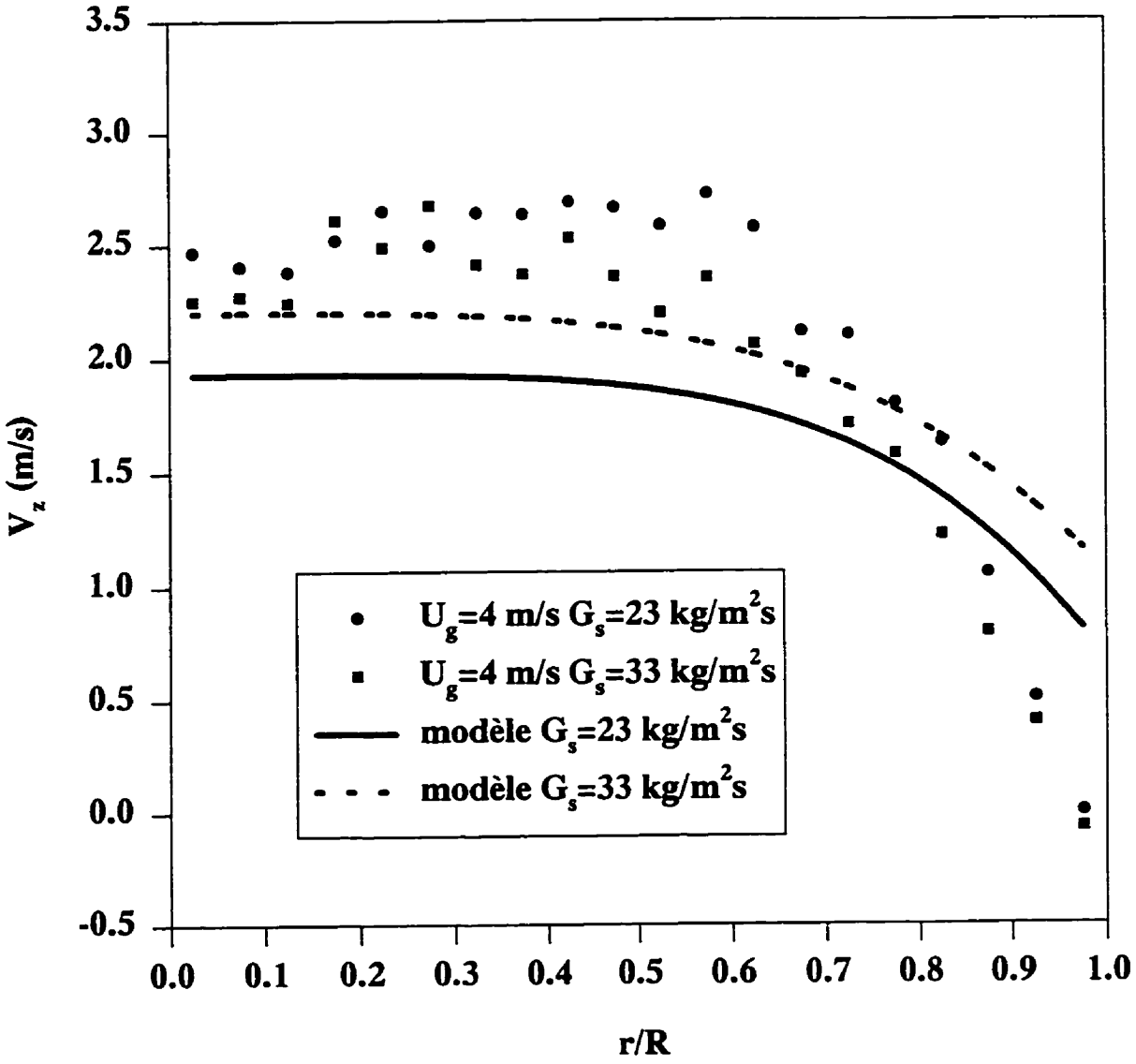

Figure 5.1 Comparaison des profils de vitesse axiale

5.1 Recommandations

Il faudrait poursuivre l'étude hydrodynamique dans de nouvelles applications et tenter d'ajuster le modèle développé au chapitre 1 aux conditions opératoires obtenues au chapitre 4 et dans de nouvelles expériences. La comparaison des prédictions et des mesures expérimentales peut permettre de renouveler et corriger les corrélations utilisées par le modèle hydrodynamique. Par exemple, une corrélation prenant en considération la variation du facteur de glissement (Eq. 1) avec le taux de circulation des solides serait intéressante. Il faut aussi chercher à comprendre le comportement d'une particule ayant des caractéristiques différentes de l'ensemble des particules du lit. De façon générale, les modèles éprouvent une certaine difficulté à capter l'essence de l'écoulement dans le cas de particules ayant des propriétés semblables et ne sont pas adaptés pour prédire le comportement de particules différentes. On pourrait ainsi songer à un nouveau modèle hydrodynamique incluant l'effet de la taille des particules. Il y a cependant des limites inférieures quant à la taille possible d'une particule radioactive. Il faut que le temps de l'activation neutronique soit compatible avec les possibilités du laboratoire de génie nucléaire. Il est à peu près impossible pour l'instant d'entrevoir la fabrication de particules plus petites que 300 μm pour l'utilisation dans le lit fluidisé circulant.

Il serait également intéressant de poursuivre des études dans le lit fluidisé circulant en utilisant une méthode expérimentale différente et/ou complémentaire à la technique de poursuite d'une particule radioactive. Par exemple, les distributions de temps de séjour des particules et du gaz peuvent être mesurées à l'aide des détecteurs radioactifs. Le profil de porosité peut également être mesuré à l'aide d'une sonde à capacitance ayant été développée au département. Toutes ses informations sont rarement disponibles pour de mêmes conditions d'opération sur un montage expérimental.

En fait, le lit fluidisé circulant est un montage expérimental qui offre beaucoup de possibilités. Plusieurs (deux ou même trois) étudiants pourraient utiliser le montage et l'adapter à leurs besoins. Il serait notamment intéressant d'opérer le lit fluidisé circulant à hautes températures.

Enfin, la dernière recommandation est plus générale et concerne tous les montages expérimentaux quelques peu complexes. Il serait intéressant qu'une attention particulière soit portée sur la comptabilisation de tous les documents relatifs aux montages expérimentaux. Il arrive trop souvent que les plans des montages, les manuels d'utilisation des appareils de mesure, les garanties et les noms des fournisseurs des équipements, les courbes de calibration, etc. ne soient pas disponibles. Cette mesure permettrait sûrement de sauver du temps aux nouveaux venus qui héritent d'un montage et d'appareils existants.

RÉFÉRENCES

ABED, R. (1983), The Characterization of Turbulent Fluid-Bed Hydrodynamics, in *Fluidization IV*, ed. D. Kunii and R. Toei, Engineering Foundation, New York 137.

AVIDAN, A. A. (1980) *Bed Expansion and Solid Mixing in High Velocity Fluidized Beds*, Ph. D. Dissertation, City College, New York.

AVIDAN, A. A., EDWARDS M. et H. OWEN (1990), Fluid-Catalytic Cracking, Past and Future Challenges, *Rev. Chem. Eng.* **6** 1.

BADER, R., FINDLAY, J. et T. M. KNOWLTON (1988), Gas/Solids Flow Pattern in a 30.5 cm Diameter Circulating Fluidized Bed, in *Circulating Fluidized Bed Technology II*, P. Basu and J. F. Large Eds., Pergamon Press, New York, NY, pp.123-137.

BAI, D., ZHI, J. X., JIN, Y. et Z. YU (1995), Internal Recirculation Flow Structure in Vertical Upflow Gas-Solids Suspensions: Part II Flow Structure Predictions, *Pow. Tech.* **85,** 178-188.

BEAM, G. B., WIELOPOLSKI, L., GARDNER, R. P., et K. VERGHESE (1978) Monte Carlo calculation of efficiencies of right-circular cylindrical NaI detectors for arbitrarily located point sources, *Nucl. Inst. Meth.* **154**, 501.

BERRUTI, F.; CHAOUKI, J.; GODFROY, L.; PUGSLEY, T. S. et G. S. PATIENCE (1995), Hydrodynamics of Circulating Fluidized Bed Risers: A Review, *Can. J. Chem. Eng.* 73, 579.

BEVINGTON, P. R. (1969) *Data Reduction and Error Analysis for Physical Sciences*, McGraw-Hill.

BOLKAN-KENNY, Y. G., PUGSLEY, T. S. et F. BERRUTI (1994), Computer Simulation of the Performance of Fluid Catalytic Cracking Risers and Downers, *Ind. Eng. Chem. Res.* 33, 3043.

BRERETON, C. M. H. et J. R. GRACE (1993) Microstructural aspects of the behaviour of circulating fluidized beds, Chem. Eng. Sci. **48** ,2565.

BROADBENT, C. J., BRIDGEWATER, J., PARKER, D. J., KENINGLEY, S. T. et P. KNIGHT (1993) Phenomenological study of a batch mixer using a positron camera. *Powder Techn.* **76**, 317.

CANKURT, N. T. et J. YERUSHALMI (1978), Gas Backmixing in High Velocity Fluidized Bed, in *Fluidization*, eds. J. F. Davidson and D. L. Keairns, Cambridge University Press, London, 387.

CASSANELLO, M, LARACHI, F., MARIE, M.-N., GUY, C., et J. CHAOUKI (1995), Ind. Eng. Chem. Res. **34**, 2971.

CHAOUKI, J., LARACHI, F. et M. P. DUDUKOVIC (Eds) (1997) *Non-invasive Monitoring of Multiphase Flows*, Elsevier Science, New York, NY, 585p.

CONTRACTOR, R. M.; PATIENCE, G. S.; GARNETT, D. I.; HOROWITZ, H. S.; SISLER, G. M. et H. E. BERGNA (1994), A New Process for *n*-butane Oxidation to Maleic Anhydride using a Circulating Fluidized Bed Reactor, in *Circulating Fluidized Bed Technology*, ed. A. A. Avidan, American Institute of Chem. Eng., New York, 387.

CONTRACTOR, R. M.; PELL, M.; WEINSTEIN, H. et H. J. FEINDT (1992), The Rate of Solids Loss in a Circulating Fluidized Bed Following a Loss of Circulation Accident, in *Fluidization VII*, eds. O. E. Potter and D. J. Nicklin., Engineering Foundation, New York., 243.

CURL, R. L. et M. L. MCMILAN (1966), Accuracy in Residence Time Measurements, *AICHE J.* **12**, 819-822.

CYBENKO, G. (1989) Approximation by superpositions of sigmoidal functions. *Math. Control. Syst.* **2**, 303.

DEVANATHAN, N., MOSLEMIAN, D. et M. P. DUDUKOVIC (1990) Flow mapping in bubble columns using CARPT. *Chem. Eng. Sci.* **45** 2285.

DING, J. et GIDASPOW (1990), A Bubbling Fluidization Model Using Kinetic Theory of Granular Flow, *AICHE J.* **36**, 523-538.

DUDUKOVIC, M. P., DEVANATHAN, N. et R. HOLUB, "Multiphase Reactors: Models and Experimental Verification", Rev. Inst. Franc. Pét. **46**, 439-465 (1991).

GODFROY, L., LARACHI, F., KENNEDY, G., GRANDJEAN, B. P. A. et J. CHAOUKI (1997a), On-Line Flow Visualization in Multiphase Reactors using Neural Networks, *Appl. Radiat. Isot.* **48**, 225-235.

GODFROY, L., PATIENCE, G. S. et J. CHAOUKI (1997b) Radial Hydrodynamics in Risers, submitted to Ind. Eng. Chem. Res. (chapitre 1 de la these)

GODFROY, L., LARACHI, F., KENNEDY, G. et J. CHAOUKI (1996a), Simultaneous Measurement of the 3-D Position and Velocity of a Single Radioactive Particle in a CFB Riser at High Velocity, preprint of *Proc. 5th Int. Conf. Circulating Fluidized Bed*, Bejing, China, May 1996.

GRACE J. R. (1996), Riser Geometry on CFB Particle and Fluid Dynamics, in preprint of *Proc. 5th Int. Conf. Circulating Fluidized Bed*, Bejing, China, May 1996, pp. PL2 1-16.

GRACE, J. R., A. A. AVIDAN et T. M. KNOWLTON, Eds. (1997), *Circulating Fluidized Beds*, J. R. Grace, A. A. Avidan and T. M. Knowlton, Eds., Blackie Academic & Professional, London, 585 p.

GRACE, J. R. et K. S. LIM (1997), Reactor Modeling for High-Velocity Fludized Beds in Circulating Fludized Beds, in *Circulating Fluidized Beds*, J. R. Grace, A. A. Avidan and T. M. Knowlton, Eds., Blackie Academic & Professional, London, pp. 505-524.

HARRIS, B. J.; DAVIDSON, J. F. et Y. XUE (1994), Axial and Radial Variation of Flow in Circulating Fluidized Bed Risers, in *Circulating Fluidized Bed Technology IV*, ed. A. A. Avidan, American Institute of Chemical Engineers, New York, 103.

HARRIS, B. J. et J. F. DAVIDSON (1994), Modelling Options for Circulating Fluidized Beds: A Core/Annulus Depositions Model, in *Circulating Fluidized Bed IV*, A. A. Avidan, Ed., American Institute of Chemical Engineers, New York, 32-39.

HARTGE, E. U., RENSNER D. et J. WERTHER (1988), Solids Concentration and Velocity in Circulating Fluidized Beds, in *Circulating Fluidized Bed Technology II*, P. Basu and J.F. Large, Eds., Pergamon Press, New York, 165-180.

HERB, B.; TUZLA, K. et J. C. CHEN (1989), Distribution of Solids Concentration in Circulating Fluidized Bed, in *Fluidization VI*, eds. J. R. Grace, L.W. Schemilt and M. A. Bergougnou, Eds., Engineering Foundation, New York ,65.

HORIO, M., MORISHITA, K., TACHIBANA, O. et N. MURATA (1988), Solids Distribution and Movement in Circulating Fluidized Beds, in *Circulating Fluidized Bed Technology II*, P. Basu and J.F. Large, Eds., Pergamon Press, New York, 147-154.

HORIO, M., KUROKI, H. et M. OGASAWARA (1993), The Flow Structure of a Three-dimensional Ciculating Fluidized Bed Oberved by the Laser Sheet Technique. in preprint of *Proc. 4th Int. Conf. Circulating Fluidized Bed*, Pennsylvania, USA, August 1st-5th 1993.

HORNIK, K., STINCHCOMBE, M., et WHITE H. (1989) Multilayer feedforward networks are universal approximators. *Neur. Net.* **2**, 359.

ISHII, H., NAKAJIMA, T. et M. HORIO (1989), The Clustering Annular Flow Model in Circulating Fluidized Beds, *J. Chem. Eng. Japan* **22**, 484-490.

JENKINS, J. T. et S. B. SAVAGE (1983), A Theory for the Rapid Flow of Identical, Smooth, Nearly Elastic, Spherical Particles, *J. Fluid. Mech.* **130**, 178-202.

JOHNSON, P.C. et R. JACKSON (1987), Frictional-Collisional Constitutive Relations for Granular Materials with Application to Plane Shearing, *J. Fluid. Mech.* **176**, 67-73.

KATOH, Y., KANEKO, S., et M. MIYAMOTO (1993), Flow Pattern and Velocity Distribution on Fluidized Particles in a Riser of Circulating Fluidized Beds, in *Preprints 4th Int. Conference on Circulating Fluid Beds*, A. A. Avidan, Ed., Somerset, PA, U.S.A., Aug. 1-5 1993, American Institute of Chemical Engineers, New York, 332-337.

KONDUKOV, N. B., KORNILAEV, A. N., SKACHKO, I. M., AKHROMENKOV, A. A. et A. S. KRUGLOV (1964), An Investigation of the Parameters of Moving Particles in a Fludized Bed by a Radioisotopic Method, *Int. J. Chem. Eng.* **4**, 43-47.

LARACHI, F., KENNEDY, G. et J. CHAOUKI (1994), A -ray detection system for 3-D particle tracking in multiphase reactors. *Nucl. Instr. Meth. Phys. Res.* **A338**, 568.

LARACHI, F., CASSANELLO, M., MARIE, M.-N., CHAOUKI, J. et C. GUY (1995a) Solids circulation patterns in three-phase fluidized beds containing binary mixtures of particles as inferred from RPT. *Trans. Inst. Chem. Eng.* **73**, 263.

LARACHI, F., LORD, E., CHAOUKI, J., CHAVARIE, C. et L. A. BEHIE (1995b), Phenomenological study of solids mixing in a binary liquid fluidized bed. *Proceeding of Fluidization VIII, Tours, France*, 385.

LARACHI, F., CHAOUKI, J., KENNEDY, G. et M. P. DUDUKOVIC (1996), Radiation Particle Tracking in Multiphase Reactors: Principle and Applications, to appear in *Tomography and Velocimetry Techniques for Non-invasive Flow Measurements in Multiphase Flows in Process Industry*, Eds Chaouki J., Larachi F., Dudukovic M.P., to appear in Elsevier Science B.V.

LIN, J. S., CHEN, M. M. et B. T. CHAO (1985), A novel radioactive particle tracking facility for measurement of solids motion in gas fluidized beds, *AIChE J.* **31**, 465.

LIPPMANN, R. P. (1987), Introduction to computing with neural nets, *IEEE ASSP* **4**, 4.

LOUGE, M. Y., MASTORAKOS, E. et J. T. JENKINS (1991), The Role of Particle Collisions in Pneumatic Transport, *J. Fluid. Mech.* **231**, 345-359.

LUN, C. K. K., SAVAGE, S. B., JEFFREY, D. J. et N. CHEPURNIY (1984), Kinetic Theories for Granular Flow: Inelastic Particles in Couette Flow and Slightly Inelastic Particles in a General Flow-field, *J. Fluid. Mech.* **140**, 223-256.

MARTIN, M. P.; TURLIER, P. et J. R. BERNARD (1992), Gas and Solid Behavior in Cracking Fluidized Beds, *Pow. Tech.* **70**, 249.

MATSEN, J. M. (1976), Some Characteristics of Large Solids Circulation Systems in *Fluidization Technology*, D. L. Keairns, Ed., Hemisphere, New York, 135 p.

MINEO, H. (1989), High Velocity Circulating Fluidized Beds, Ph. D. Dissertation, University of Tokyo, Japan.

MORRIS, A. J., MONTAGNE, G. A. et WILLIS M. J. (1994) Artificial neural networks: Studies in process modeling and control. *Chem. Eng. Res. Des.* **72**, 3.

MOSLEMIAN, D., (1987) Study of Solids Motion and Heat Transfer in Gas-Fluidized Bed, Ph. D. Dissertation, University of Illinois at Urbana-Chamaign, USA.

MOSLEMIAN D., DEVANATHAN N. et M. P. DUDUKOVIC (1992) Radioactive particle tracking for investigation of phase recirculation and turbulence in multiphase systems. *Rev. Sci. Inst.* **63**, 4361.

NAUMAN, E. B. (1981), Invited Review : Residence Time Distributions and Micromixing, *Chem. Eng. Commun.* **8**, 53-131.

Nieuwland, J. J., Van Sint Annaland, M., Kuipers, J. A. A. et W. P. M. van Swaaij (1996a), Hydrodynamic Modeling of Gas/Particles Flows in Riser Reactors, *AICHE J.* **42**, 1569-1582.

NIEUWLAND, J. J., MEIJER, R., KUIPERS, J. A. M. et W. P. M. VAN SWAAIJ (1996b), Measurements of Solids Concentration and Axial Solids Velocity in Gas-Solid Two-phase Flows, *Pow. Tech.* **87**, 127-139.

NORMANDIN A., GRANDJEAN B. P. A. et THIBAULT J. (1993) PVT data analysis using neural network models, *I&EC Res.* **32**, 970.

OKI, K., WALAWENDER, W. P. et L. T. FAN (1978), The measurement of Local Velocity of Solids Particles, *Pow. Tech.* **18**, 171-178.

PATIENCE, G. S. (1990), Circulating Fluidized Beds : Hydrodynamics and Reactor Modeling, Ph. D. dissertation, École Polytechnique de Montréal, Quebec, Canada.

PATIENCE, G. S., CHAOUKI, J., BERRUTI, F. et R. WONG (1992), Scaling Considerations for Circulating Fluidized Bed Risers, *Pow. Tech.* **72**, 31.

PATIENCE, G.S. et P. L. MILLS (1994), Modelling of Propylene Oxidation in a Circulating Fluidized-Bed Reactor, in *New Development in Selective Oxidation II*, eds. V. C. Corberan and S. Vic Bellon, Elsevier, New York, 1.

PATIENCE, G. S. et J. CHAOUKI (1995), Solids Hydrodynamics in the Fully Developed Region of CFB Risers, in *Fluidization VIII*, preprints, Tours, May 14, 33.

PATIENCE, G. S., CHAOUKI, J., et F. BERRUTI (1996), Gas Phase Hydrodynamics in Circulating Fluidized Bed Risers, in *Multiphase Reactor and Polymerization System Hydrodynamics*, ed. N. P. Cheremisinoff, Texas 255.

PITA, J. A. et S. SUNDARESAN (1993), Developing Flow of Gas-Particle Mixture in a Vertical Riser, *AICHE J.* **39**, 541.

PRESS H. W., FLANNERY B. P., TEUKOLSKY S. A. et VETTERLING W. T. (1988) *Numerical Recipes, the Art of scientific Computing*, Cambridge University Press, London.

PUGSLEY, T. S., PATIENCE, G. S., BERRUTI, F. et J. CHAOUKI (1992), Modelling of the Oxidation of *n*-Butane to Maleic Anhydride in a Circulating Fluidized Bed Reactor, *Ind. Eng. Chem. Res.* **31**, 2652.

PUGSLEY, T. S., BERRUTI, F., GODFROY, L., CHAOUKI, J. et G. S. PATIENCE (1994), A predictive Model for the Gas-Solid Flow Structure in Circulating Fluidized Bed Risers, in *Circulating Fluidized Bed Technology IV*", ed. A. A. Avidan, American Institute Chem. Eng., New York, 40.

QIAN, C. et J. LI (1994), Particle Velocity Measurement in CFB with Integrated Probe, in *Circulating Fluidized Bed IV*, A. A. Avidan, Ed., American Institute of Chemical Engineers, New York, 274-278.

REH, L. (1995) New and Efficient High-Temperature Processes with Circulating Fluid Bed Reactors, *Chem. Eng. Tech.* **18**, 75.

RHODES, M. J., WANG, X. S., CHENG, H. et T. HIRAMA (1992a), Similar Profiles of Solids Flux in Circulating Fluidized-Bed Risers, *Chem. Eng. Sci.* **47**,1635.

RHODES, M., ZHOU, S. et H. BENKREIRA (1992b), Flow of Dilute Gas Suspensions, *AICHE J.* **28**, 1913-1915.

ROY D., LARACHI F., LEGROS R. et CHAOUKI J. (1994) A study of Solid Behaviour in Spouted Beds Using 3-D Particle Tracking. *Can. J. Chem. Eng.* **72**, 945.

ROWE, P. N. (1962), Effect of Bubbles on Gas-Solids Contacting in Fluidized Beds, *Chem. Eng. Progr., Symp. Ser.* **58**, 42.

SEVILLE, J. P. K., SIMONS, S. J. R., BROADBENT, C. J., MARTIN, T. W., PARKER, D. J. et T. D. BEYNON (1995), Proceeding of Fluidization VIII, Tours, France, 319.

SINCLAIR, J. L. et R. JACKSON (1989), Gas-Particle Flow in a Vertical Pipe with Particle-Particle Interaction, *AICHE J.* **35**, 1473-1486.

TANNER, H., L. LI et L. REH (1994), Radial Profiles of Slip Velocity Between Gas and Solids in Circulating Fluidized Beds, in *Fluid Particle Technology*, Weimer A. W. Ed., New York, AICHE Symp. Ser. **301**, pp. 105-113.

TSOULFANIDIS, N. (1983) *Measurement and Detection of Radiation*, McGraw-Hill.

TUNG, Y., ZHANG, W., WANG, Z., LIU, X. et X. CHING (1989), Further Study on Radial Voidage Profile in a Fast Fluidized Bed, *Eng. Chem. and Metallurgy* **10**, 18.

VAN SWAAIJ, W. P. M., BUURMAN, C. et J. W. VAN BREUGEL (1970), Shear Stresses on the Wall of a Dense Gas-Solids Riser, *Chem. Eng. Sci.* **25**, 1818.

VAN ZOONEN, D. (1962), Measurements of Diffusional Phenomena and Velocity Profiles in a Vertical Riser, *Paper Congr. European Fed. Chem. Engrs. 3rd*, London A54.

VIITANEN, P. I. (1993), Tracer Studies on a Riser Reactor of a Fluidized Catalyst Cracking, *Ind. Eng. Chem. Res* **32**, 577.

WANG, T., LIN, Z. J., ZHU, C. M., LIU, D. C. et S. C. SAXENA (1993), Particle Velocity Measurements in a Circulating Fluidized Bed, *AIChE J.* **39**, 1406-1410.

WASSERMAN P. D. (1988) Combined back propagation/Cauchy machine. *International Neural Network Society 1988 First Annual Meeting, Boston sep. 6-10*, 43.

WATANABE K. S., HIROTA L., HOIU L. et HIMMELBLAU D. M. (1994) Diagnosis of multiple simultaneous fault via hierarchical artificial neural networks. *AIChE J.* **40**, 839.

YANG, G., HUANG, Z. et L. ZHAO (1983), Radial Gas Dispersion in a Fast Fluidized Bed, in *Fluidization*, eds. D. Kunii and R. Toei, Engineering Foundation, New York, 145.

YANG, Y., JIN, Y., YU, Z., WANG, Z. et D. BAI (1991), The Radial Distribution of Local Particle Velocity in a Dilute Circulating Fluidized Bed, in *Circulating Fluidized Bed Technology III*, P. Basu, M. Horio and M. Hasarani, Eds., Pergamon Press, New York, 201-206.

YANG, Y. L., JIN, Y., YU, Z. Q., ZHU, J. X. et H. T. BI (1993), Local Slip Behavior in the Circulating Fluidized Bed, *AICHE Symp. Ser.* **89**, 81-90.

ZETHRAEUS, B. (1996), A Theoretical Model for Gas-Particle Contact Efficiency in Circulating Fluid Bed Risers, *Pow. Tech.* **88**, 133-142.

ZHANG, W., TUNG, Y. et F. JOHNSSON (1991), Radial Voidage Profiles in Fast Fluidized Beds of Different Diameters, *Chem. Eng. Sci.* **46**, 3045.

Annexe I: Revue de la littérature

L'article de revue de la littérature a été publié dans un numéro spécial du "Canadian Journal of Chemical Engineering" voué spécialement aux lits fluidisés circulants. Il se veut une revue compréhensive des travaux de recherches sur l'hydrodynamique des lits fluidisés circulants. Le sujet est vaste et tente de rejoindre tout les aspects couverts par différents auteurs dans ce domaine.

Hydrodynamics of Circulating Fluidized Bed Risers: A Review

F. BERRUTI[1], J. CHAOUKI[2]*, L. GODFROY[2], T. S. PUGSLEY[1] and G. S. PATIENCE[3]

[1]*Department of Chemical and Petroleum Engineering, University of Calgary, 2500 University Dr. N.W., Calgary, Alberta, Canada T2N 1N4*

[2]*Department of Chemical Engineering, École Polytechnique de Montréal, C.P. 6079, Succ. A, Montréal, Québec, Canada H3C 3A7*

[3]*E .I. du Pont de Nemours & Co., Wilmington, DE, U.S.A. 19880-0262*

Any vessel in which solids are transported upward by a gas stream and then recycled to the bottom may be classified as a Circulating Fluidized Bed (CFB). We describe possible CFB operating regimes in the context of this broad classification and highlight commercial processes that employ CFB technology and potential applications. Process design and development require a fundamental understanding of gas and solids hydrodynamics — solids hold-up, mixing and velocity distribution. We discuss techniques used to measure solids mass flux, which is a critical parameter for both design and control. In the last decade, significant research efforts have been devoted to new experimental techniques to measure both gas and solids spatial and temporal distribution. We list these techniques and detail the different modelling approaches that have emerged based on the new data. Characterization of the data is still incomplete and the available models require further refinement to reliably predict the effect of scale, operating conditions and particle characteristics on hydrodynamics.

N'importe quel contenant dans lequel des particules sont emportées dans la direction ascendante par un courant gazeux puis recyclées par le bas peut être classé comme un Lit Fluidisé Circulant (LFC). Nous décrivons les régimes possibles des opérations dans ces LFC en tenant compte de cette définition étendue et les procédés industriels existants et potentiels qui utilisent cette technologie des LFC.

La conception et le développement des procédés exigent une compréhension fondamentale des hydrodynamics du gaz et des particules — rétention de solides, degré de mélange et distribution des vitesses. Nous discutons les différentes techniques utilisées pour mesurer le taux de circulation de solide qui est un paramètre critique pour aussi bien le design que le contrôle. Durant le dernières années, un effort significatif de recherche a été consenti au développement de nouvelles techniques expérimentales pour mesurer les distributions temporelle et spatiale des différentes caractéristiques du gaz et du solide. Nous reportons ces techniques et nous détaillons le différentes approches de modélisation qui ont été introduites en se basant sur ces nouvelles données.

La caractérisation de ces données est encore incomplète et les modèles existants doivent être encore raffinés afin de prédire adéquatement les effets d'échelle, des conditions opératoires et des caractéristiques des particules sur l'hydrodynamique.

Keywords: circulating fluidized bed, riser, hydrodynamics, modelling, radial profiles.

Gas/solid reactors are critical to numerous industrial processes in the chemical, petrochemical and metallurgical industries, in the manufacture of fine powders and ceramics and in combustion and environmental remediation. One specific type of gas/solid reactor, the Circulating Fluidized Bed (CFB) is finding significant applications industrially because of its many intrinsic properties such as efficiency, operational flexibility and overall profitability. The CFB consists of a riser in which a gas-solid suspension is transported upward. The two-phase mixture is separated at the top of the riser and solids are recycled to the bottom via a standpipe and other ancillary equipment, such as strippers, regenerators and external heat exchangers. A schematic representation of two types of circulating fluidized bed is shown in Figures 1 and 2.

The term circulating fluidized bed was first applied to alumina calciners (Reh, 1971), but many other synonyms have been used to describe this system: fast fluidized bed, riser reactor, entrained bed, transport bed, pneumatic transport reactor, recirculating solids riser, highly expanded fluid bed, dilute phase transported bed, transport line reactor and suspended catalyst bed in cocurrent gas flow. We will use the term CFB throughout to describe generically the above systems. In this review, we discuss intrinsic characteristics of the CFB riser and highlight commercial processes that employ this technology and applications that have been patented or identified in the literature. CFB process design and development requires a good understanding of gas and solids hydrodynamics — the effect of operating conditions, scale and particle characteristics on solids hold-up, gas and solids mixing and velocity profiles. Generally, to maximize profitability, gas and solids residence times are chosen to achieve the highest product yield per unit of reactor volume. Solids residence time is a function of suspension density, solids mass flux and riser height. Riser height is generally set to achieve sufficient pressure build-up to circulate solids at a high rate. High gas velocities and low solids hold-up are preferred in some applications to minimize compressor costs. However, for many catalytic reactions, lower gas velocities may be preferred because they give higher solids hold-up, thus maximizing specific activity per unit volume.

Many hydrodynamic models have been proposed to characterize the relationship between solids hold-up and gas velocity, solids mass flux, riser geometry and particle characteristics. We adopt the classification of Harris and Davidson (1994) and group them into three categories: Type I models predict only axial solids suspension density; Type II models characterize both radial and axial solids hold-up and velocity profiles; and, Type III models employ the fundamental equations of fluid dynamics. In order to discuss the merits of these different models, we first outline the different operating regimes for CFB risers.

Despite the long history of CFB research and the significant advances in the measurement and characterization of

*Author to whom correspondence may be addressed.

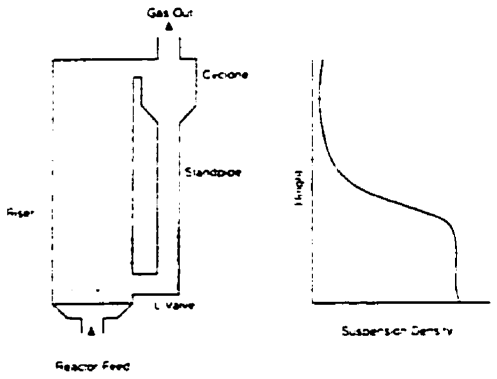

Figure 1 — Fixed Inventory System typical of CFB combustors with the characteristic axial voidage profile.

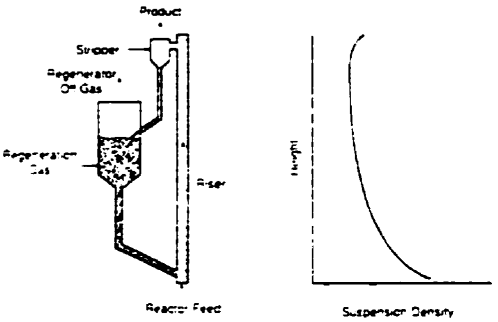

Figure 2 — Variable Inventory System typical of FCC with the characteristic axial voidage profile.

the solids hydrodynamics, several areas need more attention. Gas hydrodynamics have been studies to some degree but scale-up criteria are not very robust and require more attention. We conclude this review with suggestions in many areas that need further research.

Applications

The first documented application of gas-solid contacting in a CFB occurred when a consortium of companies, led by the engineers of the Standard Oil Development Company (now Exxon), designed the first commercial fluid catalytic cracking (FCC) unit at the Baton Rouge refinery in 1942 (Squires, 1986). Since that time, four other industrial applications have been developed: Fischer-Tropsch synthesis in synthol reactors (1950's), solids processing, including alumina calcination (1970's), high temperature operation which comprises combustion (1980's) and partial oxidation for the production of chemicals (1990's). Table 1 summarizes applications of CFB reactor technology and relevant references.

Operational flexibility is often cited as an advantage of CFB reactors over conventional technology. Other cited advantages include good gas-solids contacting at short residence times (typically less than 10 s), excellent heat and mass transfer characteristics, staged addition of gas and solids, good turndown capability and high throughout per cross-sectional area. Fast reactions are ideally suited for CFB risers. CFB technology provides unique capabilities for processes in which high selectivities are essential, coke formation or some other poisoning mechanism is rapid, gas plug flow is desirable (i.e., where product inhibition or degradation is significant), or reactions where the solids are the primary reactant and need to be withdrawn continuously. Although this mode of contacting has been commercialized for over 50 years, its industrial application to the production of chemicals is limited to the partial oxidation of *n*-butane to maleic anhydride (Contractor et al., 1994). Many processes have been patented that claim substantial advantages of this contacting regime over more conventional fixed and fluidized beds and include partial oxidation of alkanes and alkenes, epoxidation, ammoxidation and more recently oxidative dehydrogenation (see Table 1). However, they have not been commercialized because of a number of factors associated with new process development: scale-up uncertainty, process equipment complexity, need for attrition resistant catalyst and large scale requirements to justify process economics.

The two main operating parameters in CFB systems are the gas superficial velocity (U_g) and the overall solids mass flux (G_s). Typically, risers operate at gas velocities exceeding 2 m/s and solids mass fluxes greater than 10 kg/m$^2 \cdot$s. In combustion and other non-catalytic gas-solid reactions, the solids mass fluxes are generally less than 100 kg/m$^2 \cdot$s and powders belonging to the Geldart Group B classification are used. These operating conditions are significantly different from catalytic applications, where solids mass fluxes of over 250 kg/m$^2 \cdot$s are typical and Geldart Group A powders are used. Table 2 shows the typical operating characteristics of both types of units, showing that the two main applications of this technology differ widely in both design and operational characteristics.

Ideally, CFB risers operate at a relatively uniform temperature, which is achieved and maintained by a high solids recycle rate renewing the inventory of the riser. Catalytic reactions are generally carried out at relatively low temperatures (250–650°C) as compared to combustion processes (>800°C). Low temperature operation permits the use of mechanical devices to control the solids mass flux. For combustion processes, the rate is controlled by non-mechanical devices.

Regime Classification

When gas is introduced through a suitable gas distributor at the base of a column containing solid particles, different hydrodynamic regimes can be observed, depending on the particle characteristics and the magnitude of the gas superficial velocity. When the gas velocity is increased, the regimes will change from that of a packed bed to the bubbling bed, to slug flow, to the turbulent regime, to fast fluidization and eventually to pneumatic transport. Many studies have been conducted to characterize the flow regime transitions, as summarized in Kunii and Levenspiel (1991a). The following discussion on the physical characterization of CFB risers assumes that solid particles used in the fluidized system belong to either the Group A or B of the Geldart classification and refers to the block diagram represented in Figure 3. This diagram schematically illustrates the regimes of operation of gas-solid fluidized contactors in accordance with the interpretation proposed in the present review.

The onset of fluidization is typically characterized by the minimum fluidization velocity (U_{mf}), or the gas superficial velocity at which the gas-particle mixture starts behaving

TABLE 1
Milestones and Potential Applications of CFB Technology

	Reference
Fluid Catalytic Cracking (FCC)	
• Review of early history and development of the FCC process	Squires (1986)
• Review of recent process and hardware developments	King (1992)
• US capacity reached 10 Mb/d in 1992 with over 350 FCC units	Reichle (1992)
• FCC CFB catalyst regenerators described	King (1994)
Fischer-Tropsch Synthesis:	Jewel and Johnson (1951)
• Gasoline production began in a Synthol CFB in 1955	Dry (1982)
• Larger Synthol reactors came on stream in 1980 and 1982	Shingles and McDonald (1988) Silverman et al. (1986)
• History and operational experience of Synthol CFB reactors	Bartholomew (1991)
• Methanol synthesis	Chanchlani et al. (1994)
• Methanol-to-olefins	Schonfelder et al. (1994)
Solids processing:	
• AlF_3 from $Al(OH)_3$ and 98% HF	Reh (1971)
• Calcination of $Al(OH)_3$ to alumina (Al_2O_3)	Reh (1971)
• Conversion of ferric chloride to iron oxide and chlorine	Reeves et al. (1981)
• Metallurgical and inorganic chemical industries waste gas scrubbing	Reh (1986)
• Reduction of iron ore	Zhiqing (1994)
• Reduction of gold roasting	Peinemann et al. (1992)
Combustions and Applications, Environmental Remediation	
• Over 220 units in operation by 1991	Engstrom and Lee (1991)
• NO_x emission requirements	Tang et al. (1994)
• Performance testing of a large combustor	Moe et al. (1994)
• Tests using different fuels	Anders et al. (1991)
• Municipal waste incinerator	Hallstrom and Rarlsson (1991)
• Combined pressurized gasifier and atmospheric combustion	Anders et al. (1991)
• Ethane and propane cracking	Koyama and Ranoff (1992)
• de NO_x/de SO_x	Herrmann and Weisweiler (1994)
Potential heteregeneous catalytic applications:	
1. Paraffin Oxidation	
• Partial oxidation of n-butane to maleic anhydride	Contractor (1994) Pugsley et al. (1992)
• Oxidative coupling of methane to ethane and ethylene	Baerns et al. (1994) Dutta and Jazayeri (1992) Santamaria et al. (1991)
• Oxidation of alkane to alcohols and ketones: – isobutane to ter-butylalcohol – propane to acetone – isopropyl alcohol and butane to methyl ethyl ketone	Lyons (1993)
• Methane to CO and H_2	Lewis et al. (1949)
2. Ammoxidation	
• Acrylonitrile from propylene	Beuther et al. (1978)
• Benzonitrile from toluene and acrylonitrile from propylene	Gianetto et al. (1990)
• Acrylonitrile and methacrylonitrile from propylene and butene	Huibers (1969)
• Tetraphthalonitrile from p-xylene	Huibers (1969)
• Acylonitrile and methacrylonitrile from propane and i-butane	Kahney and McMinn (1976)
3. Allylic Oxidation	
• Maleic anhydride from C4 to C6 fractions	Rollman (1952)
• Acrolein from propylene process patent	Johnson (1963)
• Acrolein from propylene	Callahan et al. (1970) Patience and Mills (1994) Rollman (1952)
• Phthalic anhydride from o-xylene and naphtalene	Wainwright and Hoffman (1974)
• Phthalic anhydride from o-xylene	Gelbein (1981)
4. Epoxidation	
• Ethylene oxide from ethylene	Rollman (1952) Park and Gau (1986)
5. Dehydrogenation	
• Anaerobic oxidation of butane to butadiene	Tmenov et al. (1980)
• Alkane oxidative dehydrogenation	Murchison et al. (1993) Sanfilippo et al. (1992)
• Ethyl benzene to styrene and ethyl toluene to vinyltoluene	Debras et al. (1992)
• Butadiene from butane and butenes	Woskow (1969, 1970)
• Ethylene from ethane	Coudurier et al. (1993)
6. Other	
• Glyoxal from ethylene glycol	Gallezot et al. (1993)
• Methanol from formaldehyde	Zaza et al. (1991)

TABLE 2
Operating Characteristics of Fast Fluidized Bed Catalytic Reactors and Combustors

Characteristic	Catalytic Reactors	Combustors
Superficial velocity	4–10 m/s	2–6 m/s
Solids circulation rate	> 250 kg/m^2 · s	5–100 kg/m^2 · s
Particle diameter	50–196 μm	250–506 μm
Geldart Classification	A	B
Temperature	250–650°C	> 800°C
Riser Diameter	1–2 m	8–10 m
Pressure	≥ 100 kPa	100 kPa
Solids reinjection system	mechanical	non-mechanical valves
Exit geometry	smooth, abrupt	abrupt

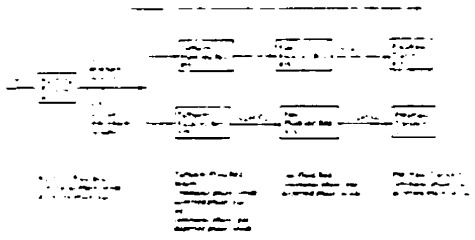

Figure 3 — Fluidization regimes with characteristic transition gas velocities.

in a liquid-like manner. According to the two-phase theory of fluidization, as U_{mf} is exceeded, gas bubbles may appear throughout the bed enhancing the degree of solids mixing. A bubbling fluidized bed is characterized by a gas-solid mixture where the solids are the continuous phase and the gas the dispersed phase. As the gas superficial velocity is increased, particles may become entrained by the gas stream leaving the top of the bed. Depending upon the length of the freeboard region above the bed, particles may leave the column. Cyclones are installed to return elutriated solids back to the bed. Conceptually, a bubbling fluidized bed equipped with a cyclone may be considered as a circulating fluidized bed.

When the increasing gas superficial velocity reaches a certain critical value, U_c, the bed is said to become turbulent (Chehbouni et al., 1994). A turbulent fluidized bed is characterized by two different coexisting regions: a lower region, where the solids are the continuous phase and the gas the dispersed phase and an upper region, where the gas is the continuous phase and solids are dispersed. Under these conditions particle carryover through the top of the column becomes more significant. Figure 3 indicates that the operating regimes beyond the transition velocity, U_c, will follow two different paths depending upon the design of the CFB system, i.e. whether or not the solids mass flux is a dependent or independent operating variable, corresponding to the operation as a Fixed Inventory System (FIS) or a Variable Inventory System (VIS), respectively.

Figure 1 and 2 illustrate the difference between FIS and VIS designs as outlined by Kobro and Brereton (1986) and Kunii and Levenspiel (1991b). There is no controllable solids storage inventory in a FIS; setting the gas velocity and solids charged to the reactor establishes the solids hold-up in the riser and solid mass flux. In a VIS, an additional vessel is located in the return leg; gas velocity and mass flux are varied to achieve a desired solids hold-up in the riser. However, for the same powder and riser geometry, the pressure drop in fully developed region (the section of the riser away from entrance or end effect where the hydrodynamic parameters are invariant with height) in either design should be the same when operated at the same mass flux and gas velocity.

If the solids mass flux through a turbulent fluidized bed is not an independent variable, the system may be defined as a FIS turbulent bed. The time averaged axial distribution of the solids suspension density is typically characterized by a sigmoidal profile, shown in Figure 1, approximately constant along the dense bed and exponentially decaying along the freeboard.

When the gas velocity reaches another specific value, the onset of fast fluidization is observed. This regime is characterized by only one region: gas is the continuous phase and solids, typically moving upward in the centre and downward at the wall, are dispersed. Under these conditions, the time averaged axial distribution of the bed density is characterized by an exponentially decaying porfile from the entrance region to the location where fully developed flow conditions are achieved, as illustrated in Figure 2. A pneumatic transport reactor is characterized by a very dilute gas solid flow (gas is the continuous phase) with little or no particle backflow at the wall. Bi et al. (1994) define three velocities that characterized the transition to this regime, only one of which is stable U_{CA}. The other two velocities delineate transitions into unstable regimes induced by blowers, standpipes or riser geometry.

In a VIS the operating regimes of the CFB system may change as illustrated in Figure 3. When U_{tr} is reached, the regime changes from a VIS turbulent bed to fast fluidization. This may be true as long as the imposed solids mass flux does not exceed the saturation carrying capacity of the gas, which Geldart (1986) defines as the solids loading that causes the gas-solid suspension to collapse into dense phase or slugging flow at the bottom of the column. Otherwise, the transition will occur a higher gas superficial velocity, and the transition velocity U_{tr} will be a function of the imposed solids mass flux. Similarly to a FIS, Bi et al. (1994) defined three velocities to characterize the change from fast fluidization. Once again, only U_{CA} characterizes the transition into pneumatic transport regime. U_{CA} is also expected to be a function of G_s when the imposed solids flux exceeds the saturation carrying capacity of the gas.

Numerous publications deal with the experimental determination of the transition velocities between bubbling and turbulent fluidization, and between turbulent and fast fluidization (e.g. Schnitzlein and Weinstein, 1988; Perales et al., 1991; Brereton and Grace, 1992; Chehbouni et al., 1994). A more comprehensive list is provided by Chehbouni et al.

(1994). Additional research is needed to better define the gas transition velocities in the case of a VIS, in accordance with the proposed regime formulation of Figure 3. Perales et al. (1991) and Chehbouni et al. (1994) determined the transition velocity to fast fluidization for a fixed inventory system based on data for the time to empty the bed in the absence of solids recycle as a function of the gas superficial velocity.

CFB operating regimes have been defined in several different and controversial ways during the past decade. Yerushalmi and Cankurt (1978) defined the CFB as a fluidized bed operating at gas velocities exceeding the minimum transport velocity. Kwauk et al. (1986) and Takeuchi et al. (1986) stated that an inflection point separating a dense phase at the bottom from a dilute phase at the top of the riser was necessary. Recently, Karri and Knowlton (1991) suggested that the fast fluidization region can be defined by two transition velocities for a given solids mass flux: the choking velocity, and the velocity corresponding to the minimum pressure drop on the ΔP vs. U_g diagram (onset of pneumatic transport). Yang (1994) defined the incipient fast fluidization velocity as the velocity at which the solids start to reflux adjacent to the wall to form a dense phase at the bottom of the riser. On the basis of the qualitative description of the operation regimes of fluidized bed systems proposed above in Figure 3, a CFB can be defined as any system (either FIS or VIS), involving solids recirculation, operating at gas velocities exceeding U_c. It may be operated under turbulent fluidization, fast fluidization or pneumatic transport regimes. This broad definition is consistent with many experimental observations reported in the literature dealing with the general appearance of the bed and discussed later in the present view. In this paper, the discussion focuses mainly on systems where the gas velocity and solids mass flux are independent variable (VIS), and concentrates on the fast fluidization regime which is often difficult to clearly characterized in view of the complexity in the definition of the regime boundaries, especially in the VIS operation.

Most of the work reported in the literature describe hydrodynamics of small scale risers — 3 to 15 m tall from 0.02 to 0.15 m in diameter. In particular, the exit configuration, either smooth or abrupt, has led to different experimental findings related to the gas-solid suspension densities. Also, various configurations of the solids reinjection systems at the base of the riser have been used by different authors (L-valve, V- valve, J-valve). In summary, a word of caution is needed regarding the extrapolation of findings obtained with a specific configuration to risers that are geometrically dissimilar. The following sections will attempt to generalize the experimental results available in the literature, and to provide guidelines for a reliable interpretation of experimental data, for a better understanding of the complex features of CFB risers.

Solids Mass Flux

The gas-solid suspension density within the riser is greatly influenced by both gas superficial velocity and solids mass flux, and therefore, these operating parameters directly affect heat transfer, mass transfer, and chemical reaction rates. The control of the solids mass flux is achieved by varying the operating conditions at the level of the solids reinjection system. In the case of mechanical valves (e.g. slide valve), the valve operation controls the solids mass through the CFB loop. Mechanical valves have moving parts which are not suitable for high temperature applications, but have the advantage of better control of solids circulation, and the ability to achieve higher solids mass fluxes because of a lower pressure drop. In the case of non-mechanical valves, the solid mass flux is controlled by aeration of the standpipe. Solids flow through non-mechanical valves as a result of drag on the particles by the aeration gas. Non-mechanical devices use only aeration and piping geometry to control the flow rate of solids, have no moving parts, are inexpensive, and can be manufactured easily.

Accurate measurement of gas superficial velocity and solids mass flux is critical in experimental investigations of the riser flow structure so that results of various researchers can be compared. However, quantifying the solids mass flux is problematic. Ideally, it should be on-line and easily calibrated, e.g. for gas velocity. A number of different techniques have been developed and tested to provide a reliable method for mesuring and controlling the solids mass fluxes. Most of these methods involve determining the solids mass flux based on the particle velocity in the downcomer side of the CFB. Burkell et al. (1988) reviewed some of these techniques, which included: closing a permeable valve in the return leg and timing the solids accumulation, timing the descent of identifiable particles at the standpipe wall, recording the force imparted by returning particles as they fall downward from the cyclone, measuring the pressure drop across a constriction in the return loop, and estimating the solids flow from a heat balance on a calorimetric section in the standpipe. They conclude that the first two methods, while easily calibrated, are poor on-line techniques. The remaining methods provided adequate on-line measurement, but careful calibration was necessary. For instance, the measurement of the time of descent of particles at the standpipe wall may appear to be a simple and accurate calibration technique. However, Patience and Chaouki (1991) showed that wall velocities were typically half the bulk velocity calculated based on the mean residence times of the particle in the return leg. Milne et al. (1992) described a new technique for measuring the solids mass flux in which a rigid horizontal screen attached to a vertical rod was dropped into the bulk flow of the moving packed bed in the solids return leg, and the time required for the tip of the rod to travel a prescribed distance was determined. A similar method was employed by Kuramoto et al. (1985). Such techniques, though too cumbersome for on-line measurement of solids mass flux, provide an excellent method of calibration.

Patience et al. (1990) provided a description of an alternative, on-line method, based on measurements of pressure drop in horizontal section of the CFB loop connecting the top of the riser and the primary cyclone, as well as along the riser itself. This method was shown to be reliable, non-interfering and suitable for applications involving high temperatures and large scale units. Dry et al. (1994) considered four possible differential-pressure drop measurements in a large-scale cold model CFB, and found that the riser mid-section or riser top differential pressures were the most useful parameters for on-line measurement. Pressure gradient measurements, which can easily be performed along CFB risers, provide a clear indication of the development of the flow and, in particular, of the axial location along the riser where the flow can be considered fully developed, corresponding to a pressure gradient which is invariant with height. Patience and Chaouki (1991) suggested that the radioactive tracers could be the most direct, non-interfering technique to measure solids mass flux. On-line calibration using radioactive tracers would give a sensitive and reliable method amenable to any scale.

Solids Hydrodynamics

The gas and solids flow structure in CFB risers is inherently very complex. As a result of this complexity, accurate experimental measurements are difficult and attempts at hydrodynamic modelling have not been entirely successful. Risers exhibit an axial solids hold-up distribution showing a certain degree of densification at the bottom of the column where the solids are introduced from the standpipe. The solids holdup decreases along the riser as the solids are accelerated by the high velocity gas stream. Provided the riser is long enough, fully developed flow conditions will be reached corresponding to a solids holdup which is approximately invariant with height. Some riser exit geometries enhance local backmixing or internal recirculation at the top that results in an increase in the suspension density. Experimental observations clearly show that the slip velocities in CFB risers, defined as the difference between interstitial gas velocity and particle velocity, exceed single particle terminal velocities.

Several modelling efforts making various assumptions regarding the gas and solids flow structure and employing very different mathematical formulations have appeared in the recent literature. Harris and Davidson (1994) classified the variety of models that have been published into three broad groups: (I) those that predict the axial variation of the solids suspension density, but not the radial variation, (II) those that predict the radial variation by assuming two or more regions, such as core-annulus or clustering annular flow models, (III) those that employ the fundamental equations of fluid dynamics to predict two phase gas-solid flow. As discussed by Harris and Davidson (1994), the attractiveness of the type III models is in their generality and ability to deal with complex geometries, but the nature of the constituent equations for two-phase gas-solids flow must be questioned, and the numerical complexity alone often discourages their use. Proponents of the type I and II models cite ease of understanding and usage along with generally very good agreement with experimental data as the main advantages. However, detractors argue that the assumptions of the flow structure associated with such models oversimplify the complex experimentally observed flow patterns. One important consideration in selecting a modelling approach is its intended application: type I and II models may be best employed as design tools to investigate the effects of operating conditions and riser dimensions on the riser flow structure. In addition, they may be easily coupled with reaction kinetic models to simulate the performance of CFB reactors (e.g. Pugsley et al., 1992; Patience and Mills, 1993; Bolkan-Kenny et al., 1994). Type III models, on the other hand, are well suited to investigate the riser local flow structure and the impact of geometry, such as the corner effects in CFB combustors, or unique inlet configurations such as those studied by Pita and Sundaresan (1993). The three classes of models described may be further characterized by the mathematical approach taken. This characterization is obvious for type III models in which a system of equations contains the continuity, momentum, and pseudo-thermal energy balances, and constitutive relations are solved. However, types I and II may involve the use of correlations based on experimental data, referred to as the "lumped approach", or a combination of correlations and fundamental relationships.

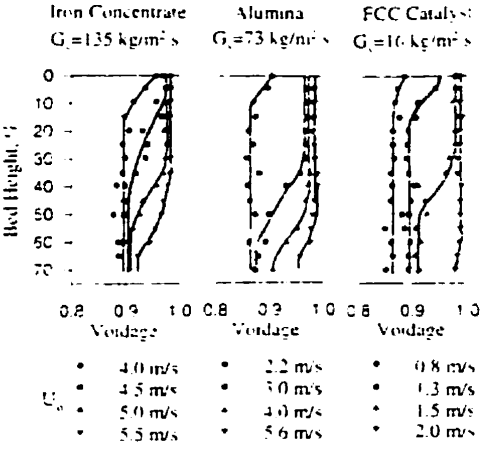

Figure 4 — Axial voidage profiles (Kwauk et al., 1986).

AXIAL SOLIDS DISTRIBUTION — TYPE I MODELS

Many studies have appeared in the literature dealing with axial solids distribution along CFB risers (e.g. Yerushalmi et al., 1976; Kwauk et al., 1986; Arena et al., 1991; Bai et al., 1992a). It is most often represented as either a plot of the radially averaged solids suspension density or voidage versus height as shown in Figure 4. This profile is experimentally determined from the pressure distribution along the riser, recognizing that the suspended solids constitute the major contributor to the pressure drop (Louge and Chang, 1990),

$$\rho_p (1 - \varepsilon) = -\left(\frac{1}{g}\right)\frac{dP}{dz} \quad \ldots\ldots\ldots\ldots\ldots\ldots \quad (1)$$

This formation ignores acceleration, which is significant at the base of the riser as shown by Weinstein and Li (1989), gas and solids wall friction, and gas density.

The experimental work of Yerushalmi et al. (1976) is generally considered as the pioneering academic study of the axial solids distribution in circulating fluidized bed risers. They discussed the densification at the riser base and proposed several advantages of operating in the fast fluidization regime. Kwauk et al. (1986) demonstrated the coexistence of a dense phase at the bottom of the riser below a dilute phase extending to the top of the riser, and provided a mathematical expression for describing the characteristic S-shaped voidage distribution that they experimentally measured, indicating the vague boundary between dense and dilute regions:

$$\ln\frac{(\bar{\varepsilon} - \bar{\varepsilon}_a)}{(\varepsilon^* - \bar{\varepsilon})} = \left(\frac{-1}{Z_o}\right)(Z - Z_i) \quad \ldots\ldots\ldots\ldots\ldots \quad (2)$$

where $\bar{\varepsilon}$ is the voidage at the distance Z from the top of the riser, Z_o is a characteristic length, Z_i is the height of the inflection of the curve, and ε_a and ε^* are the limiting voidage of the dense and dilute phases, respectively. They also defined fast fluidization as the regime in which the suspension density is dilute at the top and dense at the

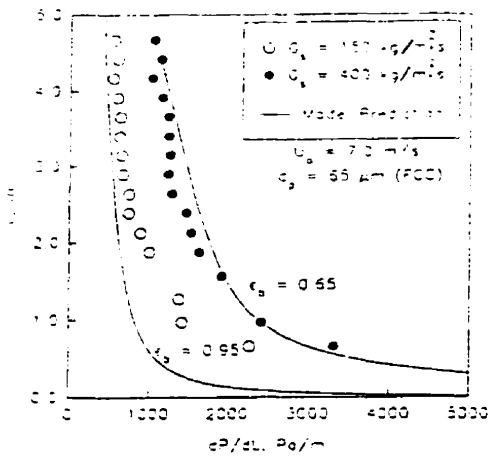

Figure 5 — Axial pressure profiles of sand in the fast fluidization regime (Pugsley et al., 1993).

bottom, with an inflection point in between. The axial voidage profiles of Kwauk et al. (1986) for different solids at constant solids mass flux, and different gas velocities are illustrated in Figure 4. Based on this work, they showed that, at a fixed solids mass flux, an increase in the gas superficial velocity caused a decrease in the solids holdup. The voidage profiles of Figure 4 also show that with increasing gas superficial velocity, the inflection point, Z_i, first appears near the top of the riser, then moves downward, and eventually disappears. In accordance with the earlier discussion this would represent a transition through the CFB operating regimes, from turbulent fluidization to fast fluidization. The profiles at the lowest gas velocities in Figure 4a, 4b, and 4c represent on CFB operating under a solids mass flux such that the dense phase fills the entire riser, and the voidage profile is essentially constant. At the highest gas superficial velocities, the exponential voidage profile is present, indicative of operation in the fast fluidization regime. All other intermediate velocities, resulting in a point of inflection in the axial voidage profile, are characteristics of the turbulent fluidization regime. In all investigations conducted within the fast fluidization regime, experimental evidence indicates that the sigmoidal axial suspension density profile is not applicable as the gas superficial velocities used are higher than the transport velocity, U_{tr}. Under these conditions, the axial voidage distribution is found to have a typical profile described by a simple exponential decay function from the base of the riser, eventually reaching a constant value higher up in the column where the flow becomes fully developed. Figure 5 shows typical profiles obtained at a constant gas velocity and different solids mass fluxes. Even at the highet solids fluxes, the exponentially decaying profile is observed.

Kunii and Levenspiel (1991b) treated the dilute region of CFB riser by extending entrainment models developed originally for bubbling fluids beds. The riser is viewed as having a lower region of constant bulk density and an upper region where the bulk density decreases with height. Once again, according to the definition proposed in the current review, this model would only be valid for risers operating in the turbulent fluidization regime. They showed that the dilute zone height should be the same, in principle, for the same gas superficial velocity, solids mass flux and exit configuration, irrespective of the column height. This point has also been demonstrated experimentally by Horio et al. (1988). However, Weinstein et al. (1983) and Schnitzlein and Weinstein (1988) showed that the height of the dilute region may be a function of gas velocity, solids mass flux as well as solids inventory.

The model of Rhodes and Geldart (1986) extended the bubbling fluidized bed entrainment model to explain the typical $\Delta P/L$-G_s-U_g plot for Geldart A powders. Bolton and Davidson (1988) developed a similar relation for the developed a similar relation for the axial solids flux profile down the riser wall. Yang (1988) modelled the dense phase at the riser base as dense phase pneumatic transport with an annular region, and used an available pneumatic transport correlation to model the dilute region in the upper section of the riser. The height of the interface between the two regions were determined from a consideration of the overall pressure balance around the solids circulation loop. A fundamentally different approach was presented by Zhang et al. (1991) which combined Brownian motion with Random Walk theory to model the axial solids voidage distribution. The result was the familiar exponential relationships, one describing the voidage profile in the dense region, and one describing the dilute phase voidage profile. Values for the limiting voidages and the axial location of the interface were determined from previously published correlations. Fujima et al. (1991) modelled the axial voidage profiles as due to "chain growth" or cluster formation. Finally, Mori et al. (1991) and Choi et al. (1991) developed empirical correlations to predict the average axial voidage profiles.

Squires (1986) relates that it was recognized at an early stage of the commercial development of CFB risers that the relative velocity between the solids and gas — the slip velocity — could be greater by two orders of magnitude with respect to the predicted by Stokes' law. Large slip velocities result in high suspension densities (high solids volume fraction). Predicting the solids volumetric fraction in a fully developed flow stream continues to be a critical parameter in Type I models. Modelling approaches vary considerably from overly simplistic to unnecessarily complex. Kunii and Levenspiel's (1995) models is an example of the former. They propose that for Geldart group A powders the solids volumetric fraction in fully developed flow is less than 0.02, and that it is less than 0.01 for Geldart AB and B powders. This model does not account for the data published by Contractor et al. (1994) in which solids volume fractions exceeding 0.15 are reported for a 27 m tall riser. Kwauk et al. (1986) developed a correlation that relates the solids volume fraction to a Reynolds number but requires an iteration technique to solve the equations since the Reynolds number they use depends on solids velocity and volume fraction. Yang's (1988) pneumatic transport model expresses the particle velocity as the difference between gas velocity and the particle terminal velocity multiplied by a function that includes the solid friction factor. However, the correlations underestimate the slip velocities and solids volume fraction; slip velocities are not orders of magnitude greater than the Stokes' law-based particle terminal velocity.

Matsen (1976) observed that for industrial FCC risers the ratio of the gas velocity to solids velocity — the slip factor — was approximately equal to 2,

$$\psi = \frac{U_g/\varepsilon}{V_p} \qquad (3)$$

Patience et al. (1992) applied the concept of slip factor to experimental data in risers varying in diameter from 0.04 to 0.15 m and found that a value of two was a good first approximation; it varied from 5 at velocities near 2 m/s to 1.6 at gas velocities exceeding 10 m/s. Ouyang and Potter (1993b) examined a larger pool of experimental data and found that the average slip factor was 2.6 with a standard deviation of 0.9. Patience et al. (1992) proposed an empirical correlation to account for the effects of particle characteristics, riser diameter and gas velocity on the slip factor:

$$\psi = 1 + \frac{5.6}{Fr} + 0.47\, Fr_t^{0.41} \quad \ldots\ldots\ldots\ldots\ldots\ldots\ldots\ldots \quad (4)$$

where Fr is the Froude number and Fr_t is the $U_o/(gD)^{0.5}$ Froude number based on the terminal velocity of a single particle = $V_t/(gD)^{0.5}$. Rearranging Equation (3) in terms of density yields a simple relationship to calculate suspension density:

$$\rho = \frac{\rho_p}{\left(1 + \dfrac{\rho_p\, U_o}{G_s\, \psi}\right)} \quad \ldots\ldots\ldots\ldots\ldots\ldots\ldots\ldots\ldots\ldots \quad (5)$$

High slip factors ψ results in high suspension densities Equation (4) indicates that density increases with increasing particle terminal velocity and decreases with gas velocity. As the gas velocity approaches pneumatic conveying, the slip factor approaches one and the slip velocity tends towards the single particle terminal velocity. Equation (4) surprisingly predicts that the suspension density increases with riser diameter, but Avidan (1980) and Bai et al. (1992b) reported the opposite trend with respect to riser diameter. In the latter study, two units 0.14 m in diameter and 0.186 m were examined. At a gas velocity of 4.4 m/s and a solids mass flux of 86 kg/m$^2 \cdot$s, the solids volume fraction was more than double in the larger diameter unit — 0.047 compared to 0.017. In the former study, the solids volume fraction was 0.018 in a 0.15 diameter riser at a gas velocity of 4.5 m/s and a solids mass flux of 86 kg/m$^2 \cdot$s, and 0.047 in a riser 0.076 m in diameter. Both studies attributed the increased volume fraction to the wall effect. However, Contractor et al. (1992) showed that solids volume fraction decreases when additional "wall" surface, a heat transfer tube, is introduced into the riser. Further experimental work and characterization is required to relate the slip factor to particle characteristics, riser geometry and operating conditions.

The slip factor correlation provides a good check on experimental mass flux measurements: if the calculated slip factor, based on the experimental data, approaches a value of one than either the solids mass flux is overestimated or the flow regime is pneumatic transport. Values greater than five suggest that either the solids mass flux is underestimated or entrance/exit effects are significant.

Radial Solids Distribution — Type III Models

Whereas Type I models account for increased solids hold-up higher than prediced by Stokes' law, Type II models attempt to characterize the solids distribution radially and explain the reason for the higher solids hold-up. Yerushalmi et al. (1976) proposed that the increased solids hold-up was

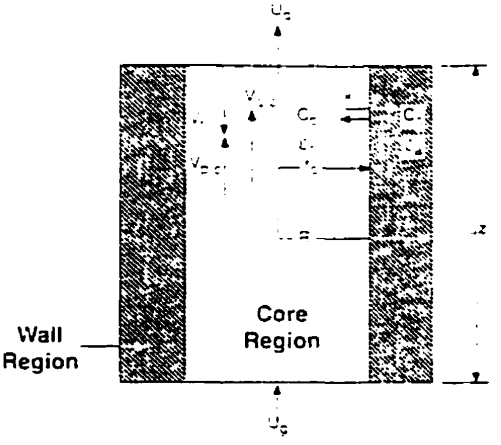

Figure 6 — Core-annular model.

attributable to an agglomeration phenomenon, called "clustering"; solids coalesce to form a larger pseudo-particle. The particle terminal velocity of the cluster is sufficiently high to account for the large slip velocities observed experimentally. These clusters are dynamic, i.e. they constantly form and disintegrate. Berruti and Kalogerakis (1989) explained the high slip velocities by assuming that the flow domain consists of two characteristic regions: a dilute gas-solid suspension preferentially travelling upward in the centre (core) and a dense phase of particle clusters or strands, as shown in Figure 6. They assume that the slip velocity in the core equals the particle terminal velocity and that the density in the annulus is equal to that at minimum fluidization. Their model assumes that solids descend along the annulus at a velocity equal to the particle terminal velocity.

Strong radial suspension density gradients have experimentally been reported with a maximum at the wall and a minimum at the centre, which agrees well with the core-annular approximation to the flow domain. Also, particle velocity and solids flux measurements across the cross-section of risers are approximately parabolic radially, often with negative velocities along the riser wall. Downward particle velocities between 0.5 and 1.5 m/s have been measured experimentally (Grace, 1990). Typical upward and downward solids flux and radial particle velocity profiles are illustrates in Figures 7 and 8.

Several different types of probes have been developed by various researchers to measure radial density profiles, particle velocities, and solids flux. These include capacitance probes (Brereton and Grace, 1993), fibre optic probes (Li et al., 1991b; Reh and Li, 1991; Horio et al., 1988; Hartge et al., 1988), iso-kinetic and non-isokinetic sampling probes (Rhodes et al., 1988; Bolton and Davidson, 1988; Bodelin et al., 1994), X-rays (Weinstein et al., 1986), high speed cinematography (Takeuchi and Hirama, 1991), laser Doppler velocimetry (Yang et al., 1991), Pitot tubes (Bader et al., 1988), and recently a laser sheet technique (Kuroki and Horio, 1994). A set of three laser sheets intersecting at right angles is applied to see the three dimensional structure of the suspension. The limination of this technique is penetration of the laser when the solids concentration is high.

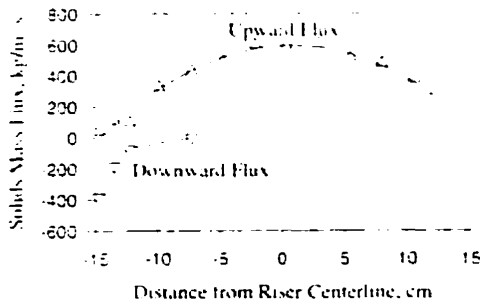

Figure 7 — Radial mass flux profiles of FCC powder in a 0.305 m diameter riser: U_t = 4.6 m/s, G_s = 147 kg/m^2·s (Bader et al., 1988)

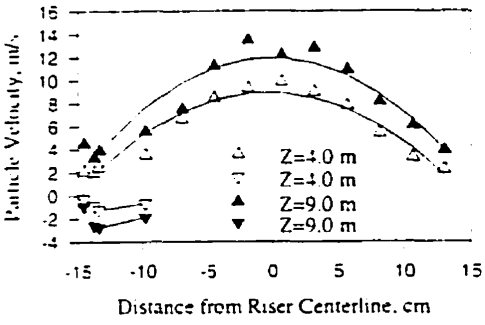

Figure 8 — Radial velocity profiles of FCC powder in a 0.305 m diameter riser: U_t = 3.7 m/s, G_s = 98 kg/m^2·s (Bader et al., 1988)

Tables 3-5 list experimental investigations relating the radial void fraction, solids velocity, and solids mass flux profiles.

Zhang et al. (1991b) reporting radial void fraction profiles for four different powders in three different risers up to 0.3 m in diameter, have found that the normalized radial void fraction was a unique function of radial distance. The observations of Herb et al. (1989), Mineo (1989), and Tung et al. (1989) support this observation. In Figure 9, Zhang et al.'s data are compared with a correlation proposed by Patience and Chaouki (1995): centreline densities are assumed equal to the average void fraction raised to the 0.4 power, i.e.

$$\frac{\bar{\varepsilon}^{+0.4} - \varepsilon_r}{\bar{\varepsilon}^{+0.4} - \bar{\varepsilon}} = 4\left(\frac{r}{R}\right)^6 \quad \ldots\ldots\ldots\ldots\ldots\ldots\ldots\ldots\ldots\ldots \quad (6)$$

The expression proposed by Zhang et al. (1991b) assumed a power of 0.191; however, this low power value underestimates the mass flux at the centreline:

$$G_{s,r} = \rho_p (1 - \epsilon_r) V_{p,r} \quad \ldots\ldots\ldots\ldots\ldots\ldots\ldots\ldots\ldots\ldots \quad (7)$$

Monceaux et al. (1986), using a sampling probe, observed what they called "similar profiles" of solids mass flux. They showed that, at a given gas velocity, radial profiles of reduced mass flux (local solids flux divided by cross-sectional mean solids flux) changed very little with changes in means solids flux in the riser. Rhodes et al. (1992a) support this concept and they proposed a model capable of simulating solids flux profiles and linking solids flux, solids hold-up and solids velocity. They suggested that the thickness of the annular region was independent of the solids mass flux and only a function of gas velocity. The conducted their experiments in two risers of 0.152 m and 0.305 m diameter. At higher gas velocities, the profiles became less parabolic in shape, and the thickness of the annular region decreased. In the larger riser, the profiles were flatter, and the relative thickness in the annulus is less than that observed in smaller risers. The actual thickness of the downflow region seems comparable in large as well as in small risers, at a given gas superficial velocity, indicating that this reverse flow is predominantly a wall effect.

A closer examination of the radial profiles of mass flux reported by Rhodes et al. (1992a) reveals that they are, in fact, not similar. For example, as shown in Figure 10, at the highest mass flux of 63 kg/m^2·s, the reduced mass flux is greatest at almost twice the average mass flux in the centre of the riser. At the lowest mass flux, 2.8 kg/m^2·s, the maximum mass flux is near the wall and the centreline is almost at a local minimum. It appears that the idea of a "similar profiles of mass flux" may be valid over a very limited range of operating conditions. Yang et al. (1991) report velocity profiles at different heights and show a significant variation in the profile from the entrance region to the exit. Thus, if a universal radial solids volume fraction profile exists and the velocity profile changes with height, the mass flux profile must also change with height, as shown in Equation (6).

Bodelin et al. (1994) report that the radial particle size distributions are essentially independent of the solids loading for dilute gas-solids suspensions. Higher solids mass fluxes result in increased internal recirculation of particles, and the suspension flowing downward along the wall contains a higher fraction of coarse particles.

Brereton (1987) observed that the core-annular flow structure characterization does not take into consideration the fluctuating nature of the flow. He proposed an intermittency index to account for the fluctuations, defined as the ratio of the standard deviation of density fluctuations at a given point to the standard deviation of density fluctuations for fully segregated two-phase flow having identical time-mean density at the same point. It varies between zero, for uniform steady flow of any mean density, and unity, for a flow of the same density consisting of clusters of loosely packed particles surrounded by particle-free gas. Based on this interpretation, the intermittency index rapidly decreased in the core moving from the bottom of the riser towards the fully developed flow region, whereas its value remained consistently in the vicinity of the wall, where the segregated flow was maintained along the entire riser. Those observations seem to be more applicable to risers where Group B particles are employed. For Group A particles, typical solids mass fluxes are larger, corresponding to higher average suspension densities. Particle interactions, including intra-particle forces, enhance the clustering behaviour and the intermittency index is expected to possess larger values throughout the riser. Brereton et al. (1993) describe the behaviour of Group A particles throughout the column similar to that of Group B particles at the base of the riser. Systematic measurements of clusters sizes and characteristics have been provided in the literature (e.g. Horio et al., 1988; Arena et al., 1991). A critical examination of the abundant

TABLE 3
Sources of Data on Local Void Fraction

Experimental Method	Comments	Reference
pitot tube / isokinetic probes	wavy annular film	Harris et al. (1994)
capacitance probes / optic fiber probes	radial profiles	Hartge et al. (1986)
capacitance probes	experimental data profiles	Herb et al. (1989)
capacitance probes / video camera	wall solids hydrodynamics	Herb et al. (1992)
optical probes	two phase flow	Hartge et al. (1988)
optical probes	cluster size distribution	Ishii et al. (1989)
optical probes	radial profiles	Zhang et al (1991)
optical fiber / dynamics pressures	radial profiles	Qian and Li (1994)
gamma ray absorption	dense wall, dilute core	Saxton and Worley (1970)
gamma ray tomography	core annulus flow	Martin et al. (1986, 1992)
gamma ray camera	k-epsilon turbulence model	Berker and Tulig (1986)
gamma ray absorption	radial profiles	Azzi et al. (1991)
X ray absorption	third order polynomial radial profile	Weinstein et al. (1986)
X ray densitometer	two phase flow	Miller and Gidaspow (1992)

TABLE 4
Sources of Data on Solids Velocity

Experimental Method	Comments	Reference
pitot tube	core-annulus flow structure	Bader et al. (1988)
pitot tube / isokinetic probe	wavy annular film	Harris et al. (1994)
laser Doppler velocimetry	radial velocity profiles	Yang et al. (1991, 1993)
particle dynamic analyser	core-annulus flow structure	Wang et al. (1993)
optical fiber probes	two phase flow	Hartge et al. (1988)
optical fiber probes	annular flow with clusters	Horio et al. (1988)
optical fiber probes	cluster velocity profiles	Ishii et al. (1989)
optical fiber probes	radial profiles	Katoh et al. (1995)
optical fiber probes / dynamic pressure	radial profiles	Qian and Li (1994)

TABLE 5
Sources of Data on Local Solids Mass Flux

Experimental Method	Comments	Reference
isokinetic sampling probes	radial profiles	Van Breugel et al. (1969) Herb et al. (1992)
non-isokinetic sampling probes	similar profiles	Monceaux et al. (1986) Rhodes et al. (1992b)
non-isokinetic sampling probes	radial profiles	Rhodes et al. (1988) Azzi et al. (1991)
non-isokinetic sampling probes	core-annulus flow	Bader et al. (1988), Rhodes (1990), Rhodes and Laussmann (1992)
non-isokinetic sampling probes		Miller and Gidaspow (1992)
non-isokinetic sampling probes	similar profiles in dilute flow, different trend at denser flow	Bodelin et al. (1994)
fiber optic probes		Hartge et al. (1993)

experimental evidence on radial solids distribution suggests that neither the core-annular flow theory nor the clustering approach alone can fully describe riser gas-solid hydrodynamics. For example, instantaneous capacitance probe data rapid periodic fluctuations in the suspension density, indicating intermittent passage of dense clusters. However, on a time-average scale, capacitance probe data obtained at several radial locations support the core-annulus approximation. It is evident that both phenomena coexist and that a rigorous interpretation should take into consideration both clusters and core-annulus. The trends in the literature indicate that the core-annulus theory will likely be the basis for improved interpretations in the future. However, data of Contractor et al. (1994) indicate that for risers operating at solids mass fluxes exceeding 400 kg/m^2 · s, the predominant flow pattern may no longer be core-annular. Under these conditions, the CFB maybe operating as a VIS turbulent bed with essentially constant radial and axial profiles.

Nakamura and Capes (1973) proposed that for vertical solids transport, when the gas velocity is decreased or the

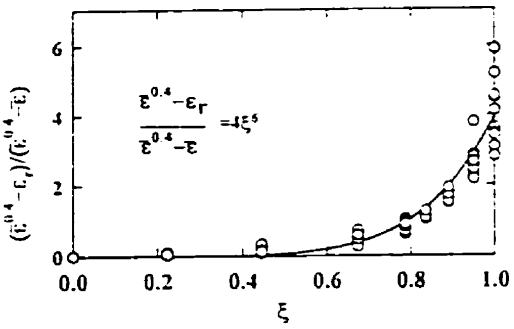

Figure 9 — Normalized radial void fraction profile (data after Zhang et al., 1991).

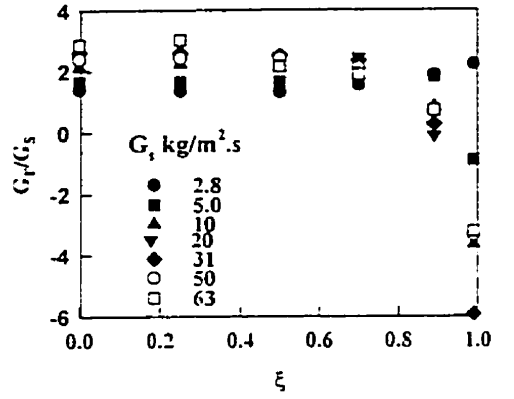

Figure 10 — Similar radial mass flux profiles (Rhodes et al., 1992a).

solids loading is increased-approaching choking conditions — the observed internal recirculation of solids may be modelled as annular flow. However, Horio et al. (1988) finding that this approximation was unable to predict their experimentally observed annular thickness, and attributing the discrepancy to cluster formation, modified the model to include cluster voidage and cluster terminal velocity. These quantities were calculated based on the measured effective cluster diameter. Ishii et al. (1989) and Horio and Takei (1991) refined the clustering-annular flow model. The former group presented a system of material and momentum balances for the gas and solid phases in which the wall-solid interfacial shear stress was calculated based using a friction fraction equal to 0.003, and the core-annulus interfacial shear stress was calculated from the experimental data for the cluster diameter and core radius. They concluded that the core-annulus interfacial shear could not be neglected in the momentum balances. The latter group further improved the clustering-annular flow model by presenting empirical relations to calculate the cluster diameter and the core-annulus interfacial shear, thus making it fully predictive. One limitation of modelling clusters is that they are dynamic and their characteristics are hard to measure, quantify or generalize.

The core-annular approximation to the flow domain has received considerable attention and is constantly being refined as experimental data continue to be published. Hartge et al. (1988) adopted this flow structure and used the Richardson-Zaki (1954) correlation to calculate the core and annular slip velocities. Their model required experimentally measured voidages and particle velocities as inputs, in order to calculate local gas and solids flows at various axial locations. Rhodes (1990) presented a similar model; requiring the average solids flux in the core and annulus and the core radius — the radial distance at which the solids flux equals zero — as inputs. The downward particle velocity in the annulus was taken as 0.2 m/s based on visual observations at the riser wall. Rhodes (1990) quantified the net core to annulus particle flux by a deposition coefficient determined from the best fit of the axial profile of the internal solids recirculation.

The major limitation of these models and that of Berruti and Kalogerakis (1989) is that they require experimental data for input, thus, they cannot be used as predictive tools. In addition, certain assumptions, such as the average annular voidage being equal to the minimum fluidization voidage, and the downward annular particle velocity being equal to the terminal settling velocity of a single particle, do not, in general, agree with recent experimental evidence. Wong et al. (1992) presented a fully predictive model for the gas and solids flow structure which combined the Berruti-Kalogerakis model with empirical correlations for the length of the acceleration zone and the voidage at the base of the riser. Also, a slip factor equal to two was assumed in the fully developed flow region. Recently several other "predictive" model have been developed (Pugsley and Berruti, 1995; Koenigsdorff and Werther, 1995; Patience and Chaouki, 1995). These models account for the radial variation of solids velocity profile and hold-up, and have been developed from a larger data base and more detailed experimental measurements.

While the core-annular flow assumption adequately describes the time averaged radial solids suspension density profiles, the instantaneous measurement of local solids suspension density with instruments such as capacitance probes indicates the rapid formation and disintegration of solids clusters. Therefore, future type II modelling, such as that by Koenigsdorff and Werther (1995), need to take both phenomena into account. Experimental evidence of this complex flow structure has, however, led to an entirely different class of mathematical models, referred to as type III models, designed to more rigorously quantify two-phase gas-solids in CFB risers.

TYPE III MODELS

The work of Adewumi and Arastoopour (1986) marked a departure from previous models which had used fundamental hydrodynamic equations to describe vertical gas-solid flow, by developing a two-dimenstional model to describe both the radial and axial gradients in pneumatic transport systems. Previous efforts had concentrated on describing the axial gradient only. The two-dimensional model consists of gas and solid phase continuity equations, and momentum balances in both the axial and radial directions. The constitutive equations include the contributions of the hydrostatic head of both phases, as well as the drag force in both the axial and radial directions, with the value of the drag coefficient taken from the standard drag curve. The constitutive equations of Berker and Tulig (1986), on the other hand, were developed from a simplified version of the k-ϵ turbulence model, where k symbolizes the turbulent kinetic energy of the gas phase, and ϵ the turbulent energy dissipation

in the gas phase. A rigorous treatment of a turbulent energy system requires the modelling of numerous turbulence correlation terms. The approach of Berker and Tulig (1986) lumped all of these correlations into two functions which accounted for the imperfect, or inelastic, response of the particles to velocity fluctuations in the gas phase. The inelastic response of the particles resulted in turbulent energy dissipation, creating a region of lower turbulent energy near the riser wall, and establishing the radial suspension density gradients observed in fully developed flow. The simplifications introduced by Berker and Tulig (1986) allow the coupling of riser hydrodynamics with a simple first order reaction scheme, and investigate the effects of the radial suspension density gradients on a fluid catalytic cracking unit. Noting the high degree of empiricism introduced in the two functions of Berker and Tulig (1986), Sinclair and Jackson (1989) concentrated on the gas-particle and particle-particle interactions which did not arise directly from the effects of gas phase turbulence. Thus, they focused on the interactions between the mean particle and gas velocity fields (i.e. drag force), the mean particle velocity field, and the fluctuating particle velocity component. In order to model the latter interaction, Sinclair and Jackson (1989) assumed that the momentum of the moving particles was sufficient to carry them through the gas film, so that the interaction occurred by direct particle-particle collisions. They noted that the major inconsistency in their formulation was the complete neglect of the random gas velocity component, which would hence be inconsistent in the limiting case of turbulent gas flow in a pipe in the absence of particles. However, for gas-solid two-phase flow, their results did predict qualitatively the effect of particle-particle collisions which was sufficient to generate the particle flow segregation experimentally observed in CFB risers, though no comparison of their predictions with experimental data was attempted. This was done later in the work of Pita and Sundaresan (1991), who compared model predictions with experimental data of Bader et al. (1988). The agreement with experimental data was excellent, but subsequent investigation of the effects of inelasticity of the particle-particle collisions and the damping action of the gas on the particle velocity fluctuations indicated an unacceptable degree of sensitivity of the model to these parameters. Pita and Sundaresan (1991) concluded that the inclusion of the gas phase turbulence effects may be necessary for accurate predictions. Yasuna et al. (1994) recently presented further comparisons of the prediction of the model of Sinclair and Jackson (1989) with published experimental data. Acceptable agreement was only obtained under very dilute flow conditions. Yasuna et al. (1994) noted that under high solids flux conditions, much of the data was obtained under developing flow conditions, and this may have been a source of inaccuracy. Neither Pita and Sundaresan (1991) nor Yasuna et al. (1994) noted the fact that comparisons were made with experiments using very fine powders. It was explicitly stated in the original work of Sinclair and Jackson (1989) that the assumption of particle-particle collisions should only be considered valid for larger particles used in applications such as mineral processing. For fine powders,the mechanism of particle-particle interaction may be significantly different, and, especially at high solids fluxes, particle-particle interaction is considered to be the key contributor to the observed segregation of solids. The most recent work in this area is that of Dasgupta et al. (1994b). These authors developed a comprehensive physical model which considered the turbulent energy effects in both the gas and solid phases, and is explicitly valid for CFBs operating at higher solids suspension densities, and circulating very fine powders. By first examining the so-called "dusty gas" limit, or the conditions of very low solids suspension densities, Dasgupta et al. (1994b) were able to determine the physical cause of the segregation of particles toward the wall required to maintain the force balance in the radial direction. The wall region becomes an area of lower turbulent energy, confirming the earlier empirical assumptions of Berker and Tulig (1986). In fact, the equations of Dasgupta et al. (1994b) were closed using a k-ϵ turbulence model developed for a constant density, homogeneous, incompressible fluid. The output of the model indicated qualitative agreement with experimental observations, and a sensitivity analysis prove that the model results were relatively insensitive to the parameters in the k-ϵ turbulence model. Dasgupta et al. (1994a) compared model predictions with the experimental data of Bader et al. (1988) and found very good agreement.

The above discussion of the type III modelling efforts suggests three main critical points. Firstly, the modelling of the turbulent flow phenomenon is very complex, and if it is considered, requires the introduction of some significant simplifying formulations. There is an ongoing commitment by the researchers in this field to develop more rigorous consideration of the turbulent flow of both the solids and gas phases, which will undoubtedly lead to even more complex models. The eventual applications of such models must be carefully considered. Secondly, no single, comprehensive model has so far been developed which is valid for all operating conditions and particle characteristics encountered in CFB risers. The early work of Sinclair and Jackson (1989) was specific to larger particles and low solids fluxes, while the recent work of Dasgupta et al. (1994a,b) was developed for higher solids fluxes and fine powders. Finally, these models are limited to the fully developed flow regions of CFB risers only, and thus give no insight into the fluid mechanical behaviour in the region of developing flow near the riser base.

A different style of type III models which avoids the introduction of a turbulence model is seen in the works of Ding and Gidaspow (1990) and Tsuo and Gidaspow (1990). These contributions consist of a generalization of the Navier-Stokes equations for two-phase flow. Such a formulation require a solid-viscosity term. The work of Ding and Gidaspow (1990) provides a predictive method for calculating the solids viscosity based on the kinetic theory of granular solids. On the other hand, the effective solids viscosity in the work of Tsuo and Gidaspow (1990) is an input based on previous experimental results. The latter model gives good agreement with experimental data, but it should be noted that the experimental data provided for comparison was generated with the CFB riser used for the effective solids viscosity calculation. Therefore, the model may suffer from a lack of generality. Gidaspow et al. (1992) extended the work of Ding and Gidaspow (1990) to CFB risers to develop a fully developed predictive hydrodynamic model. Applications of this work are shown by Gidaspow et al. (1992) and Therdthianwong and Gidaspow (1994).

BENCHMARK MODELLING TEST

Over the past decade, a significant number of hydrodynamic model have been published. A common feature of many of these studies is that models were developed from the

authors' own data comparison was generally limited to a narrow operating range and a single CFB geometry.

The need to determine the state-of-the-art of the various models and addressed during the 1992 International Conference on Fluidization in Australia, where a Benchmark Modelling Exercise was proposed to collect hydrodynamic data using several CFB test units. The geometry of the units along with the operating conditions and particle characteristics of the solids would be made available to the research community with an invitation to predict the hydrodynamics. Comparison between model predictions and experimental data would be disclosed at the 1995 International Conference on Fluidization in France.

Two experimental units were used: one 14.2 m tall and 0.2 m in diameter, the other 9 m tall and 0.4 m in diameter, employing sand and FCC powders, and air was the fluidizing medium. Data were collected over a wide range of conditions — $2.4 < U_o < 11$ m/s , $10 < G_s < 800$ kg/m^2·s. This information was given to the modellers in January 1995 with the challenge to predict axial pressure profiles, radial solids mass flux profiles, and radial solids density profiles. Ten research groups: Bernard; Sundaresan; Arastoopour and Kim; Gidaspow and Sun, Johnsson; Chaouki, Godfroy and Patience; Pugsley and Berruti; Rhodes and Wang; O'Brien and Syamlal; and Chen participated in the exercise. Comparisons between predictions and the experimental data were evaluated by Knowlton, Matsen, Geldart and King acting as a peer-committee. At Fluidization VIII in France, the results were announced at a special CFB hydrodynamics workshop: two plots were shown for each participating group — one which represented good agreement between experimental data and model predictions and the other in which the agreement was considered poor.

Although most of the groups did not attempt to model all the test conditions, the benchmark modelling exercise provided a good perspective of the state-of-the-art in CFB modelling. Only type II and type III modellers participated. Conclusions drawn from the exercise are as follows: (a) no single model adequately predicted all the conditions and trends in the data; (b) type III models did not show as good agreement with the data as did type II models; (c) some models are good over a limited range of conditions; (d) most models failed to properly represent radial density and solids mass flux profiles of FCC catalyst at the highest mass flux; (e) no model adequately predicted the increase in suspension density at the top of the riser; (f) Bernard's model prediced FCC data quite well; (g) the models of Chaouki, et al. and Pugsley and Berruti provided the best overall agreement with the experimental data; and; (h) the best type III model was created by Gidaspow and Sun which matched some significant trends in the radial mass flux profiles.

During subsequent discussion the necessity of including additional criteria in the assessment of the different models was pointed out. One of the most crucial requirements is user-friendliness and speed in generating results. The benchmark modelling test provided a fair representation of the accuracy and applicability of present hydrodynamic models and it indicated some direction for future developments.

Solids Mixing

Internal recirculation of solids in CFB risers occurs due to the interchange of solids between the heterogeneous flow structures within the riser. As a result, the residence time of any particle in the riser may vary from less than a second to more than twenty seconds. The interchange of solids is of critical importance for the control of the convective heat transfer mechanism between the solids and the riser wall in a CFB combustor (Grace, 1986b). In applications of the CFB as a catalytic reactor, internal recirculation of deactivating catalyst particles affects reactor performance. Therefore, for design purposes, it is important to known the solids residence time distribution (RTD) expected for given operating conditions and riser geometry.

Studies of the RTD are typically conducted using tracer techniques. A number of different tracer-detection methods employed in the literature for determining the solids RTD are given in Table 6. For instance, Yerushalmi and Avidan (1985) used a ferromagnetic tracer and an inductance bridge detector. On the other hand, Bader et al. (1988) and Rhodes et al. (1991) injected a sodium chloride sample and detected the tracer by dissolving the collected samples in water and measuring the electrical conductivity of the solution. However, the majority of published solids tracer experiments have been used radioactivity (Helmrich et al., 1986; Ambler et al., 1990; Patience, 1990; Viitanen, 1993). The advantages of using radioactive tracers, as indicated by Patience (1990), include versatility, non-intrusiveness, *in situ* measurement, and ease of detection. In addition, the small quantities of tracer material required for detection minimizes injection perturbation. Radioactive tracer detection in a CFB riser requires a rapid response time of the detector, otherwise the inherent accuracy is lost. This problem was encountered in the study of Ambler et al. (1990). Figure 11 shows RTD curves for the three different particle sizes injected at the base of the riser and detected at the exit; the riser was operating at a mass flux of 45 kg/m^2·s. and a gas velocity of 4.2 m/s. Internal solids recirculation is greatset for the larger particles, whose particle terminal velocity is 3.9 m/s. However, breakthrough times — the time at which radioactivity is first detected at the exit — is short; it takes 1.8s for the solids to travel along the 4.7 m rise length. The breakthrough time of the 108 μm sand particles is 0.8 s; their particle terminal velocity is only 0.6 m/s.

Effects of operating conditions on axial solids mixing have been studied by Yerushalmi and Avidan (1985), Patience et al. (1991), and Rhodes et al. (1991). Yerushalmi and Avidan (1985) observed a maximum in the effective axial solids dispersion coefficient as a function of gas superficial velocity and solids circulation rate. Examination of their axial suspension density profiles suggests that this maximum corresponds to the transition velocity from the turbulent regime to fast fluidization. Data on the effect of solids mass flux seem inconclusive, although the authors do state that axial dispersion increased slightly with increasing solids mass flux. At higher gas velocities, axial solids dispersion decreased indicating a reduction in the internal solids recirculation Rhodes et al. (1991) experimentally investigated the influence of operating conditions on axial solids mixing in two CFB risers of differing diameter (0.152 m and 0.305 m), and correlated the axial Peclet number as a function of solids mass flux and riser diameter. The correlation indicated that the axial solids dispersion decreased with increasing diameter, supporting the notion that the annular region is in fact a wall effect, hence internal recirculation is less in a large diameter riser. The correlation also showed that the axil solids dispersion decreased slightly with solids mass flux. Rhodes et al. (1991) attributed this to operation of the riser under the similar profiles condition, where the solids velocity and thus solids mixing are independent of

TABLE 6
Sources of Data on Solids Residence Time Distribution

Experimental Method	Model	Reference
salt tracer	core-annulus	Bader et al. (1988)
salt tracer	one-dimensional dispersion	Rhodes et al. (1991, 1992b)
salt tracer detected in gas phase	axial dispersion	Bai et al. (1992b)
$CaCl_2$ on alumina sorbent particles	core-annulus	Corleen et al. (1990)
(limestone) fluorescent tracer particles	size reduction	Lyngfelt and Leckner (1992)
radioactive tracer	core-annulus	Mori (1994)
radioactive tracer	core-annulus	Patience (1990)
ferromagnetic tracer	axial dispersion	Milne and Berruti (1991)
radioactive tracer	plug flow and stirred tank	Yerushalmi and Avidan (1985)
radioactive tracer	radial dispersion	Helmrich et al. (1986)
radioactive tracer	core-annulus	Viitanen (1993)

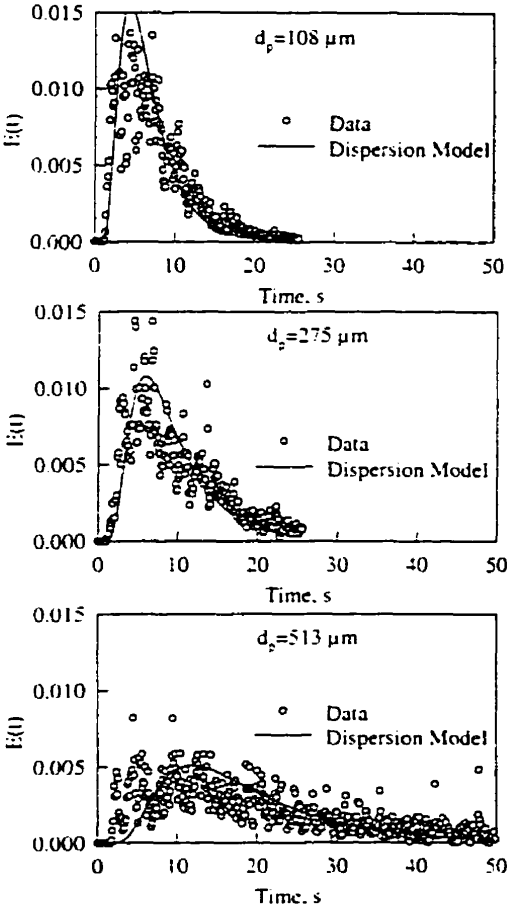

Figure 11 — Solids RTD in a 0.0828 m riser: U_g = 4.2 m/s, G_s = 45 kg/m^2·s (Patience et al., 1991).

solids mass flux. The fact that this finding contradicts that of Patience et al. (1991), who found that the solids axial dispersion increased with solids mass flux in their 0.083 m diameter riser, may be due to the effect of riser diameter. However, as shown in Figure 11, dispersion modelling does not account for all the details of the RTD curves, particularly the breakthrough times and large fluctuations. Moreover, modelling the entire riser length lumps entrance and exit effects together with the fully developed region.

In a recent study, Patience and Chaouki (1995) studied the local RTD of sand particles 513 μm, 275 μm and 108 μm in diameter, by placing a scintillation detector in the entrance region where solids hold-up is greatest, and near the riser exit in the hydrodynamically "fully" developed region of the riser. The lower detector exhibited the same response curve for all particle sizes, but the upper detector showed decreased peak heights and longer tails for the larger particles. Solids mixing at the entrance appears to be insensitive to particle properties in contrast to the fully developed region.

Helmrich et al. (1986) modelled solids RTD data by using a loop reactor model which combined plug flow and stirred tank compartments. While such models accurately describe the experimental data and give an indication of the effects of riser operating conditions and geometry on axial solids mixing, they do not physically represent the actual mechanism of solids mixing observed in CFB risers. As stated by Ambler et al. (1990), models based upon the actual flow patterns observed in the riser are fundamentally superior. Therefore, it is desirable to develop a model describing the solids RTD based upon the interchange of solids between the core and annual regions and among clusters.

Bolton and Davidson (1988) modelled the transfer of solids from the core to the annulus with a turbulent diffusion mass transfer coefficient developed by analogy with the freeboard region of a bubbling bed. However, Harris and Davidson (1994) noted an apparent inconsistency in this formulation, because turbulent diffusion from the lean core region to the dense annular zone would represent mass transfer against a solids concentration gradient. In postulating a core-to-annulus deposition model which assumed binary collisions between particles, the interchange of solids from the annulus to the core was neglected. The model of Senior and Brereton (1992) also assumed that particle-particle collisions accounted

for the movement of solids from the core region to the annulus. In addition, they modelled the reentrainment of particles from the annulus to the core as due to gas shear. Sinclair and Jackson (1989) indicated that for larger (d_p > 150 μm) and, heavier particles collisions between particles was the dominant mechanism producing particle flow segregation observed in practice. Wirth (1991) presented a model for the momentum transfer arising from collisions between discrete particles and clusters or strands of solids dispersed throughout the cross-section of a CFB riser which did not assume the existence of a core-annulus flow structure in the riser. Recent work by Pugsley and Berruti (1995) modified the work of Wirth (1991) slightly by limiting the clusters to the annular region and calculating the core-to-annulus solids interchange coefficient based on collisions between the upward flowing particles in the core and the downward flowing particles in the annulus. They calculated the annulus-to-core solids interchange coefficient so that the material balance at any axial location is satisfied: the core-to-annulus coefficient increased axially from the riser base to a constant value in the fully developed flow region, while the annulus-to-core coefficient remained essentially constant and less than the core-to-annulus coefficient. The core-to-annulus interchange coefficient increased rapidly near the base of the riser indicating that the core-annulus structure forms very quickly under the conditions of fast fluidization. Senior and Brereton (1992) found that a value of 0.20 m/s for the core-to-annulus solids interchange coefficient produced the best fit of their experimental axial suspension density profiles. This compares favourably with the work of Pugsley and Berruti (1994) with values in the range of 0.05 to 0.30 m/s for various operating conditions and riser dimensions. Based on turbulent diffusion, Bolton and Davidson (1988) calculated coefficients 50% lower than those of Pugsley and Berruti (1995).

Patience and Chaouki (1995) characterized radial transport of solids by radial dispersion and found that the value of the dispersion coefficient is approximately equal to that measured for radial gas dispersion by Martin et al. (1992) — about 0.0025 m^2/s.

Gas Hydrodynamics

Gas velocity is a key operating parameter that identifies regime transitions in gas-solids reactors. In the bubbling fluid-bed regime, significant research has been devoted to gas injection and design criteria for the grid region to optimize gas-solids contact. In fast fluidization, design criteria for gas injection are not as well defined, although its impact on the hydrodynamics is certainly not negligible. For example, Saxton and Worley (1970) described industrial risers in which oil was introduced through one, two, and three nozzles. They reported that not only did solids distribute more uniformly at the entrance with three nozzles, but that the vapour injection had a significant effect throughout the riser: suspension densities were lower with a more evenly distributed gas at the entrance than with just one or two nozzles only. Fligner et al. (1994) compared circumferential gas injection with internal injection through two nozzles in a pilot scale riser. Circumferential gas injection resulted in uniform radial densities at the entrance with a corresponding increase in conversion by 3%. Weinstein et al. (1995) suggest that the mode of gas injection into the riser impacts the acceleration (entrance) region and this effect may extend throughout the entire column, as reported by Saxton and Worley (1970). They suggest that nozzle designs should accelerate catalyst particles rapidly and uniformly over the riser cross-section to minimize entrance length and maximize reactor performance.

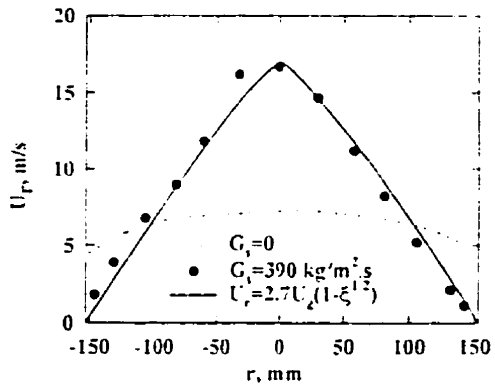

Figure 12 — Gas radial velocity profile with FCC catalyst in a 0.3 m diameter riser: U_g = 6.3 m/s, G_s = 390 kg/m^2·s (van Breugel et al., 1969).

In the fully developed region of risers, most experimental evidence indicates that the gas is unevenly distributed across the radius: centreline velocities are typically as much as two to three times superficial velocities, and wall velocities are zero. Van Breugel et al. (1969) measured gas velocity profiles using iso-kinetic sampling in a 0.3 m diameter riser operating at a gas velocity of 6.3 m/s and a mass flux of 390 kg/m^{2}s. Centreline veolocities were close to 17 m/s and the radial profile was approximately triangular in shape, as shown in Figure 12. Martin et al. (1992) report gas velocity profiles in a 0.19 m diameter unit operating at gas velocities between 3.8 and 6 m/s and mass fluxes up to 200 kg/m^{2}s. They found that the gas profiles shifted from relatively flat under dilute operating conditions to a triangular shape under dense conditions. Radial dispersion was measured by injecting a steady flow of helium iso-kinetically at the centreline, and sampling at different radial and axial positions along the riser. They characterized their data with the radial dispersion model

$$\frac{\partial C}{\partial t} + U_r \frac{\partial C}{\partial Z} = \frac{D_r}{r}\left(\frac{\partial}{\partial r}\left(r\frac{\partial C}{\partial r}\right)\right) \quad \text{..... (8)}$$

and found that the radial dispersion coefficient ranged from 20 to 30 cm^2/s; at low mass flux and 6 m/s, it reached 50 cm^2/s.

Bader et al. (1988) also described their gas tracer data using a radial dispersion model. Radial dispersion coefficients were reported at different heights along the riser and varied from 25 to 67 cm^2/s. They did not, however, account for the gas velocity profile and this could explain why their values are higher than those reported by Martin et al. (1992). Amos et al. (1993) introduced a two zone core-annulus model with radial gas dispersion in the core region, assuming a constant gas velocity in the core. Peclet numbers varied between 300 and 500, and were a strong function of mass flux. Zethraeus et al. (1992) introduced turbulent gas mixing and a local

TABLE 7
Sources of Data on Gas Mixing

Experimental Method	Model	Reference
pilot tube	—	Van Breugel (1969)
continuous CH_4	plug flow	Cankurt et al. (1978)
hydrogen tracer	axial dispersion	Li and Wu (1991)
pulse organic tracer	axial dispersion	Bai et al. (1992b)
pulse krypton	axial dispersion	Martin et al. (1992)
continuous helium tracer	axial dispersion	Bader et al. (1988)
continuous helium	radial dispersion	Yang et al. (1993)
continuous CH_4	radial dispersion	Adams (1988)
continuous helium	radial dispersion	Bader et al. (1988)
continuous helium tracer	radial dispersion	Martin et al. (1992)
argon pulse	core-annulus	Dry et al. (1987), Dry and White (1989)
helium step	core-annulus	Brereton et al. (1988)
continuous helium	core-annulus, dispersion	Li and Weinstein (1989)
continuous helium	core-annulus, backmixing	Weinstein et al. (1989)
continuous ozone	core-annulus	Kagawa et al. (1991)
continuous CO_2 tracer	core-annulus	Werther et al. (1991, 1992a, 1992b)
continuous sulphur hexafluoride	core-annulus / radial dispersion	Amos et al. (1993)
radioactive argon pulse	core-annulus	Patience and Chaouki (1993)
hot air	contact efficiency	White and Dry (1989)
continuous methane	core-annulus	Zethraeus et al. (1992)
in situ sampling	plug flow	Moe et al. (1991)
radioactive argon pulse	axial disperison	Viitanen (1993)
ozone decomposition	pseudo-homogeneous CSTR and plug flow	Ouyang et al. (1993a)

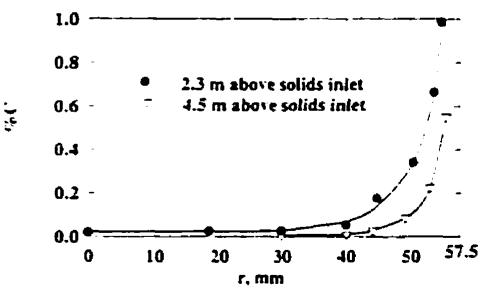

Figure 13 — Radial gas tracer concentration distribution: D = 115 m, U_g = 2.3 m/s, G_s = 32 kg/m^2·s (Yang et al., 1983).

turbulent diffusion constant to characterize their tracer data. In general, the low dispersion coefficients reported in risers indicate that radial mass transport is poor and this agrees with experimental data conducted in the NUCLA Atmospheric Circulating Fluidized Bed Combustor (Moe et al. (1994)), where two retractable probes were used to extract gas samples at 30 cm intervals over a distance of 3 m, which is a little less than half way to the centreline. They measured gas concentrations at heights of 7.6 m and 24 m and found that peaks in gaseous components appeared at the same radial distance at both heights. Furthermore, secondary air injected above the dense region did not improve gas mixing significantly. Reduced emissions, which is a result of good gas/solids contact, were obtained by better distributing the fuel inside the combustor.

A crude approximation to the gas velocity profile is the core-annulus model. Gas in the core is assumed to rise at high velocities and in the annulus it is assumed to be stagnant or to descend at a relatively low velocity:

$$\frac{\partial C_c}{\partial t} + U_c \frac{\partial C_c}{\partial Z} + \frac{2\,k}{r_c}(C_c - C_a) = 0 \quad \ldots\ldots\ (9)$$

$$\frac{\partial C_a}{\partial t} - \frac{2\,k\,r_c}{R^2 - r_c^2}(C_c - C_a) = 0 \quad \ldots\ldots\ (10)$$

This approximation has been adopted to describe the experimental data in a number of studies, as shown in Table 7. It is simple and relatively effective at capturing overall gas mixing. Werther et al. (1992) have extended the model to account for differing amounts of dispersion in the core compared to the annulus. Martin et al. (1992) explain that two coefficients are necessary when using the core-annulus model because the approximation neglects the actual profile. Patience and Chaouki (1993) adopted the core-annulus model to describe radioactive impulse tracer experiments conducted in a 0.083 m diameter riser. To characterize mass transfer across the core-annular boundary, they adopted the Gilliland-Sherwood equation based on mass transfer in wetted wall towers. They also proposed a relationship to describe the core radius from which gas velocities hence residence times, are calculated.

Weinstein et al. (1989) and Cankurt and Yerushalmi (1978) studied gas backmixing over a range of gas velocities from bubbling to turbulent and fast fluidized bed regimes. Cankurt and Yerushalmi (1978) report reduced backmixing with increasing gas velocity and suggest that it is practically negligible in fast fluidization. Yang et al. (1983) used helium as a tracer and presented data that essentially agreed with Cankurt and Yerushlami's conclusions that the central region

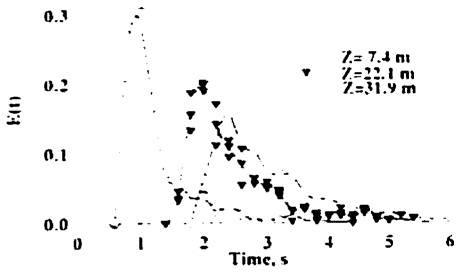

Figure 14 — Gas RTD in a commercial FCC riser: D = 1.3 m, U_g = 12 m/s, G_s = 290 kg/m^2·s (Viitanen et al., 1993).

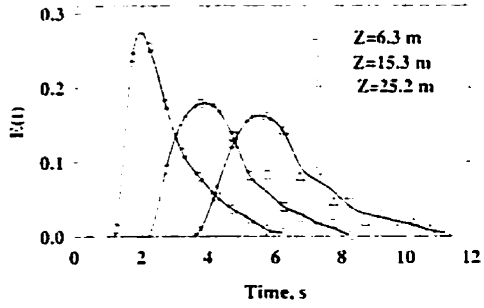

Figure 15 — Gas RTD in a 27 m tall pilot scale riser: D = 0.15 m, U_g = 5.6 m/s, G_s = 270 kg/m^2·s (Contractor et al., 1993).

of the riser is plug flow. However, they detected axial mixing in the vicinity of the wall, not mentioned in the former study. As shown in Figure 13, helium concentrations, measured at 50 mm below the injector, are essentially zero in the centre of the riser and much higher in the vicinity of the wall. Weinstein et al. (1989) agree that axial dispersion is low but they state that it approaches an asymptotic value as found by tracer injections at different radial positions and detection at different heights and across the radius. They developed elaborate sampling and injection manifolds to measure gas backmixing in the entrance region and in the fully developed region. Dispersion coefficients reported by Li and Wu (1991) vary between 0.3 and 0.8 m^2/s. However, the gas velocity profile was ignored in these studies, and the data should be reinterpreted to account for this effect. Viitanen (1993) reported tracer studies performed in a commercial FCC riser, 1.3 m in diameter and 39 m tall; some of his data are reproduced in Figure 14. Radioactive argon was used as a tracer for the gas phase and seven detectors were located along the length of the riser. The gas flow was characterized by Peclet numbers in the range of 8 to 14, and dispersion coefficients between 9 and 23 m^2/s, higher than the values reported by Li and Wu (1991). Contractor et al. (1994) published a set of tracer data using radioactive Kr in 0.15 m diameter riser operating up to at a mass flux of 600 kg/m^2·s. Figure 15 shows tracer data measured at a gas velocity of 5.6 m/s and a mass flux of 270 kg/m^2·s; the peak height decreases with distance along the riser, which indicates some axial dispersion. No gas bypassing was detected at the higher mass flux indicating that the core annular structure may not be sustained under dense phase riser transport conditions; the solids volume fraction was approximately 0.15, which is considerably higher than most experimental risers that operate at levels lower than 0.05.

A single model is not available to characterize the gas phase hydrodynamics in CFB risers. Gas injection has largely been ignored by researchers although it has been shown to impact both solids hydrodynamics and reactor performance considerably. Under dense phase transport conditions, it appears that a simple axial dispersion model is adequate to characterize gas mixing. Under dilute conditions a core-annulus model represents a good first approximation, but, to characterize riser hydrodynamics completely, both radial dispersion, and radial gas velocity must be taken into account.

Research Needs

Despite the significant achievements in this field, a number of areas require further study:

(1) Techniques for determining the transition velocity from the turbulent regime to the fast fluidization regime have been reported, but their implementation is not exact. Experimental work is needed, particularly for VIS risers operating above the saturation carrying capacity of gas. Available predictive correlations for the transition velocities must be modified to incorporate the effect of the imposed solids mass flux.

(2) Three classes of steady-state hydrodynamic models have evolved to describe the gas and solids flow structure in CFB risers. Type I model development is limited in scope and usefulness. Type II models characterize axial and radial gas-solids flow by assuming the existence of clusters or a core-annular distribution. In reality, both exist, and present models might be improved by combining elements of these approximations as shown by Koenigsdorff and Werther (1995). However, since such models will require many input parameters, which are not generally available; and, since the parameters will be difficult to quantify, they may find only limited use. There is sufficient controversy over the effect of riser diameter on axial solids hold-up; the effect of riser diameter on cluster size, frequency, shape and mean residence time should be interesting. We expect that the more rigorous type III formulations will improve with computational speed, but their development will also depend on more precise hydrodynamic measurements. Unsteady state models — apart from type III — are non-existent. They may become useful to predict conversions and selectivities in catalytic reactors, or capture efficiency of SO_2 and NO_x in combustors.

(3) CFB scaling laws predict the flow structure of large scale units based on data in much smaller units. Criteria for CFB scaling have been developed by a number of investigators (Glicksman, 1984; Glicksman 1988; Horio et al., 1986; Horio et al., 1989; Louge, 1987; Chang and Louge, 1992). These scaling laws are based on equations of continuity and momentum, on specific boundary conditions, and on the Ergun equation. But many problems remain unresolved. In many commercial applications, they entry region impacts riser performance, but the proposed scaling relationships are generally applicable to the vertical direction only. An industrial example illustrates this limitation: the 7 m square NUCLA CFB combustor suffered severe bubble cap erosion at the grid. Solids were fed into the side at a velocity of 0.3 m/s and a 45° angle through a 2 m square standpipe flush with the grid at the bottom. In a cold flow model, one would presumably pick the same gas velocity and experiment with

mass flux to approach commercial riser suspension densities. Scaling riser diameter with standpipe diameter proportionately gives the same mass flux through riser and standpipe. However, to simulate erosion it may be more appropriate to scale the standpipe geometry such that the penetration depth is proportionately smaller, or the same as in the commercial reactor. If raising the standpipe vertically so that it is no longer flush with the bottom of the grid is chosen as a remedy for bubble cap erosion, how does one choose the vertical dimension to verify the hypothesis in the experimental unit (modifying a commercial reactor is costly!)? What distance should be chosen? Should experiments be conducted at heights scaled proportionately with the riser diameter scale or should they be kept at full scale conditions to more closely approximate the acceleration region effect? These and similar questions have not been fully addressed and require more attention.

(4) Innovative design of new solids-feeding devices and gas-solids separation techniques may reduce operational complexities. The effects of scale on the entrance region may be considerable, as mentioned above, and must be taken into account in laboratory and pilot studies. Furthermore, the entrance regions of experimental CFB risers vary arbitrarily and may effect riser hydrodynamics. Design details of the entrance region must be available to facilitate the proper comparison of flow structure.

(5) Highly exothermic reactions may require internals for heat removal to maintain temperature uniformity. Research is needed on the influence of internals on hydrodynamics and catalyst attrition, as well as tube-bundle erosion. Heat transfer between the solids and the membrane walls in CFB combustors has been well documented. Heat transfer studies for the operating conditions typical of CFB catalytic reactors are now needed, including heat transfer rates between solids and submersed internals.

(6) The mechanisms of attrition and erosion, mentioned above, are understood qualitatively, but little work has been done on their quantiative evaluation and design implications. The development of attrition resistant catalysts is a key factor in the successful commercialization of any new CFB process. This is also closely linked to the effect of internals in CFB risers and entrance geometry.

(7) Commercialization of new CFB processes for the production of fine chemicals has been hindered due to scale-up concerns and operational complexities. In particular, the effect of diameter, high solids mass flux, and high pressure on the hydrodynamics are largely undocumented in the open literature.

(8) It is well known that a large fraction of fines is necessary for smooth solids circulation in the standpipe, but the effect of fines on riser hydrodynamics is not generally known. This area will require future research to improve operation and scale-up.

In conclusion, this section on research needs indicates that fundamental understanding of CFB operation continues to hinder the potential commercial applications. A great deal of concentrated research is still required in many areas. The attendees at the four international conferences on CFB technology and the last several International Fluidization conferences represented a unique balance between industry and academia. Continued interaction between these groups will be necessary to meet the challenges in CFB research, and to ascertain that CFB technology will reach its full potential.

Nomenclature

Ar_p = Archimedes number $\rho_g(\rho_p - \rho_g)\, g d_p^3/\mu$
C_a = concentration in the annulus (mol/m^3)
C_c = concentration in the core (mol/m^3)
D = riser diameter (m)
D_r = radial dispersion coefficient
d_p = particle diameter (m)
Fr = Froude number = $U_0/(gD)^{0.5}$
Fr_t = terminal Froude number = $U_t/(gD)^{0.5}$
g = gravitational acceleration (m/s^2)
G_s = overall solids mass flux (kg/m$^2 \cdot$ s)
L = length of the riser (m)
P = pressure (Pa)
r_c = core radius (m)
Re_p = particle Reynolds number $(d_p U_0 \rho_g)/\mu$
t = time (s)
U_c = transition velocity to turbulent flow (m/s)
U_{Ca} = accumulative choking velocity of minimum transport velocity (m/s)
U_{mf} = minimum fluidization velocity (m/s)
U_t = transport velocity (m/s)
U_0 = gas superficial velocity (m/s)
V_p = average particle velocity (m/s)
V_t = particle terminal velocity (m/s)
Z = coordinate along the riser (m)
Z_i = height of the inflection in voidage profile (m)
Z_0 = characteristic length (m)

Greek letters

ε_a = limiting voidage of the dense phase
ε_c = voidage in the core
$\bar{\varepsilon}$ = average cross sectional voidage
ε^* = limiting voidage of the dilute phase
μ = gas viscosity (Pa.s)
ρ = suspension density (kg/m^3)
ρ_g = gas density (kg/m^3)
ρ_p = particle density (kg/m^3)
ξ = adimentional radius
ψ = slip factor, ratio of the interstitial gas velocity to the average particle velocity average voidage

Subscript

r = radial position

Superscript

^{0} = reference condition

Abbreviations

FIS = Fixed Inventory System
VIS = Variable Inventory System

References

Adams, C. K., "Gas Mixing in Fast Fluidized Beds", in "Circulating Fluidized Bed Technology II", P. Basu and J. F. Large, Eds., Pergamon Press, New York (1988), pp. 299-306.

Adewumi, M. A. and H. Arastoopour, "Two-Dimensional Steady State Hydrodynamic Analysis of Gas-Solids Flow in Vertical Pneumatic Conveying Systems", Powder Technol. 48, 67-74 (1986).

Ambler, P. A., B. J. Milne, F. Berruti and D. S. Scott, "Residence Time Distribution in a Circulating Fluidized Bed: Experimental and Modelling Studies", Chem. Eng. Sci. 45, 2179-2186 (1990).

Amos, G., M. J. Rhodes and H. Mineo, "Gas Mixing in Gas-Solids Risers", Chem. Eng. Sci. 48, 943-949 (1993).

Anders, R., H. Beisswenger and L. Plass, "Clean and Low Cost Energy from Atmospheric and Pressurized Lurgi CFB Systems", in "Circulating Fluidized Bed Technology III", P. Basu, M. Horio and M. Hasatani, Eds., Pergamon Press, New York (1991), pp. 431–437.

Arena, U., A. Malandrino, A. Marzocchella and L. Massimilla, "Flow Structures in the Risers of Laboratory and Pilot CFB Units", in "Circulating Fluidized Bed Technology III", P. Basu, M. Horio and M. Hasatani, Eds., Pergamon Press, New York (1991), pp. 137–144.

Avidan, A. A., "Bed Expansion and Solid Mixing in High Velocity Fluidized Beds", Ph.D. Dissertation, The City College, New York (1980).

Azzi, M., P. Turlier, J. F. Large and J. R. Bernard, "Use of a Momentum Probe and Gammadensitometry to Study Local Properties of Fast Fluidized Beds", in "Circulating Fluidized Bed Technology III", P. Basu, M. Horio and M. Hasatani, Eds., Pergamon Press, New York (1991), pp. 189–194.

Bader, R., J. Findlay and T. M. Knowlton, "Gas/Solid Flow Patterns in a 30.5 cm Diameter Circulating Fluidized Bed", in "Circulating Fluidized Bed Technology II", P. Basu and J. F. Large, Eds., Pergamon Press, New York (1988), pp. 123–137.

Baerns, M., L. Mleczko, G. J. Tjatjopoulos and I. A. Vasalos, "Comparative Simulation Studies on the Performance of Bubbling and Turbulent Fluidized Bed Reactors for the Oxidative Coupling of Methane", in "Circulating Fluidized Bed Technology IV", A. A. Avidan, Ed., American Institute of Chemical Engineers, New York (1994), pp. 414–421.

Bai, D.-R., Y. Jin, Z.-Q. Yu and J.-X. Zhu, "The Axial Distribution of the Cross-Sectionally Averaged Voidage in Fast Fluidized Beds", Powder Technol. 71, 51–58 (1992).

Bai, D., J. Yi, Y. Jin and Z. Yu, "Residence Time Distributions of Gas and Solids in a CFB", in "Fluidization VII", O. E. Potter and D. J. Nicklin, Eds., Engineering Foundation, New York (1992b), pp. 195–202.

Bartholomew, C. H., "Recent Developments in Fischer-Tropsch Catalysis", in "New Trends in CO Activation", L. Guczi, Ed., Studies in Surface Science and Catalysis No. 64, Elsevier, Amsterdam, The Netherlands (1991), pp. 158–224.

Berker, A. and T. J. Tulig, "Hydrodynamics of Gas-Solid Flow in a Catalytic Cracker Riser: Implications for Reactor Selectivity Performance", Chem. Eng. Sci. 41, 821–827 (1986).

Berruti, F. and N. Kalogerakis, "Modelling the Internal Flow Structure of Circulating Fluidized Beds", Can. J. Chem. Eng. 67, 1010–1014 (1989).

Beuther, H., R. A. Innes and H. E. Swift, "Process for Preparing Acrylonitrile", U. S. Patent 4,102,914 assigned to Gulf Research and Development Co., July 25 (1978).

Bi, H. T., J. R. Grace and J-X. Zhu, "On Types of Choking in Vertical Pneumatic Systems", Int. J. Multiphase Flow 19, 1077–1092 (1994).

Bodelin, P., Y. Molodtsof and A. Delebarre, "Flow Structure Investigations in a CFB", in "Circulating Fluidized Bed Technology IV", A. A. Avidan, Ed., American Institute of Chemical Engineers, New York (1994), pp. 118–122.

Bolton, L. W. and J. F. Davidson, "Recirculation of Particles in Fast Fluidized Risers", in "Circulating Fluidized Bed Technology II", P. Basu and J. F. Large, Eds., Pergamon Press, New York (1988), pp. 139–146.

Bolkan-Kenny, Y. G., T. S. Pugsley and F. Berruti, "Computer Simulation of the Performance of Fluid Catalytic Cracking (FCC) Risers and Downers", Ind. Eng. Chem. Res. 33, pp. 3043–3052 (1994).

Bouillard, J. X. and A. L. Miller, "Experimental Investigations of Chaotic Hydrodynamic Attractors in Circulating Fluidized Beds", Powder Technol. 79, 211–215 (1994).

Brereton, C. M. H., "Fluid Mechanics of High Velocity Fluidised Beds", Ph.D. Dissertation, the University of British Columbia, Vancouver, B.C. (1987).

Brereton, C. M. H., J. R. Grace and J. Yu, "Axial Gas Mixing in a Circulating Fluidized Bed", in "Circulating Fluidized Bed Technology II", P. Basu and J. F. Large, Eds., Pergamon Press, New York (1988), pp. 307–314.

Brereton, C. M. H. and J. R. Grace, "The Transition to Turbulent Fluidization", Trans. Inst. Chem. Eng 70, 246–251 (1992).

Brereton, C. M. H. and J. R. Grace, "Microstructural Aspects of the Behaviour of Circulating Fluidized Beds", Chem. Eng Sci. 48, 2565–2572 (1993).

Brereton, C., J. R. Grace, C. J. Lim and J. Zhu, "Engineering Aspects of Recirculating Fluidized Bed Combustion", in "Chemical Reactor Technology for Environmentally Safe Reactors and Products", H. I. de Lasa, G. Dogu and A. Ravella, Eds., Kluwer Academic Publishers, The Netherlands (1993), pp. 507–536.

Burkell, J. J., J. R. Grace, J. Zhao and C. J. Lim, "Measurement of Solids Circulation Rates in Circulating Fluidized Beds", in "Circulating Fluidized Bed Technology II", P. Basu and J. F. Large, Eds., Pergamon Press, New York (1988), pp. 501–509.

Callahan, J. L., R. K. Grasselli, E. C. Milberger and H. A. Strecker, "Oxidation and Ammoxidation of Propylene over Bismuth Molybdate Catalyst", Ind. Eng. Chem. Prod. Res. Dev. 9, 134–142 (1970).

Cankurt, N. T. and J. Yerushalmi, "Gas Backmixing in High Velocity Fluidized Beds", in "Fluidization", J. F. Davidson and D. L. Keairns, Eds., Cambridge University Press, London (1978), pp. 387–393.

Chanchlani, K. G., R. R. Hudgins and P. L. Silveston, "Methanol Synthesis Under Periodic Operation: An Experimental Investigation", Can. J. Chem. Eng. 72, pp. 657–671 (1994).

Chang, H. and M. Louge, "Fluid Dynamic Similarity of Circulating Fluidized Beds", Powder Technol. 70, 259–270 (1992).

Chehbouni, A., J. Chaouki, C. Guy and D. Klvana, "Characterization of the Flow Transition between Bubbling and Turbulent Fluidization", Ind. Eng. Chem. Res. 33, 1889–1896 (1994).

Choi, J. H., C. K. Yi and J. E. Son, "Axial Voidage Profile in a Cold Mode Circulating Fluidized Bed", in "Circulating Fluidized Bed Technology III", P. Basu, M. Horio and M. Hasatani, Eds., Pergamon Press, New York (1991), pp. 131–136.

Contractor, R. M., H. E. Bergna, H. S. Horowitz, C. M. Blackstone, U. Chowdhry and A. W. Sleight, "Butane Oxidation to Maleic Anhydride in a Recirculating Solids Reactor", in "Catalysis 1987", J. W. Ward, Ed., Elsevier Science Publishers, Amsterdam (1988), pp. 645–654.

Contractor, R. M., M. Pell, H. Weinstein and H. J. Feindt, "The Rate of Solid Loss in a Circulating Fluid Bed Following a Loss of Circulation Accident", in "Fluidization VII", O. E. Potter and D. J. Nicklin, Eds., Engineering Foundation, New York (1992), pp. 243–248.

Contractor, R. M., G. S. Patience, D. I. Garnett, H. S. Horowitz, G. M. Sisler and H. E. Bergna, "A New Process for *n*-Butane Oxidation to Maleic Anhydride Using a Circulating Fluidized Bed Reactor", in "Circulating Fluidized Bed Technology IV", A. A. Avidan, Ed., American Institute of Chemical Engineers, New York (1994), pp. 387–391.

Coudurier, G., D. Decottignies, M. Loukah and J. C. Vedrine, "Vanadium and Chromium Based Phosphates as Catalysts for Oxidative Dehydrogenation of Ethane", presented at the 13th North American Meeting of the Catalysis Society, Pittsburgh, PA, May 2 (1993).

Corleen, D. C., G. E. Klinzing, Y. T. Shah and C. G. Dassori, "Hydrodynamics and Mixing of Solids in a Recirculation Fluidized Bed", Ind. Eng. Chem. Res. 29, 1785–1792 (1990).

Dasgupta, S., R. Jackson and S. Sundresan, "Turbulent Gas-Particle Flow in CFB Risers", in "Circulating Fluidized Bed Technology IV", A. A. Avidan, Ed., American Institute of Chemical Engineers, New York (1994a), pp. 367–372.

Dasgupta, S., R. Jackson and S. Sundresan, "Turbulent Gas-Particle Flow in Vertical Risers", AIChE J. 40, 215–228 (1994b).

Debras, G., J. Grootjans and L. Delorme, "Process for the Catalytic Dehydrogenation of Alkylaromatic Hydrocarbons", European Patent No. 0 482 276 A1 (1992).

Ding, J. and D. Gidaspow, "A Bubbling Fluidization Model Using Kinetic Theory of Granular Flow", AIChE J. 36, 523–538 (1990).

Dry, M. E., "The Sasol Route to Fuels", CHEMTECH 12, 744–750 (1982).
Dry, R. J., I. M. Christensen and C. C. White, "Gas-Solids Contact Efficiency in a High-Velocity Fluidized Bed", Powder Technol. 53, 243–250 (1987).
Dry, R. J. and C. C. White, "Gas Residence-Time Characteristics in a High-Velocity Circulating Fluidized Bed FCC Catalyst", Powder Technol. 58, 17–23 (1989).
Dry, R. J., R. B. White and T. Joyce, "Correlation of Solids Circulation Rate in Circulating Fluidized Bed Systems", in "Circulating Fluidized Bed Technology IV", A. A. Avidan, Ed., American Institute of Chemical Engineers, New York (1994), pp. 621–627.
Dutta, S. and B. Jazayeri, "Alternative Reactor Concepts for the Oxidative Coupling Methane", in "Fluidization VII", O. E. Potter and D. J. Nicklin, Eds., Engineering Foundation, New York (1992), pp. 445–453.
Engstrom, F. and Y. Y. Lee, "Future Challenges of Circulating Fluidized Bed Combustion Technology", in "Circulating Fluidized Bed Technology III", P. Basu, M. Horio and M. Hasatani, Eds., Pergamon Press, New York (1991), pp. 15–37.
Fligner, M., P. H. Schipper, A. V. Sapre and F. J. Krambeck, "Two Phase Cluster Model in Riser Reactors: Impact of Radial Density Distribution on Yields", Chem. Eng. Sci. 49, 5813–5818 (1994).
Fujima, Y., K. Tagashira, Y. Takahashi, S. Ohme, S. Ichimura and Y. Arakawa, "Conceptual Study on Fast Fluidization Formation", in "Circulating Fluidized Bed Technology III", P. Basu, M. Horio and M. Hasatani, Eds., Pergamon Press, New York (1991), pp. 85–90.
Gallezot, P., S. Tretjak, Y. Christidis, G. Mattioda and A. Schouteeten, "Oxidative Dehydrogenation of Ethylene Glycol on Silver Catalyst", presented at the 13th North American Meeting of the Catalysis Society, Pittsburgh, PA, May 2 (1993).
Gelbein, A. P., "Phthalic Anhydride Reaction System", U.S. Patent 4,261,899 assigned to Chem. Systems Inc., Apr. 14 (1981).
Geldart, D., "Particle Entrainment and Carryover", in "Gas Fluidization Technology", D. Geldart, Ed., John Wiley & Sons, New York (1986), pp. 123–153.
Gianetto, A., S. Pagliolico, G. Rovero and B. Ruggeri, "Theoretical and Practical Aspects of Circulating Fluidized Bed Reactors (CFBRs) for Complex Chemical Systems", Chem. Eng. Sci. 45, 2219–2225 (1990).
Gidaspow, D., R. Bezburuah and J. Ding, "Hydrodynamics of Circulating Fluidized Beds: Kinetic Theory Approach", in "Fluidization VII", O. E. Potter and D. J. Nicklin, Eds., Engineering Foundation, New York (1992), pp. 75–82.
Gilliland, F. R. and T. K. Sherwood, "Diffusion of vapors into air streams", Ind. Eng. Chem. 26, 516–523 (1935).
Glicksman, L. R., "Scaling Relationships for Fluidized Beds", Chem. Eng. Sci. 39, 1373–1379 (1984).
Glicksman, L. R., "Scaling Relationships for Fluidized Beds", Chem. Eng. Sci. 43, 1419–1421 (1988).
Glicksman, L. R., D. Westphalen, C. Brereton and J. Grace, "Verification of the Scaling Laws for Circulating Fluidized Beds", in "Circulating Fluidized Bed Technology III", P. Basu, M. Horio and M. Hasatani, Eds., Pergamon Press, New York (1991), pp. 119–124.
Grace, J. R., "Contacting Modes and Behaviour Classification of Gas-Solid and Other Two-Phase Suspensions", Can. J. Chem. Eng. 64, 353–361 (1986a).
Grace, J. R., "Heat Transfer in Circulating Fluidized Beds", in "Circulating Fluidized Bed Technology", P. Basu, Ed., Pergamon Press, New York (1986b), pp. 63–81.
Grace, J. R., "High-Velocity Fluidized Bed Reactors", Chem. Eng. Sci. 45, 1953–1966 (1990).
Hallström, C. and R. Karlsson, "Waste Incineration in Circulating Fluidized Bed Boilers: Test Results and Operating Expereiences", in "Circulating Fluidized Bed Technology III", P. Basu, M. Horio and M. Hasatani, Eds., Pergamon Press, New York (1991), pp. 417–422.
Harris, B. J. and J. F. Davidson, "Modelling Options for Circulating Fluidized Beds: A Core/Annulus Depositions Model", in "Circulating Fluidized Bed Technology IV", A. A. Avidan, Ed., American Institute of Chemical Engineers, New York (1994), pp. 32–39
Harris, B. J., J. F. Davidson and Y. Xue, "Axial and Radial Variation of Flow in Circulating Fluidized Bed Risers", in "Circulating Fluidized Bed Technology IV", A. A. Avidan, Ed., American Institute of Chemical Engineers, New York (1994), pp. 103–110.
Hartge, E. U., Y. Li and J. Werther, "Analysis of the Local Structure of the Two-Phase Flow in a Fast Fluidized Bed", in "Circulating Fluidized Bed Technology", P. Basu, Ed., Pergamon Press, New York (1986), pp. 153–160.
Hartge, E. U., D. Rensner and J. Werther, "Solids Concentration and Velocity in Circulating Fluidized Beds", in "Circulating Fluidized Bed Technology II", P. Basu and J. F. Large, Eds., Pergamon Press, New York (1988), pp. 165–180.
Helmrich, H., K. Schurgerl and K. Janssen, "Decomposition of $NaHCO_3$ in Laboratory and Bench Scale Circulating Fluidized Reactors", in "Circulating Fluidized Bed Technology", P. Basu, Ed., Pergamon Press, New York (1986), pp. 161–166.
Herb, B., K. Tuzla and J. C. Chen, "Distribution of Solids Concentration in Circulating Fluidized Bed", in "Fluidization VI", J. R. Grace, L. W. Schemilt and M. A. Bergougnou, Eds., Engineering Foundation, New York (1989), pp 65–72.
Herb, B., S. Dou, K. Tuzla and J. C. Chen, "Solid Mass Fluxes in Circulating Fluidized Beds" Powder Technol. 70, 197–205 (1992).
Hermann, E. and W. Weisweiler, "Circulating Fluidized-Bed Reactor as Reaction System for Catalytic Gas-Solid Reactions", Int. Chem. Eng. 34, 198–209 (1994).
Horio, M., A. Nonaka, Y. Sawa and I. Muchi, "A New Rule for Fluidized Bed Scale-Up", AIChE J. 32, 1466–1482 (1986).
Horio, M., K. Morishita, O. Tachibana and M. Murata, "Solids Distribution and Movement in Circulating Fluidized Beds", in "Circulating Fluidized Bed Technology II", P. Basu and J. F. Large, Eds., Pergamon Press, New York (1988), pp. 147–154.
Horio, M., H. Ishii, Y. Kobukai and N. Yamanishi, "A Scaling Law for Circulating Fluidized Beds", J. Chem. Eng. Japan 22, 587–592 (1989).
Horio, M. and Y. Takei, "Macroscopic Structure of Recirculating Flow of Gas and Solids in Circulating Fluidized Beds", in "Circulating Fluidized Bed Technology III", P. Basu, M. Horio and M. Hasatani, Eds., Pergamon Press, New York (1991), pp. 207–212.
Huibers, D. Th. A., "Process for the Production of Acrylonitrile or Methacrylonitrile", U.S. Patent 3,478,082 assigned to the Lummus Company, Nov. 11 (1969).
Ishii, H. and I. Murakami, "Evaluation of the Scaling Law of Circulating Fluidized Beds in Regards to Cluster Behavior", in "Circulating Fluidized Bed Technology III", P. Basu, M. Horio and M. Hasatani, Eds., Pergamon Press, New York (1991), pp. 125–130.
Ishii, H., T. Nakajima and M. Horio, "The Clustering Annular Flow Model of Circulating Fluidized Beds", J. Chem. Eng. Japan 22, 484–490 (1989).
Jewel, J. W. and W. B. Johnson, "Method for Synthesis of Organic Compounds", U.S. Patent 2,543,974 assigned to M. W. Kellog Co., Mar. 6 (1951).
Johnson, A. J., "Oxidation of Olefins to Unsaturated Aldehydes and Ketones", U.S. Patent 3,102,147 assigned to Shell Oil Company, Aug. 27 (1963).
Kahney, R. H. and T. D. McMinn, "Parafin Ammoxidation Process", U.S. Patent 4,000,178 assigned to Monsanto Company, Dec. 28 (1976).
Kagawa, H., H. Mineo, R. Yamazaki and K. Yoshida, "A Gas-Solid Contacting Model for Fast Fluidized Bed", in "Circulating Fluidized Bed Technology III", P. Basu, M. Horio and M. Hasatani, Eds., Pergamon Press, New York (1991), pp. 551–556.
Karri, S. B. R. and T. M. Knowlton, "A Practical Definition of the Fast Fluidization Regime", in "Circulating Fluidized Bed Technology III", P. Basu, M. Horio and M. Hasatani, Eds., Pergamon Press, New York (1991), pp. 67–72.

Karri, S. B. R. and T. M. Knowlton, "Comparison of Group A and Group B Powders in Underflow Standpipes", in "Fluidization VII", O. E. Potter and D. J. Nicklin, Eds., Engineering Foundation, New York (1992), pp. 345–352.

Kato, K., T. Takarada, T. Tamura and K. Nishino, "Particle Hold-Up Distribution in a Circulating Fluidized Bed", in "Circulating Fluidized Bed Technology III", P. Basu, M. Horio and M. Hasatani, Eds., Pergamon Press, New York (1991), pp. 145–150.

Katoh, Y., S. Kaneko and M. Miyamoto, "Flow Pattern and Velocity Distribution on Fluidized Particles in a Riser of Circulating Fluidized Beds", in "Preprints of 4th International Conference on Circulating Fluid Beds", A. A. Avidan, Ed., Somerset, PA, U.S.A., Aug. 1-5, 1993, American Institute of Chemical Engineers, New York (1993), pp. 332–337.

King, D., "Fluidized Catalytic Crackers: An Engineering Review", in "Fluidization VII", O. E. Potter and D. J. Nicklin, Eds., Engineering Foundation, New York (1992), pp. 15–26.

King, D., "Model Predicting Average Densities in Commercial FCC CFB Regenerators", in "Circulating Fluidized Bed Technology IV", A. A. Avidan, Ed., American Institute of Chemical Engineers, New York (1994), pp. 500–503.

Kobro, H. and C. Brereton, "Control and Fuel Flexibility of Circulating Fluidized Bed", in "Circulating Fluidized Bed Technology", P. Basu, Ed., Pergamon Press, New York (1986), pp. 263–272.

Koenigsdorff, R. and J. Werther, "Gas-Solids Mixing and Flow Structure Modeling of the Upper Dilute Zone of a Circulating Fluidized Bed", Powder Technol. 82, 317–329 (1995).

Koyama, H. and J. S. Dranoff, "Modelling the Thermal Cracking of Ethane and Propane in a Non-Isothermal Vertical Pneumatic Transport Reactor", Ind. Eng. Chem. Res. 31, 2265–2272 (1992).

Kunii, D. and O. Levenspiel, "Fluidization Engineering", Butterworth-Heinemann, Stoneham, MA (1991a), pp. 61–94.

Kunii, D. and O. Levenspiel, "Flow Modeling of Fast Fluidized Beds", in "Circulating Fluidized Bed Technology III", P. Basu, M. Horio and M. Hasatani, Eds., Pergamon Press, New York (1991b), pp. 91–98.

Kunii, D. and O. Levenspiel, "The Vertical Distribution of Solids in Circulating Fluidized Beds, CFB", in "Fluidization VIII" preprints, Tours, May 14 (1995) pp. 17–24.

Kuramoto, M., T. Furusawa and D. Kunii, "Development of a New System for Circulating Fluidized Particles within a Single Vessel", Powder Technol. 44, 77–84 (1985).

Kuroki, H. and M. Horio, "The Flow Structure of a Three-Dimensional Circulating Fluidized Bed Observed by the Laser Sheet Technique, in "Circulating Fluidized Bed Technology IV", A. A. Avidan, Ed., American Institute of Chemical Engineers, New York (1994), pp. 77–84.

Kwauk, M., N. Wang, Y. Li, B. Chen and Z. Shen, "Fast Fluidization at ICM", in "Circulating Fluidized Bed Technology", P. Basu, Ed., Pergamon Press, Toronto, ON (1986) pp. 33–62.

Lewis, W. K., E. R. Gilliland and W. A. Reed, "Reaction of Methane with Copper Oxide in a Fluidized Bed", Ind. Eng. Chem. 41, 1227–1237 (1949).

Li, J., Y. Tung and M. Kwauk, "Energy Transport and Regime Transition in Particulate-Fluid Two-Phase Flow", in "Circulating Fluidized Bed Technology II", P. Basu and J. F. Large, Eds., Pergamon Press, New York (1988), pp. 75–87.

Li, J. and H. Weinstein, "An Experimental Comparison of Gas Backmixing in Fluidized Beds Across the Regime Specturm", Chem. Eng. Sci. 44, 1697–1705 (1989).

Li, J., L. Reh and M. Kwauk, "Application of the Principle of Energy Minimisation to the Dynamics of Circulating Fluidized Bed", "Circulating Fluidized Bed Technology III", P. Basu, M. Horio and M. Hasatani, Eds., Pergamon Press, New York (1991a), pp. 105–112.

Li, H., Y. Xia, Y. Tung and M. Kwauk, "Micro-Visualisation of Two-Phase Structure in a Fast Fluidized Bed", in "Circulating Fluidized Bed Technology III", P. Basu, M. Horio and M. Hasatani, Eds., Pergamon Press, New York (1991b), pp. 183–188.

Li, Y. and M. Kwauk, "The Dynamics of Fast Fluidization", in "Fluidization", J. R. Grace and J. M. Matsen, Eds., Plenum Press, New York (1980), pp. 537–544.

Li, Y. and P. Wu, "A Study on Axial Gas Mixing in a Fast Fluidized Bed", in "Circulating Fluidized Bed Technology III", P. Basu, M. Horio and M. Hasatani, Eds., Pergamon Press, New York (1991), pp. 581–586.

Louge, M. in J. Mustonen, Ed., Proc. 9th Conf. FBC, Boston, ASME, New York 1193-1197 (1987).

Louge, M. and H. Chang, "Pressure and Voidage Gradients in Vertical Gas-Solid Risers", Powder Technol. 60, 197–201 (1990).

Lyngfelt, A. and B. Leckner, "Residence Time Distribution of Sorbent Particles in a Circulating Fluidized Bed Boiler", Powder Technol. 70, 285–292 (1992).

Lyons, J. E., "The Molecular Design, Synthesis and Application of New Catalytic Systems for the Selective Oxidation of Hydrocarbons to Fuels and Chemical Products", presented at the 13th North American Meeting of the Catalysis Society, Pittsburgh, PA, May 2 (1993).

Martin, M. P., P. Turlier, J. R. Bernard and G. Wild, "Gas and Solid Behavior in Cracking Circulating Fluidized Beds", Powder Technol. 70, 249–258 (1992).

Matsen, J. M., "Some Characteristics of Large Solids Circulation Systems" in "Fluidization Technology", D. L. Keairns, Ed., Hemisphere, New York (1976), 135–149.

Miller, A. and D. Gidaspow, "Dense, Vertical Gas-Solid Flow in a Pipe", AIChE J 38, 1801–1815 (1992).

Milne, B. J. and F. Berruti, "Modeling the Mixing of Solids in Circulating Fluidized Beds", in "Circulating Fluidized Bed Technology III", P. Basu, M. Horio and M. Hasatani, Eds., Pergamon Press, New York (1991), pp. 575–580.

Milne, B. J., F. Berruti and L. A. Behie, "Solids Circulation in an Internally Circulating Fluidized Bed (ICFB) Reactor", in "Fluidization VII", O. E. Potter and D. J. Nicklin, Eds., Engineering Foundation, New York (1992), pp. 235–242.

Mineo, H., "High Velocity Circulating Fluidized Beds", Ph.D. Dissertation, University of Tokyo, Tokyo, Japan (1989).

Moe, T. A., M. D. Mann, A. K. Henderson and D. R. Hajicek, "Pilot-scale CFBC Systems: A Valuable Tool for Design and Permitting", in "Circulating Fluidized Bed Technology IV", A. A. Avidan, Ed., American Institute of Chemical Engineers, New York (1994), pp. 91–97.

Monceaux, L., M. Azzi, Y. Molodtsof and J. F. Large, "Overall and Local Characterization of Flow Regimes in a Circulating Fluidized Bed", "Circulating Fluidized Bed Technology", P. Basu, Ed., Pergamon Press, New York (1986), pp. 185–191.

Mori, S., Y. Yan, K. Kato, K. Matsubara and D. Liu, "Hydrodynamics of a Circulating Fluidized Bed", in "Circulating Fluidized Bed Technology III", P. Basu, M. Horio and M. Hasatani, Eds., Pergamon Press, New York (1991), pp. 113–118.

Mori, S., "Particles Behavior and Flow Pattern in a Circulating Fluidized Bed", in "Circulating Fluidized Bed Technology IV", A. A. Avidan, Ed., American Institute of Chemical Engineers, New York (1994), pp. 240–246.

Murchison, C. B., G. E. Vrieland, B. Khazai and E. D. Weihl, "Anaerobic Oxidation of Butane to Butadiene on Magnesium Molybdate Catalyst", presented at the 13th North American Meeting of the Catalysis Society, Pittsburgh, PA, May 2 (1993).

Nakamura, K. and C. E. Capes, "Vertical Pneumatic Conveying: A Theoretical Study of Uniform and Annular Particle Flow Models", Can. J. Chem. Eng. 51, 39–46 (1973).

Ouyang, S., J. Lin and O. E. Potter, "Ozone Decomposition in a 0.254 m Diameter Circulating Fluidized Bed Reactor", Powder Technol. 74, 73–78 (1993a).

Ouyang, S. and O. E. Potter, "Consistency of Circulating Fluidized Bed Experimental Data", Ind. Eng. Chem. Res. 32, 1041–1045 (1993b).

Park, D. W. and G. Gau, "Simulation of Ethylene Epoxidation in a Multibubular Transport Reactor", Chem. Eng. Sci. 41, 143–150 (1986).

Patience, G. S., "Circulating Fluidized Beds: Hydrodynamics and Reactor Modelling", Ph.D. Dissertation, École Polytechnique de Montréal, Montréal, Québec (1990).

Patience, G. S., J. Chaouki and B. P. A. Grandjean, "Solids Flow Metering From Pressure Drop Measurement in Circulating Fluidized Beds", Powder Technol. 61, 95-99 (1990).

Patience, G. S. and J. Chaouki, "Solids Circulation Rate Determined by Pressure Drop Measurements", in "Circulating Fluidized Bed Technology III", P. Basu, M. Horio and M. Hasatani, Eds., Pergamon Press, New York (1991), pp. 627-632.

Patience, G. S., J. Chaouki and G. Kennedy, "Solids Residence Time Distribution in CFB Reactors", in "Circulating Fluidized Bed Technology III", P. Basu, M. Horio and M. Hasatani, Eds., Pergamon Press, New York (1991), pp. 599-604.

Patience, G. S., J. Chaouki, F. Berruti and R. Wong, "Scaling Considerations for Circulating Fluidized Bed Risers", Powder Technol. 72, 31-37 (1992).

Patience, G. S. and J. Chaouki, "Gas Phase Hydrodynamics in The Riser of a Circulating Fluidized Bed", Chem. Eng. Sci. 48, 3195-3205 (1993).

Patience, G. S. and P. L. Mills, "Modelling of Propylene Oxidation in a Circulating Fluidized-Bed Reactor", in "New Developments in Selective Oxidation II", V. C. Corberan and S. Vic Bellon, Eds., Elsevier, New York (1994) pp. 1-18.

Patience, G. S. and J. Chaouki, "Solids Hydrodynamics in the Fully Developed Region of CFB Risers", in "Fluidization VIII" preprints, Tours, May 14 (1995), pp. 33-40.

Peinemann, B., W. Stockhausen and L. Mackenzie, "Experience with the Circulating Fluid Bed for Gold Roasting and Alumina Calcination", in "Fluidization VII", O. E. Potter and D. J. Nicklin, Eds., Engineering Foundation, New York (1992), pp. 921-928.

Perales, J. F., T. Coll, M. F. Llop, L. Puigjaner, J. Arnaldos and J. Casal, "On the Transition from Bubbling to Fast-Fluidization Regimes", in "Circulating Fluidized Bed Technology III", P. Basu, M. Horio and M. Hasatani, Eds., Pergamon Press, New York (1991), pp. 73-78.

Pita, J. A. and S. Sundaresan, "Developing Flow of a Gas-Particle Mixture in a Vertical Riser", AIChE J., 39, 541-552 (1993).

Pita, J. A. and S. Sundaresan, "Gas-Solid Flow in Vertical Tubes", AIChE J. 37, 1009-1018 (1991).

Pugsley, T. S., G. S. Patience, F. Berruti and J. Chaouki, "Modeling the Oxidation of *n*-Butane to Maleic Anhydride in a Circulating Fluidized Bed Reactor", Ind. Eng. Chem. Res. 31, 2652-2660 (1992).

Pugsley, T. S. and F. Berruti, "A Core-Annulus Solids Interchange Model for Circulating Fluidized Bed and FCC Risers", in "Fluidization VIII" preprints, Tours, May 14 (1995), pp. 449-455.

Pugsley, T. S., F. Berrutiand A. Chakma, "Computer Simulation of a Novel Circulating Fluidized Bed Pressure-Temperature Swing Adsorber for Recovering Carbon Dioxide from Flue Gases", Chem. Eng. Sci. 49, 4465-4481 (1994).

Pugsley, T. S., "Experimental Investigation and Hydrodynamic Modelling of High Density Risers", Ph.D. Dissertation, University of Calgary, Calgary, Alberta (1994).

Pugsley, T. S., F. Berruti, L. Godfroy, J. Chaouki and G. S. Patience, "A Predictive Model for the Gas-Solid Flow Structure in circulating Fluidized Bed Risers", in "Circulating Fluidized Bed Technology IV", A. A. Avidan, Ed., American Institute of Chemical Engineers, New York (1994), pp. 40-47.

Qian, C. and J. Li, "Particle Velocity Measurement in CFB with an Integrated Probe", in "Circulating Fluidized Bed Technology IV", A. A. Avidan, Ed., American Institute of Chemical Engineeres, New York (1994), pp. 274-278.

Reeves, J. W., R. W. Sylvester and D. F. Wells, "Chlorine and Iron Oxide from Ferric Chloride — Apparatus", U.S. Patent 4,282,185 assigned to E. I. du Pont de Nemours and Co., Inc., Aug. 4, (1981).

Reh, L., "Fluidized Bed Processing", Chem. Eng. Prog. 67, 58-63 (1971).

Reh, L., "The Circulating Fluidized Bed Reactor — A Key to Efficient Gas/Solid Processing", in "Circulating Fluidized Bed Technology", P. Basu, Ed., Pergamon Press, New York (1986), pp. 105-118.

Reh, L. and J. Li, "Measurement of Voidage in Fluidized Beds by Optical Probes", in "Circulating Fluidized Bed Technology III", P. Basu, M. Horio and M. Hasatani, Eds., Pergamon Press, New York (1991), pp. 163-170.

Reichle, A. D., "Fluid Catalytic Cracking Hits 50 Year Mark on the Run", Oil Gas J. 90 (20), 41-48 (1992).

Rhodes, M. J. and D. Geldart, "The Hydrodynamics of Recirculating Fluidized Beds", in "Circulating Fluidized Bed Technology", P. Basu, Ed., Pergamon Press, New York (1986), pp. 193-200.

Rhodes, M. J., P. Laussmann, F. Vilain and D. Geldart, "Measurement of Radial and Axial Solids Flux Variations in the Riser of a Circulating Fluidized Bed", in "Circulating Fluidized Bed Technology II", P. Basu and J. F. Large, Eds., Pergamon Press, New York (1988), pp. 155-164.

Rhodes, M. J., "Modelling the Flow Structure of Upward Flowing Gas-Solids Suspensions", Powder Techlol. 60, 27-38 (1990).

Rhodes, M. J., S. Zhou, T. Hirama and H. Cheng, "Effects of Operating Conditions on Longitudinal Mixing in a Circulating Fluidized Bed Riser", AIChE J. 37, 1450-1458 (1991).

Rhodes, M. J. and P. Laussmann, "A Simple Non-isokinetic Sampling Probe for Dense Suspensions", Powder Technol. 70, 141-151 (1992).

Rhodes, M. J., X. S. Wang, H. Cheng and T. Hirama, "Similar Profiles of Solids Flux in Circulating Fluidized-Bed Risers", Chem. Eng. Sci. 47, 1635-1643 (1992a).

Rhodes, M., S. Zhou, T. Hirama and H. Cheng, "Effects of Operating Conditions and Scale on Solids Mixing in Risers of Circulating Fluidized Beds", in "Fluidization VII", O. E. Potter and D. J. Nicklin, Eds., Engineering Foundation, New York 249-256 (1992b).

Richardson, J. F. and W. N. Zaki, "Sedimentation and Fluidisation: Part 1", Trans. Instn. Chem. Engrs. 32, 35-53 (1954).

Rollman, W. F., "Selective Oxidation with Suspended Catalyst", U.S. Patent 2,604,479 assigned to Standard Oil Development Company, July 22 (1952).

Roy, R. and J. F. Davidson, "Similarity Between Gas-Fluidized Beds at Elevated Temperature and Pressure", in "Fluidization VI", J. R. Grace, L. W. Shemilt and M. A. Bergougnou, Eds., Engineering Foundation, New York (1989), pp. 293-300.

Rudolph, V., Y. O. Chong and D. J. Nicklin, "Standpipe Modelling for Circulating Fluidized Beds", in "Circulating Fluidized Bed Technology III", P. Basu, M. Horio and M. Hasatani, Eds., Pergamon Press, New York (1991), pp. 49-64.

Sanfilippo, D., F. Buonomo, G. Fusco, M. Lupieri and I. Miracca, "Fluidized Bed Reactors for Paraffins Dehydrogenation", Chem. Eng. Sci. 47, 2313-2318 (1992).

Santamaria, J. M., E. E. Miro and E. E. Wolf, "Reactor Simulation Studies of Methane Oxidative Coupling on a $Na/NiTiO_3$ Catalyst", Ind. Eng. Chem. Res. 30, 1157-1165 (1991).

Saxton, A. L. and A. C. Worley, "Modern Catalytic Cracking Design", Oil Gas J. 68, 82-99 (1970).

Schnitzlein, M. and H. Weinstein, "Flow Characterization in High-Velocity Fluidized Beds Using Pressure Fluctuations", Chem. Eng. Sci. 43, 2605-2614 (1988).

Schonfelder, H., J. Hinderer, J. Werther and F. J. Keil, "Methanol to Olefins-Prediction of the Performance of Circulating Fluidized-Bed Reactor on the Basis of Kinetic Experiments in a Fixed-Bed Reactor", Chem. Eng. Sci. 49, pp. 5377-5390 (1994).

Senior, R. C. and C. Brereton, "Modelling of Circulating Fluidized-Bed Solids Flow and Distribution", Chem. Eng. Sci. 47, 281-296 (1992).

Shingles, T. M. and A. F. McDonald, "Commercial Experience with Synthol CFB Reactors", in "Circulating Fluidized Bed Technology II", P. Basu and J. F. Large, Eds., Pergamon Press, New York (1988), pp. 43-50.

Silverman, R. W., A. H. Thompson, A Steynberg, Y. Yukawa and T. Shingles, "Development of a Dense Phase Fluidized

Bed Fisher-Tropsch Reactor" in "Fluidization V", K. Ostergaard and A. Sorenson, Eds., Engineering Foundation, New York (1986), pp. 441–448.
Sinclair, J. L. and R. Jackson, "Gas-Particle Flow in a Vertical Pipe with Particle-Particle Interactions", AIChE J. 35, 1473–1486 (1989).
Squires, A. M., "The Story of Fluid Catalytic Cracking: The First Circulating Fluid Bed", in "Circulating Fluidized Bed Technology", P. Basu, Ed., Pergamon Press, New York (1986), pp. 1–19.
Takeuchi, H., T. Hirama, T. Chiba, J. Biswas and L. S. Leung, "A Quatitative Definition and Flow Regime Diagram and for Fast Fluidization", Powder Technol. 47, 195–199 (1986).
Takeuchi, H. and T. Hirama, "Flow Visualisation in the Riser of a Circulating Fluidized Bed", in "Circulating Fluidized Bed Technology III", P. Basu, M. Horio and M. Hasatani, Eds., Pergamon Press, New York (1991), pp. 177–182.
Tang, J. T. and R. A. Curran, "Challenges and Strategies for CFB Boilers to Meet Stringent Emissions", in "Circulating Fluidized Bed Technology IV", A. A. Avidan, Ed., American Institute of Chemical Engineers, New York (1994), pp. 766—773.
Tmenov, D. N., N. I. Svintson and L. P. Shapovalova, A. V. Tabakov, M. L. Dvoretskii, G. I. Vasil'ev and G. P. Shestovkii, "Unsaturated Hydrocarbons", German Patent DE 2902220 assigned to Institute of Physical-Organic Chemistry and Coal Chemistry, July 31 (1980).
Therdthianwong, A. and D. Gidaspow, "Hydrodynamics and SO_2 Sorption in a CFB Loop", in "Circulating Fluidized Bed Technology IV", A. A. Avidan Ed., American Institute of Chemical Engineers, New York (1994), pp. 351–358.
Tsuo, Y. P. and D. Gidaspow, "Computation of Flow Patterns in Circulating Fluidized Beds", AIChE J. 36, 885—896 (1990).
Tung, Y., W. Zhang, Z. Wang, X. Liu and X. Ching, "Further Study of Radial Voidage Profiles in a Fast Fluidized Beds", Eng., Chemistry and Metallurgy 10, 18–23 (1989).
Van Breugel, J. W., J. J. M. Stein and R. J. de Vries, "Isokinetic Sampling in a Dense Gas-Solids Stream", Proc. Instn. Mech. Engrs. 184 , 18–23 (1969).
Van der Stappen, M. L. M., J. C. Schouten and C. M. van den Bleek, "Application of Deterministic Chaos Analysis to Pressure Fluctuation Measurements in a 0.96 m^2 CFB Riser", in "Circulating Fluidized Bed Technology IV", A. A. Avidan, Ed., American Institute of Chemical Engineers, New York (1994), pp. 54–61.
Viitanen, P. I., "Tracer Studies on a Riser Reactor of a Fluidized Catalyst Cracking Plant", Ind. Eng. Chem. Res. 32, 577–583 (1993).
Wainwright, M. S. and T. W. Hoffman, "The Oxidation of *o*-Xylene in a Transported Bed Reactor", in "Chemical Reaction Engineering II", H. M. Hulburt, Ed., Advances in Chemistry Series No. 133 American Chemical Society, Washington, DC (1974), pp. 669–685.
Wang, T., Z. J. Lin, C. M. Zhu, D. C. Liu and S. C. Saxena, "Particle Velocity Measurements in a Circulating Fluidized Bed", AIChE J. 39, 1406–1410 (1993).
Weinstein, H., R. A. Graf, M. Meller and M. J. Shao, "The Influence of the Imposed Pressure Drop Across a Fast Fluidized Bed", in "Fluidazation IV", D. Kunii and R. Toei, Eds., Engineering Foundation, New York (1983), pp. 299–306.
Weinstein, H., M. Shao and M. Schnitzlein, "Radial Variation in Solid Density in High Velocity Fluidization", in "Circulating Fluidized Bed Technology II", P. Basu, Ed., Pergamon Press, New York (1986), pp. 201–206.
Weinstein, H. and J. Li, "An Evaluation of the Actual Density in the Acceleration Section of Vertical Risers", Powder Technol. 57, 77–79 (1989).
Weinstein, H., H. J. Feindt, L. Chen, R. A. Graff, M. Pell, R. M. Contractor and S. P. Jordan, "Riser Gas Feed Nozzle Configuration Effects on the Acceleration and Distribution of Solids", in "Fluidization VIII" Preprints, Tours, May 14 (1995) pp. 121–127.
Werther, J., E. U. Hartge, M. Kruse and W. Nowak, "Radial Mixing of Gas in the Core Zone of a Pilot Scale CFB", in "Circulating Fluidized Bed Technology III", P. Basu, M. Horio and M. Hasatani, Eds., Pergamon Press, New York (1991), pp. 593–598.
Werther, J., E. U. Hartge and M. Kruse, "Gas Mixing and Interphase Mass Transfer in the Circulating Fluidized Bed", in "Fluidization VII", O. E. Potter and D. J. Nicklin, Eds., Engineering Foundation, New York (1992a), pp. 257–264.
Werther, J., E. U. Hartge and M. Kruse, "Radial Gas Mixing in the Upper Dilute Core of a Circulating Fluidized", Powder Technol., 70, 293–301 (1992b).
Werther, J., E. U. Hartge and D. Rensner, "Measurement Techniques for Gas-Solid Fluidized-Bed Reactors", Int. Chem. Eng. 33, 18–27 (1993).
White, C. C. and R. J. Dry, "Transmission Characteristics of Gas in a Circulating Fluidized Bed", Powder Technol., 57, 89–94 (1989).
White, C. C., R. J. Dry and O. E. Potter, "Modelling Gas Mixing in a 9 cm Diameter Circulating Fluidized Bed", in "Fluidization VII", O. E. Potter and D. J. Nicklin, Eds., Engineering Foundation, New York (1992) pp. 265–273.
Wirth, K. E., "Fluid Mechanics of Circulating Fluidized Beds", Chem. Eng. Tech. 14, 29–38 (1991).
Wong, R., T. Pugsley and F. Berruti, "Modelling the Axial Voidage Profile and Flow Structure in Risers of Circulating Fluidized Beds", Chem. Eng. Sci. 47, 2301–2306 (1992).
Woskow, M. Z., "Dehydrogenation Process", U. S. Patent 3,420,912 assigned to Petro-Tex Corp., Jan. 7 (1969).
Woskow, M. Z. "Dehydrogenation Process Using Manganese Ferrite", U. S. Patent 3,513,216 assigned to Petro-Tex Corp., May (1970).
Yang, G., Z. Huang and L. Zhao, "Radial Gas Dispersion in a Fast Fluidized Bed", in "Fluidization", D. Kunii and R. Toei, Eds, Engineering Foundation, New York, NY (1983), pp. 145–152.
Yang, Y., Y. Jin, Z. Yu, Z. Wang and D. Bai, "The Radial Distribution of Local Particle Velocity in a Dilute Circulating Fluidized Bed", in "Circulating Fluidized Bed Technology III", P. Basu, M. Horio and M. Hasatani, Eds., Pergamon Press, New York (1991), pp. 201–206.
Yang, Y. L., Y. Jin, Z. Q. Yu and Z. W. Wang, "Investigation on Slip Velocity in the Riser of Dilute CFB", Powder Technol. 73, 67–73 (1993).
Yang, W. C., "A Model for the Dynamics of a Circulating Fluidized Bed Loop", in "Circulating Fluidized Bed Technology II, P. Basu and J. F. Large, Eds., Pergamon Press, Oxford, (1988), pp. 181–191.
Yang, W. C., "Incipient Fast Fluidization Boundary and Operational Maps for Circulating Fluidized Bed Systems", in "Circulating Fluidized Bed Technology IV", A. A. Avidan, Ed., American Institute of Chemical Engineers, New York (1994), pp. 62–69.
Yasuna, J. S. Elliott, H. Westersund, I. Gamwo and J. Sinclair, "Assessing the Predictive Capabilities of a Gas/Solids Flow Model which Includes Particle-Particle Interactions", in "Circulating Fluidized Bed Technology IV", A. A. Avidan, Ed., American Institute of Chemical Engineers, New York (1994), pp. 340–344.
Yerushalmi, J., D. H. Turner and A. M. Squires, "The Fast Fluidized Bed", Ind. Eng. Chem. Process Des. Dev. 15, 47–53 (1976).
Yerushalmi, J., N. T. Cankurt, D. Geldart and B. Liss, "Flow Regimes in Vertical Gas-Solids Contact Systems", AICHE Symp. Ser. 74, No. 176, 1 (1978).
Yerushalmi, J. and N. T. Cankurt, "Further Studies of the Regimes of Fluidization", Powder Technol. 24, 187–205 (1979).
Yerushalmi, J. and A. Avidan, "High Velocity Fluidization", in "Fluidization", J. F. Davidson, R. Clift and D. Harrison, Eds., Academic Press, London (1985) pp. 225–229.
Zaza, P., A. de la Torre and A. Renken, "Direct Dehydrogenation of Methanol to Formaldehyde in a Circulating Fluidized Bed", Chem.Ing.-Tech 63, pp. 640-642 (in German) (1991).
Zethraeus, B., C. Adams and N. Berge, "A Simple Model for Turbulent Gas Mixing in CFB Reactors", Powder Technol. 69, 101–106 (1992).

Zhang, H., Y. Xie, Y. Chen and M. Hasatani, "Mathematical Modeling for Longitudinal Voidage Distribution of Fast Fluidized Beds", in "Circulating Fluidized Bed Technology III", P. Basu, M. Horio and M. Hasatani, Eds., Pergamon Press, New York (1991a), pp. 151–156.

Zhang, W., Y. Tung and F. Johnsson, "Radial Voidage Profiles in Fast Fluidized Beds of Different Diameters", Chem. Eng. Sci. 46, pp. 3045–3052 (1991b).

Zhiqing, U., "Application Collocation", in "Advances in Chemical Engineering", Vol. 20. M. Kwauk, Ed., Academic Press, New York (1994), pp. 39–83.

Manuscript received December 16, 1994; revised manuscript received September 11, 1995; accepted for publication September 13, 1995.

Annexe II: Article soumis au Groupe Français de Génie des Procédés

Le congrès français de Génie des Procédés, organisé par le Groupe Français de Génie des Procédés, est une manifestation biennale permettant aux scientifiques chercheurs, enseignants et aux industriels de se rencontrer, de présenter leurs travaux, de prendre connaissance des développements récents de la discipline et de définir les enjeux futurs.

L'article qui suit a été présenté au 5^{e} congrès tenu du 19 au 21 septembre 1995 à Lyon en France. Le thème du congrès était: "La maîtrise de la complexité rencontrée dans les procédés". L'un des thèmes secondaires était: "Nouvelles techniques pour l'observation de la complexité" et c'est sous ce thème que l'article a été proposé.

Le but visé par cet article est de faire connaître la technique de poursuite d'une particule radioactive à la communauté scientifique francophone. L'essentiels des objectifs spécifiques visés, des résultats, des analyses et la portée de cet article ont été repris dans l'article publié dans "International Journal of Applied Radiation and Isotopes" (voir chapitre 2). C'est la raison pour laquelle cet article a été mis en annexe. Les résultats y sont présentés d'une façon quelque peu différente et pourront éclaircir certains points relatifs à la technique de poursuite d'une particule radioactive.

Visualisation d'écoulements des réacteurs polyphasiques en temps réel

L. Godfroy*, F. Larachi*, B. Grandjean**, G. Kennedy*** et J. Chaouki*c
*Dépt. Génie Chimique, École Polytechnique de Montréal
***Dépt. Génie Mécanique, École Polytechnique de Montréal
Casier Postal 6079, Succ. Centre-Ville, Montréal, (Québec), Canada, H3C 3A7

**Dépt. Génie Chimique, Université Laval
Faculté des Sciences et de Génie, Cité Universitaire, Québec,(Québec),Canada, G1K 7P4
cAuteur à qui toutes correspondances doivent être adressées

Résumé
Récemment, une technique de poursuite d'une particule radioactive permettant une étude hydrodynamique locale a été développée. Cette technique permet la détermination de la position et de la vitesse d'une particule mimant la phase tracée. La résolution spatiale de la technique a été vérifiée pour trois radio-isotopes dans un milieu dense et dans un milieu dilué. Il est démontré que l'or (^{198}Au) est le meilleur radio-isotope à utiliser dans les deux milieux testés. Enfin, un réseau neuronal s'est montré un moyen efficace pour réduire le temps de calcul de la position instantanée de la particule radioactive. À l'aide d'un réseau neuronal, la position de la particule est déterminée en un temps largement en deçà de la période d'échantillonnage de 10 millisecondes, ce qui permet une visualisation en temps réel des écoulements rapides.

I. INTRODUCTION

Les écoulements polyphasiques sont omniprésents dans les procédés industriels (lits fluidisés, colonnes à bulles, réacteurs biologiques, etc.) Malgré leurs vastes applications, la conception de ces réacteurs reste encore hasardeuse à cause de la complexité des écoulements présents. La maîtrise de cette complexité s'intensifie au fur et à mesure que l'information sur les structures locales devient disponible. Afin de caractériser localement l'écoulement, deux catégories de méthodes retiennent l'attention, les méthodes structurales et les méthodes dynamiques. Les méthodes structurales permettent de déterminer la densité ou la rétention locale de la phase tracée alors que les méthodes dynamiques permettent de déterminer le champ de vitesse. L'une des méthodes dynamiques la plus prometteuse est la poursuite d'une particule radioactive. Cette technique a l'avantage d'être non-intrusive et ne perturbe aucunement l'écoulement. Cette technique permet la détermination de la position instantanée (X,Y,Z) d'une particule à l'aide des résultats du comptage de huit scintillateurs NaI (Tl) pendant de courtes périodes d'échantillonnage Δt. Une fois la position instantanée de la particule déterminée (à Δt près), il est possible d'effectuer plusieurs analyses. Il est possible de déterminer le champ de vitesse et d'analyser le caractère chaotique de l'écoulement (1). Cette technique s'est avérée un outil performant pour déterminer le champ de vitesse à l'intérieur d'un lit fluidisé triphasique (1), d'un lit-à-jet (2), d'un lit fluidisé liquide-solide (3) et est présentement à l'étude pour un lit fluidisé circulant.

Rappelons ici les étapes à suivre afin de déterminer la position d'une particule (4). Après l'étape de calibration où 3 paramètres sont déterminés, un dictionnaire de 19200 positions (60 positions axiales, 8 positions radiales et 40 positions azimutales) contenant les valeurs prédites pour chacun des détecteurs est calculé. Une fois ce dictionnaire créé, la position grossière de la particule est déterminée en minimisant la somme pondérée des carrés des différences entre le comptage prédit par le modèle et le comptage expérimental. À ce stade, la position de la particule n'est pas déterminée de façon précise et la recherche des coordonnées optimales est poursuivie en faisant l'approximation que les détecteurs sont localement ponctuels. Cette recherche à l'intérieur du dictionnaire, combinée à la recherche locale, prend plus de temps que la période d'échantillonnage sur une station de travail RISC 6000 (IBM 375). Il est par conséquent impossible de déterminer la position de la particules en temps réel sur un ordinateur personnel d'acquisition de données.

II. PROBLÉMATIQUE

Jusqu'à maintenant, la technique de poursuite d'une particule radioactive s'est montrée efficace lorsque les vitesses de la phase tracée sont inférieures à 2 m/s pour des Δt de 30 millisecondes. Afin d'appliquer la technique à de plus grandes vitesses, par exemple dans le cas des lits fluidisés circulants, il faut réduire la période d'échantillonnage. En réduisant la période d'échantillonnage, le nombre de coups dans les détecteurs diminue, ce qui augmente l'incertitude relative et détériore la résolution spatiale. Le problème est donc de vérifier s'il est possible, tout en réduisant la période d'échantillonnage, de déterminer la position de la particule avec une bonne précision. Le premier objectif de ce travail est donc d'étendre l'applicabilité de la technique à des périodes d'échantillonnage de 10 millisecondes (ms) i.e. que la position de la particule est déterminée 100 fois par seconde. Cette période permet en principe de mesurer des vitesses allant jusqu'à 6 m/s. Enfin la détermination de la position de la particule à l'aide du modèle développé demande un temps de calcul plus long que la période d'échantillonnage, ce qui rend impossible la visualisation de la position de la particule en temps réel. Le second objectif est donc d'étudier un moyen de rendre possible la visualisation en temps réel en utilisant un réseau neuronal avec rétropropagation.

III. MODÈLE PHÉNOMÉNOLOGIQUE

La figure 1 illustre le montage expérimental. Il s'agit de deux rangées superposées de 4 détecteurs (7,6cmX7,6cm) disposés à angles droits autour de la colonne. Afin de déterminer les paramètres optimaux du modèle, la particule radioactive est placée à 30 endroits différents où les impulsions des rayons γ sont comptées et enregistrées à toutes les 10 ms pendant 10 s. Le nombre de coups enregistré sur 10 s permet de déterminer trois paramètres (R, la radioactivité, τ, le temps mort et μ_r, le coefficient d'atténuation linéaire dans le réacteur) pour chacun des systèmes de détection à l'aide du modèle phénoménologique suivant:

$$C(x,y,z) = \frac{\upsilon R \phi \Delta t \epsilon}{1 + \upsilon R \phi \tau \epsilon} \qquad (1)$$

où $C(x,y,z)$ est le nombre de coups enregistrés pendant la période d'échantillonnage Δt, υ est le nombre de rayon γ émis par désintégration, ϕ est le rapport photopic/total et où ϵ est l'efficacité totale de détection. Cette dernière est la probabilité que le photon émerge du réacteur sans interaction pour interagir avec le détecteur en y déposant au moins une partie de son énergie. L'efficacité totale de détection est donnée par l'équation (2) et est évaluée

à l'aide d'un calcul Monte-Carlo sur toute la surface du détecteur (Ω):

$$\epsilon = \iint_{\Omega} \frac{\vec{r} \cdot \vec{n}}{r^3} e^{-(\mu_r e_r + \mu_p e_p)} \left(1 - e^{-\mu_s e_s} \right) d\Sigma \qquad (2)$$

où μ_r, μ_p et μ_s sont respectivement les coefficients d'atténuation linéaire du réacteur, de la paroi et du scintillateur. De la même façon e_r, e_p et e_s sont les épaisseurs traversées par le photon dans le réacteur, dans la paroi et dans le scintillateur.

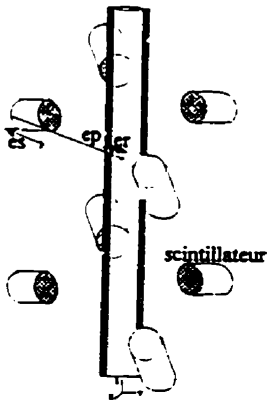

Figure 1: Schéma du montage

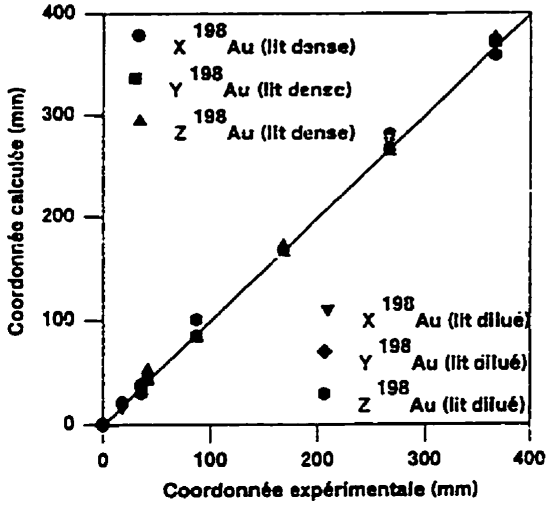

Figure 2: Comparaison des valeurs des coordonnées

Afin de vérifier l'applicabilité de la technique à des périodes d'échantillonnage de 10 ms, six expériences ont été effectuées, trois avec la colonne remplie d'eau (lit dense) et trois avec la colonne vide (lit dilué). Trois radio-isotopes différents ont été testés, le molybdène (^{99}Mo), l'or (^{198}Au) et le scandium (^{46}Sc), émettant respectivement des rayons γ de 140 keV, 410 keV et 1005 keV. Le choix des radio-isotopes s'est fait de manière à couvrir une grande plage d'énergie des rayons γ. Pour une meilleure comparaison, l'activité de chacune des sources a été choisie de façon à ce que le nombre total de rayons γ émis soit équivalent à celui d'une source de 50 μCi de scandium (^{46}Sc). La figure 2 compare quelques valeurs instantanées calculées par le modèle (à chaque 10 ms) et les valeurs géométriques des coordonnées où la particule est maintenue en place. Quel que soit le radio-isotope utilisé et la densité du milieu, on constate que les valeurs moyennes des coordonnées X, Y et Z ne sont pas significativement différentes. Le modèle prédit des coordonnées non-biaisées par rapport aux coordonnées géométriques.

Afin d'aller chercher le plus d'informations sur l'hydrodynamique, il est intéressant de connaître lequel des radio-isotopes présente la meilleure résolution spatiale. Par exemple, pour quantifier le champ de turbulence, il faut diminuer le plus possible les fluctuations liées à la technique de mesure. Il s'agit donc de trouver lequel des radio-isotopes a les plus faibles valeurs d'écarts types σ_x, σ_y et σ_z des coordonnées X, Y et Z calculées. Le tableau 1 présente les valeurs typiques de σ_x, σ_y et σ_z au centre de la colonne. Les valeurs expérimentales des écarts types σ_x sont toujours comparables aux valeurs de σ_y étant donné la symétrie dans l'emplacement des détecteurs autour de la colonne. Comme le montre le tableau 1, ^{198}Au est le meilleur radio-isotope dans le milieu dilué, puisque les écarts types

sont les plus faibles. ^{198}Au est aussi le meilleur radio-isotope dans le milieu dense car il présente l'écart type $\sigma_{3D}=\sqrt{(\sigma_x^2 + \sigma_y^2 + \sigma_z^2)}$ le plus petit. ^{198}Au permet de déterminer la position de la particule à 8.8 mm (σ_{3D}) près dans le milieu dilué et à 6.5 mm près dans le milieu dense. Il est donc préférable d'utiliser un traceur à base d'or afin d'améliorer la résolution spatiale. Il est à noter que les différences entre les radio-isotopes est beaucoup moindre en milieu dense qu'en milieu dilué. Les écarts types en milieu dense sont toujours plus faibles qu'en milieu dilué. Ceci vient du fait que l'atténuation, plus importante en milieu dense, rend le nombre de coups enregistrés plus sensibles à la position, ce qui améliore la sensibilité.

Tableau 1: Valeurs typiques des écarts types de coordonnées calculées au centre de la colonne.

	σ_x (mm)	σ_y (mm)	σ_z (mm)
^{99}Mo (milieu dilué)	6.3	6.6	7.1
^{198}Au (milieu dilué)	4.6	4.1	6.3
^{46}Sc (milieu dilué)	5.7	5.9	7.9
^{99}Mo (milieu dense)	2.1	2.3	6.3
^{198}Au (milieu dense)	2.6	2.4	5.5
^{46}Sc (milieu dense)	4.1	4.1	7.4

Puisque le modèle arrive à localiser correctement la particule dans les deux milieux et pour les trois radio-isotopes, il est possible de vérifier si le modèle est capable de prédire les fluctuations dans le calcul des coordonnées. Il est possible de démontrer que la variance σ_x^2 (et similairement pour σ_y^2 et σ_z^2) est donné par la relation suivante (5), où N est le nombre de détecteurs:

$$\frac{1}{\sigma_x^2} = \sum_{j=1}^{N} C_j \frac{\partial \ln C_j}{\partial x} \qquad (3)$$

Les valeurs prédites de l'écart type sont généralement en accord avec ceux du modèle comme le montre la figure 3. C'est donc dire que le modèle permet non seulement de déterminer les coordonnées d'une particule radioactive mais qu'il est aussi capable de prédire l'écart type associé aux coordonnées calculées. Les fluctuations dans les positions calculées sont dominées par les fluctuations dans les comptages mesurés qui eux sont liés à la nature même du phénomène de désintégration radioactive. Ce résultat, des plus importants, ouvre la voie à plusieurs simulations. En effet, il est possible d'optimiser la position des détecteurs afin de maximiser la résolution spatiale (minimiser l'écart type σ_{3D}) à l'intérieur d'un volume de mesure. Un autre calcul intéressant pouvant être effectué est d'optimiser, pour une radioactivité donnée, la disposition du réseau de détecteurs. Ce calcul est intéressant lorsque la technique de poursuite d'une particule radioactive est utilisée sur une grosse colonne.

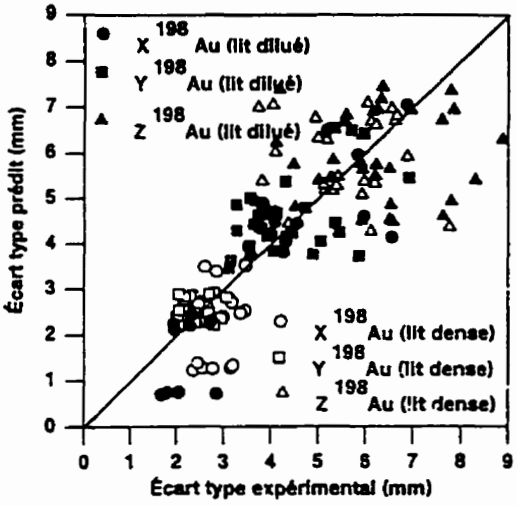

Figure 3: Comparaison des écarts types des positions

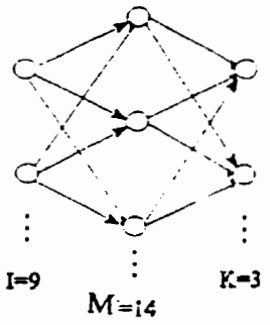

Figure 4: Illustration du réseau neuronal

Comme l'ont démontrées les figures 2 et 3, le modèle phénoménologique est précis et permet d'obtenir de bonnes résolutions. Le problème est qu'il requiert des calculs complexes nécessitant un temps machine important. Il est donc intéressant de voir si d'autres avenues permettent de calculer beaucoup plus rapidement les coordonnées X, Y et Z directement à partir des comptages des huit détecteurs. Un schéma de régression multi-variable comme un réseau neuronal peut être utilisé pour calculer les coordonnées X,Y, et Z de façon beaucoup plus rapide.

IV. RÉSEAU NEURONAL

Les réseaux neuronaux sont connus pour être efficaces pour saisir les relations non-linéaires existant entre les variables dans les systèmes complexes (6) et (7). En fait, un réseau neuronal peut être vu comme un modèle de régression non-linéaires à plusieurs paramètres liant les variables d'entrées aux variables de sorties. Plusieurs applications de ces réseaux ont été rapportées, principalement dans le domaine de la modélisation et du contrôle des procédés de même qu'en analyse de défaillance. Pour plus de renseignements sur les réseaux neuronaux, les lecteurs sont référés aux ouvrages (8) et (9). La figure 4 illustre le réseau neuronal utilisé. La première colonne est la couche d'entrée et elle est constituée des réponses normalisées des huit détecteurs. La dernière colonne est la sortie normalisée des coordonnées. La normalisation des variables a pour but de ramener la plage de variation de toutes les variables entre -1 et +1 ou 0 et +1 dépendamment de la variable. La colonne centrale est la couche cachée du réseau et comprend M noeuds. Les auteurs (10) et (11) ont démontré qu'un réseau neuronal est capable d'approximer n'importe quelle fonction pourvu que le nombre de noeuds cachés (M) soit suffisamment élevé. Le nombre de noeuds cachés doit être déterminé expérimentalement par essais et erreurs et augmente avec la complexité du système. Les relations liant les variables sont les suivantes:

$$H_j = \frac{1}{1 + e^{-\sum_{i=1}^{9} W_{ij} U_i}} \qquad 1 \le j \le M-1$$

$$S_k = \frac{1}{1 + e^{-\sum_{j=1}^{J} W_{jk} H_j}} \qquad 1 \le k \le 3 \qquad (4)$$

La valeur des variables U_9 et H_M est fixée à 1 et sont connues sous le nom de variables de biais. Ainsi un réseau neuronal à 14 noeuds cachés a été utilisé. La détermination des 159 paramètres du réseau, connu comme étant l'apprentissage du réseau, nécessite beaucoup de données. Il est évidemment beaucoup trop fastidieux de générer expérimentalement toutes les données nécessaires à la détermination des paramètres du réseau. Les données contenues dans le dictionnaire sont donc utilisées pour déterminer les paramètres du réseau. Ainsi 12250 données ont été sélectionnées parmi les 19200 contenues dans le dictionnaire afin de déterminer les 159 paramètres. Les quelques 7000 données restantes sont utilisées pour tester la validité du réseau neuronal. Les paramètres sont déterminés par régression non-linéaire à l'aide de la méthode de Marquardt (12). Le réseau neuronal remplace la partie recherche de la position. Les coordonnées de la particule sont déterminés en 0.16 ms sur une station de travail RISC 6000 (IBM 375), ce qui est environ 500 fois plus rapide qu'avec la résolution phénoménologique. Avec le réseau neuronal, un ordinateur personnel 80486 (66 MHz) détermine les coordonnées en 0.5 ms, ce qui permet la visualisation des écoulements en temps réel. Il est à noter que le modèle phénoménologique est toujours utilisé afin de déterminer les paramètres optimaux et de générer le dictionnaire des comptages. La figure 5 compare les coordonnées Y et Z obtenues à l'aide du modèle phénoménologique seul et du réseau neuronal pour un lit fluidisé triphasique. On ne peut faire la distinction entre les valeurs obtenues des deux façons sauf dans la partie du bas du réacteur où l'écart est de moins de 14 mm.

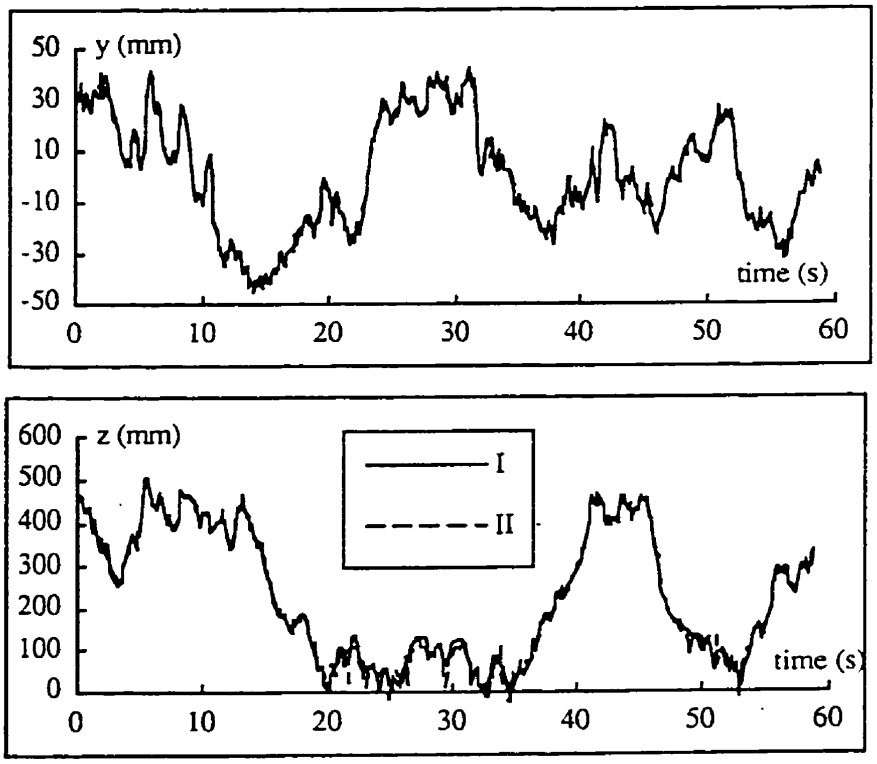

Figure 5: Comparaison des coordonnées calculées par le modèle phénoménologique (I) et par le réseau neuronal (II).

V. CONCLUSION

Il a été démontré qu'il est possible de déterminer la position d'une particule radioactive à une fréquence de 100 Hz. Afin de réduire l'écart type dans les positions calculées, il est préférable d'utiliser l'or (^{198}Au) tant en lit dense qu'en lit dilué. Il a également été montré que le modèle phénoménologique est capable d'estimer les écarts types des coordonnées de la particule radioactive. Enfin, l'utilisation d'un réseau neuronal permet le calcul de la position de la particule en un temps largement en deça de la période d'échantillonnage, ce qui ouvre désormais la voie à des expériences où la position sera calculée en temps réel.

Bibliographie

(1) Larachi F., Cassanello M., Marie M. N., Chaouki J., Guy C., Experimental Characterization of the solid phase chaotic dynamics in three-phase fluidization, Trans. IChemE (in press).

(2) Roy D. ,Larachi F. , Legros R. ,Chaouki J., A study of solid behavior in spouted beds using 3-D particle tracking, Can. J. Chem. Eng., 72, 945-952 (1994)

(3) Larachi F., Lord E., Chaouki J., Chavarie C., Behie L. A., Phenomenological study of solids mixing in a binary liquid fluidized bed, Fluidization VIII, Tours, France 1995 (in press)

(4) Larachi F., Kennedy G., Chaouki J., A γ-ray detection system for 3-D particle tracking in multiphase reactors, Nucl. Inst. Meth. Phys. Res., A338, 568-576 (1994)

(5) Larachi F., Godfroy L., Grandjean B. P. A., Kennedy G., Chaouki J., On line flow visualisation in multiphase reactors using neural networks, Int. J. Modelling Simulation (in press)

(6) Wasserman P. D., Neural Computing: theory and practice, ANZA Research Inc., Van Nortrand Rheinhold, New York, 43-60 (1989)

(7) Lippman R. P., An introduction to computing with neural nets, IEEE ASSP, 4 au 22 avril (1987)

(8) Morris A. J., Montague G. A. , Willis M. J., Artificial neural networks: studies in a process modelling and control, Trans. Inst. Chem. Eng. 72, Part A, 3-19 (1994)

(9) Watanabe K. , Hirota S. , Hou L. , Himmelblau D. M. , Diagnosis of multiple simultaneous fault via hierarchilal artificial neural networks, AICHE J. 40 839-848 (1994)

(10) Cybenko G., Approximation by superposition of sigmoidal functions, Math. Control. Syst., 2, 303-314 (1989)

(11) Hornik K. , Stincombe M. ,White H., Multilayer feedforward networks are universal approximators, Neu. Net. 2, 356-366 (1989)

(12) Press H. W. ,Flannery B. P.,Teukolsky S. A. ,Vetterling W. T. , Numerical recipes, the art of scientific computing, Cambridge University Press, London, 307-312 (1988)

Annexe III Détails du montage expérimental

La conception de montage expérimental représente une contribution originale au projet d'étude. Pour cette raison, ce dernier est présenté plus en détail ici que dans les articles des chapitres 3 et 4.

A3.1 Réalisation du montage

Cette section cherche à établir brièvement quelles ont été les contributions apportées dans la première phase du projet: la réalisation du montage expérimental. La première tâche de mon doctorat fut de construire un lit fluidisé circulant. Je me suis donc occupé de la conception et la construction d'un lit fluidisé circulant d'une hauteur de 7 m et d'un diamètre interne de 8.2 cm. Le schéma de montage est présenté à la Figure A3.1. Ce réacteur met en contact un gaz (de l'air) et des particules de sables (d_p=150 µm). Le gaz passe une seule fois dans la colonne de réaction. Il est alimenté au bas du lit, juste au-dessus d'un distributeur (plaque perforée). Il transporte, jusqu'aux cyclones, les particules introduites dans le lit à l'aide de 4 orifices placés juste au dessus du distributeur. Les cyclones séparent le mélange gaz-solides. Les solides sont réintroduits dans le bas du lit. Les solides sont toujours en train de circuler en boucle fermée (d'où le nom de lit fluidisé circulant). La Figure A3.2 présente schématiquement la tuyauterie du lit fluidisé circulant. Deux rotamètres (R1 et R2) mesurent le débit d'air fluidisant. L'un mesure l'air primaire qui est alimenté avec le gaz naturel à la tête du brûleur. L'autre mesure l'air secondaire qui est alimenté dans une chambre de mélange, connexe au brûleur. Les équations de calibration de ces rotamètres sont inscrites à l'arrière de ces rotamètres. Enfin, 3 rotamètres (R3, R4, R5) permettent l'alimentation étagée de l'air dans la partie cylindrique de retour des particules au bas du lit. Le débit d'air alimenté dans cette partie est directement proportionnel au taux de circulation de solides. Ainsi, le débit d'air ternaire contrôle le taux de circulation des solides. Le débit d'air à ajouter pour l'obtention d'un certain taux de circulation

dépend entre autres de la vitesse superficielle du gaz. Les courbes de calibration des rotamètres R3, R4 et R5 sont présentées à l'annexe IV.

L'originalité de ce nouveau design de lit est la façon dont les solides sont introduits dans la colonne de réaction (Figure AIII.3). Des résultats préliminaires obtenus à l'Université de Calgary nous indiquaient qu'il était possible d'obtenir de très hauts taux de circulation de solides (G_s>400 kg/m^2.s pour une vitesse superficielle de gaz de 6 m/s). De telles conditions opératoires sont très intéressantes. Elles se rapprochent des conditions opératoires des lits fluidisés circulants utilisés comme réacteurs catalytiques pour lesquels peu de données sont disponibles dans la littérature. De plus, le lit est équipé d'un brûleur au gaz naturel permettant de chauffer facilement le gaz jusqu'à 200 °C. Très peu de groupes de recherche ont la possibilité d'étudier l'hydrodynamique à chaud. Ce montage expérimental peut facilement être modifié pour des recherches futures.

Pour l'instant, seulement des expériences à froid de poursuites d'une particule radioactive ont été conduites. La raison en est simple, nous n'avons pas encore de traceur radioactif résistant à haute température. Une brève description de la procédure à suivre pour effectuer une expérience de poursuite d'une particule radioactive est annexée au présent document (annexe VI)

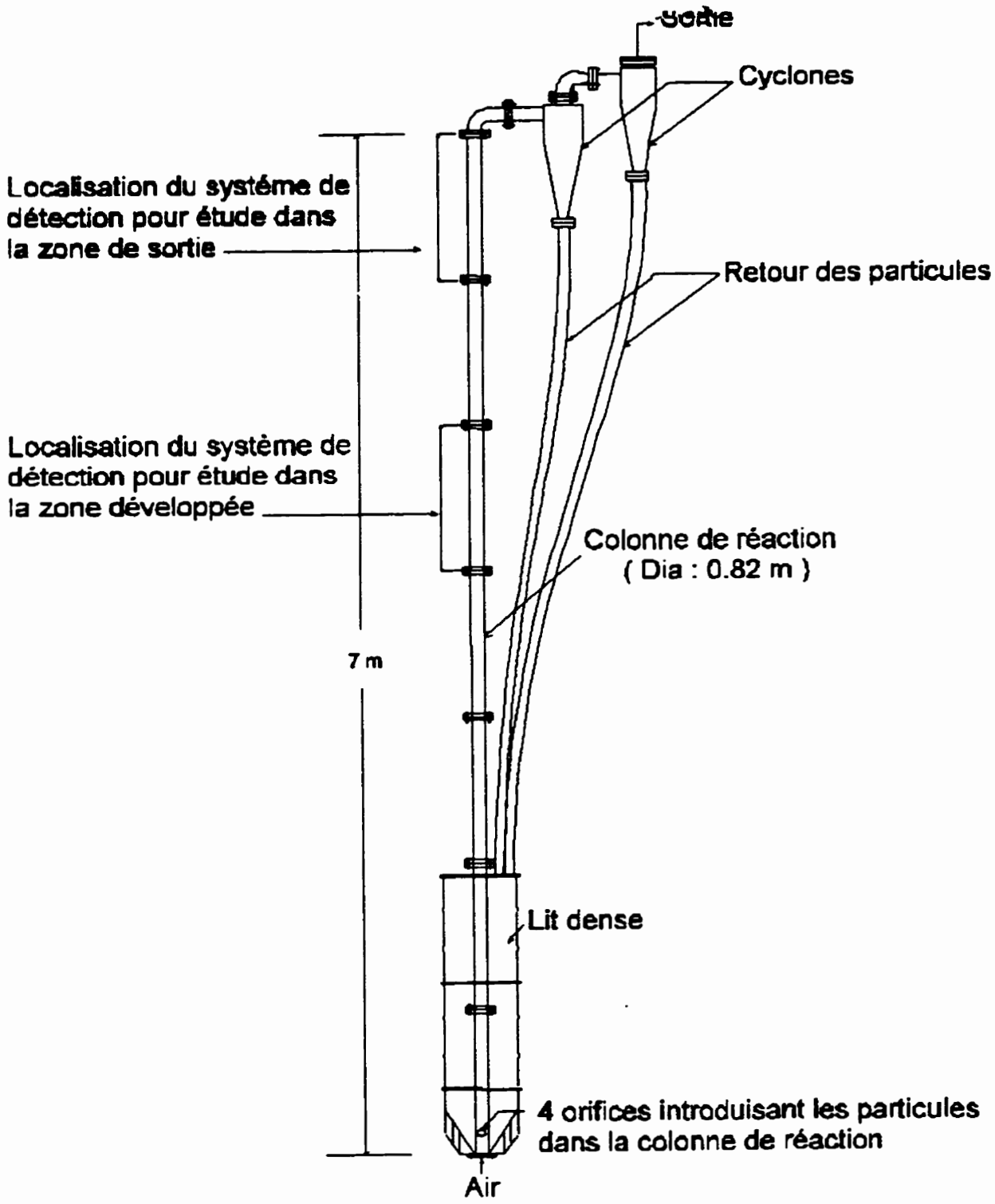

Figure AIII.1 Schéma du montage

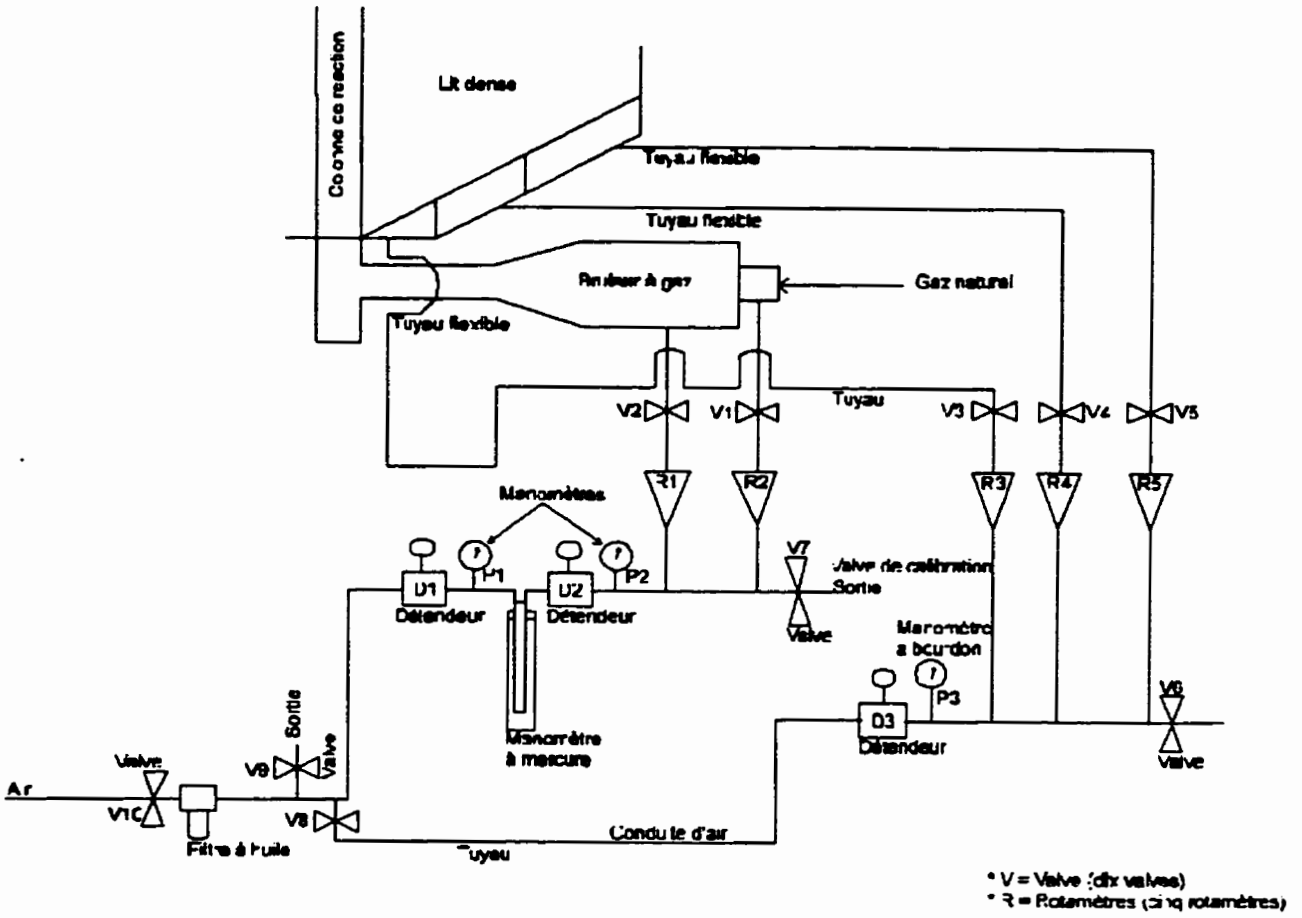

Figure AIII.2 Schéma de la tuyauterie

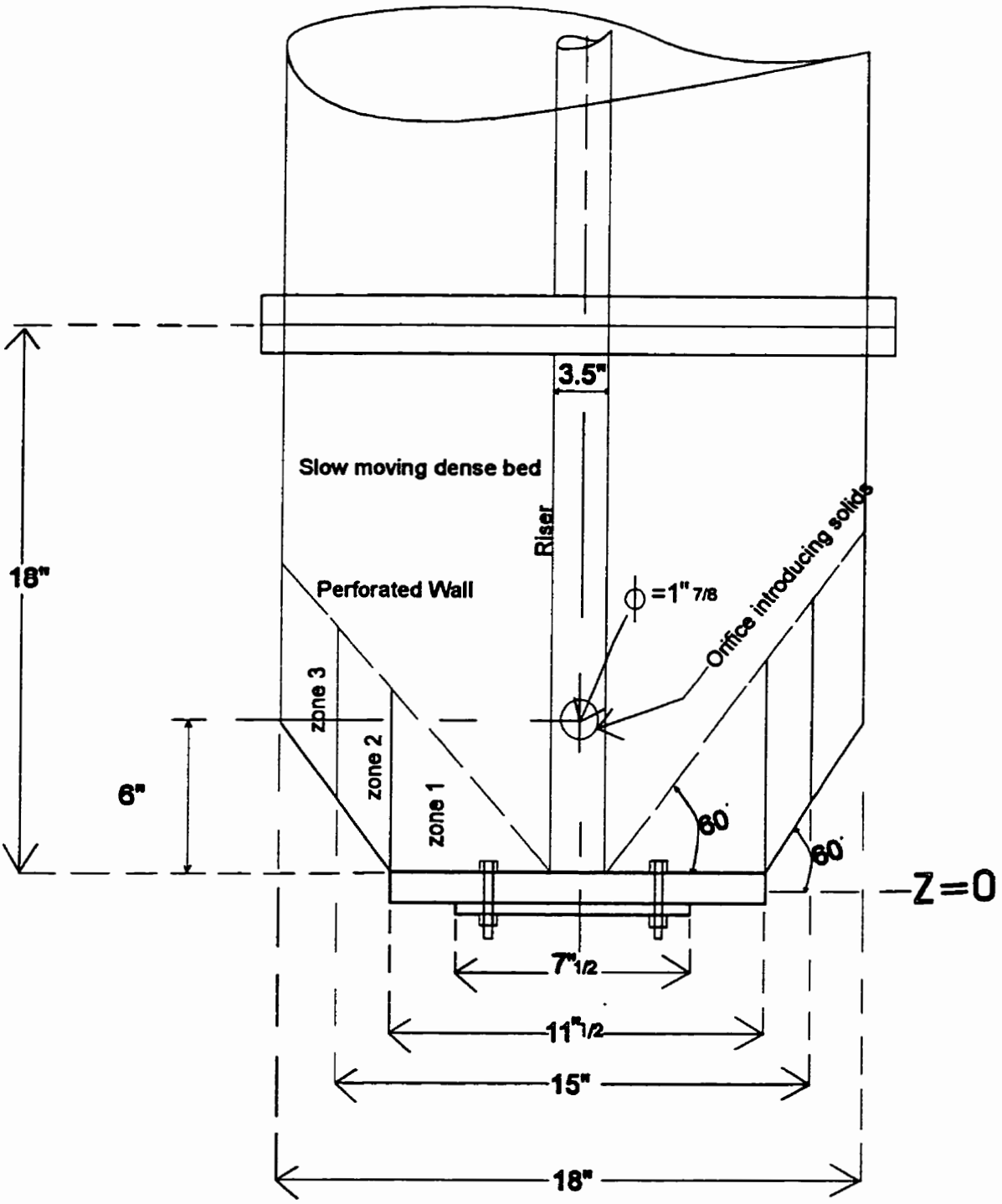

Figure AIII.3 Schéma du bas du lit

Annexe IV Courbes de calibration des rotamètres R3, R4 et R5.

Les courbes de calibration des rotamètres R3, R4 et R5 sont présentées aux Figures AIV.1, AIV.2 et AIV.3. La pression jauge dans les rotamètres est constante et égale à 300 kPa. Le débit volumique d'air est mesuré une température de 24 °C et une pression absolue de 749 mmHg.

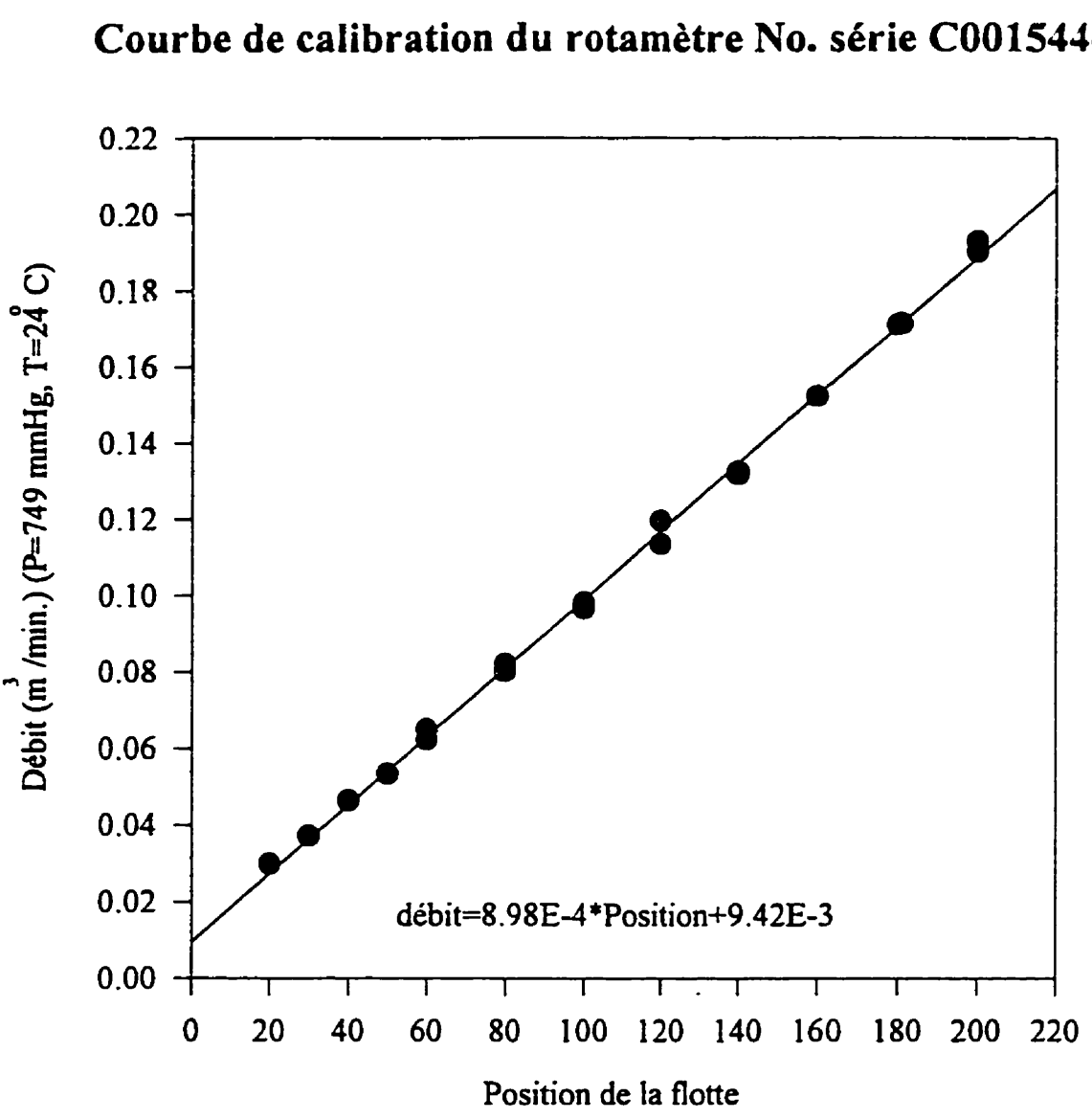

Figure AIV.1 Courbe de calibration du rotamètre R3 (P=300 kPa)

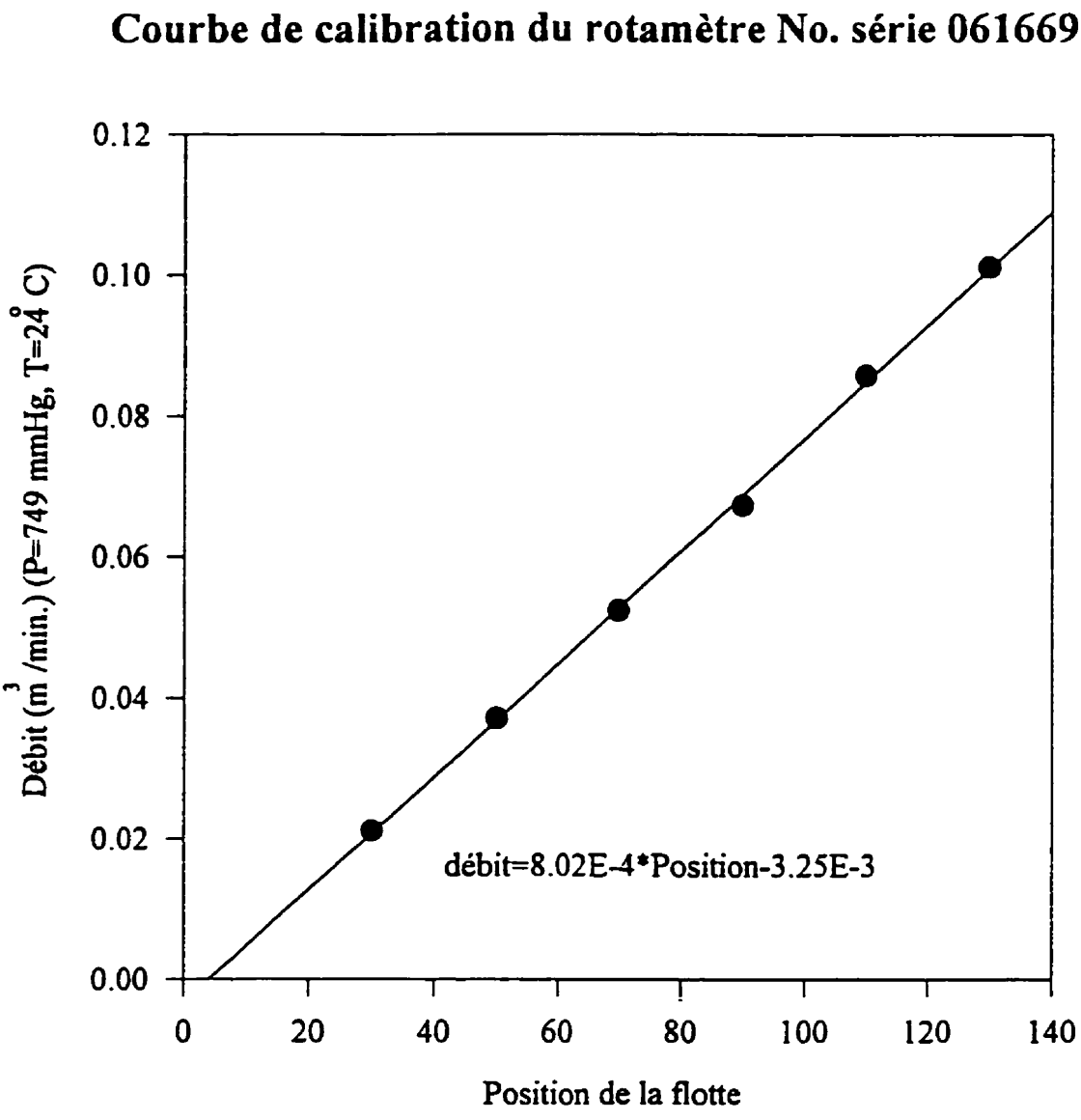

Figure AIV.2 Courbe de calibration du rotamètre R4 (P=300 kPa)

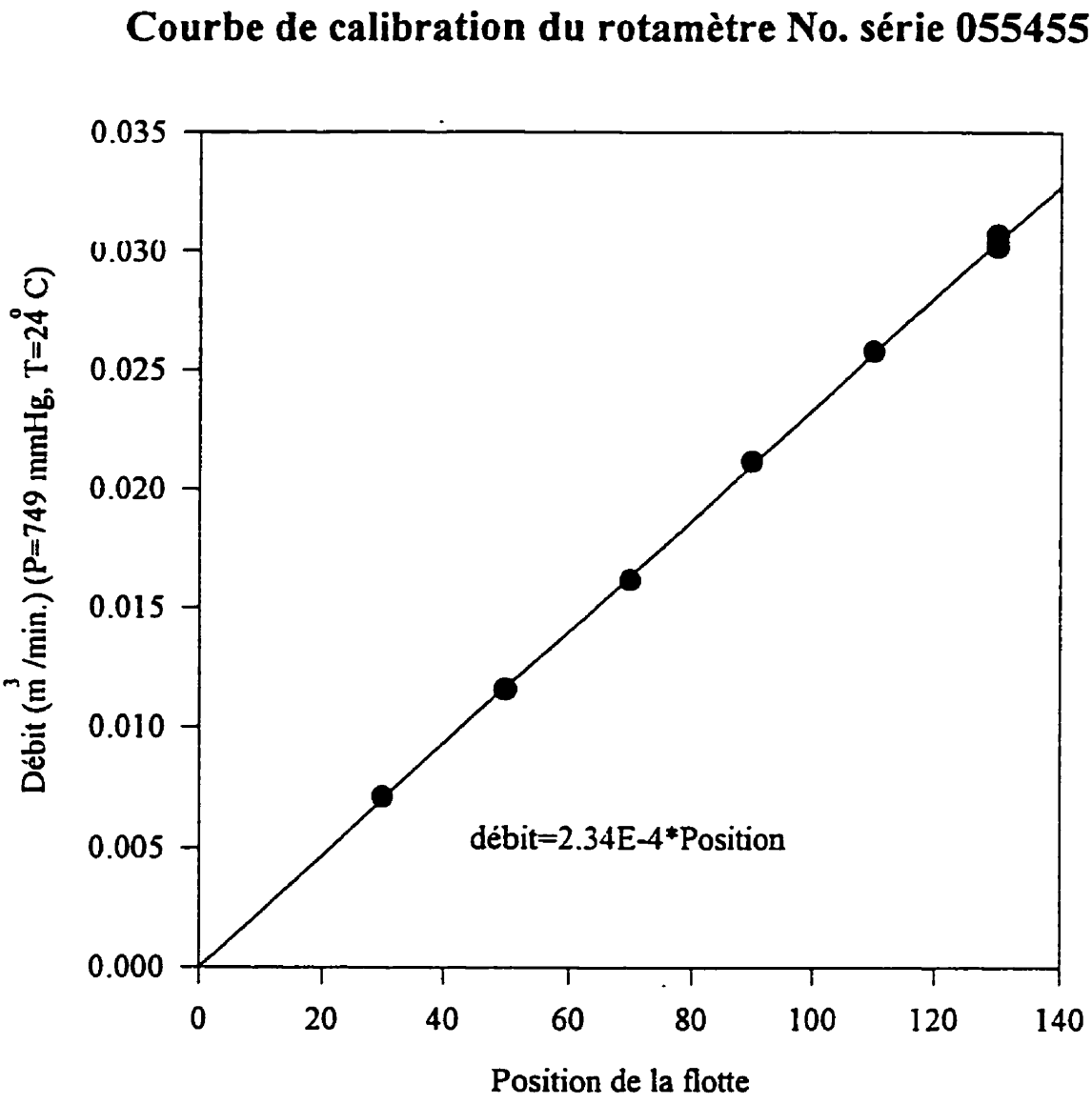

Figure AIV.3 Courbe de calibration du rotamètre R5 (P=300 kPa)

Annexe V Courbe de calibration du capteur différentiel de pression

La courbe de calibration du capteur différentiel de pression utilisé pour la mesure de la perte de charge est présenté à la Figure AV.1. La réponse du capteur de pression varie de -2.5 V à +2.5 V. Le voltage est mesuré à l'aide d'un micro-ordinateur d'acquisition des données. Le capteur de pression permet la mesure de la perte de charge comprise entre -60 et +60 cmH_2O.

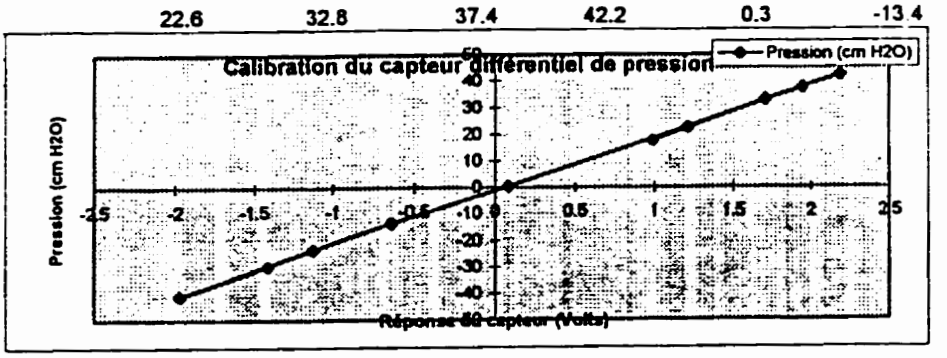

fichier: prescali.xls

Voltage (v)	cm H2O	17.5
0.990314453	17.5	
1.212177402	22.6	
1.708116426	32.8	
1.942872988	37.4	
2.185955	42.2	
0.084544531	0.3	
-0.637178105	-13.4	
-1.12411502	-23.2	
-1.972008418	-40.9	
-1.416654688	-29.6	

$$\text{Pression mesurée}\left[\text{cm } H_2O\right] = 19.8604 * \text{voltage}[V] - 1.337$$

Figure AV.1 Courbe de calibration du capteur différentiel de pression pour la mesure de la perte de charge axiale.

Annexe VI: Procédure expérimentale

Pour réaliser une expérience de poursuite d'une particule radioactive, il faut préparer une particule (mélange or-résine époxy d_p=500 µm, ρ_p=2000 kg/m^3) et l'activer pendant environ 32 heures dans le réacteur "Slowpoke" du département de génie énergétique. Ensuite, il faut effectuer une calibration. Dans un premier temps, les gains de chacun des détecteurs sont ajustés à l'aide d'un analyseur de spectre afin de s'assurer du bon fonctionnement de chacun des détecteurs. Par la suite, il faut générer des comptages expérimentaux qui permettront d'ajuster les paramètres du modèle phénoménologique reliant le comptage des détecteurs à la position de la particule. La calibration du modèle phénoménologique permettra par la suite de déterminer la position instantanée de la particule connaissant le comptage instantané de chacun des détecteurs. Cette opération doit s'effectuer dans des conditions aussi proches que possible de celles où la poursuite aura lieu. Il s'agit de positionner la particule à 90 endroits différents dans le lit et à en mesurer le comptage pendant 10 s de façon à avoir un comptage moyen de faible incertitude. La comparaison des comptages prédits par le modèle et des comptages mesurés expérimentalement permet l'optimisation, pour chacun des détecteurs, des paramètres du modèle. Comme la densité à l'intérieur du lit est faible (ρ_{lit}< 100 kg/m^3), l'atténuation est faible et ce paramètre n'est pas optimisé. On peut facilement montrer que la sensibilité du modèle à une variation de l'atténuation est faible. Les 2 paramètres à être optimisés sont: l'activité et le temps mort. L'optimisation utilise l'algorithme du simplex (Press et coll. 1988) pour la détermination des paramètres optimaux. L'activité optimale est proche de l'activité réelle (+-10%) qui peut être mesurée avec précision au laboratoire de génie énergétique (≈ 100 µCi). Le temps mort des détecteurs est d'environ 9 µs.

Une fois la calibration terminée, il faut introduire la particule dans le réacteur. Cette opération est un peu plus compliquée qu'on pourrait le croire; il faut se rappeler que le diamètre de la particule n'est que de 500 µm et que la manipulation est délicate. Ensuite, il ne reste qu'à fixer les débits d'air pour obtenir la vitesse superficielle et le taux de circulation de solides désiré.

Après une quinzaine de minutes, l'écoulement est en régime permanent et le système d'acquisition est démarré.

Annexe VII Caractérisation de la taille des particules de sable

Deux expériences de tamisage ont permis de déterminer le diamètre moyen des particules utilisées dans les expériences dans le lit fluidisé circulant. Le diamètre moyen des particules est de 150 µm.

Tableau AVII.1 Résultats du tamisage

Tamis	masse vide (g)	tamis+sable (g)	m_i (g)	X_i	dp_i (µm)
250 µm	299.3	427.9	128.6	.219	250
212 µm	422.1	552.7	130.6	.222	231
180 µm	302.8	423.4	120.6	.205	196
150 µm	296.2	347.3	51.1	.087	165
106 µm	283.9	363.1	79.2	.135	122
63 µm	291.0	314.6	23.6	.04	84.5
vide	403.4	456.8	53.4	.091	50

L'équation permettant de calculer le diamètre moyen des particules est la suivante :

$$\frac{1}{dp} = \frac{1}{\sum x_i / dp_i} \qquad \text{(AVII.1)}$$

Le diamètre moyen des particules déterminé par la première expérience de tamisage est de 145 µm.

Tableau AVII.2 Résultats du tamisage (essai répété)

Tamis	masse (g)	vide	tamis+sable (g)	m_i (g)	X_i	dp_i (µm)
250 µm	300.2		682.8	382.6	.414	250
212 µm	422.6		536.8	114.2	.123	231
180 µm	303.0		473.4	170.4	.185	196
150 µm	296.4		364.0	67.6	.0733	165
106 µm	284.1		385.2	101.1	.1096	122
63 µm	291.3		319.3	28.8	.0304	84.5
vide	403.4		461.6	58.2	.0631	50

Le diamètre moyen des particules déterminé par la deuxième expérience de tamisage est de 155 µm. Conclusion: Les expériences de tamisage démontrent que le diamètre moyen des particules est de 150 µm.

Les pages qui suivent donnent plus de détails sur la détermination du diamètre moyen des particules à partir d'une expérience de tamisage. De l'information est également fournie sur les diamètres d'ouverture des tamis et sur le fournisseur du sable.

Annexe VIII Réquisition pour l'achat de 8 détecteurs radioactifs

ÉCOLE POLYTECHNIQUE

CAMPUS DE L'UNIVERSITÉ DE MONTRÉAL
CASE POSTALE 6079 - SUCCURSALE "A"
MONTRÉAL (QUÉBEC) CANADA
H3C 3A7

DATE

BON DE COMMANDE
PURCHASE ORDER

N° C- 83754 -GC

À INSCRIRE SUR CORRESPONDANCE, COLIS, FACTURES, FEUILLES DE LIVRAISON.
TO BE INDICATED ON CORRESPONDENCE, PARCELS, INVOICES, PACKING SLIPS

EG & G Labserco
1182, South Service Road West
Oakville, Ontario
L6L 5T7

A/S Goorge Trap

93007 - 12094

ENVOIS POSTAUX
PARCEL POST SHIPMENTS

ÉCOLE POLYTECHNIQUE
CAMPUS DE L'UNIVERSITÉ DE MONTRÉAL
CASE POSTALE 6079 - SUCCURSALE "A"
MONTRÉAL (QUÉBEC) CANADA
H3C 3A7

EXPÉDIER À - *SHIP TO*

ÉCOLE POLYTECHNIQUE
CAMPUS DE L'UNIVERSITÉ DE MONTRÉAL
2900 ÉDOUARD-MONTPETIT
MONTRÉAL (QUÉBEC) CANADA
H3T 1J4

RÉCEPTION PORTE #3 / *RECEIVING #3*
FERMETURE: 12H00 À 13H00
CLOSED: NOON TO 1H00 PM

CONDITIONS - *TERMS*	À EXPÉDIER - *SHIP VIA*	F.A.B. - *F.O.B.*	À LIVRER LE - *DATE REQUIRED*
Net 30 days		Oakville, Ontario	

QTÉ - *QTY*	DESCRIPTION	PRIX - *PRICE*	MONTANT - *AMOUNT*
8	Model 925-Scint (Ace-Mate) Workstation (Bench Top enclosure) including: preamplifier-amplifier-single channel analyser-ratemeter-bias supply	1,930.00$	15,440.00$
8	Model Ace-MCS 1 slot multichannel scaler board (including MCS software package VGA compatible)	1,230.00$	9,840.00$
8	Model 266 PMT Base	330.00$	2,640.00$
8	Teledyne isotopes model S-1212-I NaI detector 3" x 3" crystal 7.5% resolution	2,011.00$	16,088.00$
8	MC36-S SHV cable, 30' length	125.00$	1,000.00$
8	MC-24-12 BNC cable, 12 length	27.00$	216.00$
8	MC-24-S BNC cable, 30' lenght	73.00$	584.00$
8	MC-25-S BNC cable, 30' lenght	73.00$	584.00$
	Quotation: 2184A		

EXEMPTIONS: TVQ - PST - TPS - GST - DOUANE - CUSTOMS - EX

NO D'INSCRIPTION T.P.S. - G.S.T. REGISTRATION NO.: R 107585226

FACTURES - *INVOICES*
Les factures en triplicata doivent être envoyées à
Invoices in triplicate have to be sent to

ÉCOLE POLYTECHNIQUE
SERVICE DES FINANCES
CAMPUS DE L'UNIVERSITÉ DE MONTRÉAL
CASE POSTALE 6079, SUCCURSALE "A"
MONTRÉAL (QUÉBEC) CANADA H3C 3A7

L'École Polytechnique se réserve le droit d'annuler cette commande si elle n'est pas complétée selon les spécifications et conditions ci-dessus mentionnées.
École Polytechnique reserves the right to cancel this order if not completed according to specifications and conditions mentioned herein.

POUR RENSEIGNEMENTS, COMMUNIQUER AVEC:
FOR INQUIRIES RE:

Faïçal Larachi R-097187 TÉL: (514) 340-4469
TÉLÉCOPIEUR: (514) 340-4211

BON DE COMMANDE N°

LA CORPORATION DE L'ÉCOLE POLYTECHNIQUE

Lorraine Godin
RESPONSABLE DE L'APPROVISIONNEMENT
(514) 340-4795

4- CENTRE - DÉPARTEMENT - *INSTITUT - SERVICE*

IMAGE EVALUATION
TEST TARGET (QA–3)

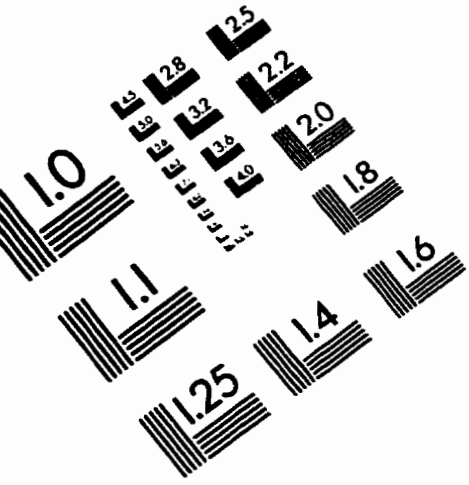

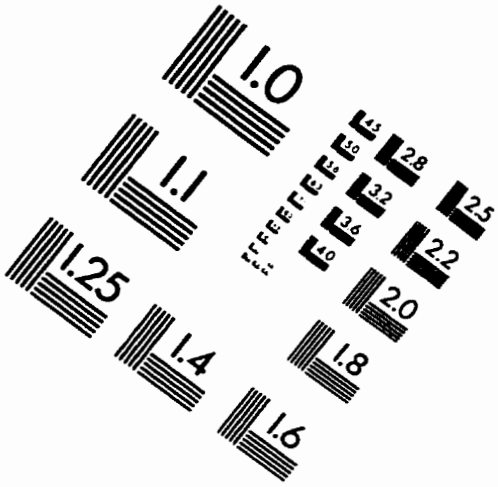

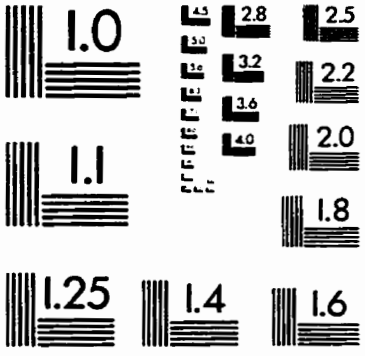

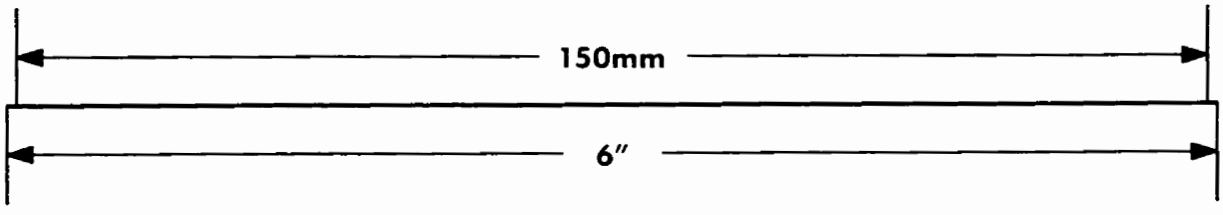

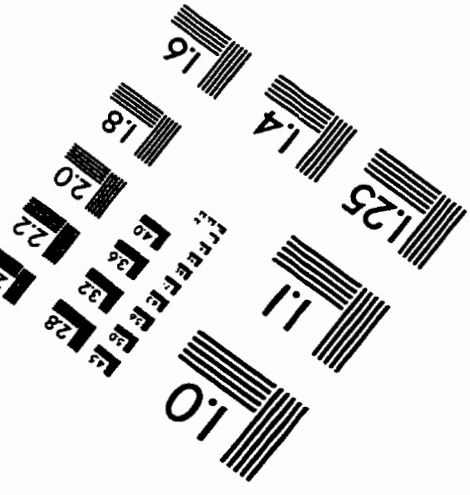

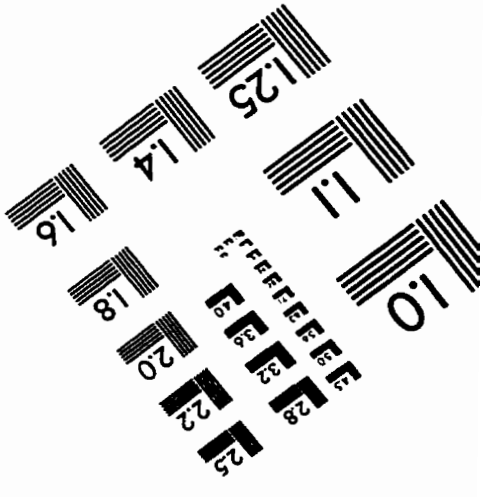

APPLIED IMAGE, Inc
1653 East Main Street
Rochester, NY 14609 USA
Phone: 716/482-0300
Fax: 716/288-5989